

École Centrale de NANTES

ÉCOLE DOCTORALE

SCIENCES ET TECHNOLOGIES  
DE L'INFORMATION ET MATHÉMATIQUES

Année 2011

N ° attribué par la bibliothèque

□□□□□□□□□□

# Contribution à la commande de robots marcheurs bipèdes

## THÈSE DE DOCTORAT

Discipline : Automatique et Informatique Appliquée

Spécialité : Robotique

Présenté

et soutenue publiquement par

**Ting WANG**

Le 8 Décembre 2011, devant le jury ci dessous

*Président*

...

...

...

*Rapporteurs*

Mazen

ALAMIR

Directeur de Recherche, CNRS, à GIPSA-Lab

Olivier

BRUNEAU

Maître de Conférences à l'Université de Versailles Saint Quentin

*Examineurs*

Gabriel

ABBA

Professeur à l'École Nationale d'Ingénieurs de Metz

Rodolphe

GELIN

Chef des projets collaboratifs à Aldebaran Robotics

Yannick

AOUSTIN

Maître de Conférences à l'Université de Nantes

Christine

CHEVALLEREAU

Directeur de Recherche, CNRS, à l'IRCCyN

Directeur de thèse : Christine CHEVALLEREAU

ED : .....



# Contents

<b>Introduction</b>	<b>1</b>
<b>1 Walking control of an under-actuated planar biped robot</b>	<b>7</b>
1.1 Introduction . . . . .	7
1.2 Description of the studied robot . . . . .	8
1.2.1 Biped model . . . . .	8
1.2.2 Walking gait . . . . .	10
1.3 Dynamic model during different walking phases . . . . .	11
1.3.1 Lagrange formulation . . . . .	11
1.3.2 Swing phase model . . . . .	13
1.3.3 Impact model . . . . .	13
1.3.4 Hybrid model of walking . . . . .	16
1.4 A control law for tracking parametrized reference trajectory . . . . .	16
1.4.1 The reference trajectory . . . . .	17
1.4.2 Calculation of the input torques . . . . .	18
1.4.3 Stability analysis . . . . .	19
1.5 Two control laws for tracking time-variant reference trajectory . . . . .	23
1.5.1 The reference trajectory . . . . .	24
1.5.2 A control law based on choice of controlled outputs . . . . .	24
1.5.3 Stability analysis . . . . .	26
1.5.4 Stability test in a reduced dimensional space . . . . .	28
1.5.5 An event-based feedback controller . . . . .	30
1.6 Simulation results of three controllers . . . . .	31
1.6.1 A cyclic motion and approximated motion . . . . .	32
1.6.2 Results of the control law for tracking parametrized reference trajectory	34
1.6.3 An example of a control law tracking only actuated joints . . . . .	36
1.6.4 An example of the event-based feedback controller . . . . .	38
1.6.5 Results of stability analysis with different choices of controlled outputs	40
1.6.6 A method for pertinent choice of controlled outputs . . . . .	43
1.6.7 Comparison of three control laws . . . . .	46
1.7 Conclusions . . . . .	47

<b>2</b>	<b>Walking control of a 3D biped robot</b>	<b>49</b>
2.1	Introduction . . . . .	49
2.2	Description of the studied biped robot . . . . .	50
2.3	Dynamic model during different walking phases . . . . .	51
2.3.1	Swing phase model . . . . .	52
2.3.2	ZMP dynamics . . . . .	53
2.3.3	Impact model . . . . .	54
2.4	Parametrization of the reference trajectory . . . . .	54
2.5	A control law considering ground contact and stability . . . . .	55
2.5.1	ZMP controller . . . . .	57
2.5.2	Swing ankle rotation controller . . . . .	57
2.5.3	Partial joint angles controller . . . . .	58
2.5.4	Modification of the tracked errors caused by impact . . . . .	59
2.5.5	Calculation of the input torques . . . . .	61
2.5.6	Hybrid zero dynamics . . . . .	61
2.5.7	Stability analysis at a fixed-point . . . . .	63
2.6	Simulation results . . . . .	63
2.6.1	Reference trajectory . . . . .	64
2.6.2	The effect of different controlled partial joints on the walking stability	65
2.6.3	Description of the simulator . . . . .	65
2.6.4	The robustness of the control law for the rigid ground model . . .	67
2.6.5	The robustness of the proposed control law for the soft ground model	70
2.7	Comparison of several control laws . . . . .	72
2.7.1	A control law without the regulation of $ZMP_y$ . . . . .	73
2.7.2	A control law without the regulation of $ZMP_x$ . . . . .	77
2.7.3	A control law without the regulation of $ZMP$ . . . . .	81
2.7.4	A classical control law without the regulation of $ZMP$ . . . . .	85
2.7.5	Comparisons of five control laws . . . . .	87
2.8	Conclusions . . . . .	88
<b>3</b>	<b>Steering control of the 3D biped robot</b>	<b>89</b>
3.1	Introduction . . . . .	89
3.2	Stability analysis of the extended system with yaw motion . . . . .	90
3.3	Stabilization of the yaw motion . . . . .	92
3.4	Steering control of the walking . . . . .	95
3.4.1	Steering control of robot to walk along a desired direction . . . . .	95
3.4.2	Steering control of robot to pass through a door . . . . .	98
3.4.3	Steering control of robot to reach a destination . . . . .	100
3.5	Conclusions . . . . .	102

<b>4</b>	<b>Walking control of a 3D biped robot with foot rotation</b>	<b>103</b>
4.1	Introduction . . . . .	103
4.2	Description of the studied biped robot . . . . .	104
4.3	Dynamic model during different walking phases . . . . .	106
4.3.1	Dynamic model during single support phase . . . . .	108
4.3.2	ZMP dynamics . . . . .	108
4.3.3	Impact model . . . . .	109
4.4	Parametrization of the reference trajectory . . . . .	109
4.5	A control law considering ground contact and stability . . . . .	111
4.5.1	ZMP controller . . . . .	111
4.5.2	Swing ankle rotation controller . . . . .	111
4.5.3	Partial joint angles controller . . . . .	112
4.5.4	Calculation of the input torques . . . . .	113
4.5.5	Stability analysis . . . . .	114
4.6	Simulation results . . . . .	114
4.6.1	Simulation results of an example without foot rotation phase . . . . .	115
4.6.2	Simulation results of the walking with foot rotation phase . . . . .	119
4.7	Conclusions . . . . .	136
	<b>Conclusions and perspectives</b>	<b>137</b>
<b>A</b>	<b>Calculation details of the control law</b>	<b>153</b>
A.1	Calculation of ${}^s\omega_n$ and ${}^s\dot{\omega}_n$ . . . . .	153
A.2	Simplification of calculations for swing ankle rotation controller . . . . .	153
A.3	Simplification of calculations for partial joint angles controller . . . . .	155
A.4	Calculation of zero dynamics . . . . .	156
A.5	Calculation of joint accelerations . . . . .	157
<b>B</b>	<b>Steering control for different legs</b>	<b>159</b>
<b>C</b>	<b>Publications</b>	<b>161</b>



# List of Figures

1.1	Photo of RABBIT . . . . .	9
1.2	Geometrical parameters of RABBIT . . . . .	10
1.3	The studied biped . . . . .	11
1.4	Walking phases . . . . .	12
1.5	Description of $\theta$ . . . . .	17
1.6	Poincaré map. . . . .	21
1.7	The modification of the reference path. . . . .	31
1.8	Stick-diagram for the first step of the periodic walking gait . . . . .	32
1.9	Joint profiles of the obtained periodic motion over two steps, where the small circles represent $q_f^*$ . . . . .	33
1.10	Joint rate profiles of the obtained periodic motion over two steps, where the small circles represent $\dot{q}_f^*$ . . . . .	33
1.11	The difference of the real values and desired values of $q_u$ and $\dot{q}_u$ at the end of each step for the control law based on tracking parametrized reference trajectory. . . . .	35
1.12	Phase-plane plots for $q_i$ , $i = 1, \dots, 5$ for the control law based on tracking parametrized reference trajectory. The straight lines correspond to the impact phase, where the state of the robot changes instantaneously. The initial state is represented by a (red) star. . . . .	35
1.13	The torques of the swing leg for the control law based on tracking parametrized reference trajectory, where $\Gamma(3)$ notes the torque of hip and $\Gamma(4)$ notes the torque of knee. . . . .	36
1.14	The difference of the real values and desired values of $q_u$ and $\dot{q}_u$ at the end of each step for the control law based on choice of controlled outputs with $M_1 = [0, 0, 0, 0]^T$ . . . . .	37
1.15	Phase-plane plots for $q_i$ , $i = 1, \dots, 5$ for the control law based on choice of controlled outputs with $M_1 = [0, 0, 0, 0]^T$ . The straight lines correspond to the impact phase, where the state of the robot changes instantaneously. The initial state is represented by a (red) star. . . . .	37
1.16	The difference of the real values and desired values of $q_u$ and $\dot{q}_u$ at the end of each step for the event-based feedback control law. . . . .	39

1.17	Phase-plane plots for $q_i$ , $i = 1, \dots, 5$ for the event-based feedback control law. The straight lines correspond to the impact phase, where the state of the robot changes instantaneously. The initial state is represented by a (red) star. . . . .	39
1.18	The torques of the swing leg for the event-based feedback control law, where $\Gamma(3)$ notes the torque of hip and $\Gamma(4)$ notes the torque of knee. . . . .	40
1.19	$\max  \lambda_{1,2} $ versus $M_1(j)$ , $j = 1, 2, 3, 4$ , when the other three components of $M_1$ are zero. . . . .	41
1.20	The difference of the real values and desired values of $q_u$ and $\dot{q}_u$ at the end of each step for the control law based on choice of controlled outputs with $M_1 = [0, 0, -2.06, 0]^T$ . . . . .	42
1.21	Phase-plane plots for $q_i$ , $i = 1, \dots, 5$ for the control law based on choice of controlled outputs with $M_1 = [0, 0, -2.06, 0]^T$ . The straight lines correspond to the impact phase, where the state of the robot changes instantaneously. The initial state is represented by a (red) star. . . . .	42
1.22	The torques of the swing leg for the control law based on choice of controlled outputs with $M_1 = [0, 0, -2.06, 0]^T$ , where $\Gamma(3)$ notes the torque of torso and $\Gamma(4)$ notes the torque of knee. . . . .	43
1.23	The height of the swing foot at the end of the step $Z_{sw}(T^d)$ with respect to the effective eigenvalues of the Poincaré map, $\max  \lambda_{1,2} $ . . . . .	45
1.24	The stable domain of $M_1(2)$ and $M_1(3)$ for two groups of solution, which is described with contour line $\max  \lambda_{1,2}  = 1$ . . . . .	45
1.25	The difference of the real values and desired values of $q_u$ and $\dot{q}_u$ at the end of each step for the control law based on choice of controlled outputs with $M_1 = [1.91, -4, -3, -1.41]$ . . . . .	46
1.26	The torques of the swing leg for the control law based on choice of controlled outputs with $M_1 = [1.91, -4, -3, -1.41]$ , where $\Gamma(3)$ notes the torque of hip and $\Gamma(4)$ notes the torque of knee. . . . .	47
2.1	Photo of HYDROID . . . . .	51
2.2	Biped Model . . . . .	52
2.3	The support foot . . . . .	53
2.4	The definition of $\theta$ . . . . .	55
2.5	Block diagram of the control system. . . . .	56
2.6	Stick-diagram for one step of the periodic walking gait in sagittal plane . .	64
2.7	$\max  \lambda_{1,2,3} $ versus $M_1(j, 1)$ , $j = 6, 7$ , when the other 9 components of $M_1$ are zero. . . . .	65
2.8	Block diagram of the simulator. . . . .	66
2.9	The walking motion of first three steps with the proposed control law. . . .	67
2.10	Position of ZMP with the proposed control law using the rigid ground model: the position of ZMP moves periodically and is always within the limits. . .	68
2.11	The tracking errors of $q_2$ with the proposed control law using the rigid ground model. . . . .	68



2.12	Height of feet with the proposed control law using the rigid ground model.	69
2.13	Phase-plane plots for $q_i, i = 1, 2, 3, 4$ with the proposed control law using the rigid ground model. The initial state is represented by a (red) star. . .	69
2.14	Ground reaction force (GRF) of the soft ground model. . . . .	70
2.15	Position of ZMP in the feet sole with the proposed control law using the soft ground model: the position of ZMP moves periodically and returns to the limits fastly after impact. . . . .	71
2.16	Height of feet with the proposed control law using the soft ground model. .	71
2.17	Phase-plane plots for $q_i, i = 1, 2, 3, 4$ with the proposed control law using the soft ground model. The initial state is represented by a (red) star. . . .	72
2.18	The tracking errors of $q_2$ with the proposed control law using the soft ground model. . . . .	72
2.19	Position of ZMP in the foot sole for the control law without the regulation of $ZMP_y$ : the position of ZMP moves periodically and is always within the limits but $ZMP_y$ does not track $ZMP_y^d$ . . . . .	75
2.20	Phase-plane plots for $q_i, i = 1, 2, 3, 4$ for the control law without the regulation of $ZMP_y$ . The initial state is represented by a (red) star. . . . .	76
2.21	Height of feet for the control law without the regulation of $ZMP_y$ . . . . .	76
2.22	Position of ZMP in the foot sole for the control law without the regulation of $ZMP_x$ : the position of ZMP moves periodically but $ZMP_x$ is out of the limit during a short time. . . . .	79
2.23	Phase-plane plots for $q_i, i = 1, 2, 3, 4$ for the control law without the regulation of $ZMP_x$ . The initial state is represented by a (red) star. . . . .	80
2.24	Height of feet for the control law without the regulation of $ZMP_x$ . . . . .	80
2.25	Position of ZMP in the foot sole for the control law without the regulation of ZMP. . . . .	82
2.26	Phase-plane plots for $q_i, i = 1, 2, 3, 4$ for the control law without the regulation of ZMP. The initial state is represented by a (red) star. . . . .	82
2.27	Height of feet for the control law without the regulation of ZMP. . . . .	83
2.28	Position of ZMP in the foot sole for the control law without the regulation of ZMP: the position of $ZMP_x$ is out of the limits when the larger initial errors are introduced. . . . .	83
2.29	Phase-plane plots for $q_i, i = 1, 2, 3, 4$ for the control law without the regulation of ZMP when the larger initial errors are introduced. The initial state is represented by a (red) star. . . . .	84
2.30	Height of feet for the control law without the regulation of ZMP when the larger initial errors are introduced. . . . .	84
2.31	The tracking errors of $q_2$ for the classical control law. . . . .	85
2.32	Height of feet with the classical control law, for the right foot a zoom is done along the vertical axis to show the unexpected rotation of the stance foot. .	86
2.33	COP in the feet sole for the classical control law. . . . .	86
2.34	The walking motion of first two steps with the classical control law. . . . .	87

3.1	Description of walking direction . . . . .	90
3.2	The positions of the feet at impacts with initial error of states, where the red points denote the midpoint of two feet. The robot departs from the direction of $x_s$ axis. . . . .	91
3.3	The modification of the reference path $u^d$ . . . . .	93
3.4	Scheme of the steering control law. . . . .	96
3.5	The positions of the feet at impacts under event-based feedback control, where the red points denote the midpoint of two feet. The robot walks along the direction of $x_s$ axis . . . . .	96
3.6	The direction angle of left foot $q_l$ , right foot $q_r$ and the walking direction angle $q_0$ , where the straight lines in figures of $q_l$ and $q_r$ denote the single support phases. $q_0$ converges to $180^\circ$ . . . . .	97
3.7	The positions of the feet at impacts under event-based feedback control, where the red points denote the midpoint of two feet. The robot walks along the direction of $-x_s$ axis . . . . .	98
3.8	The layout of the robot and the targets. . . . .	99
3.9	The positions of the feet at impacts for passing through the door, where the red points denote the midpoint of two feet. The walking path converges to the desired one $y^d = -0.5$ . . . . .	99
3.10	The direction angle of left foot $q_l$ , right foot $q_r$ , and the walking direction angle $q_0$ , where the straight lines in figures of $q_l$ and $q_r$ denote the single support phases. $q_0$ is regulated to obtain $y^d = -0.5$ at first, then it converges to $0^\circ$ so the robot walks along the $x_s$ axis as shown in Fig. 3.9. . . . .	100
3.11	The positions of the feet at impacts for reaching two destinations at $[6, 1]$ and $[6, -1]$ respectively. . . . .	101
3.12	The relative distance of the robot and the destination at $[6, 1]$ . . . . .	101
4.1	HYDROID: biped robot with arms. . . . .	105
4.2	In case (a), the stance foot contacts the ground completely, the center of pressure of the forces on the foot, P, remains strictly within the interior of the footprint. In this case, the foot will not rotate, $q_1 = 0$ and thus the system is fully actuated. In case (b), the center of pressure has moved to the toe, that allows the foot to rotate, $q_1 \neq 0$ , thus the system is now under-actuated. . . . .	106
4.3	Human walking gait through one cycle, beginning and ending at heel strike. Percentages showing contact events are given at their approximate location in the cycle. Adapted from [Rose and Gamble, 1994]. . . . .	107
4.4	Walking gait of the studied robot with foot rotation phase. Adapted from [Tlalolini, 2008]. . . . .	108

4.5	The definition of $\theta$ during fully support phase (a) and foot rotation phase (b). Note that the definition of joint angle for the ankle and knee, i.e., $q_3$ and $q_5$ , are different from that of the robot's model shown in Fig. 2.4. This is because the definition of coordinate systems for the two joints are changed in the new robot model. . . . .	110
4.6	Stick-diagram for one step of the periodic walking gait in 3D space and sagittal plane. . . . .	115
4.7	$\max  \lambda_{1,2,3} $ versus $M_1(j, 1)$ , $j = 2, 16$ , when the other 22 components of $M_1$ are zero. . . . .	116
4.8	Height of feet for the walking without foot rotation phase. . . . .	117
4.9	Position of ZMP in the foot sole for the walking without foot rotation phase: the position of ZMP moves periodically and is always within the limits. . .	117
4.10	Phase-plane plots for $q_i, i = 2, 3, 4, 5$ for the walking without foot rotation phase. The initial state is represented by a (red) star. . . . .	118
4.11	The corresponding torques of $q_i, i = 2, 3, 4, 5$ for the walking without foot rotation phase. . . . .	118
4.12	The walking motion of the robot without foot rotation phase during first three steps. . . . .	119
4.13	Stick-diagram for one walking step with foot rotation phase in 3D space. .	120
4.14	Stick-diagram for one walking step with foot rotation phase in sagittal plane.	120
4.15	Foot rotation angle $q_1$ and height of feet for the walking including foot rotation phase. . . . .	121
4.16	$\max  \lambda_{1,2,3} $ versus $M_1(4, 1)$ , when the other 22 components of $M_1$ are zero.	122
4.17	Block diagram of the simulator for the walking with foot rotation phase. .	123
4.18	Height of feet for the walking including foot rotation phase. . . . .	124
4.19	Position of ZMP in the foot sole for the walking including foot rotation phase: the position of ZMP moves periodically. $ZMP_y$ is always within the limits and $ZMP_x$ is zero during under-actuated phase. . . . .	124
4.20	Phase-plane plots for $q_i, i = 2, 3, 4, 5$ for the walking including foot rotation phase. The initial state is represented by a (red) star. . . . .	125
4.21	The corresponding torques of $q_i, i = 2, 3, 4, 5$ for the walking including foot rotation phase. . . . .	125
4.22	The tracking errors of $q_2$ and $q_3$ for the walking including foot rotation phase.	126
4.23	The tracking errors of $q_{14}$ and $q_{15}$ for the walking including foot rotation phase. . . . .	126
4.24	Rotation angle of the stance foot in the sagittal plane and its desired values. Note that in the first step it is $q_1$ and in the next step is written as $q_{16}$ , and so forth. . . . .	127
4.25	The walking motion of the robot with foot rotation phase during first three steps. . . . .	127
4.26	Height of feet for the proposed control law considering initials errors and $-20\%$ modeling errors. . . . .	129

4.27	The tracking errors of $q_2$ and $q_3$ for the proposed control law considering initials errors and $-20\%$ modeling errors. . . . .	129
4.28	Position of ZMP for the proposed control law considering initials errors and $-20\%$ modeling errors. $ZMP_y$ is always within the limits and $ZMP_x$ is zero during under-actuated phase. . . . .	130
4.29	Phase-plane plots for $q_i, i = 2, 3, 4, 5$ for the proposed control law considering initials errors and $-20\%$ modeling errors. The initial state is represented by a (red) star. . . . .	131
4.30	The corresponding torques of $q_i, i = 2, 3, 4, 5$ for the proposed control law considering initials errors and $-20\%$ modeling errors. . . . .	131
4.31	Position of ZMP for the proposed control law considering initials errors and $+10\%$ modeling errors. $ZMP_x$ almost reaches the edge of the heel during the fully support phase. . . . .	132
4.32	The tracking errors of $q_2$ and $q_3$ for the proposed control law considering initials errors and $+10\%$ modeling errors. . . . .	132
4.33	Position of CoP in the foot sole for the walking with foot rotation phase under the classical control law: it moves out of the foot sole after walking two steps. . . . .	134
4.34	Height of feet for the walking with foot rotation phase under the classical control law. . . . .	134
4.35	The walking motion of the robot with foot rotation phase under the classical control law. . . . .	135
4.36	Phase-plane plots for $q_i, i = 2, 3, 4, 5$ for the walking with foot rotation phase under the classical control law. The initial state is represented by a (red) star.	135
B.1	The walking direction angle of the left foot before the impact of the first step with different $\delta q_0$ . The red point denotes the moment at Poincaré section when $\delta q_0$ is introduced in the feedback event-based control law. . . . .	160
B.2	The walking direction angle of the right foot before the impact of the second step with different $\delta q_0$ . Here the straight line denotes the right leg is supported by the ground in the first leg. The red point denotes the moment at Poincaré section where $\delta q_0$ is introduced in the feedback event-based control law. . . . .	160

# Introduction

Research on biped humanoid robots is currently one of the most attractive topics in the field of robotics. Many biped walking robots have been manufactured since 1970s, such as WL-12 [Yamaguchi et al., 1993], H5 [Nagasaka et al., 1999], ASIMO [Sakagami et al., 2002], HRP-2 [Kaneko et al., 2004], QRIO [Ishida, 2004], JOHNNIE [Buschmann et al., 2007], Lola [Buschmann et al., 2009]. Among them ASIMO of HONDA and HRP of AIST are well known biped humanoid robots. Although more and more human-like biped robot platforms have been developed, the realization of stable walking of bipeds remains challenging.

Compared to human walking, the walking of bipedal robots looks awkward and has less energetic efficiency. The *foot rotation phase*, where the stance heel lifts from the ground and the stance foot rotates about the toe, allows robot to reduce significantly the cost criterion for fast motions [Huang et al., 2001], [Tlalolini et al., 2009]. Work in [Kuo, 2002] shows that plantarflexion of the ankle, which initiates heel rise and toe roll, is the most efficient method to reduce energy loss at the subsequent impact of the swing leg. This motion is also necessary for the aesthetics of mechanical walking. Thus, it is extremely important and interesting to study the walking control of a humanoid robot with rotation of the feet, and that is also the ultimate goal of this thesis. However, the foot rotation phase is an under-actuated phase and the stability analysis is necessary during the design of the control law. In order to study the control of under-actuated biped robots and the principle of stability analysis using Poincaré method, our work starts with the research on RABBIT which is an under-actuated planar biped robot with point feet (4 actuated joints and 5 DOF). Based on this research, the walking control of a 3D biped robot with flat-feet but without arms (14 actuated joints) and the control of a 3D biped robot with arms (26 actuated joints) are studied. In the first two robot models, the walking phase only consists of single support phase and impact or instantaneous double support phase. In order to obtain a more human-like walking, the foot rotation phase is considered in the third robot model. As a preliminary study of our robot, the control laws proposed in this thesis use the principle of our earlier research. Specifically, the reference trajectory of the joint angles and ZMP have been off-line computed using the optimization techniques to minimize the consumed torques [Chevallereau and Aoustin., 2001], [Tlalolini et al., 2011]. Our objective is to propose new control laws to satisfy the constraint of contact and to study the stability of walking, i.e., the convergence of periodical walking. The thesis is organized as follows.

In Chapter 1, the stable walking control of an under-actuated planar biped robot is

studied. The biped model consists of five links, connected together to form two legs with knees and a torso (Fig. 1.3). It has point feet without actuation between the feet and ground, so the ZMP heuristics is not applicable, and thus under actuation must be explicitly addressed in the walking controller design.

There exist various studies about the walking control of the under-actuated mechanical systems [Fantoni and Lozano, 2002], [Anderle and Celikovsky, 2009], [Grizzle et al., 2005], [Zikmund and Moog, 2006], [Chemori and Loria, 2004]. Most controllers of these systems are based on tracking reference motions. In the existing research of the biped, there are two groups of method which depend on the differences of reference trajectory. The first one is based on reference trajectory as a function of time and the latter one is time invariant. In the second method, for example, the method of virtual constraints, a state quantity of the biped which is strictly monotonic (i.e., strictly increasing or decreasing) along a typical walking gait, is used to replace time in parameterizing a periodic motion of the biped. When the reference walking motion is parametrized with respect to a scalar valued function of the state of the robot instead of time, the controller is time invariant, which helps analytical tractability. In addition, when such a control has converged, the configuration of the planar robot at the impact is the desired configuration. Moreover, it has been observed that for the same robot and for a same known cyclic motion, a control law based on a reference trajectory as a function of the state of the robot, produces a stable walking. Whereas a control law based on reference motion as a function of time produces an unstable walking [Chevallereau, 1999]. For the above reasons, many walking controllers are designed successfully based on this virtual constraints method for the planar bipeds in the previous work [Grizzle et al., 2001], [Chevallereau et al., 2003], [Plestan et al., 2003], [Westervelt et al., 2003]. In [Shih et al., 2007] and [Chevallereau et al., 2009], this control methodology has been extended to a 3D walking robot with 2 degree of under-actuation. However, the reference motion which is parametrized as a function of the state of the robot instead of time is not usual in robotics, while the definition of reference motion described as a function of time is more traditional. In addition, it is difficult to find the strictly monotonic state for some robots, for example, quadruped with a curvet gait, or biped with frontal motion [Kuo, 1999], [Fukuda et al., 2006].

Based on these observations, it is challenging and significantly important to propose a tool to analyze the stability of a control based on tracking reference motion as a function of time and to propose solution to obtain stable walking. This is exactly the purpose of Chapter 1. The Poincaré method is used to numerically analyze the stability of limit cycles for hybrid zero dynamics (HZD) of the robot. It has been proved that the closed-loop system is stable if and only if the eigenvalues of the linearized Poincaré map (ELPM) have magnitude strictly less than one [Morris and Grizzle, 2009], [Westervelt et al., 2007, Chap. 4]. Therefore, the control problem can be viewed as the problem of modifying the ELPM. Two control strategies are explored for the studied robot. The first strategy is using event-based feedback control to modify ELPM. [Grizzle, 2003] shows that the event-based feedback control could be used for the hybrid system with impulse effects such as the walking system of the biped robot. Here it is extended to a 2D biped robot with time-varying reference trajectory. It shows that this method is still usable, a vector of



parameters that is updated at each impact is introduced to modify the walking stride to stride.

The main contribution of Chapter 1 is the proposition of the second control law. In contrast to the first control strategy, our second method does not need supplementary feedback controller. It is based on the choice of controlled outputs. When the controlled outputs are selected to be the actuated coordinates, most periodic walking gaits for this robot are unstable. In [Wang et al., 2009] the effect of controlled outputs selection on the walking stability was studied. It shows that the stable walking can be obtained by some pertinent choices of controlled outputs. These pertinent choices are not obvious. Is there a method to help with many judicious choices of controlled outputs to improve the stability? By studying some walking characteristics of many stable cases, we found that the height of swing foot is nearly zero for all the stable walking at the desired moment of impact for one step. Consequently, that is viewed as a necessary condition proposed in Chapter 1. Based on this condition, the choice of controlled outputs is constrained, and then two stable domains for the controlled outputs selection are given. Finally, we compared the control property of our second control law with the method of virtual constraints [Grizzle et al., 2001], [Chevallereau et al., 2003], [Plestan et al., 2003], [Westervelt et al., 2003]. It shows that when the controlled outputs are chosen pertinently, the velocity of the joints with our method converge faster than that with the method of virtual constraints.

As a following work, the principles of the control law and the method of stability analysis in Chapter 1 are extended to the biped robot with feet. In Chapter 2, some stable walking control methods for a 3D bipedal robot with 14 joint actuators are proposed. As shown in Fig. 2.2, the 3D robot is comprised of a torso and two identical legs that are independently actuated and terminated with flat-feet.

The walking of biped robot with feet can be composed of different phases such as single support (SS) with flat foot, SS with foot rotation around the metatarsal axis and double support etc. During every walking phase, there is a corresponding dynamic model and condition of contact with the ground. Thus an appropriate control law has to be implemented for each phase. Generally, the sequence of type of contact with the ground is imposed but it is obtained only if the conditions of ground reaction force, friction cone and zero moment point (ZMP) are satisfied. The ZMP is firstly introduced by Vukobratovic [Vukobratovic et al., 1990]. It is defined as a point about which the horizontal ground reaction moment of the ground reaction force is zero. When this point is inside the support polygon, the robot will not rotate about the edges of the foot so the foot remains flat on the ground. In this case, the ZMP is identical to the CoP (center of pressure) [Goswami, 1999].

In the earlier studies, many biped robots adopt a control strategy where the desired trajectories of joint angles are firstly designed based on the ZMP condition and then the feedback control is executed for the designed ones [Vukobratovic et al., 1990]. However, the contact condition cannot be satisfied in presence of perturbation. Therefore, most of the recent walking control strategies use ZMP and they are generally divided into two approaches.

First method is the periodical replaying of trajectories for the joint motions recorded in advance like in [Vukobratovic et al., 1990], which are then applied to the real robot with a

little on-line modification. [Huang et al., 2000] and [Kim et al., 2006] proposed their real-time modification systems consisting of body posture control, actual ZMP control and landing time control based on sensor's informations. These researches explicitly divide the problem into subproblems of planning and control.

The second method generates a joint-motion in real time, feeding back the present state of the system to be in accordance with the pre-provided goal of the motion, where planning and control are managed in a unified way [Takeuchi, 2001], [Sugihara et al., 2002], [Ferreira et al., 2006], [Coros et al., 2010], [Mitobe et al., 2000], [Kajita et al., 2001]. Two of the more famous users of these methods are Honda Robot Asimo [K.Hirai et al., 1998] and Kawada's humanoid HRP-2 [S.Kajita et al., 2003], [S.Kajita et al., 2006]. Especially, the control of ZMP proposed in [S.Kajita et al., 2003] was applied for the robot NAO in the work of [Gouaillier, 2009].

In the above researches the robot is usually modeled as an inverse pendulum. The inverse pendulum approximation is studied in [Miura and Shimoyama, 1984] for the control of the Biper-3 robot. In this approach, the whole mass of the robot is concentrated in one point, and the system dynamics are approximated using a simple inverted pendulum whose base represents the support foot during the single support phase. Kajita et al. [Kajita and Tani, 1991], [Kajita and Tani, 1995], [Kajita et al., 2001] extended the inverse pendulum approach and tested its validity on various robots. Errors between the computed motion of the inverted pendulum and the real motion of the robot must be compensated by feedback control. One solution is to use the actuated ankle joint and apply a small correcting torque. However, the single mass inverted pendulum is a non-minimum phase system, which imposes problems for controlling of the ZMP. Therefore [Napoleon et al., 2002] proposed an extension toward a two mass inverted pendulum to overcome this deficiency. [Sugihara and Nakamura, 2002] proposed a method to manipulate the CoG using the whole body motion, and to control the evolution of the inverted pendulum through ZMP manipulation.

The method that we developed belongs to a class of method that divides the problem into definition of reference motion and control. The control strategy can be viewed as an on-line modification of reference motion. In opposite to the methods based on inverted pendulum, a complete dynamic model is used. Our control law consists of ZMP controller, swing ankle rotation controller and partial joint angles controller. In the ZMP controller, the 2 positions of the calculated ZMP in the horizontal plane are regulated to follow the desired evolution of the ZMP. Since two torques will be used to insure that the ZMP evolution is correct, this means that not all the joints can be controlled directly. Because all of our work is done with a hypothesis that the ground is flat and the reference trajectory was planned to satisfy the condition of that the robot touches the ground with flat-foot, therefore, if the motion of all the joints can't track the desired trajectory, the swing foot will not touch the ground with flat-foot. As a result, the support foot in the next step will not be flat, thus the control law will not be valid. The swing ankle rotation controller is used to solve this problem, in which the pitch and roll angle of the swing foot are controlled to follow their desired values. As in the case of under-actuated robot studied in Chapter 1, the stability of the control depends on the choice of the controlled outputs.



As a consequence, the choice of controlled outputs of the partial joint angles controller depends on the stability analysis of the walking gait under closed-loop control.

In short, the ZMP controller and swing ankle controller are used to ensure the stability condition of supported foot and transferred foot respectively. The partial joint angles controller is used to track the reference trajectory and satisfy the stable condition of the overall control law. This control strategy is original for the biped robot with foot walking in 3D. As said in the beginning, almost all the existing on-line walking controllers are applied to compensate for the ZMP error. However, the general weakness of the previous methods is that they require considerable experimental hand tuning and these methods are poorly documented. Compared to these studies, our control law has the following advantages. The proposed method can be viewed as an on-line modification of the reference trajectory in order to insure the satisfaction of the constraint of contact. The main point is that the effect of this on-line modification on the stability of walking is studied based on rigorous stability analysis, not by testing on the robot which requires considerable experimental hand tuning.

In Chapter 3, the control of the walking direction without the modification of the original reference trajectory is studied for the same biped robot studied in Chapter 2. The robot is expected to be able to move all over the working place when it works in human environment. Thus we need the precise steering control not merely the simple straight walking. Therefore, the objective of this chapter is to adjust the net yaw rotation of the robot over a step in order to steer the robot to walk along paths with mild curvature.

The walking direction control has been proposed by using the sophisticated trajectory planning of CoG (center of gravity) and swing foot motion [Kajita et al., 2002], rhythmic oscillators [S.Aoi et al., 2004], slip motion between sole and floor [Miura et al., 2008], or the torsional deflection at the supporting foot [Oda and Ito, 2010]. Since the walking control system proposed in Chapter 2 is based on tracking the off-line calculated joint motion, an interesting feature of our walking direction control is that one is able to control the robot's motion along various paths with limited curvature using only a single predefined periodic motion.

This work is extended from the previous studies for a 3D under-actuated biped robot [Shih et al., 2010] and [Chevallereau et al., 2010]. The principle of our steering control is to append an event-based feedback controller to distribute set point commands to all the actuated joints in order to achieve a desired amount of turning, as opposed to the continuous corrections used in [Gregg and Spong, 2010]. Different from the other studies, with our method the stability during steering is maintained.

Finally, in Chapter 4, the walking control law proposed in Chapter 2 is extended to a humanoid robot with two arms. In addition, the walking phase describing the foot rotation around the metatarsal axis at the end of single support phase is included in the walking.

For walking gaits that include foot rotation, various *ad-hoc* control solutions have been proposed in the previous literatures. For example, in [Takahashi and Kawamura, 2001] the robot is controlled to track desired trajectories during foot rotation phase. The toe is modeled as a free joint because the input torque can not be applied to it. This kind of model produces a non-holonomic constraints system, of which the degree of freedom

degenerates. [Yi, 2000] proposed a walking control law for a biped robot with a compliant ankle mechanism. A pseudo static walking gait with dynamic gait modification method is presented by adjusting the position of a hip joint. The controller has two feedbacks, inner feedback for motor control and outer feedback for reference trajectory control. Besides of these, many researches considered the foot rotation phase in the jumping control [Hyon et al., 2006], [Goswami and Vadakkepat, 2009] or the running control of the robots [Kajita et al., 2007]. However, none of them can guarantee the stability in the presence of the under-actuation that occurs during heel roll or toe roll. The approach developed in [Choi and Grizzle, 2005] [Westervelt et al., 2007, Chap. 10] considers also a walking gait with foot rotation and the walking stability during this phase is analyzed. The work in [Chenglong et al., 2006] further elaborates on the Poincaré stability analysis of walking gaits that include foot-rotation; in particular, the issue of the state dimension varying from one phase to another is emphasized. It shows that the feedback design methodology presented for robots with point feet can be extended to obtain a provably asymptotically stabilizing control law that integrates the fully actuated and under-actuated phases of walking.

Our work is extended from [Chevallereau et al., 2008], in which a control strategy for simultaneously regulating the position of the ZMP and the joints of the robot was proposed for a biped robot in 2D. In addition, the proposed controller is based on a path-following control strategy, i.e., the reference trajectory is not defined as a function of time. This method with parametrized reference trajectory can deal with the under-actuation problem during foot rotation phase. Therefore, since in Chapter 2 the proposed control law with this kind of reference trajectory has been used successfully for the walking control of robot with flat-feet, the same control system can be used directly in the new robot with foot rotation phase. In order to consider all the effects of stance foot rotation on the dynamic models of robot, the foot rotation angle is viewed as an actuated joint angle to be considered in the joint configuration vector and used to calculate the forces and torques. As a result, a nominal torque at the toe of stance foot is calculated by using the dynamic model. In fact, during foot rotation phase, because the position of ZMP along  $x$  axis is zero so this torque is zero. Therefore, the proposed control law can be used in both of fully-actuated phase and foot rotation phase. Moreover, the stability during the foot rotation phase can also be taken into account, that is exactly what is missing in previous studies for walking gaits with foot rotation.

# Chapter 1

## Walking control of an under-actuated planar biped robot

### 1.1 Introduction

The primary objective of this chapter is to present three walking control laws that can achieve an asymptotically stable, periodic walking gait for an under-actuated planar biped robot.

The studied biped robot is RABBIT [Chevallereau et al., 2003] and it evolves only in the sagittal plane. It consists of five links connected to form two legs with knees and a torso (see Fig. 1.1) and it has point feet without actuation between the feet and ground. First, the dynamic model of the robot during different walking phases are obtained by using the method of Lagrange. Next, a classical control strategy for under-actuated biped robots is presented at first. It is called virtual constraints method, in which a state quantity of the biped that is strictly monotonic along a typical walking gait, is used to replace time in parameterizing a periodic motion of the biped [Chevallereau et al., 2003], [Plestan et al., 2003], [Westervelt et al., 2003], [Chevallereau et al., 2009]. With this parameterized reference trajectory, the controller is time invariant. When such a control has converged, the configuration of the planar robot at the impact is the desired configuration. Moreover, it has been observed that for the same robot and for a same given cyclic motion, a control law based on a parameterized reference trajectory produces a stable walking, whereas a control law based on reference trajectory as a function of time produces an unstable walking [Chevallereau, 1999]. However, the parameterized reference trajectory is not usual in robotics, while the definition of that as a function of time is more traditional. In addition, it is difficult to find the strictly monotonic state for some robots, for example, robot-semiquad [Aoustin et al., 2005], quadruped with a curvet gait, or biped with frontal motion [Kuo, 1999], [Fukuda et al., 2006].

Based on these observations, it is challenging and significantly important to propose a tool to analyze the stability of a control based on tracking reference trajectory as a function of time and to propose a solution to obtain stable walking. Therefore, the other

two walking control laws are proposed to track the reference trajectory expressed as a function of time. The second control law is obtained using event-based feedback control to improve the walking stability, that is, the convergence of periodical walking. [Grizzle, 2003] shows that it could be used for the hybrid system with impulse effects such as the walking system of the biped robot. With this control law, a vector of parameters that are updated just after each impact is introduced to modify the walking stride to stride. In this chapter it is extended to 2D biped robot with time-variant reference trajectory. It shows that this method is still usable.

In contrast with the second control strategy, the third method does not need supplemental feedback controller. It is based on the choice of controlled outputs. For a robot has  $m$  actuators and point feet without actuation, the posture of the robot in the sagittal plane depends on  $m + 1$  joint configuration variables but only  $m$  controlled outputs can be chosen. For simplicity, the  $m$  controlled variables are defined as a linear combination of  $m + 1$  joint configuration variables. The most important question addressed in this control law is how this linear combination can be chosen in order to ensure walking stability. The stability analysis is done with the method of Poincaré section, which is the classical technique for determining the existence and stability properties of periodic orbits [Morris and Grizzle, 2009], [Westervelt et al., 2007, Chap. 4]. By introducing zero dynamics, the stability of the walking gait under closed-loop control is evaluated in a reduced dimensional space [Chevallereau et al., 2009], [Plestan et al., 2003], [Westervelt et al., 2003]. The numerical analysis shows that the stable walking can be obtained by using some pertinent choices of controlled outputs. However, these pertinent choices are not obvious. Therefore, some walking characteristics of many stable cases are analyzed and a method to help with the selection of controlled outputs is proposed. Finally, three control methods are compared with each other.

This chapter is organized as follows. At first the studied robot is introduced in Section 1.2 and its dynamic models during different walking phases are presented in Section 1.3. Next, a previous control law based on tracking parametrized reference trajectory is introduced in Section 1.4. As a following work, other two control laws based on tracking time-variant reference trajectory are proposed in Section 1.5. At last, Section 1.6 gives the simulation results under these three control laws and the conclusions are given in Section 1.7.

## 1.2 Description of the studied robot

### 1.2.1 Biped model

The studied robot is modeled based on RABBIT shown in Fig. 1.1. RABBIT was designed and built between 1997-2001 by several French research laboratories such as IRCCyN, LMS Poitiers, LSIIT, LAG, LVR Bourges, LRP, INRIA Rhone-Alpes and INRIA Sophia-Antipolis. A group of researchers constituted by IRCCyN, LGIPM Metz, LMS, GAL, LVR, LIRMM, LRP and LSS worked about this prototype in the project of ROBEA

"Walking and Running Control of a Biped Robot" between 2001 and 2004.

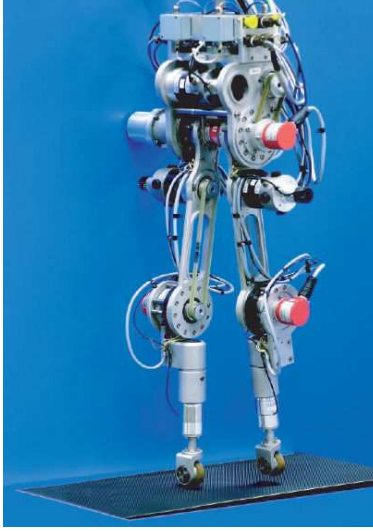


Figure 1.1: Photo of RABBIT

RABBIT was conceived to be the simplest mechanical structure that is still representative of human walking. It is composed of a torso and two identical legs with point feet. The knees and the hips are actuated and they are one degree of freedom (DOF) rotational joints. Since RABBIT does not have foot, the ZMP heuristic is not applicable, and thus under-actuation problem must be explicitly addressed in the feedback control design, leading to the development of new feedback stabilization methods.

The studied biped robot is modeled in the sagittal  $xz$  plane. According to the mechanical structure of RABBIT, the model has a torso and two symmetric legs connected at a common point called the hip, and both leg ends are terminated in points. Obviously, there are 5 rigid links connected 4 ideal revolute joints at the knees and hips. Each revolute joint is independently actuated and the point of contact between the stance leg and ground is under-actuated. Its geometric is shown in Fig. 1.2. The values of geometrical parameters and other parameters are given in Table 1.1 and Table 1.2, where:

- $m_i$  is the mass of the  $i^{th}$  link with  $i = 1, \dots, 5$ , and  $i = 1, 3$  denote the shins,  $i = 2, 4$  denote the thighs and  $i = 5$  denotes the torso.
- $L_i$  is the length of the  $i^{th}$  link.
- $S_i$  is the vector of the center-of-mass coordinates of the  $i^{th}$  link.
- $I_i$  is the moment of inertia of the  $i^{th}$  link with respect to the  $y$ -axis .
- $I_A$  is the moment of inertia of each actuator with respect to the  $y$ -axis .

The posture of the biped is described by the vector  $q = [q_1, \dots, q_5]^T$  (see Fig. 1.3). Since there is no actuation between the stance leg and ground, the unactuated variable is defined as  $q_u = q_1$ , then the vector of actuated variables is written as  $q_a = [q_2, \dots, q_5]^T$ .

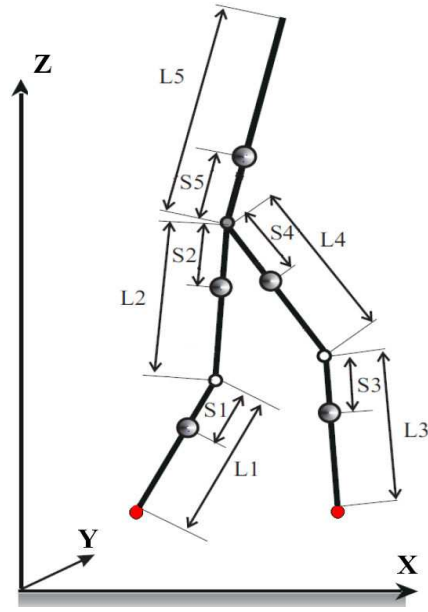


Figure 1.2: Geometrical parameters of RABBIT

### 1.2.2 Walking gait

The gait is composed of single support phases and double support phases. *The single support phase* or *swing phase* is defined to be the phase of locomotion where only one leg is in contact with the ground. Conversely, *double support* is the phase where both feet are on the ground. It is supposed to be instantaneous and the associated impact can be modeled as a rigid contact [Hurmuzlu and Marghitu, 1994]. At impact, the swing leg neither slips nor rebounds, while the former stance leg releases without interaction with the ground. After that, both two legs exchange the role and the next single support phase will begin. The alternating phases of single support and double support (or impact) are defined as the *walking* of robot, see Fig. 1.4.

Body	shin ( $i = 1, 3$ )	thigh ( $i = 2, 4$ )	torso ( $i = 5$ )
$m_i$ (kg)	3.2	6.8	17.053
$L_i$ (m)	0.4	0.4	0.625
$S_i$ (m)	0.127	0.163	0.143
$I_i$ ( $kg \cdot m^2$ )	0.1	0.25	1.869

Table 1.1: Geometrical parameters and dynamic parameters of the biped robot

Maximum torque $\Gamma_{max}$ ( $N \cdot m$ )	150
Moment of inertia $I_A$ ( $kg \cdot m^2$ )	0.83

Table 1.2: Parameters of actuator

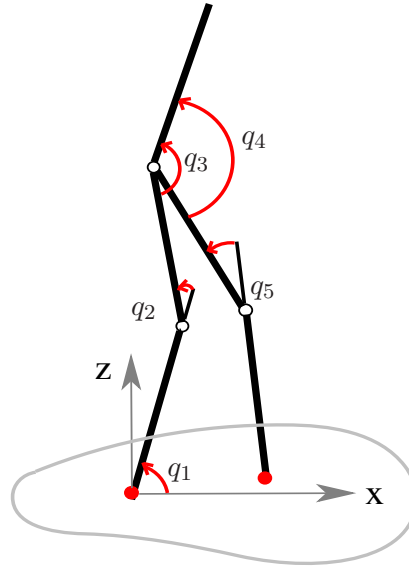


Figure 1.3: The studied biped

## 1.3 Dynamic model during different walking phases

### 1.3.1 Lagrange formulation

The dynamic model of a robot with several degrees of freedom can be obtained with the method of Lagrange, which consists of first computing the kinetic energy and potential energy of each link, and then summing terms to compute the total kinetic energy  $K$ , and the total potential energy  $E_p$ . For the biped robot described by a set of generalized coordinates  $q = [q_1, \dots, q_n]^T$ , the Lagrangian is denoted by:

$$\mathcal{L}(q, \dot{q}) = K(q, \dot{q}) - E_p(q) \quad (1.1)$$

where  $\dot{q} = [\dot{q}_1, \dots, \dot{q}_n]^T$  is the vector of velocity,  $K$  is the total kinetic energy and  $E_p$  is the total potential energy. The Lagrange equations are commonly written in the form:

$$\frac{d}{dt} \frac{\partial \mathcal{L}}{\partial \dot{q}} - \frac{\partial \mathcal{L}}{\partial q} = Q_{ex} \quad (1.2)$$

where  $Q_{ex}$  represents the sum of the external forces and torques (moments) acting on the robot. According to (1.1), (1.2) can be rewritten as:

$$\frac{d}{dt} \frac{\partial K}{\partial \dot{q}} - \frac{\partial K}{\partial q} + \frac{\partial E_p}{\partial q} = Q_{ex} \quad (1.3)$$

The kinetic energy of the system is a quadratic function in the joint velocities such that:

$$K = \frac{1}{2} \dot{q}^T D \dot{q} \quad (1.4)$$

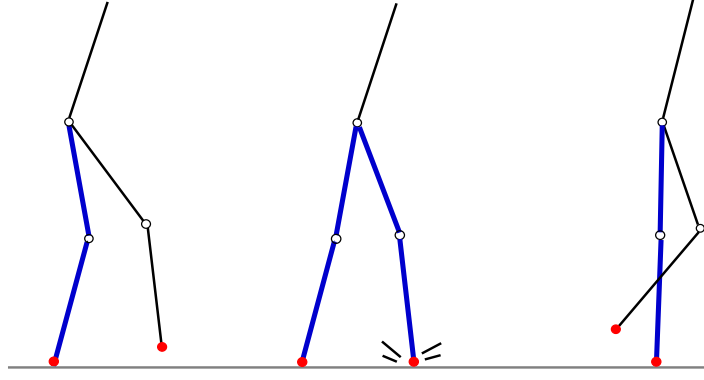


Figure 1.4: Walking phases

where  $D$  is a  $n \times n$  symmetric and positive definite inertia matrix of the robot. Its elements are function of the joint positions. Since the potential energy  $E_p$  is a function of the joint positions, (1.3) and (1.4) lead to:

$$D\ddot{q} + C(q, \dot{q})\dot{q} + G(q) = Q_{ex} \quad (1.5)$$

where

- $D_{n \times n}$  is inertia matrix.
- $C_{n \times n}$  is Coriolis matrix.
- $G_{n \times 1}$  is gravity vector.

The matrices  $D$ ,  $C$  and  $G$  can be calculated as [Dombre and Khalil, 1999]:

$$\left\{ \begin{array}{l} G = \frac{\partial E_p}{\partial q} \\ A = \frac{\partial^2 K}{\partial \dot{q}^2} \\ C_{ij} = \sum_{k=1}^n c_{i,jk} \dot{q}_k \text{ with :} \\ c_{i,jk} = \frac{1}{2} \left[ \frac{\partial D_{ij}}{\partial q_k} + \frac{\partial D_{ik}}{\partial q_j} - \frac{\partial D_{jk}}{\partial q_i} \right]. \end{array} \right. \quad (1.6)$$

For the studied robot, the computation of the sum of the external forces and torques  $Q_{ex}$  is presented for two cases:

**Force acting at the foot:** Supposing that a force  $F_{ex} = [F_x, F_z]^T$  is acting on the foot at the point  $X_{pi} = [X_{pix}, X_{piz}]^T$ , we have:

$$Q_{exi} = \left( \frac{\partial X_{pi}}{\partial q} \right)^T F_{ex} \quad (1.7)$$



**Torques acting at a revolute connection of two links:** Supposing that a torque  $\tau$  is applied at a revolute joint connected two links and let  $\theta_j^{rel}$  be the associated relative angle, we have:

$$Q_{exj} = \left( \frac{\partial \theta_j^{rel}}{\partial q} \right)^T \tau. \quad (1.8)$$

### 1.3.2 Swing phase model

As shown in Fig. 1.3, the swing phase model is created in the generalized coordinates  $q = [q_1, \dots, q_n]^T$ , where the unactuated variable is defined as  $q_u = q_1$  and the vector of actuated variables is written as  $q_a = [q_2, \dots, q_5]^T$ . Since the robot's legs are identical, in the stance phase, it will be assumed without loss of generality that leg-1 (left leg) is in contact with the ground. Moreover, the Cartesian position of the stance leg end will be identified with the origin of the  $xz$ -axes of the inertial frame.

Using the Lagrange formulation presented in Subsection 1.3.1, the dynamic model can be written as:

$$D(q_a)\ddot{q} + H(q, \dot{q}) = B\Gamma \quad (1.9)$$

where  $H_{5 \times 1} = C(q_a, \dot{q}) + G(q)$  and  $D$  depends only on  $q_a$  because the kinetic energy is invariant under rotations of the body.  $B$  is obtained according to (1.8) and the definition of  $q$  in Fig. 1.3, there is:

$$B = \begin{bmatrix} \mathbf{0}_{1 \times 4} \\ \mathbf{I}_4 \end{bmatrix}. \quad (1.10)$$

Here and in the following contents,  $\mathbf{I}_n$  denotes the identity matrix of dimension  $n \times n$ .

### 1.3.3 Impact model

An impact occurs when the swing leg contacts the ground. The impact is modeled as a contact between two rigid bodies. Our objective is to obtain an expression for the generalized velocity just after the impact of the swing leg with the walking surface in terms of the generalized velocity and position just before the impact. The model from [Hurmuzlu and Chang, 1992] is used here. The one difference is noted in the list of hypotheses [Westervelt et al., 2007]:

- HI1) an impact results from the contact of the swing leg end with the ground;
- HI2) the impact is instantaneous;
- HI3) the impact results in no rebound and no slipping of the swing leg;
- HI4) at the moment of impact, the stance leg lifts from the ground without interaction;
- HI5) the externally applied forces during the impact can be represented by impulses;

- HI6) the actuators cannot generate impulses and hence can be ignored during impact;
- HI7) the impulsive forces may result in an instantaneous change in the robot's velocities, but there is no instantaneous change in the configuration.

The development of impact model involves the reaction forces at the leg ends, and thus required  $(N + 2)$ - DoF, i.e., 7 -DoF model of the robot, see Fig. 1.2. Thus the Cartesian position and velocity of the center of gravity are appended to the generalized configuration variables  $q$ . The extended generalized configuration variables in the double support phase are denoted by:  $q_e = [q, x_g, z_g]^T$ . Using  $q_e$  in the method of Lagrange results in:

$$D_e(q_a)\ddot{q}_e + H_e(q_e, \dot{q}_e) = B_e\Gamma + Q_{exf}, \quad (1.11)$$

where  $\Gamma = [\Gamma_1, \Gamma_2, \Gamma_3, \Gamma_4]^T$  is the vector of input torques and  $Q_{exf}$  represents the vector of external forces action on the robot due to the contact between the leg ends and the ground. According to the definition of  $q_e$ ,  $D_e$  can be described by:

$$D_e = \begin{bmatrix} D(q_a) & \mathbf{0}_{5 \times 2} \\ \mathbf{0}_{2 \times 5} & m_{to}\mathbf{I}_2 \end{bmatrix}. \quad (1.12)$$

where  $m_{to}$  is the total mass of the robot.

Here we use "-" to denote the moment just before impact and "+\*" to denote the moment just after impact but before the exchange of legs. From Hypothesis HI7, during the impact, the biped's configuration variables do not change, that means:

$$q_e^{+*} = q_e^- \quad (1.13)$$

However, the generalized velocities undergo a jump during the impact. This jump is linear with respect to the joint velocity before the impact  $\dot{q}^-$  [Westervelt et al., 2007]. Under Hypothesis HI1 – HI7, "integrating" (1.11) over the "duration" of the impact and using (1.7) gives:

$$\begin{bmatrix} D(q_a^-) & \mathbf{0}_{5 \times 2} \\ \mathbf{0}_{2 \times 5} & m_{to}\mathbf{I}_2 \end{bmatrix} (\dot{q}_e^{+*} - \dot{q}_e^-) = \left( \frac{\partial X_{pi}(q^-)}{\partial q_e} \right)^T F_{ex} \quad (1.14)$$

where the subscript  $i$  denotes that leg- $i$  is the swing leg before impact, the Cartesian position of the end of leg- $i$   $X_{pi}$  can be expressed in terms of the Cartesian position of the center of gravity and the robot's angular coordinates as:

$$X_{pi} = \begin{bmatrix} x_g \\ z_g \end{bmatrix} - \mathbf{f}_i(q) \quad (1.15)$$

where  $\mathbf{f}_i = [\mathbf{f}_{ix}, \mathbf{f}_{iz}]$  is determined from the robot's parameters (links lengths, masses, positions of the center of mass). Next, (1.15) leads to:

$$\frac{\partial X_{pi}}{\partial q_e} = \begin{bmatrix} -\frac{\partial \mathbf{f}_i}{\partial q} & \mathbf{I}_2 \end{bmatrix}_{2 \times 7}. \quad (1.16)$$

Substituting (1.16) into (1.14) yields:

$$\begin{bmatrix} D(q_a^-) & \mathbf{0}_{5 \times 2} \\ \mathbf{0}_{2 \times 5} & m_{to} \mathbf{I}_2 \end{bmatrix} (\dot{q}_e^{+*} - \dot{q}_e^-) = \begin{bmatrix} -\frac{\partial \mathbf{f}_i(q^-)^T}{\partial q} \\ \mathbf{I}_2 \end{bmatrix} F_{ex} \quad (1.17)$$

The vector  $F_{ex}$  of the ground reaction impulse can be expressed using the last two lines of the matrix equation in (1.17):

$$F_{ex} = m_{to} \left( \begin{bmatrix} \dot{x}_g^{+*} \\ \dot{z}_g^{+*} \end{bmatrix} - \begin{bmatrix} \dot{x}_g^- \\ \dot{z}_g^- \end{bmatrix} \right) \quad (1.18)$$

Since two legs touch the ground during the impact, according to (1.15), there is:

$$\begin{bmatrix} \dot{x}_g^{+*} \\ \dot{z}_g^{+*} \end{bmatrix} = \frac{\partial \mathbf{f}_i(q^-)}{\partial q} \dot{q}^{+*}, \quad \begin{bmatrix} \dot{x}_g^- \\ \dot{z}_g^- \end{bmatrix} = \frac{\partial \mathbf{f}_j(q^-)}{\partial q} \dot{q}^-, \quad (1.19)$$

where the subscript  $j$  denotes the stance leg before impact.

Substituting (1.19) and (1.18) into (1.17), the robot's angular velocity vector after impact is given by a linear expression with respect to the velocity before impact:

$$\dot{q}^{+*} = I(q^-) \dot{q}^- \quad (1.20)$$

with

$$I(q^-) = (D + m_{to} \frac{\partial \mathbf{f}_i^T}{\partial q} \frac{\partial \mathbf{f}_i}{\partial q})^{-1} (D + m_{to} \frac{\partial \mathbf{f}_i^T}{\partial q} \frac{\partial \mathbf{f}_j}{\partial q}). \quad (1.21)$$

Since we are assuming a symmetric walking gait, we can avoid using two single support models, one for each leg playing the role of the stance leg, by relabeling the coordinates at impact. The coordinates must be relabeled because the roles of the legs must be swapped: the former swing leg is now in contact with the ground and is poised to take on the role of the stance leg. Combining (1.13) with (1.20) and defining "+" denotes the moment after impact and after the exchange of legs, the joint configuration and velocity becomes:

$$\begin{cases} q^+ &= E q^- \\ \dot{q}^+ &= E I(q^-) \dot{q}^- \end{cases}, \quad (1.22)$$

where  $E$  is a  $(5 \times 5)$  matrix which describes the transformation of two legs, and it is:

$$E = \begin{bmatrix} 1 & 1 & 1 & -1 & -1 \\ 0 & 0 & 0 & 0 & 1 \\ 0 & 0 & 0 & 1 & 0 \\ 0 & 0 & 1 & 0 & 0 \\ 0 & 1 & 0 & 0 & 0 \end{bmatrix}. \quad (1.23)$$

### 1.3.4 Hybrid model of walking

An overall model of walking is obtained by combining the swing phase model and the impact model to form a system with impulse effects. It can be expressed as a nonlinear hybrid system containing two state manifolds (called "charts" in [Guckenheimer and Johnson, 1995]). Define the state variables of robot as  $x = [q, \dot{q}]^T$ , so the state before impact is noted as  $x^- = [q^-, \dot{q}^-]^T$ , and the state after impact and after the exchange of legs is noted as  $x^+ = [q^+, \dot{q}^+]^T$ . With the application of (1.9) and (1.22), a complete walking motion of the biped robot is written as

$$\Sigma : \begin{cases} \dot{x} = \mathbf{f}(x) + \mathbf{g}(x) u_\tau & x^- \notin S \\ x^+ = \Delta(x^-), & x^- \in S \end{cases}, \quad (1.24)$$

with

$$\mathbf{f}(x) = \begin{bmatrix} \dot{q} \\ -D^{-1}(q_a)H(q, \dot{q}) \end{bmatrix}, \quad \mathbf{g}(x) = \begin{bmatrix} \mathbf{0}_{5 \times 4} \\ D^{-1}(q_a)B \end{bmatrix}, \quad u_\tau = \Gamma$$

and

$$x^+ = \Delta(x^-) = \begin{bmatrix} E \\ EI(q^-) \end{bmatrix} x^-.$$

where  $S$  is a hyper surface at which solutions of the differential equation undergo a discrete transition that is modeled as an instantaneous reinitialization of the differential equation.  $S$  is called the impact surface and  $S = \{(q, \dot{q}) | Z_{sw}(q) = 0, X_{sw}(q) > 0\}$ , where  $Z_{sw}$ ,  $X_{sw}$  describe the position coordinates of swing foot along  $z$  and  $x$  axis respectively. Here  $X_{sw}(q) > 0$ , because the swing leg is supposed to be placed strictly ahead of the stance leg.

The equation (1.24) means that a trajectory of the hybrid model is specified by the swing phase model until an impact occurs when the state of robot attains the set  $S$ . At this point, the impact of the swing leg with the walking surface results in a change in the velocity components of the state vector. The impulse model of the impact compresses the impact event into an instantaneous moment in time, resulting in a discontinuity in the velocities. The ultimate result of the impact model is a new initial condition from which the swing phase model evolves until the next impact. In order for the state not to be obliged to take on two values at the impact moment, the impact event is described in terms of the values of the state just before impact and after impact. These values are represented by the left and right limits,  $x^-$  and  $x^+$ , respectively. Solutions are taken to be right continuous and must have finite left and right limits at impact.

## 1.4 A control law for tracking parametrized reference trajectory

This section will propose a previously studied control strategy of the under-actuated biped robot, i.e. the method of virtual constraints, which has been proved very successful in designing feedback controllers for stable walking in planar under-actuated bipeds

[Chevallereau et al., 2003], [Plestan et al., 2003], [Westervelt et al., 2003], [Westervelt et al., 2002]. Since not all the joints can be controlled for the studied under-actuated robot, the stability of the periodic walking gait under the closed-loop control law must be analyzed. In order to simplify the stability analysis, the definition of zero dynamics will be introduced.

### 1.4.1 The reference trajectory

Using optimization techniques developed in [Djoudi et al., 2005], an optimal cyclic motion  $q^d(t)$  has been defined for the robot Rabbit described in Section 1.2. The most important point of the method of virtual constraints is that  $q^d(t)$  is parametrized by a quantity that only depends on the states of robot and is strictly monotonic like time  $t$  during the walking phase. By using this method, the closed-loop system does not depend on the time  $t$  thus only the kinematic evolution of the robot's state is regulated but not its temporal evolution. That means the control law is defined to follow a joint path but not a joint motion.

In a forward human walking motion, the  $x$ -coordinate of the hip is monotonically increasing. Hence, if the virtual stance leg is defined by the line that connects the stance foot to the stance hip, the angle of this leg in the sagittal plane is monotonic and it can replace the time  $t$  to parametrize  $q^d$ . As shown in Fig. 1.5, because the shin and the thigh have the same length, this angle can be computed by:

$$\theta = q_1 + q_2/2. \quad (1.25)$$

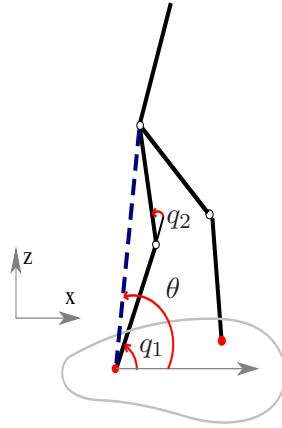


Figure 1.5: Description of  $\theta$

Next, because the obtained reference trajectory is a set of discrete points, in order to approximate the desired cyclic motion for each of the five configuration coordinates, a one-dimensional Bezier polynomial [Bezier, 1972] with order  $J = 5$  is chosen to describe the reference trajectory. It is:

$$h^d(s) = \sum_{k=0}^J \alpha_k \frac{J!}{k!(J-k)!} s^k (1-s)^{J-k}, \quad (1.26)$$

where the coefficient  $\alpha_k$  is determined to minimize the distance between the optimal trajectory and reference trajectory at the discrete points, and

$$s = \frac{\theta - \theta_i}{\theta_f - \theta_i} \quad (1.27)$$

is the normalized parameter varying on the cyclic motion from 0 to 1.  $\theta_i$  and  $\theta_f$  are the values of  $\theta$  at the beginning and end of a step respectively. Using (1.27), the parametrized reference trajectory in (1.26) can also be written as  $h^d(\theta)$ , and it is such that:

$$\begin{cases} q^d(t) &= h^d(\theta) \\ \dot{q}^d(t) &= \frac{\partial h^d(\theta)}{\partial \theta} \dot{\theta} \\ \ddot{q}^d(t) &= \frac{\partial^2 h^d(\theta)}{\partial \theta^2} \dot{\theta}^2 + \frac{\partial h^d(\theta)}{\partial \theta} \ddot{\theta} \end{cases} \quad (1.28)$$

Here and in the following contents the superscript "d" means the desired value. In [Djoudi et al., 2005], the evolution of the joints variables  $q^d$  was assumed to be polynomial function of a scalar path parameter such as  $s$  in (1.27). The coefficients of the polynomial functions were chosen to optimize a torque criterion and to insure a cyclic motion for the biped. Finally, some discrete points of the reference trajectory  $q^d(t)$ ,  $\dot{q}^d(t)$ ,  $\ddot{q}^d(t)$  were calculated thus they are supposed to be known in this thesis. From these results, in (1.28)  $h^d(\theta)$ ,  $\frac{\partial h^d(\theta)}{\partial \theta}$  and  $\frac{\partial^2 h^d(\theta)}{\partial \theta^2}$  can be deduced by (1.26) and its differential coefficients, so they are also supposed to be known in the following contents.

### 1.4.2 Calculation of the input torques

Since only the actuated joints are controlled and their joint configurations are  $q_2, q_3, q_4, q_5$ , the controlled variables are written as:

$$u = Mq \quad (1.29)$$

with

$$M = \begin{bmatrix} \mathbf{0}_{4 \times 1} & \mathbf{I}_4 \end{bmatrix}. \quad (1.30)$$

The unactuated joint angle  $q_1$  is not controlled at all. The 4 outputs that must be zeroed by the control law are:

$$y = u - u^d(\theta) \quad (1.31)$$

where  $u^d(\theta)$  is the desired value of the controlled vector  $u$ . The PD controller is used to obtain  $u = u^d$ , the expected acceleration  $\ddot{u}$  is defined as:

$$\ddot{u} = \ddot{u}^d - \frac{K_d}{\varepsilon}(\dot{u} - \dot{u}^d) - \frac{K_p}{\varepsilon^2}(u - u^d), \quad (1.32)$$

where  $K_p > 0$ ,  $K_d > 0$ , and  $\varepsilon > 0$ . According to the definition of  $u$ , here  $\ddot{u}^d$ ,  $\dot{u}^d$  and  $u^d$  can be calculated by  $M$  and the obtained reference trajectory in (1.28).

$$\begin{cases} u^d(\theta) &= Mh^d(\theta) \\ \dot{u}^d(\theta) &= M\frac{\partial h^d(\theta)}{\partial \theta}\dot{\theta} \\ \ddot{u}^d(\theta) &= M\left(\frac{\partial^2 h^d(\theta)}{\partial \theta^2}\dot{\theta}^2 + \frac{\partial h^d(\theta)}{\partial \theta}\ddot{\theta}\right) \end{cases} \quad (1.33)$$

Next is how to compute the input torques based on (1.32). Because  $u^d$  and its differential coefficients are functions of  $\theta$ , using (1.25), (1.29),  $q$  can be described by:

$$q = T_q^{-1} \begin{bmatrix} \theta \\ u \end{bmatrix}. \quad (1.34)$$

with

$$T_q = \begin{bmatrix} 1 & 0.5 & 0 & 0 & 0 \\ 0 & 1 & 0 & 0 & 0 \\ 0 & 0 & 1 & 0 & 0 \\ 0 & 0 & 0 & 1 & 0 \\ 0 & 0 & 0 & 0 & 1 \end{bmatrix}. \quad (1.35)$$

Thus, substituting (1.34) into the dynamic model during the swing phase (1.9) yields:

$$D_T \begin{bmatrix} \ddot{\theta} \\ \ddot{u} \end{bmatrix} + H(q, \dot{q}) = B\Gamma, \quad (1.36)$$

where  $D_T = DT_q^{-1}$ . Defining  $D_T$  and  $H$  as:

$$D_T = \begin{bmatrix} D_{T11(1 \times 1)} & D_{T12(1 \times 4)} \\ D_{T21(4 \times 1)} & D_{T22(4 \times 4)} \end{bmatrix}, \quad H = \begin{bmatrix} H_{1(1 \times 1)} \\ H_{2(4 \times 1)} \end{bmatrix}, \quad (1.37)$$

(1.36) can be rewritten as:

$$\begin{cases} D_{T11}\ddot{\theta} + D_{T12}\ddot{u} + H_1 = 0 \\ D_{T21}\ddot{\theta} + D_{T22}\ddot{u} + H_2 = \Gamma \end{cases} \quad (1.38)$$

Substituting (1.32) and (1.33) into the first line of (1.38),  $\ddot{\theta}$  is solved at first:

$$\ddot{\theta} = \frac{-H_1 - D_{T12}U_a}{D_{T11} + D_{T12}M\frac{\partial h^d(\theta)}{\partial \theta}} \quad (1.39)$$

with

$$U_a = M\frac{\partial^2 h^d(\theta)}{\partial \theta^2}\dot{\theta}^2 - \frac{K_d}{\varepsilon}(\dot{u} - \dot{u}^d) - \frac{K_p}{\varepsilon^2}(u - u^d). \quad (1.40)$$

Then the input torques can be calculated by substituting  $\ddot{\theta}$  in the second line of (1.38):

$$\Gamma = D_{T22}U_a + (D_{T21} + D_{T22}M\frac{\partial h^d(\theta)}{\partial \theta})\ddot{\theta} + H_2. \quad (1.41)$$

### 1.4.3 Stability analysis

Many robot motions are naturally periodic. The periodic behavior is also called limit cycle. Limit cycles can be stable (attracting), unstable (repelling) or non-stable (saddle) [Hiskens, 2001]. The classical technique for determining the existence and stability properties of periodic orbits in nonlinear system is using Poincaré map [Parker and Chua, 1989],

[Seydel, 1994]. A periodic solution corresponds to a fixed-point of a Poincaré map. Stability of the periodic solution is equivalent to stability of the fixed-point. It is well known how to use numerical methods to compute a Poincaré map and to find fixed-points [Parker and Chua, 1989]. The drawback in such a direct approach is that it does not yield sufficient insight for feedback design and synthesis. Therefore, an extension of the notion of the zero dynamics to the hybrid models arising in bipedal locomotion leads to a feedback design process in which Poincaré stability analysis can be directly and insightfully incorporated into feedback synthesis [Westervelt et al., 2007]. Moreover, thanks to zero dynamics, the stability of full order system can be evaluated by analyzing a lower-dimensional system [Morris and Grizzle, 2005], [Morris and Grizzle, 2009], [Westervelt et al., 2003].

For the hybrid closed-loop system consisting of a biped robot, its environment, and a given feedback controller, the objective during the stability analysis phase is to be able to determine if periodic orbits exist and, if they exist, whether they are asymptotically stable. This subsection provides a brief review of the general principles of Poincaré map, zero dynamics and their applications in the stability analysis of the studied robot.

### Poincaré map

In general, the dynamic model during swing phase can be viewed as an ordinary differential equation (ODE) in  $\mathbb{R}^n$ :

$$\dot{x}(t) = \mathcal{F}(x) \quad (1.42)$$

where  $x \in \mathbb{R}^n$  and  $\mathcal{F}: \mathbb{R}^n \rightarrow \mathbb{R}^n$ . The solution of (1.42) is defined by:

$$x(t) = \phi(x_0, t) \quad (1.43)$$

where the initial condition satisfies:  $x_0 = \phi(x_0, t_0)$  and  $\phi$  is called the *flow* of  $x$ .

A Poincaré map effectively samples the flow of a periodic system once every period. The concept is illustrated in Fig. 1.6. If the limit cycle is stable, oscillations approach the limit cycle over time. The samples provided by the corresponding Poincaré map approach a fixed-point. A non-stable limit cycle results in divergent oscillations. For such a case the samples of the Poincaré map diverge.

To define a Poincaré map, we consider the limit cycle  $\psi$  shown in Fig. 1.6. Let  $\mathcal{S}$  be a hyperplane transversal to  $\psi$  at  $x^*$ , the trajectory emanating from  $x^*$  will again encounter  $\mathcal{S}$  at  $x^*$  after  $T$  seconds, where  $T$  is the minimum period of the limit cycle. Due to the continuity of the flow  $\phi$  with respect to initial conditions, trajectories starting on  $x^*$  in a neighborhood of  $x^*$  will, in approximately  $T$  seconds, intersect  $x^*$  in the vicinity of  $x^*$ . Hence  $\phi$  and  $\mathcal{S}$  define a mapping:

$$x_{k+1} = P(x_k) := \phi(x_k, \tau(x_k)) \quad (1.44)$$

where  $\tau(x_k) \approx T$  is the time taken for the trajectory to return to  $\mathcal{S}$ . The Poincaré map is defined as  $P: \mathcal{S} \rightarrow \mathcal{S}$  and  $\mathcal{S}$  is called Poincaré section. Fig. 1.6 shows that:

$$x^* = P(x^*) = P(P(x^*)) = \dots \quad (1.45)$$



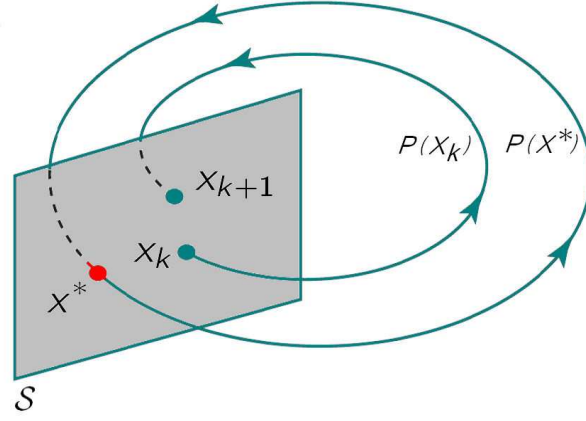


Figure 1.6: Poincaré map.

The point like  $x^* \in \mathcal{S}$  in (1.45) is called the fixed-point of Poincaré map  $P$ .

Stability of the Poincaré map (1.44) is determined by linearizing  $P$  at the fixed-point  $x^*$ , that gives rise to a linearized system:

$$\delta x_{k+1} = A \delta x_k \quad (1.46)$$

where  $\delta x_k = x_k - x^*$  denotes the perturbations at the fixed-point, the square matrix  $A$  is the Jacobian linearization of  $P$  at  $x^*$ . Using the Taylor series to linearize  $P$  at the fixed-point  $x^*$ ,  $A$  approximates to the first-order derivative of  $\phi$  evaluated at  $x^*$  [Bergmann, 2004]:

$$A = \frac{\partial \phi(x^*, T)}{\partial x} = \begin{bmatrix} \frac{\partial \phi^1}{\partial x^1} & \cdots & \frac{\partial \phi^1}{\partial x^n} \\ \vdots & \cdots & \vdots \\ \frac{\partial \phi^n}{\partial x^1} & \cdots & \frac{\partial \phi^n}{\partial x^n} \end{bmatrix}. \quad (1.47)$$

where  $\phi^i$  and  $x^i$  represent the  $i^{th}$  component of  $\phi$  and  $x$  respectively.

The eigenvalues of  $A$  determine the stability of the Poincaré map  $P$ , and hence the stability of the periodic solution [Khalil, 2002].

**Theorem 2.1:** *A fixed-point of the Poincaré map is exponentially stable, if, and only if, the eigenvalues of  $A$  have magnitude strictly less than one.*

In fact, besides of Theorem 2.1, there are other two cases [Hiskens, 2001]:

- If all the eigenvalues of  $A$  lie outside the unit circle, the Poincaré map is unstable.
- If some of the eigenvalues of  $A$  lie outside the unit circle, the Poincaré map is non-stable.

## Zero dynamics

For a system modeled by ordinary differential equations (in particular, without impact dynamics), the maximal internal dynamics of the system that is compatible with the output

being identically zero is called the *zero dynamics* [Isidori, 1995], [Isidori and Moog, 1988], [Nijmeijer and van der Schaft, A. J., 1989]. The control law proposed in Subsection 1.4.2 consists of defining a set of outputs, the number of which equals to the number of inputs, and then designing a feedback controller that asymptotically drives the output to zero. It uses a method of computed torque which can be seen as an indirect mean of designing a set of zero dynamics for the robot. Since the torque is calculated only during swing phase, if the impact model is incorporated into the notion of the maximal internal dynamics compatible with the output being identically zero, a zero dynamics of the complete model of the biped robot is obtained, which is called *hybrid zero dynamics* (HZD). As a result, the task of stability analysis of the complete model can be converted to that of the HZD using the restricted Poincaré map [Morris and Grizzle, 2005], [Morris and Grizzle, 2009], [Westervelt et al., 2003]. Since, in general, the dimension of the HZD is considerably less than the dimension of the original model itself, the stability can be tested in a reduced dimensional space.

According to the definition of zero dynamics, the output of the control law in (1.31) is zero, that means  $u = u^d$ , thus  $q, \dot{q}$  can be described by  $\theta, \dot{\theta}$  and  $u^d, \dot{u}^d$  using (1.34). Next, substituting them into the first equation of (1.38) yields:

$$\begin{cases} D_{T11}(q)\ddot{\theta} + D_{T12}(q)\ddot{u}^d(\theta) + H_1(q, \dot{q}) = 0 \\ q = T_q^{-1}[\theta, u^d(\theta)]^T, \quad \dot{q} = T_q^{-1}[\dot{\theta}, \dot{u}^d(\theta)]^T \end{cases} \quad (1.48)$$

where  $u^d(\theta), \dot{u}^d(\theta), \ddot{u}^d(\theta)$  have been obtained in (1.33), so  $\ddot{\theta}$  can be calculated directly, next  $\ddot{q}$  and  $\Gamma$  can be gotten by using (1.34) and (1.41) respectively. Compared to (1.38), it is quite obvious that (1.48) is a system of 2 dimensions with states  $\theta, \dot{\theta}$ , while (1.38) is a system of 10 dimensions with states  $q, \dot{q}$ . It shows that the introduction of zero dynamics helps to the simplification of analysis.

### Stability test in a reduced dimensional space

The stability analysis of walking can be obtained by using the Poincaré method. If the state of the robot remains on the hybrid zero dynamics manifold, that is, the zero dynamics during swing phase (1.48) and the dynamics of impact, the stability can be analyzed in a reduced dimensional space.

Different Poincaré section can be considered. Usually, for biped, the Poincaré section is defined just before the impact, so the switch surface of the dynamic model of robot (see (1.24))  $S = \{(q, \dot{q}) | Z_{sw}(q) = 0, X_{sw}(q) > 0\}$  is chosen as the Poincaré section. A restricted Poincaré map is defined from  $S \cap \mathcal{Z}$  to  $S \cap \mathcal{Z}$ , where  $\mathcal{Z} = \{(q, \dot{q}) | y(q) = 0, \dot{y}(q) = 0\}$  denotes zero dynamics (see (1.31)). The key point is that since in  $\mathcal{Z}$  the state of the robot can be parametrized by two independent variables  $\theta$  and  $\dot{\theta}$ , in  $S \cap \mathcal{Z}$ , the state of the robot can be represented only by one variable,  $x^z = \dot{\theta}$ . The reference trajectory  $h^d(\theta)$  in (1.28) gives a fixed-point  $x^{z*} = \dot{\theta}(\theta_f^*)$ , where  $\theta_f^* \in S$  is the desired value of  $\theta$  just before impact.

The restricted Poincaré map  $P^z : S \cap \mathcal{Z} \rightarrow S \cap \mathcal{Z}$  induces a discrete-time system  $x_{k+1}^z = P^z(x_k^z)$ . The corresponding theorem is proposed in [Morris and Grizzle, 2009]:

**Theorem 2.2:** *For  $\varepsilon$  sufficiently small in (1.32), the linearization of  $P^z$  about a fixed-point determines exponential stability of the full order closed-loop robot model.*

It is worth mentioning that the traditional control system without  $\varepsilon$  requires that an invariant surface of the ODE portion of the model be rendered finite-time attractive through a continuous feedback [Bhat and Bernstein, 2000], but not Lipschitz continuous feedback. However, the result established here will weaken this requirement to attractivity at a sufficiently rapid exponential rate, thereby permitting the use of smooth feedback control laws.

Next, define  $\delta x_k^z = x_k^z - x^{z*}$ , the Poincaré map linearized about the fixed-point  $x^{z*}$  gives rise to a linearized system,

$$\delta x_{k+1}^z = A^z \delta x_k^z, \quad (1.49)$$

where  $A^z$  is a one-dimensional numerical value because  $x^{z*}$  only has one component. It is calculated by the numerical method:

$$A^z = \frac{P^z(x^{z*} + \Delta x^z) - P^z(x^{z*} - \Delta x^z)}{2\Delta x^z} \quad (1.50)$$

The quantity  $\Delta x^z$  is a small perturbation introduced to calculate the linearized model. The calculation of matrix  $A^z$  requires an evaluation of the function  $P^z(x^{z*} \pm \Delta x^z)$ . It starts at the moment just before impact, then the impact model considering the exchange of legs is used, and next the zero dynamics during swing phase follows that until the moment just before impact. Besides of this numerical analysis method, some simple analytical conditions, which guarantee the existence of a cyclic motion and the convergence toward this motion has been deduced in [Chevallereau et al., 2004].

This section proposed a previously studied control strategy, i.e. the method of virtual constraints, in which the reference trajectory is parametrized by a strictly monotonic variable of the robot. The results of stability analysis and walking simulation will be shown in the Subsection 1.6.2. As written in Section 1.1, it is challenging and significantly important to propose a tool to analyze the stability of a control based on tracking reference trajectory as a function of time and to propose a solution to obtain stable walking. Therefore, in the next section, the other two walking control laws will be proposed to track time-variant reference trajectory.

## 1.5 Two control laws for tracking time-variant reference trajectory

This section will present a control law based on the choice of controlled outputs and an event-based control law to track the reference trajectory expressed as a function of time. Different from the method of virtual constraints proposed in the previous subsection, where the stability test only depends on the reference trajectory, here some parameters of these two control laws are adjusted based on the result of stability analysis of hybrid zero dynamics (HZD), that is used to ensure the stability of walking.

### 1.5.1 The reference trajectory

In order to compare the properties of different control laws, the reference trajectory mentioned in Subsection 1.4.1 is used in this section. Because it is described as a set of some discrete points, so as to approximate the desired cyclic motion for each of the five configuration coordinates, a one-dimensional Bezier polynomials such as (1.26) is chosen to describe the reference trajectory. It is:

$$h^d(s) = \sum_{k=0}^J \alpha_k \frac{J!}{k!(J-k)!} s^k (1-s)^{J-k}, \quad (1.51)$$

where the coefficient  $\alpha_k$  is determined to minimize the distance between the optimal trajectory and reference trajectory at the discrete points.

$$s = \frac{\tau}{T} \quad (1.52)$$

is the normalized time varying on the cyclic motion from 0 to 1. The cyclic motion has been defined for one cyclic step from  $t = 0$  to  $t = T$ . Here  $\tau$  is used to replace  $t$  to represent the time during one step. In the control strategy the desired trajectory is restarted at each impact. During the  $(k+1)^{th}$  step, the relation between  $\tau$  and the real time  $t$  is:

$$\tau_{k+1} = t - \sum_{i=1}^k T_i, \quad (1.53)$$

where  $T_i$  is the real duration of the  $i^{th}$  step. The reference trajectory described as a function of time  $\tau$  means it is only defined for single support phase. No matter how long the walking cycle is during the  $i^{th}$  step, after impact the desired trajectory is always  $q^d(0)$ . Since it is  $\tau$  that is used in the control law but not  $t$ , if the duration of one step is longer than the expected one, in the following contents the robot motion will not try to catch the lost time.

Next, the reference trajectory in (1.51) is written as  $h^d(\tau)$  and it is such that:

$$\begin{cases} q^d(\tau) &= h^d(\tau) \\ \dot{q}^d(\tau) &= \frac{\partial h^d(\tau)}{\partial \tau} \\ \ddot{q}^d(\tau) &= \frac{\partial^2 h^d(\tau)}{\partial \tau^2} \end{cases} \quad (1.54)$$

According to some discrete points of the known reference trajectory, in (1.54)  $h^d(\tau)$ ,  $\frac{\partial h^d(\tau)}{\partial \tau}$  and  $\frac{\partial^2 h^d(\tau)}{\partial \tau^2}$  can be deduced by (1.51) and its differential coefficients, so they are supposed to be known in the following contents.

### 1.5.2 A control law based on choice of controlled outputs

#### Definition of the controlled outputs

Since the robot is equipped with  $m$  actuators, only  $m$  outputs can be controlled. In many papers, the controlled variables are simply the actuated variables. In fact, the choice

of the controlled variables directly affects the behavior of the robots [Chevallereau et al., 2009]. For the same desired periodic motion, the stability of the closed-loop system can be dramatically improved through a judicious choice of the controlled variables. For simplicity, the analysis is limited to the case that the controlled variables  $u$  are linear combination of the configuration variables. They are expressed as:

$$u = M \begin{bmatrix} q_u \\ q_a \end{bmatrix} = \begin{bmatrix} M_1 & M_2 \end{bmatrix} \begin{bmatrix} q_u \\ q_a \end{bmatrix}, \quad (1.55)$$

where  $M$  is a  $(4 \times 5)$  matrix to be determined,  $q_u = q_1$  denotes the unactuated variable and  $q_a = [q_2, \dots, q_5]^T$  is the vector of actuated variables. To obtain a simple expression of  $q$  with respect to  $u$  and  $q_u$ ,  $M_2$  is imposed to be invertible. The 4 outputs that must be zeroed by the control law are:

$$y = u - u^d(\tau) \quad (1.56)$$

where  $u^d(\tau)$  is the desired evolution of the controlled variables. For this cyclic motion, the reference motion  $u^d$  and its differential coefficients are defined by

$$\begin{cases} u^d(\tau) &= M q^d(\tau) \\ \dot{u}^d(\tau) &= M \dot{q}^d(\tau) \\ \ddot{u}^d(\tau) &= M \ddot{q}^d(\tau) \end{cases} \quad (1.57)$$

Because the reference trajectory is expressed as the function of time, so the torques depend on the state of the robot and time  $\tau$ . To be able to consider the closed-loop state as an autonomous system, the state is extended as  $X = [x, \tau]'$ , and the studied system (1.24) can be rewritten as:

$$\Sigma_e : \begin{cases} \dot{X} &= \mathbf{f}_e(X) + \mathbf{g}_e(X) u_\tau(X) & X^- \notin S_\tau \\ X^+ &= \Delta_e(X^-) & X^- \in S_\tau \end{cases}, \quad (1.58)$$

where

$$\mathbf{f}_e(X) = \begin{bmatrix} \mathbf{f}(x) \\ 1 \end{bmatrix}, \quad \mathbf{g}_e(X) = \begin{bmatrix} \mathbf{g}(x) \\ \mathbf{0}_{1 \times 4} \end{bmatrix}, \quad \Delta_e = \begin{bmatrix} \Delta \\ 0 \end{bmatrix},$$

and  $S_\tau = \{(q, \dot{q}, \tau) | Z_{sw}(q(\tau)) = 0, X_{sw}(q(\tau)) > 0\}$  is the impact surface.

### Calculation of the input torques

Using  $q_u = q_1$  and (1.55), the current configuration of the robot can be expressed as:

$$q = T_c \begin{bmatrix} q_u \\ u \end{bmatrix}, \quad (1.59)$$

with

$$T_c = \begin{bmatrix} 1 & \mathbf{0}_{1 \times 4} \\ -M_2^{-1} M_1 & M_2^{-1} \end{bmatrix} \quad (1.60)$$

Substituting (1.59) and (1.60) into (1.9), the dynamic model during swing phase is rewritten as:

$$D(q_a) \begin{bmatrix} 1 & \mathbf{0}_{1 \times 4} \\ -M_2^{-1}M_1 & M_2^{-1} \end{bmatrix} \begin{bmatrix} \ddot{q}_u \\ \ddot{u} \end{bmatrix} + H(q, \dot{q}) = B\Gamma \quad (1.61)$$

Defining:

$$D = \begin{bmatrix} D_{11(1 \times 1)} & D_{12(1 \times 4)} \\ D_{21(4 \times 1)} & D_{22(4 \times 4)} \end{bmatrix}, \quad H = \begin{bmatrix} H_{1(1 \times 1)} \\ H_{2(4 \times 1)} \end{bmatrix}, \quad (1.62)$$

and substituting (1.62) into (1.61), it yields:

$$\begin{cases} (D_{11} - D_{12}M_2^{-1}M_1)\ddot{q}_u = -D_{12}M_2^{-1}\ddot{u} - H_1(q, \dot{q}) \\ \Gamma = (D_{21} - D_{22}M_2^{-1}M_1)\ddot{q}_u + D_{22}M_2^{-1}\ddot{u} + H_2(q, \dot{q}) \end{cases} \quad (1.63)$$

The first equation of (1.63) permits to solve  $\ddot{q}_u$ , and then using it in the second equation of (1.63) we can obtain:

$$\Gamma = \frac{(D_{21} - D_{22}M_2^{-1}M_1)(-D_{12}M_2^{-1}\ddot{u} - H_1)}{D_{11} - D_{12}M_2^{-1}M_1} + D_{22}M_2^{-1}\ddot{u} + H_2 \quad (1.64)$$

where the choice of  $M_2^{-1}M_1$  is chosen to ensure that the denominator of equation (1.64) is not zero for the studied reference motions.

To zero the output in (1.56), the control law is defined as:

$$\ddot{u} = \ddot{u}^d(\tau) - \frac{K_d}{\varepsilon}(\dot{u} - \dot{u}^d) - \frac{K_p}{\varepsilon^2}(u - u^d), \quad (1.65)$$

where  $K_p > 0$ ,  $K_d > 0$ , and  $\varepsilon > 0$ . Using the control (1.65) in (1.64), the input torques  $\Gamma$  can be calculated.

### 1.5.3 Stability analysis

#### Zero dynamics

Before the analysis of stability, the zero dynamics [Isidori, 1995] is defined at first using the same way as in Subsection 1.4.3. There are two objectives of introducing the zero dynamics. Firstly, we want to study the effect of the uncontrolled variable  $q_u$  on the property of the closed-loop system with a perfect control law. The second objective is to analyze the stability of walking in a reduced dimensional space.

According to the definition of the zero dynamics, if the output is zero, with (1.56) and the first line of (1.63), the zero dynamics is written as:

$$\begin{cases} u(t) = u^d(\tau) \\ (D_{11} - D_{12}M_2^{-1}M_1)\ddot{q}_u = -D_{12}M_2^{-1}\ddot{u}^d(\tau) - H_1(q, \dot{q}) \end{cases} \quad (1.66)$$

Based on  $u = u^d$  and (1.59),  $q, \dot{q}$  can be replaced by  $u^d, \dot{u}^d$  and  $q_u, \dot{q}_u$ . In addition, since the zero dynamics can also be expressed with the variables  $q_u$  and  $q_a$ , using the equation (1.55) and (1.57), there is:

$$M_1q_u + M_2q_a = u = M_1q_u^d + M_2q_a^d \quad (1.67)$$

Because  $M_2$  is invertible, by connecting (1.66), (1.59) and (1.67), there exists:

$$\begin{cases} q = T_c[q_u, u^d]^T, & \dot{q} = T_c[\dot{q}_u, \dot{u}^d]^T \\ (D_{11}(q) - D_{12}(q)M_2^{-1}M_1)\ddot{q}_u = -D_{12}(q)(M_2^{-1}M_1\ddot{q}_u^d + \ddot{q}_a^d) - H_1(q, \dot{q}) \end{cases} \quad (1.68)$$

This equation clearly shows that the behavior of the robot will be affected by the value of  $M_2^{-1}M_1$ . In fact, according to the definition of the controlled variables  $u$  in (1.55), the introduction of  $M_1$  permits to take into account the tracking error of the uncontrolled variable  $q_u$ . In the following contents we impose that  $M_2 = \mathbf{I}_4$ , which is an identity matrix. When  $M_1 = [0, 0, 0, 0]^T$ , the controlled variables are simply the actuated variables  $q_a$  (see (1.55)).

Obviously, the dynamic properties of the zero dynamics during swing phase depend on the particular choice of the reference motion  $u^d(\tau)$  or  $q^d(\tau)$ . For the same desired periodic motion, the choice of the controlled variables directly affects the zero dynamics in (1.68). It will be illustrated with the simulation results in Subsection 1.6.5.

### Modification of the tracking errors caused by impact

According to [Westervelt et al., 2007, Chap. 5], while the feedback control law ((1.63) and (1.65)) has created a zero dynamics of the stance phase, it has not created a *hybrid zero dynamics* (HZD), that is, the zero dynamics considering the impact model (1.22). If the control law could be modified so as to create a HZD, the study of the swing phase zero dynamics (1.66) and the impact model would be sufficient to determine the stability of the complete system of the robot, thereby leading to a reduced dimensional stability test [Morris and Grizzle, 2009]. Because the reference trajectory depends on  $\tau$  and before impact its final value  $\tau_f$  may be different from its desired value  $T^d$ , so there will be an error between the obtained states of robot  $u(\tau_f)$  and their desired values  $u^d(T^d)$ . However, no matter how much the error is, the reference motion of  $u$  after impact, i.e., at the beginning of the next step is  $u^d(0)$ , that means discontinuity of errors will exist. Therefore, the reference motion is modified stride to stride so that it is compatible with the initial state of the robot at the beginning of each step [Chevallereau et al., 2009]. The new output for the feedback control design is:

$$y_c = u(\tau) - u^d(\tau) - u_c(\tau, y_i, \dot{y}_i). \quad (1.69)$$

This output consists of the previous output (1.56), and a correction term  $u_c$  that depends on (1.56) evaluated at the beginning of the step, specifically,  $y_i = u(0) - u^d(0)$  and  $\dot{y}_i = \dot{u}(0) - \dot{u}^d(0)$ . The values of  $y_i$  and  $\dot{y}_i$  are updated at the beginning of each step (or at impact) and held constant throughout the step. The function  $u_c$  is taken to be a four-order continuously differentiable polynomial function of  $\tau$ :

$$u_c = a_0 + a_1\tau + a_2\tau^2 + a_3\tau^3 + a_4\tau^4, \quad (1.70)$$



where the coefficients  $a_0, a_1, \dots, a_4$  are calculated such that<sup>1</sup>

$$\begin{cases} u_c(0, y_i, \dot{y}_i) &= y_i \\ \dot{u}_c(0, y_i, \dot{y}_i) &= \dot{y}_i \\ u_c(\tau, y_i, \dot{y}_i) &\equiv 0, \quad \tau \geq \frac{T^d}{2}. \end{cases} \quad (1.71)$$

With  $u_c$  designed in this way, the initial errors of the output and its differential coefficient are smoothly joined to the original values at the middle of the step, and  $u_c$  does not introduce any discontinuity on the desired trajectory, as shown in Fig. 1.7. In particular, for any initial error, the initial reference motion  $u^d$  is exactly satisfied by the second part of the step  $\tau \geq \frac{T^d}{2}$ .

To zero the new output  $y_c$  in (1.69),  $u^d$  is replaced by  $u^d + u_c$  in the control law (1.65):

$$\ddot{u} = \ddot{u}^d(\tau) + \ddot{u}_c - \frac{K_d}{\varepsilon}(\dot{u} - \dot{u}^d - \dot{u}_c) - \frac{K_p}{\varepsilon^2}(u - u^d - u_c). \quad (1.72)$$

Under the new control law defined by (1.72), the behavior of the robot is completely defined by the impact map and the swing phase zero dynamics (1.66), since  $M_2 = \mathbf{I}_4$ , (1.66) becomes:

$$\begin{cases} u(\tau) = u^d(\tau) + u_c(\tau, y_i, \dot{y}_i) \\ (D_{11} - D_{12}M_1)\ddot{q}_u = -D_{12}(\ddot{u}^d + \ddot{u}_c) - H_1(q, \dot{q}) \end{cases} \quad (1.73)$$

The zero dynamics manifold is defined by  $Z_\tau = \{(q, \dot{q}, \tau) | y_c(q) = 0, \dot{y}_c(q) = 0\}$ , (1.73) shows that this manifold can be parametrized by a 3 dimensional vector  $(q_u, \dot{q}_u, \tau)$ . When the reference trajectory is a function of the state variable proposed in Subsection 1.4.3, the zero dynamics manifold is of dimension 2, here the supplementary variable  $\tau$  must be considered. Since the robot is controlled in torque, if  $u_c$  is not introduced, the discontinuities of position and velocity cannot be imposed by the control thus the states of the robot cannot stay in the zero dynamics manifold at the impact transition. However, the introduction of  $u_c$  allows to keep the states of the robot in the hybrid zero dynamics manifold. The smooth modification of the reference motion  $u^d$  using  $u_c$  induces a smooth change of the torque and thus reaction force, which is not the case for high gain control and discontinuity of errors. Thus the introduction of the term  $u_c$  is not only useful for theoretical analysis but also practical for the experiment.

#### 1.5.4 Stability test in a reduced dimensional space

The stability analysis of walking is obtained by using the Poincaré method. As the same way as in Subsection 1.4.3, the Poincaré section is also chosen just before the impact. A restricted Poincaré map is defined from  $S_\tau \cap Z_\tau$  to  $S_\tau \cap Z_\tau$ , where  $Z_\tau = \{(q, \dot{q}, \tau) | y_c(q) =$

---

<sup>1</sup>In the specific application, the polynomial function (1.70) is used for  $0 \leq \tau \leq \frac{T^d}{2}$ ; continuity of position, velocity and acceleration is ensured at  $\tau = \frac{T^d}{2}$ . There are five conditions in (1.71) to determine five coefficients.



$0, \dot{y}_c(q) = 0\}$  denotes the zero dynamics manifold and  $S_\tau = \{(q, \dot{q}, \tau) | Z_{sw}(q) = 0, X_{sw}(q) > 0\}$  is the Poincaré section. The key point is that since in  $Z_\tau$  the state of the robot can be parametrized by three independent variables, in  $S_\tau \cap Z_\tau$ , the state of the robot can be represented only by two independent variables,  $x^z = [q_u(T), \dot{q}_u(T)]^T$ , where  $q_u$  denotes the unactuated joint. Since the reference trajectory  $q^d(\tau)$  is a cyclic motion, the corresponding fixed-point is  $x^{z*} = [q_u^d(T^d), \dot{q}_u^d(T^d)]^T$ , where  $T^d$  is the desired walking period.

The restricted Poincaré map  $P^z : S_\tau \cap Z_\tau \rightarrow S_\tau \cap Z_\tau$  induces a discrete-time system  $x_{k+1}^z = P^z(x_k^z)$ . Define  $\delta x_k^z = x_k^z - x^{z*}$ , the Poincaré map linearized about the fixed-point  $x^{z*}$  gives rise to a linearized system,

$$\delta x_{k+1}^z = A^z \delta x_k^z, \quad (1.74)$$

where the  $(2 \times 2)$  square matrix  $A^z$  is the Jacobian of the Poincaré map and is computed as follows:

$$A^z = \begin{bmatrix} A_1^z & A_2^z \end{bmatrix}_{2 \times 2}$$

with

$$A_i^z = \frac{P^z(x^{z*} + \Delta x_i^z) - P^z(x^{z*} - \Delta x_i^z)}{2\Delta x_i^z}, \quad i = 1, 2, \quad (1.75)$$

$$\text{and } \Delta x_i^z = \begin{cases} \Delta q_u, & i = 1 \\ \Delta \dot{q}_u, & i = 2 \end{cases}.$$

The quantities  $\Delta q_u, \Delta \dot{q}_u$  are small perturbations introduced to calculate the linearized model, and the denominator in (1.75) must be interpreted as the scalar perturbation used in computing  $\Delta x_i^z$ . The calculation of matrix  $A^z$  requires four evaluations of the function  $P^z(x^{z*} \pm \Delta x_i^z)$ . Each evaluation of this function is composed of the reconstruction of the vector  $[q, \dot{q}]^T$  from  $x^z$  with  $x^z \in S_\tau \cap Z_\tau$ , the calculation of the impact map (1.22), the calculation of  $y_i, \dot{y}_i$ , the calculation of  $u_c(\tau)$  and the integration of the zero dynamics during swing phase.

It should be noted that the perturbation  $\Delta x_1^z = \Delta q_u$  in  $S_\tau \cap Z_\tau$  has a complex effect on the other states of the robot. Because when the robot touches the ground with a different value of  $q_u$ , it means that the duration of the previous step has been modified and as a consequence that the actuated configuration and velocity of the robot are modified. Therefore, the controlled variables  $u$  and  $\dot{u}$  must be recalculated. Firstly, the vertical position of swing foot is written as the function of the joint coordinate or of  $q_u$  and  $u$ :  $Z_{sw}(u, q_u)$ . Next, in  $S_\tau$ ,  $Z_{sw} = 0$ , the fixed-point of the Poincaré map satisfies:  $Z_{sw}(u^d(T^d), q_u^*) = 0$ . With  $\Delta q_u$ , the state of the robot in  $S_\tau$  must satisfy  $\Delta Z_{sw} = 0$ . Since  $\Delta Z_{sw}$  can be written as:

$$\Delta Z_{sw} = \frac{\partial Z_{sw}}{\partial u} \Delta u + \frac{\partial Z_{sw}}{\partial q_u} \Delta q_u \quad (1.76)$$

or

$$\Delta Z_{sw} = \frac{\partial Z_{sw}}{\partial u} \dot{u}(T^d) \Delta t + \frac{\partial Z_{sw}}{\partial q_u} \Delta q_u, \quad (1.77)$$

to satisfy  $\Delta Z_{sw} = 0$ ,  $\Delta t$  is:

$$\Delta t = - \frac{\frac{\partial Z_{sw}}{\partial q_u}}{\frac{\partial Z_{sw}}{\partial u} \dot{u}(T^d)} \Delta q_u \quad (1.78)$$

The state of robot just before impact with the perturbation  $\Delta q_u$  is then deduced from  $[u(T^d + \Delta t), q_u^* + \Delta q_u, \dot{u}(T^d + \Delta t), \dot{q}_u^*]$ .

On the contrary, the perturbation  $\Delta x_2^z = \Delta \dot{q}_u$  in  $S_\tau \cap Z_\tau$  has less effect since all the other states of the robot are unchanged. In this case, the state of robot just before impact with the perturbation is  $[u(T^d), q_u^*, \dot{u}(T^d), \dot{q}_u^* + \Delta \dot{q}_u]$ .

According to **Theorem 2.1** and **Theorem 2.2** proposed in Subsection 1.4.3, a fixed-point of the restricted Poincaré map is locally exponentially stable, if, and only if, the eigenvalues of  $A^z$  have magnitude strictly less than one [Westervelt et al., 2007, Chap. 4]. (1.73) has showed that the choice of the controlled outputs, i.e., the choice of  $M_1$  influences the zero dynamics so it also influences the walking stability. If some  $M_1$  are chosen to yield that the eigenvalues of  $A^z$  have magnitude strictly less than one, the stable walking can be obtained, that will be shown in Subsection 1.6.5. In the same way, if a feedback control law is introduced to adjust the eigenvalues of  $A^z$  to be less than one, the stable walking can also be obtained. Next, an event-based feedback control law will be proposed to improve the walking stability like this.

### 1.5.5 An event-based feedback controller

[Grizzle, 2003] presented that if a desired periodic gait is not stable, or if the corresponding rate of convergence is not sufficiently rapid, the event-based control may be designed and integrated with the continuous, stance phase controller. It has been proved successfully to improve the stability of walking for tracking the parametrized reference trajectory in [Chevallereau et al., 2009] but not yet tested for tracking the time-variant reference trajectory. Therefore, it is interesting to apply it here and compared it with the control law based on the choice of controlled outputs.

Let  $\beta$  be a vector of parameters that is retained constant during the swing phase and updated at each impact. The output in (1.69) is modified with an additional term  $u_s(\tau, \beta)$  depending on a vector of parameters  $\beta$

$$y_s = u - u^d(\tau) - u_c(\tau, y_i, \dot{y}_i) - u_s(\tau, \beta) \quad (1.79)$$

The function  $u_s$  is taken to be a four-times continuously differentiable function of  $\tau$  similar to (1.70) such that<sup>2</sup>

$$\begin{cases} u_s(0, \beta) &= 0 \\ u_s(\frac{T^d}{2}, \beta) &= \beta \\ u_s(t, \beta) &\equiv 0, \quad 0.9T^d \leq \tau \leq T^d. \end{cases} \quad (1.80)$$

where  $\beta$  will be added to  $u$  so it is a  $4 \times 1$  vector such as  $u$ .

By introducing  $u_c$  and  $u_s$  to  $u^d$ , the resulted reference trajectory can be described by Fig. 1.7. In (1.69), when  $\tau \geq \frac{T^d}{2}$ ,  $u_c(\tau, y_i, \dot{y}_i) \equiv 0$ . Therefore, the choice of  $u_s$  in (1.80) is convenient because it does not require a re-design of the controller that created the hybrid

---

<sup>2</sup>In the specific application, the four-order polynomial is used for  $0 \leq \tau \leq 0.9T^d$ . Continuity of position, velocity and acceleration is ensured at  $\tau = 0.9T^d$ . There are five conditions in (1.80) to determine five coefficients of the four-order polynomial function of  $\tau$ .

zero dynamics. As long as the impact occurs for  $\tau \geq 0.9T^d$ , which happens when the motion is close to the periodic orbit, the final state of the robot is on the original hybrid zero dynamics independently of any modification of  $u_s$  for the previous step.

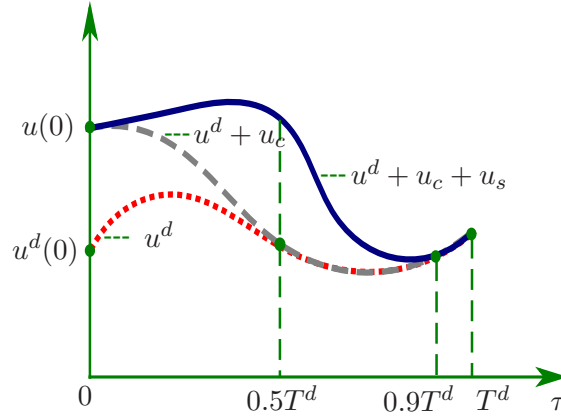


Figure 1.7: The modification of the reference path.

To zero the new output  $y_s$  in (1.79),  $u^d + u_c$  is replaced by  $u^d + u_c + u_s$  in the control law (1.72):

$$\ddot{u} = \ddot{u}^d(\tau) + \ddot{u}_c + \ddot{u}_s - \frac{K_d}{\varepsilon}(\dot{u} - \dot{u}^d - \dot{u}_c - \dot{u}_s) - \frac{K_p}{\varepsilon^2}(u - u^d - u_c - u_s). \quad (1.81)$$

Now the Poincaré map can be viewed as a nonlinear control system on  $S_\tau \cap Z_\tau$  with inputs  $\beta_k$ , where  $\beta_k$  is the value of  $\beta$  during the step  $k+1$ , namely  $x_{k+1}^z = P^z(x_k^z, \beta_k)$ . Linearizing this nonlinear system about the fixed-point  $x^{z*}$  and the nominal parameter value  $\beta^* = \mathbf{0}_{4 \times 1}$  leads to

$$\delta x_{k+1}^z = A^z \delta x_k^z + F \delta \beta_k, \quad (1.82)$$

where  $\delta \beta_k = \beta_k - \beta^*$  and  $F$  is the Jacobian of  $P^z$  with respect to  $\beta$ . Designing a feedback matrix

$$\delta \beta_k = -K \delta x_k^z \quad (1.83)$$

such that the eigenvalues of  $(A^z - FK)$  have magnitude strictly less than one will exponentially stabilize the fixed-point  $x^*$ .

## 1.6 Simulation results of three controllers

In this section, the obtained reference trajectory and its approximations used in the simulation are described at first in Subsection 1.6.1. Next, Subsection 1.6.2 shows the result of stability analysis and walking simulation of the robot with the control law for tracking parametrized reference trajectory. In the following Subsections 1.6.3-1.6.6, the simulation results of two control laws for tracking time-variant reference trajectory are

given. 1.6.3 shows that the walking gait is not stable in the case that the controlled variables are only the actuated variables and event-based feedback controller is not used. On the contrary, Subsection 1.6.4 indicates the walking gait is stable using the event-based feedback control law. It has been explained that the walking stability is influenced by the choice of controlled outputs, i.e., the choice of  $M_1$  in (1.55). Therefore, in Subsection 1.6.5 the effect of different choices of  $M_1$  on the walking stability is studied. It shows that the stable walking can be obtained by only pertinent choices of  $M_1$ . Further, a method for choosing  $M_1$  judiciously is given in Subsection 1.6.6 and two stable domains are obtained. At last, an example of  $M_1$  selected in these stable domains are compared to the previous results of three control methods proposed in Subsections 1.6.2-1.6.6.

### 1.6.1 A cyclic motion and approximated motion

Using optimization techniques developed in [Chevallereau and Aoustin., 2001], an optimal cyclic motion has been defined for the robot RABBIT described in Section 1.2. The optimization criterion is minimizing the integral of the norm of the square of torques for one meter traveling with an average velocity of  $1.6168 \text{ m/s}$ . The corresponding stick-diagram is presented in Fig. 1.8. The step length is  $0.9062 \text{ m}$  and the duration of a step is  $0.5605 \text{ s}$ . The joint profiles and angular velocities of each angle for two consecutive steps are presented in Fig. 1.9 and Fig. 1.10.

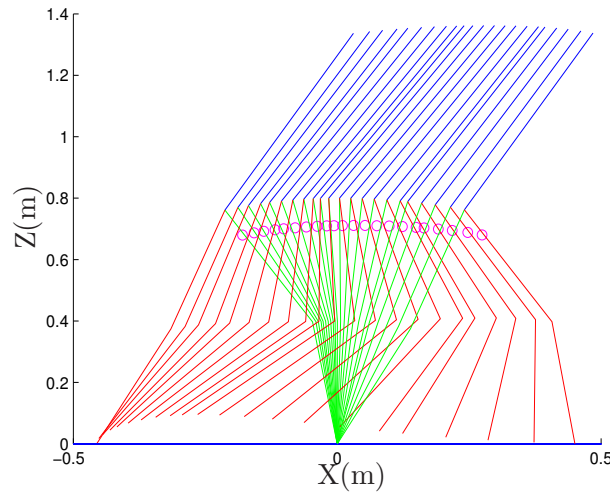


Figure 1.8: Stick-diagram for the first step of the periodic walking gait

In the walking simulation, the obtained cyclic motion is defined as Bezier polynomials for two kinds of reference trajectories (see (1.26) and (1.51)), i.e., parameterized reference trajectory and time-variant reference motion. It is worth noting that in the first reference trajectory the evolution of the posture or "shape" of the robot will be "synchronized" to an internal variable. However, in the time-variant reference trajectory, since  $q^d(\tau)$  described

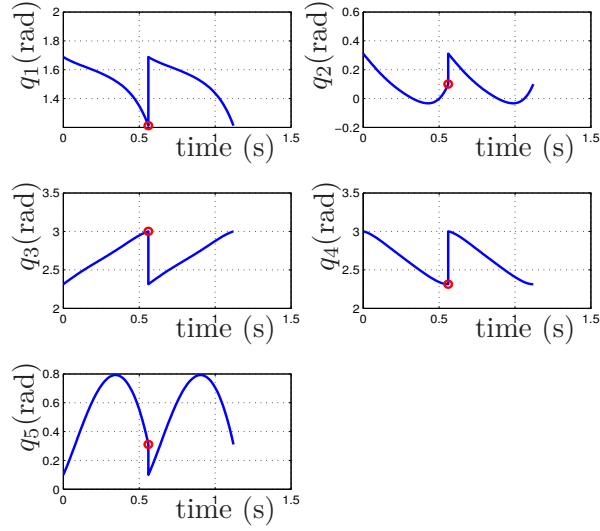


Figure 1.9: Joint profiles of the obtained periodic motion over two steps, where the small circles represent  $q_f^*$ .

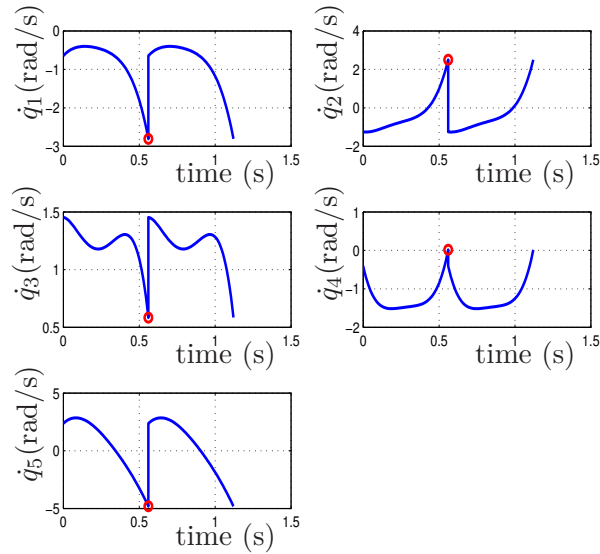


Figure 1.10: Joint rate profiles of the obtained periodic motion over two steps, where the small circles represent  $\dot{q}_f^*$ .

by (1.51) is an approximation of the initial cyclic motion, the motion defined by  $u^d(\tau)$  and the final cyclic state of the unactuated variable cannot define a perfect cyclic motion. Accordingly  $x^{z*} = [q_u^d(T), \dot{q}_u^d(T)]^T$  is not a perfect cyclic point for the Poincaré map  $P^z$ .

To solve this problem, the time-variant reference motion is slightly modified by introducing the polynomial  $u_s(\tau, \beta)$  which is proposed in Subsection 1.5.5. The fixed-point of the control law is then  $(x^{z*}, \beta^*)$ . In Subsection 1.5.5,  $\beta^*$  has been imposed as  $\beta^* = \mathbf{0}_{4 \times 1}$ , but now it is calculated by optimization method (fminsearch of Matlab), which is minimizing the cost function  $\|x^{z*} - P^z(x^{z*}, \beta^*)\|$ .

In a word, for both of two control laws based on tracking the approximate reference trajectory defined by (1.51), in order to obtain a perfect cyclic motion, (1.79) and (1.80) should be used in the closed-loop system with:

$$\beta = \beta^*. \quad (1.84)$$

If the event-based feedback control law (1.83) needs to be introduced to produce the stable walking,  $-K\delta x_k^z$  must be supplemented to (1.84) as the second term of  $\beta$ :

$$\beta = \beta^* - K\delta x_k^z. \quad (1.85)$$

## 1.6.2 Results of the control law for tracking parametrized reference trajectory

The stability of the control law for tracking parametrized reference trajectory has been theoretically analyzed in Subsection 1.4.3. As shown in (1.48), the property of the closed-loop system can be described by  $\theta$  and  $\dot{\theta}$ . Since for the chose fixed-point  $\theta = \theta^*$ , only  $\dot{\theta}$  needs to be considered. Therefore, in (1.50)  $x^z = \dot{\theta}$ . In general, the smaller the perturbation introduced at the fixed-point, the more accurate calculation of linearization. If the perturbation quantity introduced to the fixed-point is chosen as  $\Delta x^z = 10^{-4}$ , the obtained one-dimensional Jacobian of the linearized restricted Poincaré map is:

$$A^z = 0.6368, \quad (1.86)$$

so the only eigenvalue of  $A^z$  is  $\lambda = 0.6368 < 1$ , that means the walking will be stable.

Next, the initial errors of  $0.005 \text{ rad}$  and  $0.05 \text{ rad/s}$  are introduced to the states of unactuated joint  $q_u$  and  $\dot{q}_u$  respectively, and the initial states of other joints are modified accordingly to ensure that two feet touch the ground.

Fig. 1.11 shows that the uncontrolled joint  $q_1$  tracks the desired path  $q_1^d$ . Exactly, the track error of  $q_1$  converges to zero at the second step but that of  $\dot{q}_1$  converges to zero until the  $10^{th}$  step. The phase-plane plots of all the variables are shown in Fig. 1.12. The convergence toward a periodic motion is clear for all the controlled and uncontrolled variables. In addition, the torques can follow their desired values. For example, the torques of the swing leg (see Fig. 1.3) are given in Fig. 1.13. It shows that the desired torques are obtained just after walking one step. From these results, it is obviously that the walking is stable.

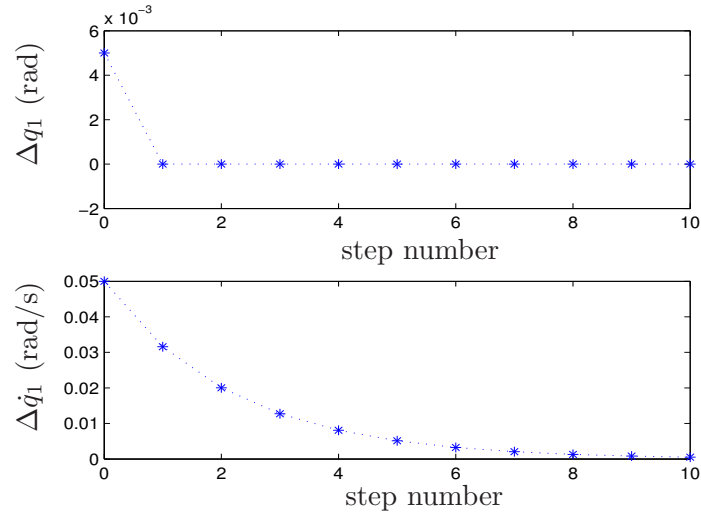


Figure 1.11: The difference of the real values and desired values of  $q_u$  and  $\dot{q}_u$  at the end of each step for the control law based on tracking parametrized reference trajectory.

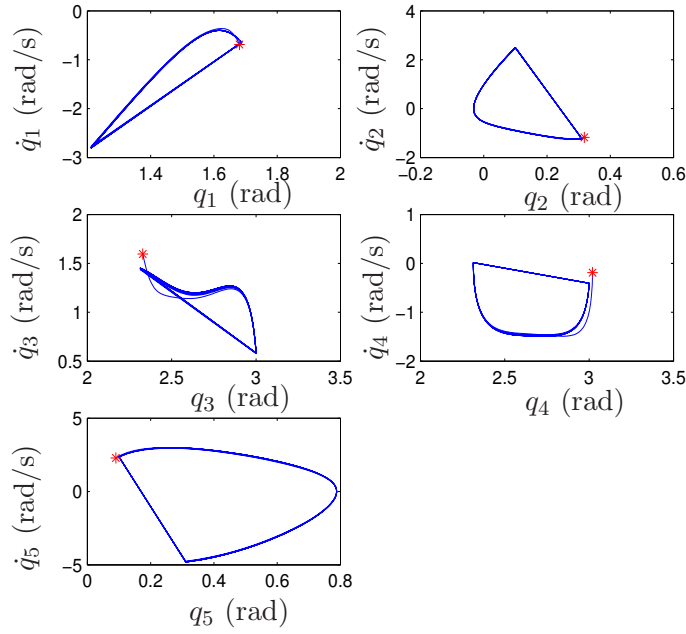


Figure 1.12: Phase-plane plots for  $q_i$ ,  $i = 1, \dots, 5$  for the control law based on tracking parametrized reference trajectory. The straight lines correspond to the impact phase, where the state of the robot changes instantaneously. The initial state is represented by a (red) star.

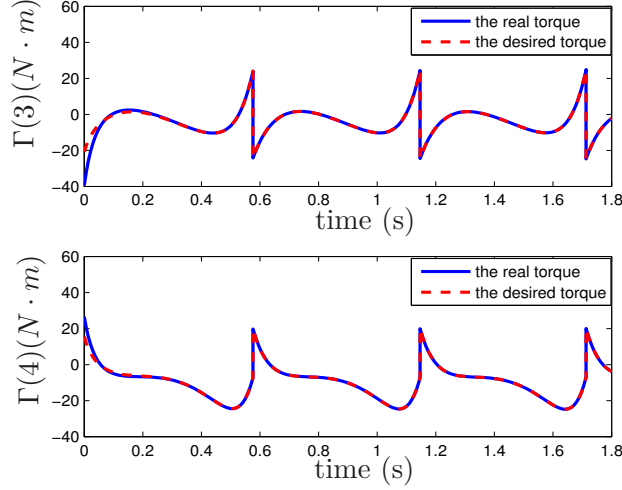


Figure 1.13: The torques of the swing leg for the control law based on tracking parametrized reference trajectory, where  $\Gamma(3)$  notes the torque of hip and  $\Gamma(4)$  notes the torque of knee.

### 1.6.3 An example of a control law tracking only actuated joints

This subsection will show the simulation results with the control law based on tracking the time-variant trajectory. The controlled variables are chosen with  $M_1 = [0, 0, 0, 0]^T$  in (1.55), since  $M_2 = \mathbf{I}_4$ , the controlled variables are only the actuated variables. The control law (1.81) is used to zero:

$$y_s = u - u^d(\tau) - u_c(\tau, y_i, \dot{y}_i) - u_s(\tau, \beta^*) \quad (1.87)$$

where  $\beta^* = [0.0003, -0.0012, 0.0005, -0.0020]^T$ . To study the stability of this control law around the periodic motion, the perturbation quantity introduced to the fixed-point in (1.74) is chosen as  $\delta x^z = [10^{-4}, 10^{-3}]^T$ , here  $x^z = [q_u, \dot{q}_u]^T$ , the Jacobian of the linearized restricted Poincaré map is computed as (1.75), yielding

$$A^z = \begin{bmatrix} 87.5469 & -6.3547 \\ 686.7508 & -49.7799 \end{bmatrix}. \quad (1.88)$$

The two eigenvalues are:

$$\begin{aligned} \lambda_1 &= 37.6069 \\ \lambda_2 &= 0.1601 \end{aligned} \quad (1.89)$$

Here the maximum eigenvalue  $\max |\lambda_{1,2}| = 37.6069 > 1$  and hence the gait will be non-stable under this controller. Next the walking simulation of robot is done to validate the result of stability analysis. Fig. 1.14 shows that the uncontrolled joint  $q_1$  does not track the desired path  $q_1^d$  even without initial error. As a result, the joint coordinates cannot converge to a periodic motion, as shown in Fig. 1.15.



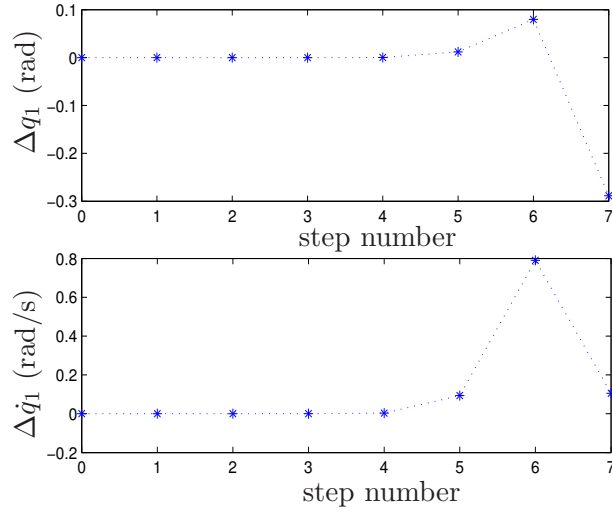


Figure 1.14: The difference of the real values and desired values of  $q_u$  and  $\dot{q}_u$  at the end of each step for the control law based on choice of controlled outputs with  $M_1 = [0, 0, 0, 0]^T$ .

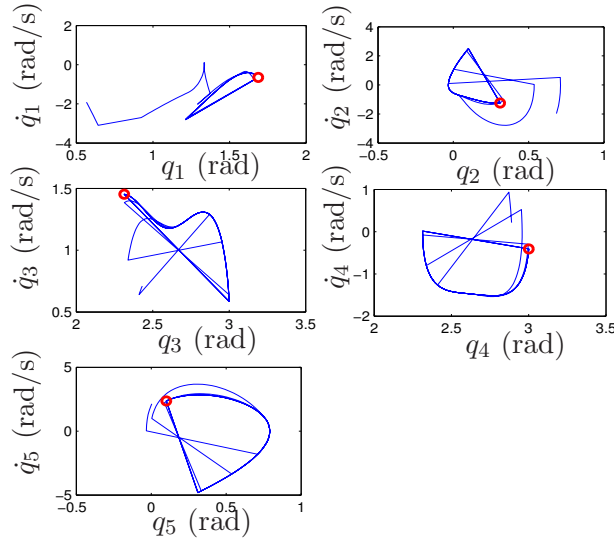


Figure 1.15: Phase-plane plots for  $q_i$ ,  $i = 1, \dots, 5$  for the control law based on choice of controlled outputs with  $M_1 = [0, 0, 0, 0]^T$ . The straight lines correspond to the impact phase, where the state of the robot changes instantaneously. The initial state is represented by a (red) star.

In the following subsections, two strategies to obtain stable walking will be considered. In the first strategy, an event-based controller is introduced to stabilize the gait, which is presented in Section 1.5.5. In the second strategy, freedom in the selection of the controlled variables is used to obtain a stable walking with only within-stride control.

### 1.6.4 An example of the event-based feedback controller

The periodic motion described before can be stabilized by introducing an event-based controller, which is defined by (1.79)-(1.83). The  $(2 \times 4)$  matrix  $F$  is computed numerically, analogously to the calculation of  $A^z$  in (1.75), yielding:

$$F = \begin{bmatrix} 0.7797 & 1.0684 & -0.5755 & -0.1786 \\ 6.0365 & 8.2404 & -4.4695 & -1.4005 \end{bmatrix} \quad (1.90)$$

The matrix  $A^z$  is given in equation (1.88). The  $(4 \times 2)$  gain matrix  $K$  is calculated via DLQR (design linear-quadratic state-feedback regulator for discrete-time state-space system), which is a function of control system toolbox in MATLAB. It calculates the optimal gain matrix  $K$  such that the state-feedback law  $\delta\beta_k = -K\delta x_k^z$  minimizes the cost function  $\sum_k (\delta x_k^z{}^T \delta x_k^z + r \delta\beta_k^T \delta\beta_k)$ , subject to the state dynamics (1.82). For  $r = 2$  we obtain:

$$K = \begin{bmatrix} 31.8912 & -2.3173 \\ 43.1182 & -3.1385 \\ -23.7987 & 1.7269 \\ -7.6435 & 0.5522 \end{bmatrix}. \quad (1.91)$$

The eigenvalues of the linearized Poincaré map in closed loop  $A^z - FK$  are:

$$\begin{aligned} \lambda &= 0.0567 \pm 0.0226i \\ |\lambda| &= 0.0610 \end{aligned} \quad (1.92)$$

It indicates that the gait will be stable with the addition of the event-based feedback controller. To illustrate the orbit's local stability, the planar biped's complete model in closed-loop is simulated with the initial state perturbed away from the fixed-point  $x^*$ . The initial errors of  $0.005 \text{ rad}$  and  $0.05 \text{ rad/s}$  are introduced respectively on  $q_u$  and  $\dot{q}_u$ , which are regarded as  $\Delta x$  to yield

$$\beta = \beta^* - K\Delta x, \quad (1.93)$$

and then the value of  $\beta$  in (1.93) is used to (1.79) to carry out the walking with the event-based feedback control law.

Fig. 1.16 shows that the tracking errors of uncontrolled variable  $q_u$  and  $\dot{q}_u$  converge to zero. The desired torques of the swing leg (see Fig. 1.3) are obtained after walking 4 steps as shown in Fig. 1.18. Compared to Fig. 1.13 we can see that the robot with event-based feedback control law consumes more energy than the control law based on tracking parametrized trajectory. Fig. 1.17 shows the phase-plane plots of all the variables. It indicates clearly that the convergence toward a periodic motion for all the controlled and uncontrolled variables. Therefore, the walking is stable with the introduction of the event-based feedback control law.

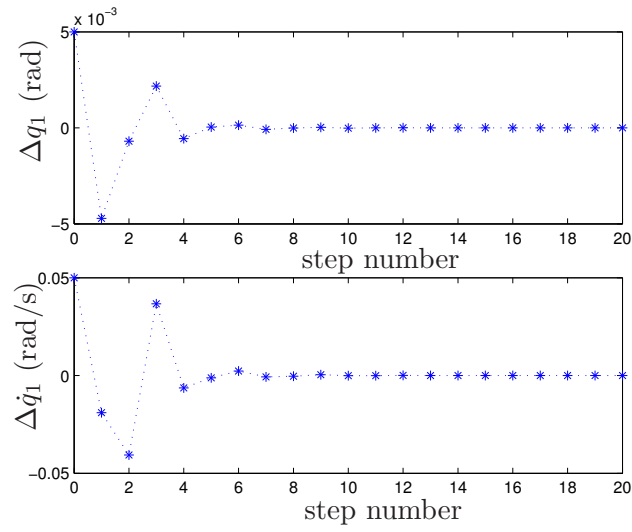


Figure 1.16: The difference of the real values and desired values of  $q_u$  and  $\dot{q}_u$  at the end of each step for the event-based feedback control law.

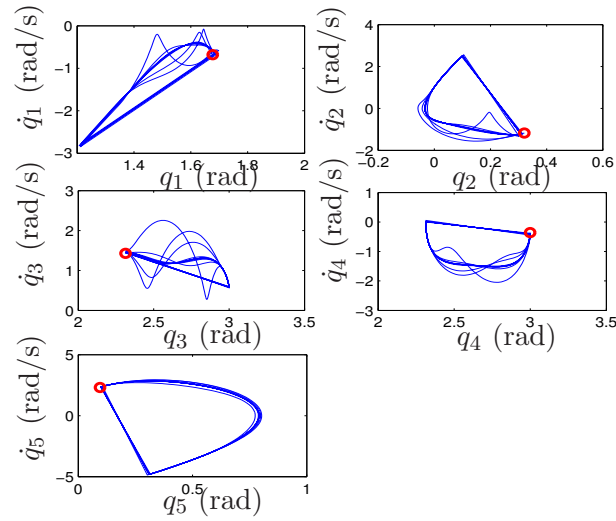


Figure 1.17: Phase-plane plots for  $q_i$ ,  $i = 1, \dots, 5$  for the event-based feedback control law. The straight lines correspond to the impact phase, where the state of the robot changes instantaneously. The initial state is represented by a (red) star.

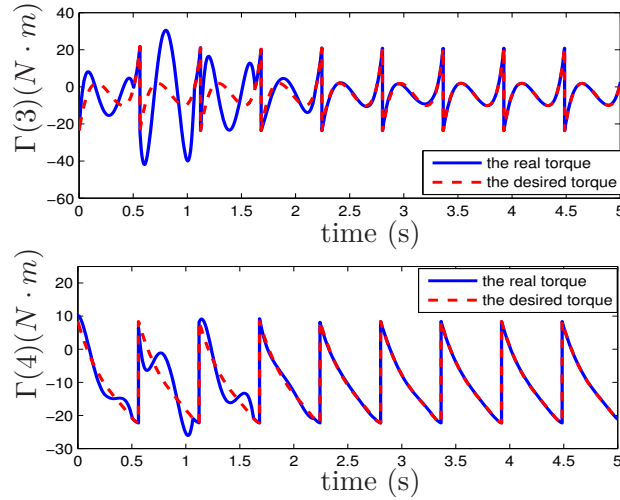


Figure 1.18: The torques of the swing leg for the event-based feedback control law, where  $\Gamma(3)$  notes the torque of hip and  $\Gamma(4)$  notes the torque of knee.

### 1.6.5 Results of stability analysis with different choices of controlled outputs

The equation (1.73) indicates that the hybrid zero dynamics depends on the choice of the controlled outputs, in fact, the choice of  $M_1$ . Subsection 1.6.3 has shown that when  $M_1 = [0, 0, 0, 0]^T$ , the walking is nonstable. Now the effect of  $M_1$  on the stability of the control law will be explored and it will be proved that the stable walking can be obtained by pertinent choice of  $M_1$  without additional event-based feedback control law.

To study the stability of this control law around the periodic motion, the eigenvalues of  $A^z$  in (1.74) are calculated, which are noted as  $\lambda_{1,2}$ . Generally, it is possible to use an optimization technique to find a vector  $M_1$  such that the maximal norm eigenvalues of  $A^z$  is less than one, as:

$$\max |\lambda_{1,2}| < 1, \quad (1.94)$$

Here an exploration technique is used to illustrate the effect of the choice of the output. We fix arbitrary three components of  $M_1$  to zero and  $\max |\lambda_{1,2}|$  are drawn as function of the fourth component of  $M_1$ . The results are shown in Fig. 1.19, where the red points note the cases such that  $\max |\lambda_{1,2}| < 1$ . In order to find these stable points, we search more precisely of  $M_1(j)$ ,  $j = 1, 2, 3, 4$  near the  $\max |\lambda_{1,2}| = 1$ . As a result, it shows that when  $M_1 = [1.96, 0, 0, 0]^T$ ,  $M_1 = [0, 2, 0, 0]^T$ ,  $M_1 = [0, 0, -2.06, 0]^T$  and  $M_1 = [0, 0, 0, -7.3]^T$ , the eigenvalues of  $A^z$  are less than one, that is, the walking will be stable.

Three main results can be found from Fig. 1.19.

1) When  $M_1$  gets into some domains, the eigenvalues of  $A^z$  can change to infinity, as a result, the swing foot cannot touch the ground, but when  $M_1$  gets out of it, the eigenvalues of  $A^z$  diminish instantaneously, as shown in  $M_1(1)$  of Fig. 1.19. It is observed that these

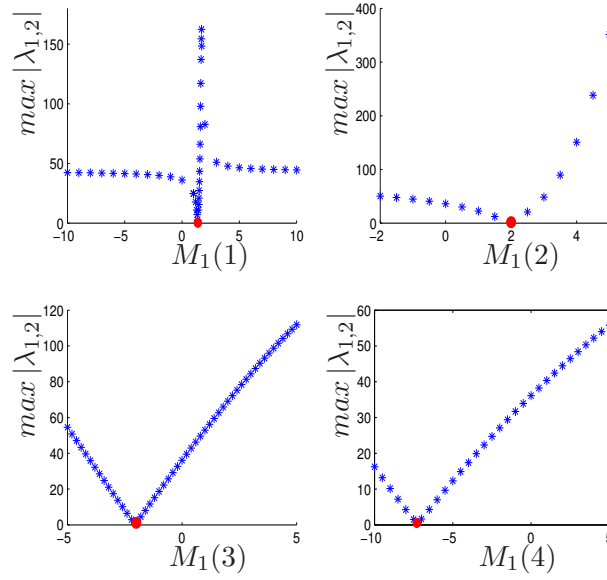


Figure 1.19:  $\max |\lambda_{1,2}|$  versus  $M_1(j)$ ,  $j = 1, 2, 3, 4$ , when the other three components of  $M_1$  are zero.

domains are due to the singularity of the controller.

*Proof:* In order to calculate the required torques  $\Gamma$  in (1.63),  $\ddot{q}_u$  must be obtained by using the first line of (1.63), which can be rewritten as:

$$\ddot{q}_u = \frac{-D_{12}\ddot{u} - H_1(q, \dot{q})}{D_{11} - D_{12}M_1}, \quad (1.95)$$

If there exist some values of  $M_1$  such that:

$$D_{11} - D_{12}M_1 = 0, \quad (1.96)$$

the controller is singularity.

During the swing phase,  $D_{11}$  and  $D_{12}$  are almost constant. At the desired impact moment  $T^d$ , there are  $D_{11} \approx 24.2445$ ,  $D_{12} \approx [13.4347, 3.6283, 0.5375, 0.0410]$ . When  $M_1 = [M_1(1), 0, 0, 0]^T$ , (1.96) is satisfied for  $M_1(1) = 1.8046$ . As shown in  $M_1(1)$  of Fig. 1.19, there is a jump of  $\max |\lambda_{1,2}|$  near this value. Using the same method, it can be deduced that when  $M_1 = [0, 6.6821, 0, 0]^T$ ,  $M_1 = [0, 0, 45.1060, 0]^T$  and  $M_1 = [0, 0, 0, 592.7751]^T$ , the controller will be singular too.

2) For some  $M_1$ , there exists a minimum  $\max |\lambda_{1,2}|$  which leads to stable walking.

3) The value of  $\max |\lambda_{1,2}|$  is very sensitive to some change of  $M_1$ . When  $M_1$  is modified a little, the stable walking gait may become unstable.

In order to illustrate the orbit's local stability, the same walking simulation is done as in Subsection 1.6.3 with the initial errors of  $0.005 \text{ rad}$  and  $0.05 \text{ rad/s}$  introduced on

$q_u$  and  $\dot{q}_u$  respectively. However,  $M_1 = [0, 0, 0, 0]^T$  is replaced by an example of stable case,  $M_1 = [0, 0, -2.06, 0]^T$ . In this case,  $\max |\lambda_{1,2}| = 0.7742$ . Some results are shown in Fig. 1.20- Fig. 1.22.

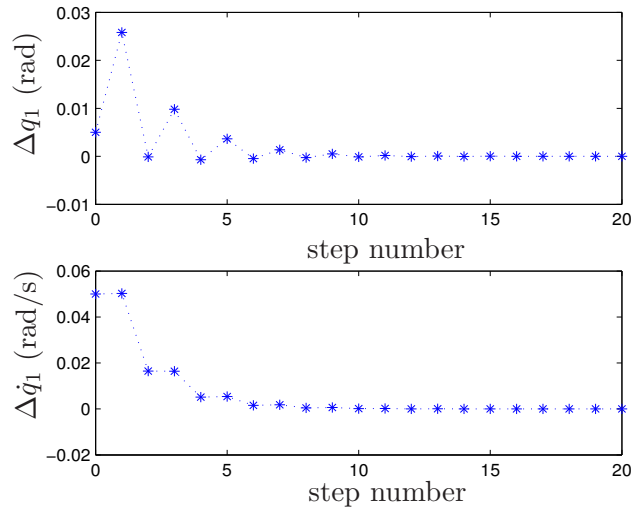


Figure 1.20: The difference of the real values and desired values of  $q_u$  and  $\dot{q}_u$  at the end of each step for the control law based on choice of controlled outputs with  $M_1 = [0, 0, -2.06, 0]^T$ .

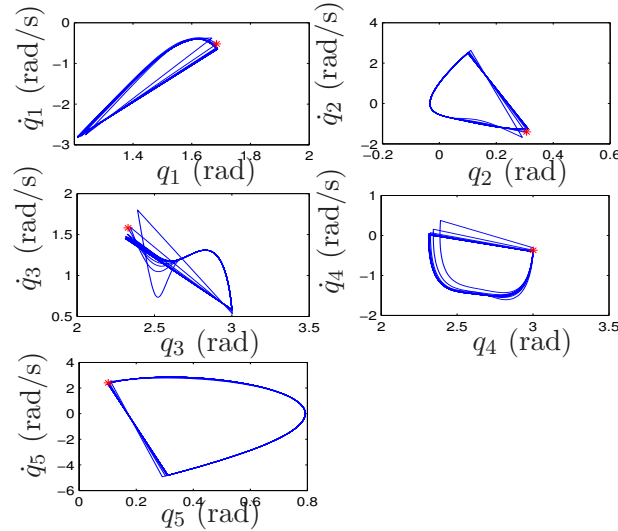


Figure 1.21: Phase-plane plots for  $q_i$ ,  $i = 1, \dots, 5$  for the control law based on choice of controlled outputs with  $M_1 = [0, 0, -2.06, 0]^T$ . The straight lines correspond to the impact phase, where the state of the robot changes instantaneously. The initial state is represented by a (red) star.

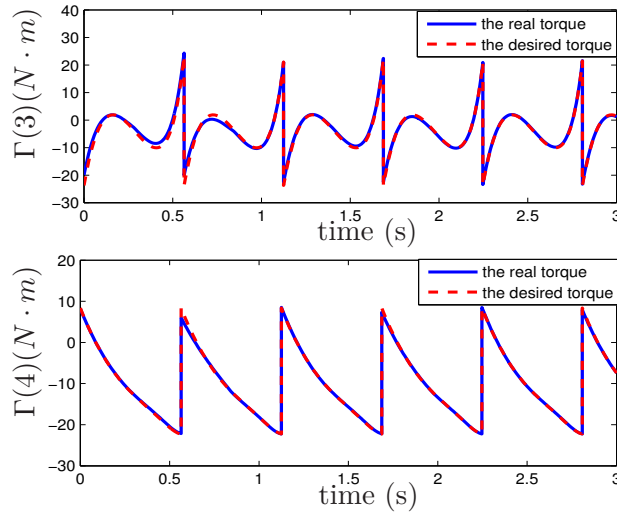


Figure 1.22: The torques of the swing leg for the control law based on choice of controlled outputs with  $M_1 = [0, 0, -2.06, 0]^T$ , where  $\Gamma(3)$  notes the torque of torso and  $\Gamma(4)$  notes the torque of knee.

By comparing these results with that of the event-based feedback controller (Fig. 1.16-Fig. 1.18), it shows that the tracking errors of  $q_u$  and  $\dot{q}_u$  converge to zero after walking 5 steps for both of two methods. With the method of feedback controller, because of the introduction of  $u_s$  in the reference trajectory (see (1.79)), the significant deformation of the trace in Fig. 1.17 occurs at the middle of one step, while it occurs at the impact moment with the method of choice of controlled outputs (see Fig. 1.21). In addition, the consumption of torques using the event-based control law are relatively high before they converge to the desired torques (see Fig. 1.18 and Fig. 1.22).

### 1.6.6 A method for pertinent choice of controlled outputs

The previous subsection has shown that some pertinent choices of controlled outputs can lead to stable walking, so the objective of this subsection is to look for a general method to make these choices.

The points 2) and 3) deduced from Fig. 1.19 show that it is possible but difficult to choose  $M_1$  leading to stable walking. In order to further illustrate that, different values of  $M_1$  are chosen to test stability. Each component of  $M_1$  is sampled between  $-10$  and  $10$  with a step of  $2.5$  to build  $9^4$  vectors  $M_1$ . For each vector  $M_1$ , the effective eigenvalues of the Poincaré map,  $\max |\lambda_{1,2}|$ , is calculated. Except some cases in which the swing foot cannot touch the ground because of the singularity of the controller, there are only 19 stable cases and 5363 unstable cases. The vectors  $M_1$  leading to stable walking are scattered and there is no obvious condition of stability that can be determined. Is there a method which is helpful in the choice of  $M_1$ ? Next, we will try to find the solution for this problem.

For all cases corresponding to different  $M_1$  which were presented in the previous para-

graph, some walking characteristics are chosen to observe whether there exists difference between the stable and unstable cases. They are:

- position of  $CoM$  (Center of Mass) at the desired impact moment  $T^d$ ,
- kinetic energy just before impact and after impact (see [Asano and Luo, 2007] and [Asano and Luo, 2008]),
- errors of uncontrolled variable  $q_u$  during the swing phase and at impact moment,
- height of swing foot  $Z_{sw}$  at  $T^d$ .

We have not observed any special relations between the effective eigenvalues of the Poincaré map  $\max |\lambda_{1,2}|$  and the first three walking characteristics, but we found  $Z_{sw} \approx 0$  at  $T^d$  for all stable cases, that is,  $\max |\lambda_{1,2}| < 1$ , see Fig. 1.23.

To calculate  $Z_{sw}$  at  $T^d$ , the equation (1.67) is used to write:

$$u(T^d) = u^d(T^d), \quad (1.97)$$

and we suppose that there exists an error  $\Delta q_u$  on the underactuated variable of biped  $q_u$ ,  $\Delta q_u = q_u(T) - q_u^d(T)$ . Considering (1.97), (1.59) and  $M_2 = I_{4 \times 4}$ , there is:

$$q(T^d) = q^d(T^d) + M_T \Delta q_u \quad (1.98)$$

where  $M_T = [1, -M_1]^T$ . Next, the height of the swing foot  $Z_{sw}(T^d)$  can be calculated using  $q(T^d)$  without simulation of the biped walking. Supposing  $\Delta q_u = 10^{-2} rad$ , which is adequate to estimate the real  $\Delta q_u$  in the walking simulation. Then  $Z_{sw}(T^d)$  for all the cases of  $M_1(j) \in [-10, 10]$ ,  $j = 1, 2, 3, 4$  are computed. Because the maximum eigenvalue of  $A^z$ , i.e.,  $\max |\lambda_{1,2}|$ , can also be calculated for each  $M_1(j)$ , so the relation between  $\max |\lambda_{1,2}|$  and  $Z_{sw}(T^d)$  can be shown in Fig. 1.23 (only the cases of  $\max |\lambda_{1,2}| < 50$  are presented), where the red points denote  $\max |\lambda_{1,2}| < 1$ , that is, the stable cases.

Based on Fig. 1.23, it can be conjectured that:

**A necessary condition for stable walking is  $Z_{sw}(T^d) \approx 0$ .**

This condition implies that the swing foot still can touch ground at  $T^d$  with an error of the unactuated variable. If there is an error on the impact moment,  $T \neq T^d$ , there will exist not only the error of configuration and velocity of unactuated variable  $\Delta q_u$ ,  $\Delta \dot{q}_u$ , but also that of controlled variables  $\Delta u$ ,  $\Delta \dot{u}$ . These errors can lead to unstable walking. The necessary condition  $Z_{sw}(T^d) \approx 0$  avoids the error on the impact moment, so the errors  $\Delta u$  and  $\Delta \dot{u}$  are avoided.

Next is how to choose  $M_1$  with this necessary condition. According to (1.98),  $Z_{sw}$  can be written with Taylor series:

$$Z_{sw}(q(T^d)) \approx Z_{sw}(q^d(T^d)) + a \Delta q_u + b \Delta q_u^2 \quad (1.99)$$

where  $a = \frac{\partial Z_{sw}(q^d(T^d))}{\partial q} M_T$  and  $b = \frac{1}{2} M_T' \frac{\partial^2 Z_{sw}(q^d(T^d))}{\partial q^2} M_T$ . Since the function of  $Z_{sw}(q(T^d))$  is highly nonlinear, here the first two terms of the Taylor series are considered, not only the first one.



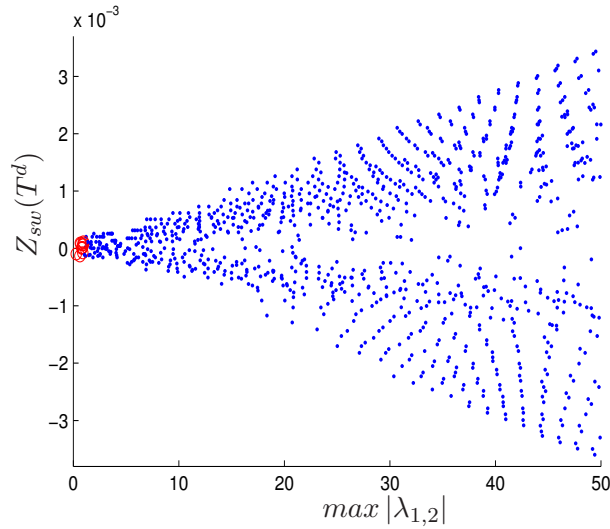


Figure 1.23: The height of the swing foot at the end of the step  $Z_{sw}(T^d)$  with respect to the effective eigenvalues of the Poincaré map,  $\max |\lambda_{1,2}|$ .

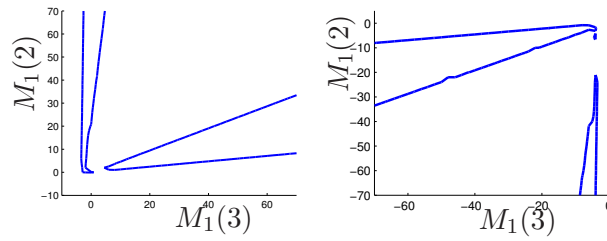


Figure 1.24: The stable domain of  $M_1(2)$  and  $M_1(3)$  for two groups of solution, which is described with contour line  $\max |\lambda_{1,2}| = 1$

If  $a$  and  $b$  satisfy:

$$a = b = 0 \quad (1.100)$$

$Z_{sw}(q(T^d))$  is close to zero for any  $\Delta q_u$ .

Two constraint equations exist in (1.100) for four components of  $M_1$ , so only two components can be chosen. The condition (1.100) leads to two groups of solution of  $M_1$ , because the equation  $b = 0$  is a second order equation as a function of  $M_1$ . For each group of solution,  $M_1(1)$  and  $M_1(4)$  are deduced from  $M_1(2)$  and  $M_1(3)$ . Then different  $M_1(2)$  and  $M_1(3)$  are searched to analyze the stability of the system, as a result, large stable domain of  $M_1$  for each group of solution are obtained, as shown in Fig. 1.24, it is described with contour line  $\max |\lambda_{1,2}| = 1$ . The system is always stable as long as  $M_1$  is chosen in these domains.

### 1.6.7 Comparison of three control laws

As soon as the stable domains of  $M_1$  are obtained, it is easy to choose the controlled outputs to yield stable walking. Since different selections of  $M_1$  may lead to different eigenvalues of the Poincaré map, which influence the properties of the control law. Therefore,  $M_1$  can be chosen according to the desired property. For example,  $M_1(2) = -4$  and  $M_1(3) = -3$  are chosen from the stable domains in Fig. 1.24, then the other two elements of  $M_1$  can be deduced from the condition (1.100) and we have  $M_1 = [1.91, -4, -3, -1.41]$ . The result of stability analysis with this  $M_1$  is  $\max |\lambda_{1,2}| = 0.2392$ . Then the planar biped's model in closed-loop is simulated with the same initial errors  $0.005 \text{ rad}$  and  $0.05 \text{ rad/s}$  introduced on  $q_u$  and its velocity respectively. The results are shown in Fig. 1.25 and Fig. 1.26.

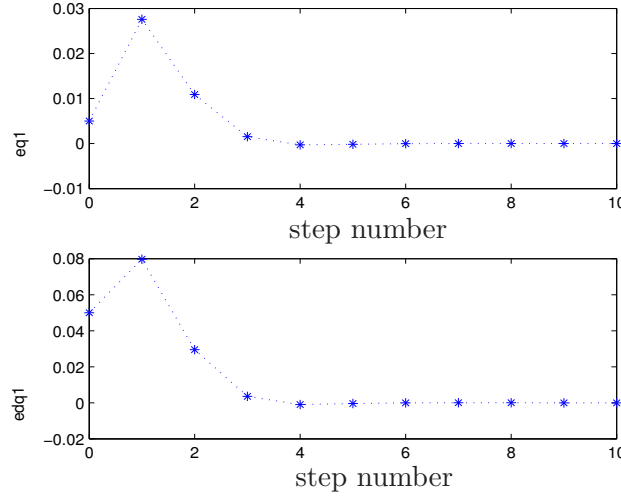


Figure 1.25: The difference of the real values and desired values of  $q_u$  and  $\dot{q}_u$  at the end of each step for the control law based on choice of controlled outputs with  $M_1 = [1.91, -4, -3, -1.41]$ .

Next, these results are compared to that of the control law based on tracking the parametrized reference trajectory, the event-based feedback control law and the same control law but with other controlled outputs, which has been shown in Subsection 1.6.5. Here the comparisons among three control methods are based on the same model of the robot, the same desired trajectory and the same method of stability analysis. It can give some conclusions as follows:

1) Comparing Fig. 1.25 and Fig. 1.26 with Fig. 1.20 and Fig. 1.22 respectively, it shows that when  $M_1 = [1.91, -4, -3, -1.41]$  and the result of stability analysis is  $\max |\lambda_{1,2}| = 0.2392$ , the tracking errors of unactuated variables  $q_u$  and  $\dot{q}_u$  converge to zero after walking 4 steps, that is better than the case of  $M_1 = [0, 0, -2.06, 0]$ , with which the result of stability analysis is  $\max |\lambda_{1,2}| = 0.7742$ . However, because the tracking errors at the end of the first step in Fig. 1.25 are bigger, the consumed torques during the second step are

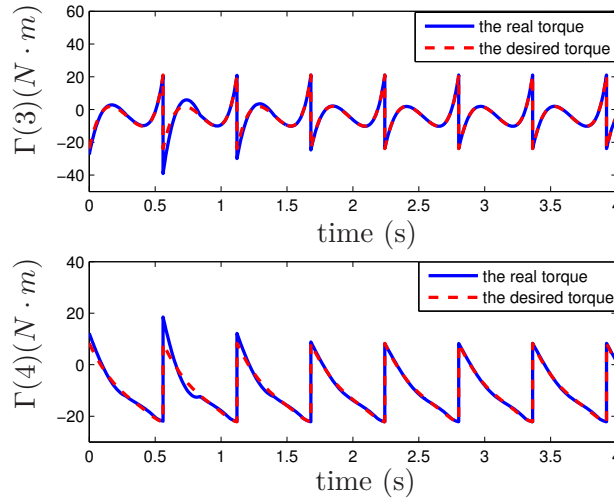


Figure 1.26: The torques of the swing leg for the control law based on choice of controlled outputs with  $M_1 = [1.91, -4, -3, -1.41]$ , where  $\Gamma(3)$  notes the torque of hip and  $\Gamma(4)$  notes the torque of knee.

bigger too. The comparisons show that the convergence properties of the control law based on choice of controlled outputs can be improved by selecting some  $M_1$ .

2) Comparing Fig. 1.25 and Fig. 1.26 with Fig. 1.16 and Fig. 1.18 respectively, it indicates that the walking with event-based control law needs more torques though the tracking errors converge more slowly.

3) Comparing Fig. 1.25 and Fig. 1.26 with Fig. 1.11 and Fig. 1.13 respectively, it shows that the tracking error of the position  $q_u$  with the control law for tracking the parametrized reference trajectory converges faster. Accordingly, its consumed torques are less than that of the control law based on the choice of controlled outputs. However, its tracking error of the velocity  $\dot{q}_u$  converges more slowly.

As stated above, the stability of walking can be improved by pertinent choice of controlled outputs, furthermore, it is possible to produce better convergent properties than the previous methods for this planar bipedal model.

## 1.7 Conclusions

This chapter presented three control laws for an under-actuated planar biped robot. The dynamic models of the studied robot during different walking phases are obtained using the method of Lagrange.

A previously studied control strategy for under-actuated biped robots is presented at first. It is called the method of virtual constraints, in which the reference trajectory is parameterized by a state quantity of the biped that is strictly monotonic along a typical walking gait. The stability analysis of the periodic walking gait under the closed-loop

control law is necessary since not all the configuration variables of the robot are controlled. Therefore, the principle of stability analysis using Poincaré map is presented. Moreover, in order to implement that in a reduced dimensional space, the zero dynamics is introduced. As a result, the stability of the closed-loop system with the control law can be analyzed in one-dimensional space.

Next, two control methods for tracking time-variant reference trajectory are proposed. One method is introducing event-based feedback control. It provides a modification term which is updated just after each impact for the reference trajectory to eliminate the tracking errors. The other method is based on choice of controlled outputs. The effect of controlled outputs selection on the walking stability was studied. It shows that the stable walking can be obtained by some pertinent choices of controlled outputs. However, these pertinent choices are not obvious. By studying some walking characteristics of many stable cases, we found that the height of swing foot is nearly zero for all the stable walking at the desired moment of impact for one step. Consequently, that is viewed as a necessary condition for stable walking proposed in this chapter. Based on this condition, the choice of controlled outputs is constrained, and then two stable domains for the controlled outputs selection are given.

Finally, the simulation results of three control methods are obtained and compared to each other. It shows that the walking with the control law for tracking parametrized reference trajectory is always stable. For the time-variant reference trajectory, the stable walking can be obtained by pertinent choice of controlled outputs or introducing event-based feedback control, where the converge properties of the former are better than that of the latter. Especially, its tracking error of the velocity converges faster than that of the first control method.

In summary, the main contributions of this chapter are:

- applying the event-based control law to the studied biped robot with time-variant reference trajectory.
- proposing a control law based on the choice of controlled outputs for the studied biped robot with time-variant reference trajectory.
- proposing a necessary condition for stable walking to choose the controlled outputs pertinently.

The work mentioned above has been presented in conferences *Humanoids'2009* [Wang et al., 2009], *IROS'2010* [Wang and Chevallereau, 2010b] and the complete version was published in the journal *Robotics and Autonomous Systems* [Wang and Chevallereau, 2011a].

# Chapter 2

## Walking control of a 3D biped robot

### 2.1 Introduction

In order to realize a stable walking of a biped robot considering rotation of stance foot during single support phase in Chapter 4, some stable walking control methods for a 3D biped robot with flat-feet are studied in this chapter. The principles of the walking control and stability analysis are almost the same as in Chapter 1. As shown in Fig. 2.2, the 3D robot which has 14 actuated joints is comprised of a torso and two identical legs that are independently actuated and terminated with flat-feet. The studied walking of this biped robot is composed of single support (SS) phases with flat foot and instantaneous double support phases. During every walking phase there is a corresponding dynamic model and condition of contact with the ground. Thus, an appropriate control law has to be implemented for each phase. Generally, the sequence of type of contact with the ground is imposed but it is obtained only when the conditions of ground reaction force, friction cone and zero moment point (ZMP) are satisfied. The ZMP firstly introduced by Vukobratovic [Vukobratovic et al., 1990] is the most important factor in achieving stable walking of humanoid robot. It is defined as a point about which the horizontal ground reaction moment of the ground reaction force is zero. When this point is inside the support polygon, the robot will not rotate about the edges of the foot and the foot remains flat on the ground.

In the early studies, many biped robots adopt a control strategy where the desired trajectories of joint angles are firstly designed based on the ZMP condition and then the feedback control is executed for the designed ones [Vukobratovic et al., 1990]. However, the contact condition cannot be satisfied in presence of perturbation. Therefore, at present almost all the walking controllers are applied to compensate for the ZMP error. However, the general weakness of those methods is that they require considerable experimental hand tuning and these methods are poorly documented [K.Hirai et al., 1998], [S.Kajita et al., 2003], [S.Kajita et al., 2006].

The control methods studied in this chapter will consider ground contact conditions and stability of walking. At first, in order to fully satisfy the conditions of contact, a control

law consisting of ZMP (zero moment point) controller, swing ankle rotation controller and partial joint angles controller is proposed. The ZMP controller guarantees that the stance foot remains in flat contact with the ground. The swing ankle rotation controller assures a flat foot impact at the end of the swinging phase. Each of these controllers creates 2 constraints on joint accelerations. Since there are 14 actuated joints in all, the partial joint angles controller is implemented to track only 10 independent variables. These controlled variables are defined as a linear combination of the 14 joint angles. The most important question addressed in this chapter is how this linear combination can be defined in order to insure a stable walking. The principle is the same as that of the control law based on choice of controlled outputs proposed in Chapter 1. In this chapter, the stability of the walking gait under closed-loop control is also evaluated with the linearization of the restricted Poincaré map of the hybrid zero dynamics. Furthermore, in order to study the influences of ZMP control on the stable walking, a control law without regulation of ZMP and two control laws only regulating one direction of ZMP respectively, i.e.,  $ZMP_x$  and  $ZMP_y$ , are presented and compared with the first control law and an earlier classical control law without the regulation of ZMP.

This chapter is organized as follows. At first, the studied robot is introduced in Section 2.2 and its dynamic models during different walking phases are presented in Section 2.3. Since the control law to be proposed is based on tracking of parametrized reference trajectory, the parametrization of the reference trajectory is introduced in Section 2.4. Next, a control law considering ground contact and stability is proposed in Section 2.5 and its simulation results are shown in Section 2.6. As a following work, Section 2.7 presents other four control laws where different directions of ZMP are regulated. Finally, the conclusions are given in Section 2.8.

## 2.2 Description of the studied biped robot

The studied biped robot is modeled based on HYDROID, which is a humanoid robot from the PHEMA Project (supported by the ANR and whose partners are LISV Versailles, IRCCyN, LNR Bordeaux and the hospital in Garches). An anthropomorphic robot is currently under construction at LISV, as shown in Fig. 2.1. It was designed as a part of the thesis of S. Alfayad [Alfayad, 2009]. The robot has 16 degrees of freedom: 3 at each ankle and hip, 1 at each knee and toe of each foot. However, the walking studied in this chapter does not include the rotation phase of the toe. Thus, two DOF associated with toes are ignored and the stance leg contacts the ground with flat-foot.

As a result, the studied robot is modeled as Fig. 2.2 [Tlalolini, 2008]. It has a torso and two identical legs with flat-feet. Each hip and ankle consists of a revolute joint with 3 DOF and the knee is a 1 DOF revolute joint, and each DOF is independently actuated. As a result, it has 14 DOF in the single support phase and 14 actuators. The joints' configurations are denoted by

$$q = [q_1, \dots, q_{14}]^T \quad (2.1)$$

where  $q_j$ ,  $j \in (1, \dots, 14)$  corresponds to the rotation about  $z_j$ . It's worth noting that the

coordinate system  $x_0y_0z_0$  is fixed on the support foot while the coordinate system  $x_sy_s z_s$  is fixed on the ground and it is called the absolute coordinate system. The origins of them are the same only during the first walking step.



Figure 2.1: Photo of HYDROID

The length and mass of each body are given in Table 2.1 and Table 2.2. All links are assumed to be massive and rigid. The inertia of each link is also taken into account, and other parameters of the robot in detail are shown in [Tlalolini et al., 2011] and [Rengifo, 2010].

$d_1, d_{15}$	$d_4, d_{12}$	$d_5, d_{11}$	$d_8$	$l_1, l_{15}$	$l_p$	$L_p$
0.185	0.392	0.392	0.190	0.05925	0.08	0.207

Table 2.1: length parameters (m)

<i>body</i>	<i>foot</i>	<i>shin</i>	<i>thigh</i>	<i>torso</i>
<i>kg</i>	0.678	2.188	5.025	24.97

Table 2.2: mass parameters

## 2.3 Dynamic model during different walking phases

The walking gait consists of single support phases where the stance foot is flat on the ground separated by impacts, that is, instantaneous double support phases where leg exchange takes place. The dynamic models for every walking phase are derived here by assuming support on leg 1. They are described as follows, and the models for support on leg 2 can be written in a similar way.

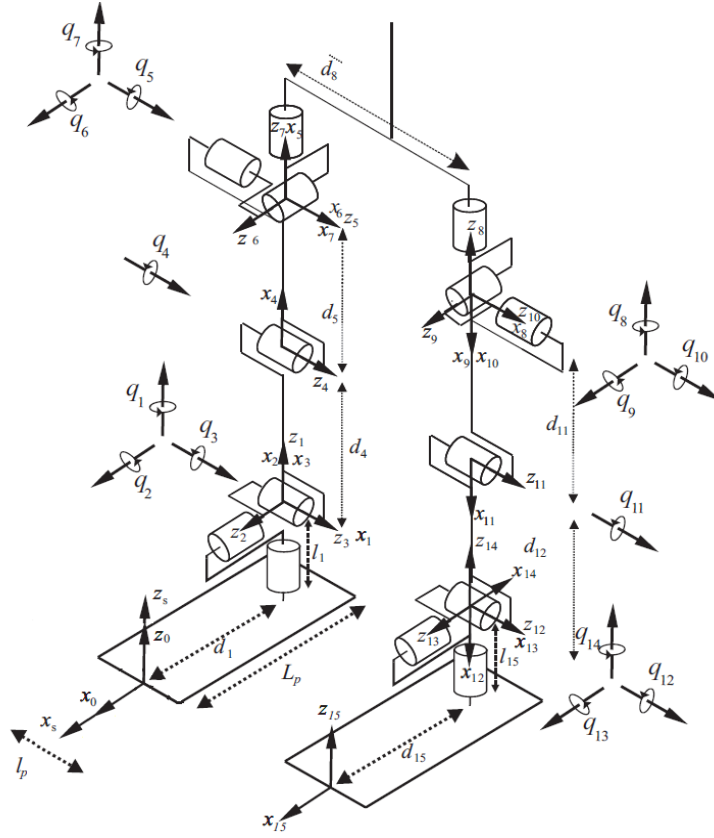


Figure 2.2: Biped Model

### 2.3.1 Swing phase model

The Newton-Euler algorithm is used to calculate the dynamic model of 3D biped robot during the single support phase [Tlalolini et al., 2010], [Tlalolini et al., 2011]. The actuator torques and the ground reaction (forces and torques) to the stance foot can be computed as soon as the joint position, velocity and acceleration are known, and they are linear functions of the acceleration  $\ddot{q}$ . Consequently, the dynamic model is represented as:

$$\begin{bmatrix} F \\ M \\ \Gamma \end{bmatrix} = NE(q, \dot{q}, \ddot{q}) = NE_1(q)\ddot{q} + NE_2(q, \dot{q}) \quad (2.2)$$

where  $NE_1(q)$  denotes all the coefficient terms of  $\ddot{q}$  and  $NE_2(q, \dot{q})$  denotes all the terms without  $\ddot{q}$  in the expression of  $NE(q, \dot{q}, \ddot{q})$  and it includes Coriolis, centrifugal and gravitational terms.  $\Gamma = [\Gamma_1, \dots, \Gamma_{14}]^T$  describes the torque of the actuated joints. Its calculation will be used in the control law.  $F$  and  $M$  compose the wrench vector exerted by the ground on the stance foot. They are expressed in the frame  $R_0: x_0y_0z_0$  and they will be used to calculate the position of ZMP.



### 2.3.2 ZMP dynamics

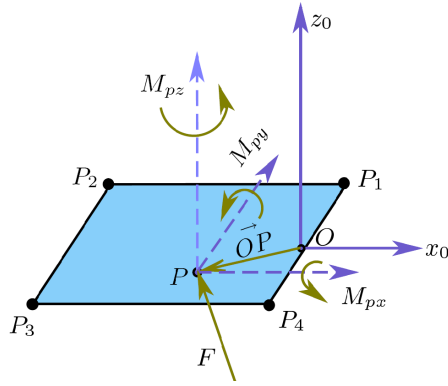


Figure 2.3: The support foot

When foot-1 is on the ground, a ground reaction force and moment can be expressed about any point in the support plane. If a point  $P$  is in the plane of the foot-1 (see Fig. 2.3), the ground reaction moment  $M_p$  of  $P$  can be calculated by:

$$M_p = M - \vec{OP} \times F \quad (2.3)$$

where  $\vec{OP}$  is the vector of  $OP$  in the reference frame  $x_0y_0z_0$ . Considering  $F, M$  are functions of  $q, \dot{q}, \ddot{q}$  and linear functions of the acceleration  $\ddot{q}$  (see (2.2)), the components of  $M_p$  along the axes  $x_0$  and  $y_0$  can be written as:

$$\begin{bmatrix} M_{px} \\ M_{py} \end{bmatrix} = f(q, \dot{q}, \ddot{q}, \vec{OP}) = W\ddot{q} + H \quad (2.4)$$

where the function  $f()$  in (2.4) depends on (2.2) and (2.3), and  $W, H$  can be obtained by:

$$H = f(q, \dot{q}, \ddot{q} = \mathbf{0}_{14 \times 1}, \vec{OP}), \quad (2.5)$$

and

$$\begin{cases} W(:, i) = f(q, \dot{q}, \ddot{q} = \mathbf{e}_{14 \times 1}, \vec{OP}) - H \\ \mathbf{e}(i) = 1, \quad i \in \{1, 2, \dots, 14\} \\ \mathbf{e}(j) = 0, \quad j \in \{1, 2, \dots, 14\} \quad \text{and} \quad j \neq i \end{cases} \quad (2.6)$$

(2.4) can be used to constrain the acceleration  $\ddot{q}$  in order that the ZMP which is such that

$$M_{px} = M_{py} = 0 \quad (2.7)$$

is at a desired point  $P$ .

### 2.3.3 Impact model

A passive impact exists at the end of the single support phase. After that, the legs swap their roles from one step to the next. Considering that the robot is symmetric, we only study a single step to deduce the complete behavior of the robot over a sequence of steps on alternating legs. In Subsection 1.3.3, the obtained model of the planar biped robot (1.22) has shown that during impact phase the biped's configuration variables do not change, but the generalized velocities undergo a jump. Therefore, the impact model for the 3D biped robot can also be written as:

$$\begin{cases} q^+ &= E q^- \\ \dot{q}^+ &= EI(q^-)\dot{q}^- \end{cases} \quad , \quad (2.8)$$

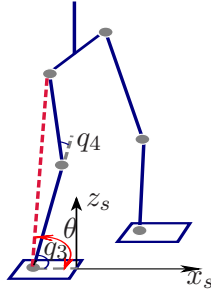
where  $-$  and  $+$  denotes the moment just before and after impact respectively,  $I(q^-)$  represents the linear jump of the joint velocity after impact and it can be calculated by the Newton-Euler algorithm (2.2) and the form of (1.11) (see [Tlalolini et al., 2010], [Tlalolini, 2008] and [Rengifo, 2010]).  $E_{14 \times 14}$  is the permutation matrix describing leg's exchange and it has been given in [Rengifo, 2010].

## 2.4 Parametrization of the reference trajectory

Starting with a reference trajectory of joint angles described as a function of time  $q^d(t)$  which has been off-line calculated through the minimization of the energy consumption in [Tlalolini, 2008], a new parametrization is proposed. Its principle has been explained in Subsection 1.4.1. By using this method, the stability can be analyzed in a lower dimensional space. In addition, only the kinematic evolution of the robot's state is regulated but not its temporal evolution. This means the control law is defined to follow a joint path but not a joint motion. It was used successfully for the walking of bipeds with point feet [Chevallereau et al., 2003], [Plestan et al., 2003], [Westervelt et al., 2003], [Chevallereau et al., 2009] and planar biped with foot rotation [Chevallereau et al., 2008]. Especially in [Chevallereau et al., 2008], this method allows the simultaneous control of the joint path and the ZMP. Moreover, it is helpful in regulating the position of ZMP in the sagittal plane. Therefore, it is still used for the 3D biped robot with flat feet but the regulation of ZMP in the frontal plane should be considered in the control law. The parametrized reference trajectory is given as follows.

It is well known that  $q^d(t)$  should be parametrized by a quantity depending on the state of the robot that is strictly monotonic like time  $t$  during the walking phase. As the same as Subsection 1.4.1, in the sagittal plane the angle of a virtual stance leg defined by the line that connects the stance foot to the stance hip is chosen to replace the time  $t$  to parametrize the reference trajectory. As shown in Fig. 2.4, because the shin and the thigh have the same length, this angle can be computed by:

$$\theta = q_3 + q_4/2. \quad (2.9)$$

Figure 2.4: The definition of  $\theta$ .

Next, similar to (1.26), a one-dimensional Bezier polynomials [Bezier, 1972] with order  $J = 11$ <sup>1</sup> is chosen to describe the reference trajectory. It is:

$$h^d(s) = \sum_{k=0}^J \alpha_k \frac{J!}{k!(J-k)!} s^k (1-s)^{J-k}, \quad (2.10)$$

where the coefficient  $\alpha_k$  is determined to minimize the distance between the optimal trajectory and reference trajectory at the discrete points.

$$s = \frac{\theta - \theta_i}{\theta_f - \theta_i} \quad (2.11)$$

is the normalized parameter varying on the cyclic motion from 0 to 1.  $\theta_i$  and  $\theta_f$  are the values of  $\theta$  at the beginning and end of a step respectively. The reference path  $h^d(s)$  which is exactly  $h^d(\theta)$  is designed in order to satisfy the conditions of contact and to be periodic including the impact model.  $h^d(\theta)$  is such that:

$$\begin{cases} q^d(t) &= h^d(\theta) \\ \dot{q}^d(t) &= \frac{\partial h^d(\theta)}{\partial \theta} \dot{\theta} \\ \ddot{q}^d(t) &= \frac{\partial^2 h^d(\theta)}{\partial \theta^2} \dot{\theta}^2 + \frac{\partial h^d(\theta)}{\partial \theta} \ddot{\theta} \end{cases} \quad (2.12)$$

According to a known reference trajectory  $q^d(t)$ ,  $\dot{q}^d(t)$ ,  $\ddot{q}^d(t)$ , in (2.12)  $h^d(\theta)$ ,  $\frac{\partial h^d(\theta)}{\partial \theta}$  and  $\frac{\partial^2 h^d(\theta)}{\partial \theta^2}$  can be deduced and they are assumed to be known in the following contents. Similarly, for every  $q^d(t)$ , there is a correspond  $\theta$  and  $ZMP^d(t)$ , then the desired position of ZMP can be described by  $\theta$  and it is written as:  $ZMP^d(\theta)$ .

## 2.5 A control law considering ground contact and stability

As shown in Fig. 2.5, the overall control law consists of ZMP controller, swing ankle rotation controller and partial joint angles controller. The former two controllers are used

<sup>1</sup>This high order is chosen to limit the difference between the optimal acceleration and reference acceleration, a smaller order can also be used.

to achieve  $ZMP = ZMP^d(\theta)$  and force the pitch and roll angle of the swing foot to be their desired values, which can lead to a good landing condition and that is helpful to insure a good contact in the next step. The third controller implements the joint path control and it is partial since the torques are already partially defined by the former two controllers. In addition, in order to create a continue and cyclic desired trajectory, the reference motion is modified after the impact phase, which has been presented in Subsection 1.5.3.

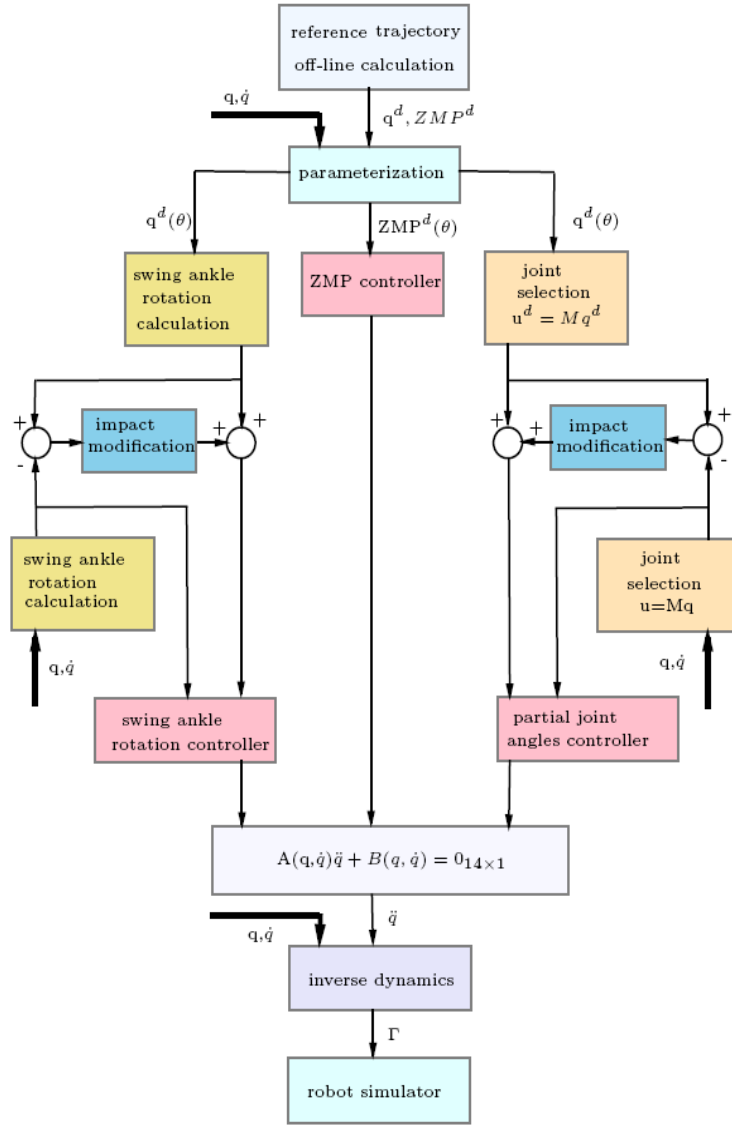


Figure 2.5: Block diagram of the control system.

### 2.5.1 ZMP controller

The objective of this controller is to obtain:

$$ZMP = ZMP^d(\theta). \quad (2.13)$$

According to the definition of ZMP, if  $P$  in Fig. 2.3 is  $ZMP^d(\theta)$ , (2.4) can be rewritten as:

$$W(q, \dot{q})\ddot{q} + H(q, \dot{q}) = \mathbf{0}_{2 \times 1} \quad (2.14)$$

where  $W$  and  $H$  are recalculated by (2.5) and (2.6) with  $\vec{OP} = ZMP^d(\theta)$ . Since our control law is a computed-torque control, the calculation of  $\ddot{q}$  is obligatory to obtain the torques  $\Gamma$  using Newton-Euler method (see (2.2)), the equation (2.14) offers two constraints to solve the acceleration  $\ddot{q}$ .

### 2.5.2 Swing ankle rotation controller

In the ZMP controller, 2 positions of ZMP in the horizontal plane are regulated to the desired ZMP, that can offer 2 dynamic equations about the joint angle, its velocity and acceleration (see (2.14)). Thus, only other  $n - 2$  outputs can be defined (where  $n = 14$  is the number of actuated joints), that means not all the joints can be controlled. Because all of our work is done with a hypothesis that the ground is flat, therefore, if the motion of all the joints cannot track the desired trajectory, the swing leg will not touch the ground with flat-foot. As a result, the support foot in the next step will not be flat, then the control law will not be valid. Thus, another controller to insure a good landing condition is necessary in the case of that not all the joint angles  $q$  are controlled. Here it is called swing ankle rotation controller and its objective is to offer some constraints about the states of the robot  $q, \dot{q}, \ddot{q}$  to force the swing foot to be flat just before impact in order to ensure that the next impact will occur in a good way. Thus the pitch and roll angle of the swing foot are controlled to track their desired values.

As shown in Fig. 2.2, the ankle with joint angles  $q_1$  denotes the ankle of the support foot. The angle  $q_{14}$  is the rotation angle of the 14<sup>th</sup> joint around the axes  $z_{14}$ . Since  $q_{14}$  does not affect whether the swing foot is flat or not, only the previous 13 joints are constrained.  ${}^sR_{13}$  denotes a  $3 \times 3$  orientation matrix from the coordinate system  $x_s y_s z_s$  to  $x_{13} y_{13} z_{13}$ :

$${}^sR_{13} = [s, n, a], \quad (2.15)$$

where  $s$ ,  $n$  and  $a$  are unitary vectors defining  $x_{13} y_{13} z_{13}$  in frame  $R_s$  respectively.  ${}^sR_{13}^d = [s^d, n^d, a^d]$  denotes the desired orientation of transformation matrix  ${}^sR_{13}$ . Small error in the orientation of the swing ankle can be defined as  $\xi$  [Luh et al., 1980]:

$$\xi = \frac{1}{2}(s \times s^d + n \times n^d + a \times a^d). \quad (2.16)$$

The derivatives of the orientation error are:

$$\begin{cases} \dot{\xi} = {}^s\omega_{13}^d - {}^s\omega_{13} \\ \ddot{\xi} = {}^s\dot{\omega}_{13}^d - {}^s\dot{\omega}_{13} \end{cases} \quad (2.17)$$

where  ${}^s\omega_{13}$  and  ${}^s\dot{\omega}_{13}$  are the angular velocity and acceleration of the joint 13 in the absolute coordinate system  $x_sy_s z_s$ .  ${}^sR_{13}$ ,  ${}^s\omega_{13}$  and  ${}^s\dot{\omega}_{13}$  in (2.15) can be efficiently computed by the forward recursive equations of the general serial robot with  $q_1, \dots, q_{13}$ , their velocity and acceleration [Khalil and Dombre, 2002] (see Appendix A.1).

Because a fact the swing foot is flat or not does not depend on the rotation components around  $z_s$  axis (see Fig. 2.2), only the first two components of  $\xi$  have to be regulated to zero:

$$\xi_{xy} = \mathbf{0}_{2 \times 1} \quad (2.18)$$

Here and in the following subsections the subscript "xy" denotes the first two lines of the vector, which correspond to the rotation around  $x_s$  direction and  $y_s$  direction respectively. (2.18) can be achieved by the PD controller:

$$\ddot{\xi}_{xy} + \frac{K_1}{\varepsilon} \dot{\xi}_{xy} + \frac{K_2}{\varepsilon^2} \xi_{xy} = \mathbf{0}_{2 \times 1}. \quad (2.19)$$

with  $K_1 > 0$ ,  $K_2 > 0$ , and  $\varepsilon > 0$ .

It is worth mentioning that the stance foot is supposed to be in flat contact with the ground, so the  $xy$  plane of  $x_0y_0z_0$  and the absolute coordinate system  $x_sy_s z_s$  are coplanar. As a consequence, (2.19) is still valid if the orientation of transformation matrix  ${}^0R_{13}$  is used instead of  ${}^sR_{13}$ . This assumption avoids absolute orientation measures. That means the control law of biped robot can be formulated using only relative joint positions  $q$ .

### 2.5.3 Partial joint angles controller

Besides of the former two sub-controllers, the control law is also designed to track the joint reference path  $q^d = h^d(\theta)$ . Unfortunately, (2.14) and (2.19) have offered 4 restrictions about the states of robot  $q, \dot{q}, \ddot{q}$ , so we can't control  $q = q^d$  directly and we only can choose 10 targets to track with. Thus, how to choose 10 controlled variables from 14 actuated joints is presented at first.

From the principle of swing ankle rotation controller, we know that the swing foot will be flat before impact under the constrain of 2 equations. It means that 2 joint angles can be determined by the other 11 joint angles in  $q_1, q_2, \dots, q_{13}$  according to the definition of  $\xi_{xy}$  in (2.15) and (2.16). Because the swing ankle is actuated by the 12<sup>th</sup> and 13<sup>th</sup> joint (see Fig. 2.2), so we can suppose that  $q_{12}$  and  $q_{13}$  have been defined using  $q_1, q_2, \dots, q_{11}$ . Thus there is no need to consider them again in the partial joint angles controller. In addition, Section 2.4 has presented that all the reference trajectory are parametrized by  $\theta$  and  $\theta = q_3 + 0.5q_4$ , so the desired trajectory for  $q_3$  and  $q_4$  are correlative:  $q_3^d(\theta) = \theta - 0.5q_4^d(\theta)$  and if  $q_4$  follows  $q_4^d$ ,  $q_3$  will also follow  $q_3^d$ . Thus only one of these two joint configuration  $q_3$  or  $q_4$  has to be controlled. As a consequence  $q_3$  is excluded here. Therefore, the joint angles that are not directly controlled via the parametrization of the reference trajectory and the swing ankle controller are:

$$Q_r = [q_1, q_2, q_4, \dots, q_{11}, q_{14}]_{11 \times 1}^T \quad (2.20)$$

$Q_r$  has 11 elements but only 10 controlled outputs can be defined. Since the second joint influences the lateral position of ZMP directly, in order to distinguish  $q_2$  from other joints in  $Q_r$  and avoid singularity in the control law, the controlled joint angles are chosen as:

$$u = Q + M_1 q_2 \quad (2.21)$$

with

$$Q = [q_1, q_4, \dots, q_{11}, q_{14}]_{10 \times 1}^T, \quad (2.22)$$

where  $M_1$  is a  $10 \times 1$  constant matrix to be determined. The next section will show that the choice of  $M_1$  affects the stability of the control law, in the sense of the convergence toward cyclic motion. The stability condition will be a criteria used to select  $M_1$ . The principle is the same as that proposed in Subsection 1.5.2.

The objective of this controller is to regulate  $u$  to track its desired value  $u^d(\theta)$ . It is regulated by a PD control:

$$\ddot{u} - \ddot{u}^d + \frac{K_d}{\varepsilon}(\dot{u} - \dot{u}^d) + \frac{K_p}{\varepsilon^2}(u - u^d) = \mathbf{0}_{10 \times 1}, \quad (2.23)$$

where  $u^d$ ,  $\dot{u}^d$ ,  $\ddot{u}^d$  can be calculated using the definition of  $u$  in (2.21) and the referenced trajectory  $q^d$ ,  $\dot{q}^d$ ,  $\ddot{q}^d$  in (2.12).

It should be noted that if  $u = u^d(\theta)$ , according to (2.21),  $Q$  is such that:

$$Q = Q^d - M_1(q_2 - q_2^d). \quad (2.24)$$

(2.24) implies that this controller can also be regarded as an on-line modification of the joint reference trajectory, which is like many existent methods. However, the advantage of our controller is that the effect of this on-line modification (or the choice of  $M_1$  in (2.24)) on stability will be studied.

#### 2.5.4 Modification of the tracked errors caused by impact

Based on the proposed three sub-controllers, the desired properties respectively are:

$$\begin{cases} y_1 &= ZMP - ZMP^d(\theta) = 0 \\ y_2 &= \xi_{xy} = 0 \\ y_3 &= u - u^d(\theta) = 0 \end{cases} \quad (2.25)$$

These sub-controllers only act for each single support phase and the impacts are passive. The reference trajectory  $u^d$  and  $ZMP^d$  are defined by taking into account the impact phase. If the desired states of robot can be obtained before the impact, the desired states after impact will be obtained too. The impact condition is a geometric condition. Thus, it can occur with some errors, especially with some errors on  $\theta$  and  $q_2$  because they are not controlled directly as other states in  $u$ . As a result, large errors on the joint position and velocity will be created after impact, that means discontinuity on  $u$  will appear because  $u^d$  and its derivatives are functions of  $\theta$  and its derivatives.

In order to avoid the discontinuity, the reference trajectory in (2.25) are modified stride to stride so that they are compatible with the initial state of the robot at the beginning of each step. The modification principle is like that has been proposed in Subsection 1.5.3. Here it is not necessary to modify  $ZMP^d(\theta)$  because the acceleration acts directly on the position of ZMP thus the discontinuities are acceptable. The new output for the feedback control design is:

$$\begin{cases} y_1 &= ZMP - ZMP^d(\theta) = 0 \\ y_{2c} &= \xi_{xy} - \xi_{xyc} = 0 \\ y_{3c} &= u - u^d(\theta) - u_c = 0 \end{cases} \quad (2.26)$$

Here  $\xi_{xyc}$  and  $u_c$  are modification terms of the original reference motions. The calculation of them is presented as follows.

Like the equation (1.70) proposed in Subsection 1.5.3, the function  $u_c$  is taken to be a four-order continuously differentiable linear function of  $\theta$ :

$$u_c = a_0 + a_1\theta + a_2\theta^2 + a_3\theta^3 + a_4\theta^4, \quad (2.27)$$

where the coefficients  $a_0, \dots, a_4$  are defined such that<sup>2</sup>

$$\begin{cases} u_c(\theta_i) &= y_{3i} \\ \frac{\partial u_c}{\partial \theta}(\theta_i) &= \frac{\dot{y}_{3i}}{\dot{\theta}_i} \\ u_c(\theta) &\equiv 0, \quad \theta \geq \frac{\theta_i^d + \theta_f^d}{2}. \end{cases} \quad (2.28)$$

where  $y_{3i}$  and  $\dot{y}_{3i}$  denote the initial values of  $y_3$  and  $\dot{y}_3$ , and they are updated at the beginning and held constant throughout the step. Specifically,  $y_{3i} = u_i - u^d(\theta_i)$  and  $\dot{y}_{3i} = \dot{u}_i - \dot{u}^d(\theta_i)$ . Here  $\theta_i^d$  and  $\theta_f^d$  are the desired initial and final value of  $\theta$  defined from  $q_i$  to  $q_f$  respectively, and they can be calculated by (2.9). As shown in Fig. 1.7, by using  $u_c$  defined in this way, the new reference trajectory starting with the current state just after the impact, are smoothly joined to the original reference trajectory at the middle of the step. In particular, for any initial error, the initial reference trajectory  $u^d$  is not modified in the second part of the step when  $\theta \geq \frac{\theta_i^d + \theta_f^d}{2}$ .

Similarly, the function of  $\xi_{xyc}$  in (2.26) is defined as the same format as (2.27):

$$\xi_{xyc} = c_0 + c_1\theta + c_2\theta^2 + c_3\theta^3 + c_4\theta^4, \quad (2.29)$$

where all the coefficients  $c_0, \dots, c_4$  are determined using the value of  $y_2$  (see (2.25)) and  $\dot{y}_2$  at the beginning of each step, that is:

$$\begin{cases} \xi_{xyc}(\theta_i) &= y_{2i} \\ \frac{\partial \xi_{xyc}}{\partial \theta}(\theta_i) &= \frac{\dot{y}_{2i}}{\dot{\theta}_i} \\ \xi_{xyc}(\theta) &\equiv 0, \quad \theta \geq \frac{\theta_i^d + \theta_f^d}{2}. \end{cases} \quad (2.30)$$

---

<sup>2</sup>The four order polynomial is used for  $\theta_i \leq \theta \leq \frac{\theta_i^d + \theta_f^d}{2}$ ; Continuity of position, velocity and acceleration is ensured at  $\theta = \frac{\theta_i^d + \theta_f^d}{2}$ .



Next, substituting these modification terms into the PD control expressions (2.19) and (2.23), we have:

$$\ddot{\xi}_{xy} - \ddot{\xi}_{xyc} + \frac{K_1}{\varepsilon}(\dot{\xi}_{xy} - \dot{\xi}_{xyc}) + \frac{K_2}{\varepsilon^2}(\xi_{xy} - \xi_{xyc}) = \mathbf{0}_{2 \times 1} \quad (2.31)$$

$$\ddot{u} - \ddot{u}^d - \ddot{u}_c + \frac{K_d}{\varepsilon}(\dot{u} - \dot{u}^d - \dot{u}_c) + \frac{K_p}{\varepsilon^2}(u - u^d - u_c) = \mathbf{0}_{10 \times 1} \quad (2.32)$$

### 2.5.5 Calculation of the input torques

With the proposed three sub-controllers, 14 equations about  $q, \dot{q}, \ddot{q}$  are obtained by (2.14), (2.19) and (2.23). Considering the impact modifications, the latter two sub-controllers are replaced by (2.31) and (2.32) to satisfy (2.26). Moreover, in (2.31) and (2.32),  $\ddot{\xi}_{xy}$ ,  $\ddot{\xi}_{xyc}$ ,  $\ddot{u}$ ,  $\ddot{u}^d$  and  $\ddot{u}_c$  are linear functions of  $\ddot{q}$ , so the two equations can be rewritten as the same format as (2.14), and they are:

$$W_s(q, \dot{q})\ddot{q} + H_s(q, \dot{q}) = \mathbf{0}_{2 \times 1} \quad (2.33)$$

and

$$W_j(q, \dot{q})_{10 \times 14}\ddot{q} + H_j(q, \dot{q})_{10 \times 1} = \mathbf{0}_{10 \times 1}, \quad (2.34)$$

where  $W_s(q, \dot{q})$ ,  $W_j(q, \dot{q})$  denotes all the coefficient terms of  $\ddot{q}$  and  $H_s(q, \dot{q})$ ,  $H_j(q, \dot{q})$  denotes all the terms without  $\ddot{q}$  in (2.31) and (2.32) respectively. The detail is presented in Appendix A.2 and A.3.

Thus, 14 new equations about  $q, \dot{q}, \ddot{q}$  can be combined as:

$$A(q, \dot{q})\ddot{q} + B(q, \dot{q}) = \mathbf{0}_{14 \times 1}, \quad (2.35)$$

with  $A = [W, W_s, W_j]^T$  and  $B = [H, H_s, H_j]^T$ . Next, the  $\ddot{q}$  can be resolved by using (see Appendix A.5):

$$\ddot{q} = -A^{-1}B \quad (2.36)$$

Then, the desired torques  $\Gamma$  can be calculated with  $\ddot{q}$ ,  $\dot{q}$  and  $q$  by using the inverse dynamics via Newton-Euler algorithm (2.2).

### 2.5.6 Hybrid zero dynamics

Subsection 1.4.3 has presented the principle of stability analysis in a reduced dimensional space using Poincaré method with the help of zero dynamics and hybrid zero dynamics (HZD).

According to the definitions of HZD, the controller with impact modifications (2.14), (2.31) and (2.32) creates the HZD, with which the behavior of the robot is completely defined by the impact map and the zero dynamics during swing phase (2.26). The Poincaré section is chosen at  $\theta = 0.4\theta_i^d + 0.6\theta_f^d$ . At this instant the swing foot does not touch the ground, and since  $\theta \geq \frac{\theta_i^d + \theta_f^d}{2}$  the value of the controlled variables are not affected by  $u_c$

and  $\xi_{xyc}$  (see Fig. 1.7). A restricted Poincaré map is defined from  $S_\theta \cap Z$  to  $S_\theta \cap Z$ , where  $Z = \{(\theta, q, \dot{q}) | y_1 = 0, y_{2c} = 0, \dot{y}_{2c} = 0, y_{3c} = 0, \dot{y}_{3c} = 0\}$  (see (2.26)) and  $S_\theta = \{(\theta, q, \dot{q}) | \theta = 0.4\theta_i^d + 0.6\theta_f^d\}$  is the Poincaré section. The key point is that the state of the robot can be parametrized by three independent variables  $x = [q_2, \dot{q}_2, \dot{\theta}]^T$  in  $S_\theta \cap Z$ . The reduction of the states dimension is explained as follows.

In  $S_\theta \cap Z$ ,  $u_c = 0$  and  $\xi_{xyc} = 0$ , thus the third line of (2.26) yields  $u = u^d$ . Based on the definition of  $u$  in (2.21), we have:

$$Q = u^d(\theta) - M_1 q_2. \quad (2.37)$$

We can see that  $Q$  is determined by  $\theta$ ,  $q_2$  and  $M_1$ . Similarly, the second line of (2.26) gives  $\xi_{xy} = 0$ , in this case  $q_{12}$  and  $q_{13}$  can be calculated by  $q_1, q_2, \dots, q_{11}$  according to the definition of  $\xi_{xy}$  in (2.15) and (2.16). Furthermore, from the definition of  $Q$  and  $\theta$  (see (2.22), (2.23) and (2.37)), we can deduce that  $q_{12}$  and  $q_{13}$  depends on  $q_2$ ,  $\theta$  and  $M_1$ . Thus the calculation of  $q_{12}$  and  $q_{13}$  can be denoted as a function  $f_q()$ :

$$[q_{12}, q_{13}] = f_q(q_2, \theta, M_1). \quad (2.38)$$

(2.22) and (2.9) imply that there exists a linear relation between  $q$  and  $Q$ ,  $q_{12}$ ,  $q_{13}$ ,  $\theta$ ,  $q_2$ :

$$q = M_{14} [Q, q_{12}, q_{13}, \theta, q_2]_{14 \times 1}^T \quad (2.39)$$

where  $M_{14}$  is a  $14 \times 14$  constant matrix.

Equations (2.37) and (2.39) show that the full configuration of the robot  $q$  is determined by  $q_2$ ,  $\theta$ ,  $M_1$  and the reference trajectory. Consequently, a simplified expression of  $q, \dot{q}$  is defined as:

$$[q, \dot{q}] = f_{HZD}(q_2, \theta, \dot{q}_2, \dot{\theta}, M_1, C_{q^d}) \quad (2.40)$$

where  $C_{q^d}$  denotes all the known terms introduced by the reference trajectory  $q^d$  and its derivatives.

In consequence the acceleration  $\ddot{q}$  can be expressed as a function of  $q_2$ ,  $\theta$ ,  $\dot{q}_2$ ,  $\dot{\theta}$ ,  $\ddot{q}_2$ ,  $\ddot{\theta}$  and it depends on  $M_1$  and  $C_{q^d}$ . Thus (2.26) corresponds to:

$$\begin{cases} W_{HZD}(q, \dot{q}) \begin{bmatrix} \ddot{q}_2 \\ \ddot{\theta} \end{bmatrix} + H_{HZD}(q, \dot{q}) = \mathbf{0}_{2 \times 1} \\ [q, \dot{q}] = f_{HZD}(q_2, \theta, \dot{q}_2, \dot{\theta}, M_1, C_{q^d}) \end{cases} \quad (2.41)$$

Apparently, the second line of (2.41) is obtained by swing ankle rotation controller and partial joint angles controller, which have been supposed to be perfect according to the definition of zero dynamics. The first line of (2.41) is deduced by the ZMP controller (2.14), where  $W_{HZD}(q, \dot{q})$  denotes all the coefficient terms of  $\ddot{q}_2$  and  $\ddot{\theta}$ , and  $H_{HZD}(q, \dot{q})$  denotes all the terms without these terms. Their calculations are given in Appendix A.4.

Obviously, with definition of  $HZD$ , (2.41) can replace the original resulted dynamic equation (2.35) to describe the behavior of the robot from the Poincaré section until the impact. Just before the impact the complete sates of the robot are calculated by using the

second line of (2.41). Then the model of impact is used and  $u_c$ ,  $\xi_{xyc}$  can be calculated. The behaviour of the robot from the beginning of the next step to the Poincaré section is then calculated by equation of HZD that is similar to (2.41) but includes the modification terms of the reference trajectory  $u_c$ ,  $\xi_{xyc}$ .

### 2.5.7 Stability analysis at a fixed-point

It has been proposed that if the dimension of the state space is  $n$  and the relative degree of the system is  $r$ , the dimension of its zero dynamics system is  $n - r$  [Sira-Ramirez, 1990], [Varghese et al., 1991]. For the studied robot the dimension of the state space is  $n = 2 \times 14$ , the relative degree of ZMP controller is zero and that of other two sub-controllers are 2 for each controlled output so the dimension of HZD is  $2 \times 14 - (2 + 10) \times 2 = 4$ . The equation (2.41) shows that these 4 variables are  $q_2, \dot{q}_2, \theta, \dot{\theta}$ . In fact, for the stability analysis, the Poincaré section is chosen such that  $\theta = \theta^*$ , thus the dimension of Poincaré return map is just 3.

The known cyclic motion  $q^d(\theta)$  gives a fixed-point  $x^{z*} = (q_2^d(\theta^*), \dot{q}_2^d(\theta^*), \dot{\theta}^*)$  for the proposed control law for any value of  $M_1$ , where  $\theta^* = 0.4\theta_i^d + 0.6\theta_f^d$ .

The restricted Poincaré map  $P^z : S_\theta \cap Z \rightarrow S_\theta \cap Z$  induces a discrete-time system  $x_{k+1} = P^z(x_k)$ . [Morris and Grizzle, 2009] states that, for  $\varepsilon$  sufficiently small in (2.31) and (2.32), *the linearization of  $P^z$  about a fixed-point determines exponential stability of the full order closed-loop robot model*. Define  $\delta x_k = x_k - x^*$ , the Poincaré map linearized about the fixed-point  $x^*$  gives rise to a linearized system,

$$\delta x_{k+1} = A^z \delta x_k, \quad (2.42)$$

where the  $(3 \times 3)$  square matrix  $A^z$  is the Jacobian matrix of the Poincaré map, and it can be calculated using:

$$A^z = \begin{bmatrix} A_1^z & A_2^z & A_3^z \end{bmatrix}_{3 \times 3}$$

with

$$A_i^z = \frac{P^z(x^{z*} + \Delta x_i^z) - P^z(x^{z*} - \Delta x_i^z)}{2\Delta x_i^z}, \quad i = 1, 2, 3 \quad (2.43)$$

$$\text{and } \Delta x_i^z = \begin{cases} \Delta q_2, & i = 1 \\ \Delta \dot{q}_2, & i = 2 \\ \Delta \dot{\theta}, & i = 3 \end{cases}.$$

**Theorem 2.1** and **Theorem 2.2** proposed in Subsection 1.4.3 have stated that a fixed-point of the restricted Poincaré map is locally exponentially stable, if, and only if, the eigenvalues of  $A^z$  have magnitude strictly less than one .

## 2.6 Simulation results

The equation (2.41) shows that the dynamic property of the system is influenced by the choice of  $M_1$ , exactly, the choice of joint angles to be controlled or the modification of

reference motion (see (2.24)). One objective of this part is to study the influence of choice of  $M_1$  on the stability and to obtain some  $M_1$  to stabilize the walking. The other objective is to test our control law in a simulator of robot with a rigid ground model and a soft ground model respectively.

### 2.6.1 Reference trajectory

The reference trajectory to be tracked using the proposed control law have been calculated off-line via the optimization techniques [Tlalolini, 2008], [Tlalolini et al., 2010]. The cyclic walking gait is composed of successive single support phases and impulsive impacts with full contact between the sole of the feet and the ground. The evolution of the joints are chosen as spline functions. The parameters to define the spline functions are determined using an optimization under constraints on the dynamic balance, on the ground reactions, on the validity of impact, on the torques, and on the joints velocities. The considered cost function is represented by the integral of the torques norm. The torques and the constraints are computed at sampling times during one step to evaluate the cost function for a feasible walking gait. The obtained stick-diagram for one step of the periodic walking gait in sagittal plane is presented in Fig. 2.6. The step length is  $0.9853\text{ m}$  and the duration of a step is  $0.4598\text{ s}$ .

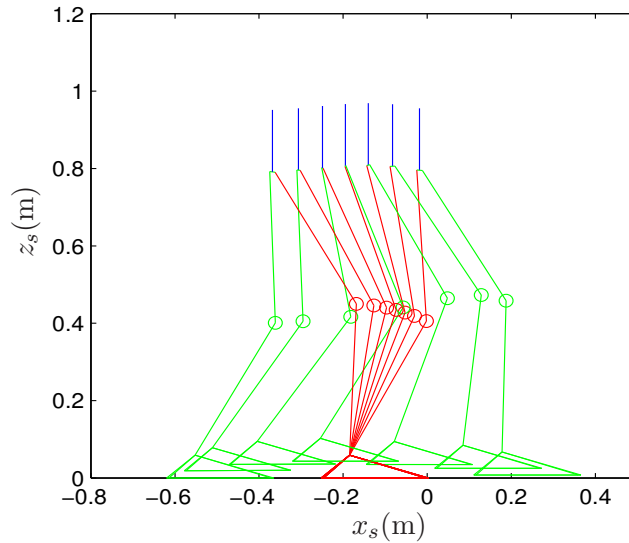


Figure 2.6: Stick-diagram for one step of the periodic walking gait in sagittal plane

### 2.6.2 The effect of different controlled partial joints on the walking stability

An exploration technique is used to illustrate the effect of the choice of  $M_1(10 \times 1)$ . Firstly, arbitrary 9 components of  $M_1$  are fixed to zero, then the largest magnitude of the eigenvalues of  $A^z$ , i.e.,  $\max |\lambda_{1,2,3}|$ , are drawn as functions of the 10<sup>th</sup> component of  $M_1$ . If they are less than 1, the resulted walking is stable. By using this method,  $\max |\lambda_{1,2,3}|$  for  $M_1(j, 1)$ ,  $j = 1, \dots, 10$  are obtained but only in the cases of  $j = 6, 7$  the stable points are in evidence and they are shown in Fig. 2.7, where the red circles denote the largest magnitude of eigenvalues of  $A^z$  are less than one, that means the stable cases exist. It also shows that the eigenvalues of  $A^z$  are larger than 1 when  $M_1 = \mathbf{0}_{10 \times 1}$ , which means the walking is not stable. In fact, in this case the controlled joint angles are  $u = [q_1, q_4, \dots, q_{11}, q_{14}]^T$  (see (2.21)) and the reference trajectory  $Q^d$  is not modified by the tracking error of  $q_2$  (see (2.24)).

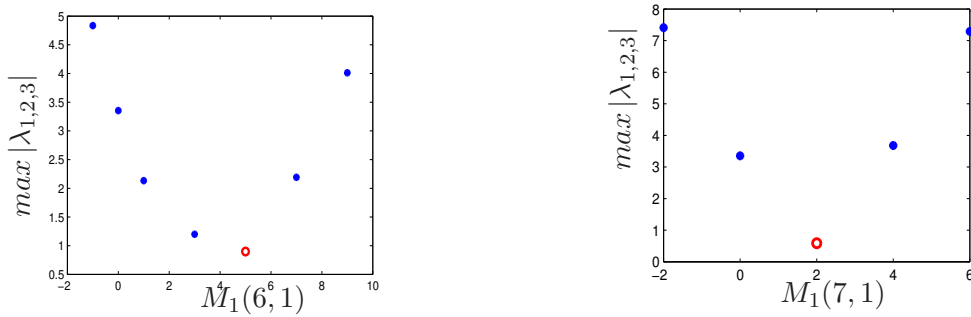


Figure 2.7:  $\max |\lambda_{1,2,3}|$  versus  $M_1(j, 1)$ ,  $j = 6, 7$ , when the other 9 components of  $M_1$  are zero.

### 2.6.3 Description of the simulator

The simulator is developed by C. Rengifo in his PhD thesis [Rengifo, 2010]. Its main objective is to calculate the impact and contact forces between foot and ground for biped robot walking simulation. The foot is supposed to be rigid and composed of four contact points  $P_1$ ,  $P_2$ ,  $P_3$  and  $P_4$  (see Fig. 2.3). If one of these points is in contact with the ground, the corresponding ground reaction force (GRF) is computed by solving a linear complementarity problem (LCP) [Acary et al., 2008] using the input torque and dynamic models. Since the punctual contact at each corner of the foot  $P_1, \dots, P_4$  is considered, the slipping, rolling or take-off of the foot can be modeled.

The block diagram of the simulator is shown in Fig. 2.8. The simulator requires a modeling that is convenient for any contact with the ground. Thus the robot is parametrized by a vector  $q_s = [X, \alpha, q]^T$  where  $X$  denotes the position of the frame  $x_0y_0z_0$  attached to the right foot, and  $\alpha$  is the euler angle that defines the orientation of frame  $x_0y_0z_0$  with respect to a fixed frame  $x_sy_s z_s$ . As soon as GRF is calculated, the vector of acceleration

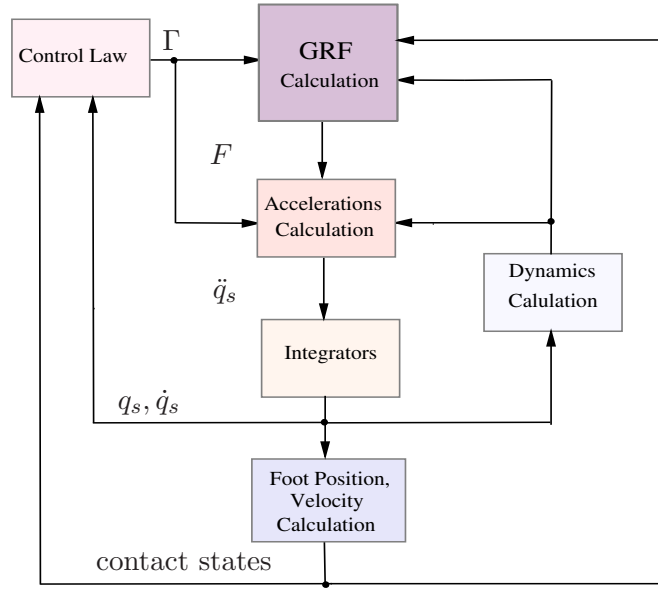


Figure 2.8: Block diagram of the simulator.

of the robot  $\ddot{q}_s$ <sup>3</sup> can be calculated according to a dynamic model [Rengifo, 2010]:

$$\ddot{q}_s = \begin{bmatrix} {}^0\dot{V}_0 \\ {}^0\dot{\omega}_0 \\ \ddot{q} \end{bmatrix} = \mathbf{A}^{-1}(q)(-\mathbf{H}(q, \dot{q}, {}^0\omega_0, \alpha) + \begin{bmatrix} \mathbf{0}_{3 \times 1} \\ \mathbf{0}_{3 \times 1} \\ \Gamma \end{bmatrix}) + \mathbf{D}(q, \alpha)F, \quad (2.44)$$

where  $\alpha$ ,  ${}^0\dot{V}_0$  and  ${}^0\dot{\omega}_0$  are respectively the orientation, linear and angular acceleration of the frame zero with respect to an inertial frame.  $\mathbf{A}_{20 \times 20}$  is the inertia matrix,  $\mathbf{H}_{20 \times 1}$  is a vector including Coriolis, centrifugal and gravitational terms, and  $\mathbf{D}_{20 \times 24}$  is the transposed of the Jacobian matrix relating the cartesian positions of the vertices of the foot and the joint positions. All of them are obtained via Newton-Euler method described as the module "Dynamics Calculation" shown in Fig. 2.8. In addition,  $\Gamma_{14 \times 1}$  is the control input,  $F_{24 \times 1}$  is the reaction forces vector resulted from the module "GRF Calculation" for 8 vertices of two feet.

Finally, by integrating the obtained joint acceleration  $\ddot{q}_s$ , the corresponding position and velocity are obtained and they will be used in the calculation of dynamic models. The control law uses only the joint position and velocity, which are parts of  $q_s$  and  $\dot{q}_s$ . Moreover, they are also used to compute the current position and velocity of the feet. From that we can know the contact states of two feet, specifically, which leg is actually in support and whether the impact occurs or not. These informations are useful for the calculations of control law and GRF.

<sup>3</sup>Although the acceleration is denoted as  $\ddot{q}_s$ , it is not the second derivative of  $q_s$  since the angular velocity  ${}^0\omega_0$  is not the derivative of  $\alpha$ , but  ${}^0\omega_0 = \Omega(\alpha)\dot{\alpha}$ .

### 2.6.4 The robustness of the control law for the rigid ground model

The flat rigid ground model is chosen at first to do the simulation. According to Fig. 2.7, when we choose  $M_1(6, 1) = 5$ , the walking should be stable, so it is used to determine the controlled outputs in (2.21) for the partial joint angles controller. For the simulation, an initial error of  $0.01 \text{ rad}$  is introduced on  $q_2$  and a velocity error of  $0.01 \text{ rad/s}$  is introduced on  $\dot{q}_2$  and  $\dot{\theta}$ , the errors on the other joints are introduced to have a double support configuration. The simulation results demonstrate the effective of the control law and the robot can realize a stable and periodic walking, as shown in Fig. 2.9.

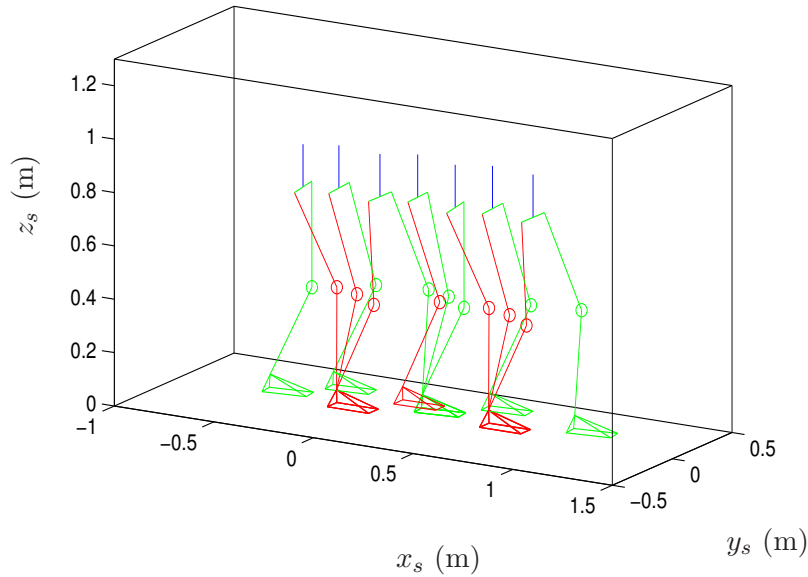


Figure 2.9: The walking motion of first three steps with the proposed control law.

The evolution of ZMP and its desired values are shown in Fig. 2.10. Although there exist a few sudden changes of ZMP which are artifacts of the method LCP used to calculate GRF, it shows that  $ZMP$  can track  $ZMP^d$  so the ZMP controller is validated. If the height of four vertices of each foot  $P_1$ ,  $P_2$ ,  $P_3$  and  $P_4$  are the same, that means the foot is flat during the walking. For the proposed control law since the  $ZMP$  is regulated to  $ZMP^d$ , the stance foot remains flat on the ground and the walk can be achieved as shown in Fig. 2.12. Fig. 2.12 describes the height of four points  $P_1, \dots, P_4$  for two feet respectively and it shows the traces of  $P_1, \dots, P_4$  are always the same, that means the supported foot remains flat on the ground and the swing foot is also flat as prescribed for the reference motion, which can validate the swing ankle rotation controller. The evolution of the error on  $q_2$  (the joint not directly controlled) is shown in Fig. 2.11. At the beginning the error increases to satisfy the condition on the ZMP but after that and step by step this error decreases and the cyclic desired motion is reached. The phase-plane plots of the joints are shown in Fig. 2.13. The convergence toward a periodic motion is clear for the uncontrolled

joint angle  $q_2$  and the controlled joint angles  $q_1, q_3, q_4$ . These results also indicate that the choice of controlled partial joints using the stability analysis is effective.

In summary, the simulations results shows that the proposed control law can lead to stable walking with initial errors on the states of robot. Moreover, we test the control law with 10% modeling errors on the inertia parameters used in the dynamic model, the obtained walking movement is also stable.

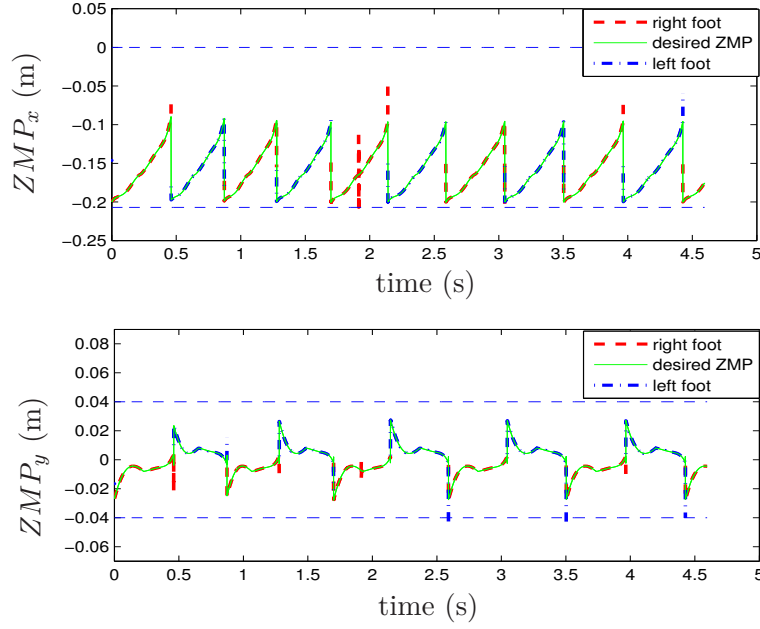


Figure 2.10: Position of ZMP with the proposed control law using the rigid ground model: the position of ZMP moves periodically and is always within the limits.

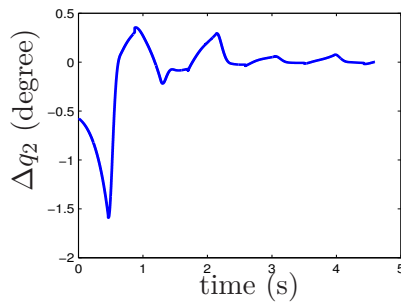


Figure 2.11: The tracking errors of  $q_2$  with the proposed control law using the rigid ground model.



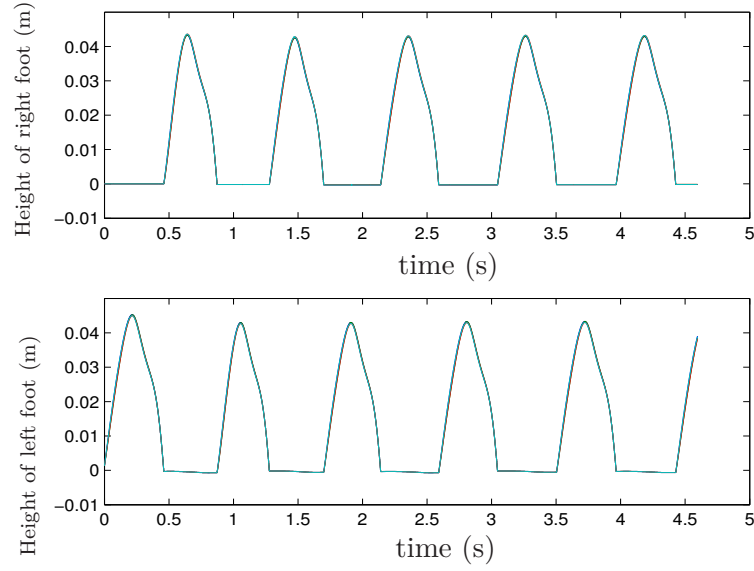


Figure 2.12: Height of feet with the proposed control law using the rigid ground model.

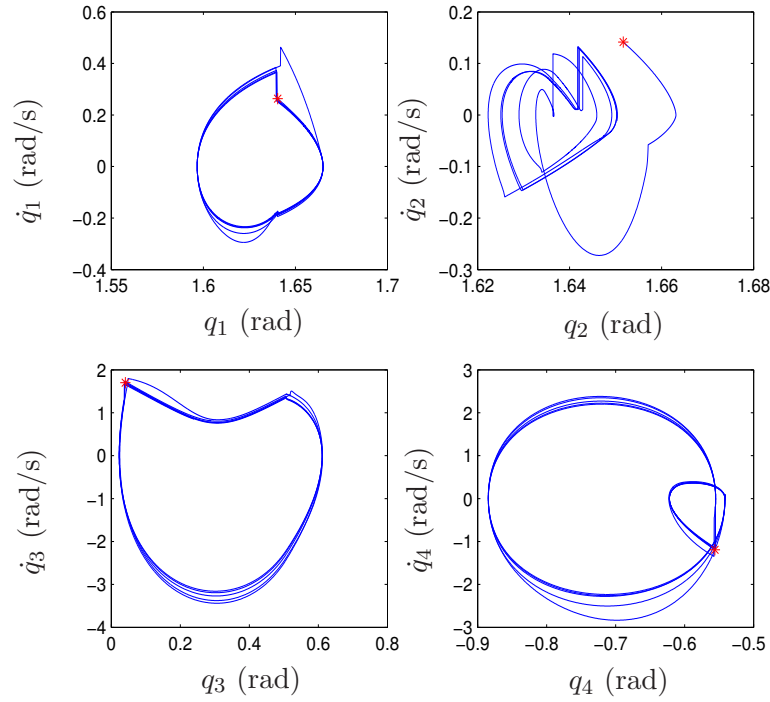


Figure 2.13: Phase-plane plots for  $q_i, i = 1, 2, 3, 4$  with the proposed control law using the rigid ground model. The initial state is represented by a (red) star.

### 2.6.5 The robustness of the proposed control law for the soft ground model

In order to further test the proposed control law, now a soft ground model is used in the simulator [Rengifo et al., 2009]. The same initial errors are introduced to every joint position and velocity as presented in the previous subsection.

Since the soft ground model is used, the foot can penetrate into the ground, and then the ground reaction force (GRF) changes acutely at the impact moment (see Fig. 2.14). As a result, the center of pressure (COP) is out of the polygon of support foot, but the ZMP is controlled quickly after the impact, as shown in Fig. 2.15. Consequently, the height of stance foot and the tracking error of  $q_2$  shake a little in the beginning of swing phase but at once recovers to zero (see Fig. 2.16 and Fig. 2.18). The phase planes for  $q_i, i = 1, 2, 3, 4$  are shown in Fig. 2.17. It worth noting that  $ZMP$  cannot track  $ZMP^d$  perfectly because the ground model used in the simulation is different from that supposed in the control law. However, the simulations results show that the robustness of the control law can resist this modeling error step by step.

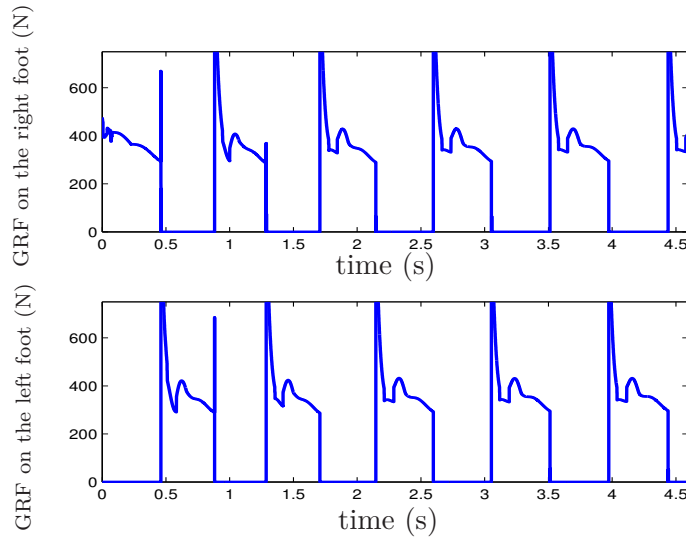


Figure 2.14: Ground reaction force (GRF) of the soft ground model.

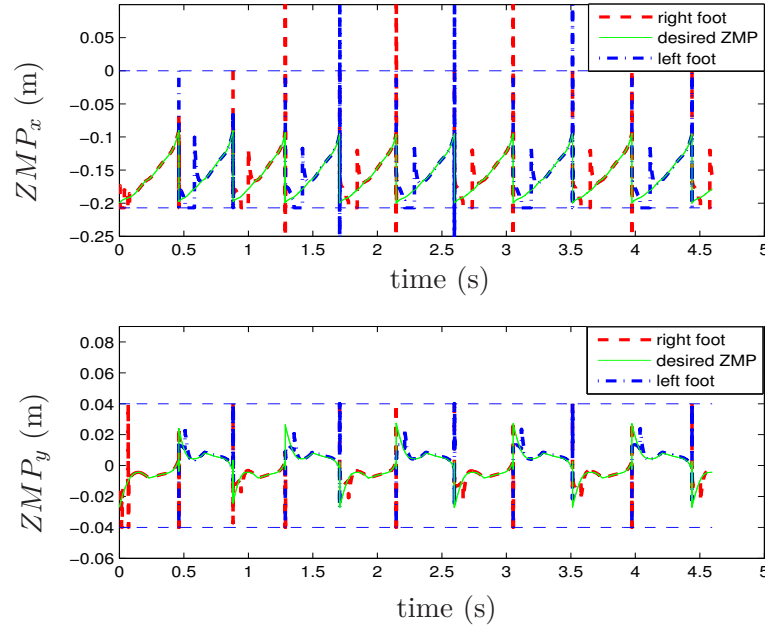


Figure 2.15: Position of ZMP in the feet sole with the proposed control law using the soft ground model: the position of ZMP moves periodically and returns to the limits fast after impact.

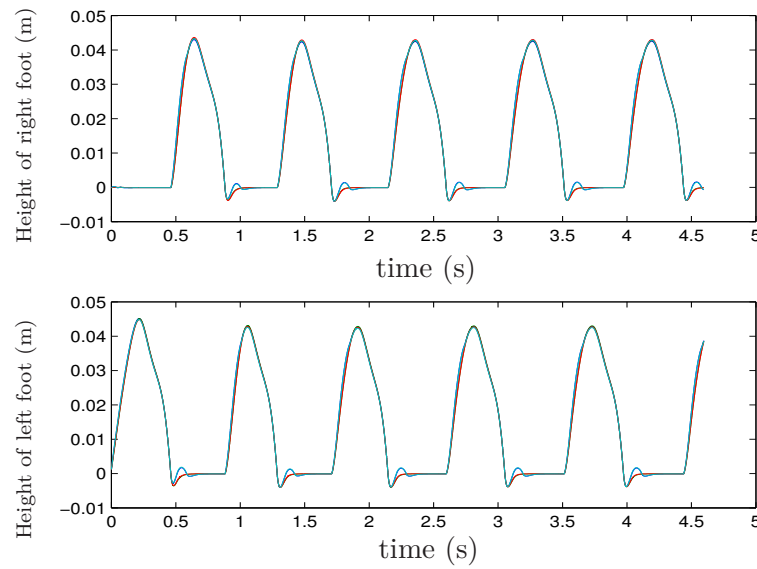


Figure 2.16: Height of feet with the proposed control law using the soft ground model.

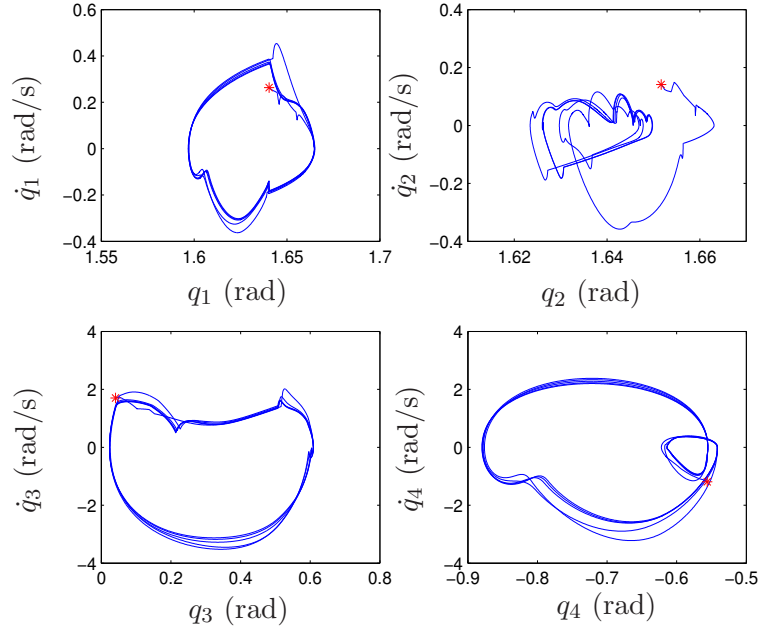


Figure 2.17: Phase-plane plots for  $q_i, i = 1, 2, 3, 4$  with the proposed control law using the soft ground model. The initial state is represented by a (red) star.

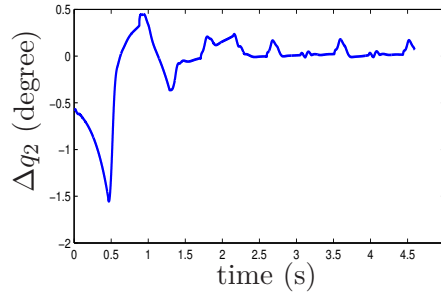


Figure 2.18: The tracking errors of  $q_2$  with the proposed control law using the soft ground model.

## 2.7 Comparison of several control laws

One critical strategy for preventing a humanoid from falling is to take control actions at the actuated joints that ensures a desired contact of the foot with the ground. In the lateral direction, this often means ensuring that the foot does not roll on an edge (to avoid twisting the ankle). In the forward direction, this means that the stance foot should not pitch. In order to satisfy the desired contact condition, in Section 2.5, the position of ZMP along  $x_s$  and  $y_s$  axis are controlled together. However, it has been shown that this control method is not absolutely necessary. In [Mitobe et al., 2010], ZMP is controlled without

being associated with horizontal position change of the center of mass (COM) along  $y_s$  axis. A new method is presented for controlling the ZMP by using harmonic oscillation of a spring mass system mounted on the robot body. The oscillation makes swing motion of the ZMP to right and left, and then the ZMP motion generates a rhythmical walk gait. [Ito et al., 2008] proposes a biped control method for the frontal plane motion based on the ZMP position feedback. The ZMP trajectory is invariant in the lateral plane of the biped robot, in which the ZMP moves from one side to the other and vice versa. This method does not require the reference motion of the upper body and the motion replanning or modification of the reference motion are free against environmental variation. In the following contents, three control laws based on the control method proposed in the Section 2.5 will be presented to study the influence of the control of the ZMP along different directions on the walking stability. There are respectively a control law without regulation of lateral position of ZMP, a control law without regulation of forward position of ZMP and a control law without regulation of ZMP. Moreover, they will be compared with a classical control law where ZMP is not adjusted at all and only joint angles are tracked.

### 2.7.1 A control law without the regulation of $ZMP_y$

#### Principle of the control law

If the lateral direction of ZMP, i.e,  $ZMP_y$  is not controlled, the output of the original control law in (2.26) can be rewritten as:

$$\begin{cases} y_1 &= ZMP_x - ZMP_x^d(\theta) = 0 \\ y_{2c} &= \xi_{xy} - \xi_{xyc} = 0 \\ y_{3c} &= u_e - u_e^d(\theta) - u_{ec} = 0 \end{cases} \quad (2.45)$$

where the first equation denotes the control of  $ZMP_x$ , which is related to  $M_{py}$  in (2.4) so the control is realized by the second row of (2.14). The second equation of (2.45) is the swing ankle rotation controller, which is the same as (2.26). Since the control of  $ZMP$  is reduced by one dimension, the partial joint angles controller has to be increased by one dimension. Fig. 2.2 shows that  $q_2$  influences  $ZMP_y$  directly, since  $ZMP_y$  is not regulated, it is useful to control the joint ankle  $q_2$  to achieve the stable walking. According to definition of  $u$  in (2.21) and (2.22),  $q_2$  can be included in the new controlled partial joints and we have:

$$u_e = [q_1, q_2, q_4, \dots, q_{11}, q_{14}]_{11 \times 1}^T. \quad (2.46)$$

Consequently, the desired values of  $u_e$ , which is denoted by  $u_e^d$ , can be obtained by  $q^d$  and (2.46). The modification term  $u_{ec}$  in (2.45) is defined similar to (2.27) and (2.28). At last, the partial joint angles controller (2.32) is rewritten as:

$$\ddot{u}_e - \ddot{u}_e^d - \ddot{u}_{ec} + \frac{K_d}{\varepsilon}(\dot{u}_e - \dot{u}_e^d - \dot{u}_{ec}) + \frac{K_p}{\varepsilon^2}(u_e - u_e^d - u_{ec}) = \mathbf{0}_{11 \times 1} \quad (2.47)$$

Using the same simplification method of (2.32) (see Appendix A.3), (2.47) can also be written as a linear function of  $\ddot{q}$  like (2.34):

$$W_{je}(q, \dot{q})_{11 \times 14} \ddot{q} + H_{je}(q, \dot{q})_{11 \times 1} = \mathbf{0}_{11 \times 1}, \quad (2.48)$$

where  $W_{je}(q, \dot{q})$  denotes all the coefficient terms of  $\ddot{q}$  and  $H_{je}$  denotes all the terms without  $\ddot{q}$  in (2.47).

As proposed in Subsection 2.5.5, the  $ZMP_x$  controller and swing ankle rotation controller can be described by the second row of (2.14) and (2.33). Using them and (2.48), 14 new equations about  $q, \dot{q}, \ddot{q}$  can be combined as:

$$A(q, \dot{q})\ddot{q} + B(q, \dot{q}) = \mathbf{0}_{14 \times 1}, \quad (2.49)$$

with  $A = [W_2, W_s, W_{je}]^T$  and  $B = [H_2, H_s, H_{je}]^T$ . Here  $W_2$  and  $H_2$  are the second row of  $W$  and  $H$ .

Next, the  $\ddot{q}$  is resolved directly:

$$\ddot{q} = -A^{-1}B \quad (2.50)$$

Then, the desired torques  $\Gamma$  can be calculated with  $\ddot{q}, \dot{q}$  and  $q$  by using the inverse dynamics via Newton-Euler algorithm (2.2).

### Stability analysis

In Subsection 2.5.6, the states of robot  $q, \dot{q}$  are replaced by  $q_2, \theta, \dot{q}_2, \dot{\theta}$  to analyze the stability of the closed-loop system using the definition of HZD in (2.26). For the studied robot the dimension of the state space is  $n = 2 \times 14$ , the relative degree of ZMP controller is zero, and that of other two sub-controllers are 2 for each controlled output so the dimension of  $HZD$  will be  $2 \times 14 - (2 + 11) \times 2 = 2$ . In the new control system, if (2.45) is satisfied, since  $q_2$  has been controlled directly in  $u_e$ , on the zero dynamics  $q, \dot{q}$  can be replaced by  $\theta, \dot{\theta}$ , that means (2.40) is rewritten as:

$$[q, \dot{q}] = f_{HZDx}(\theta, \dot{\theta}, C_{q^d}) \quad (2.51)$$

Next the acceleration  $\ddot{q}$  can be expressed as a function of  $\theta, \dot{\theta}, \ddot{\theta}$  like (2.41). Thus (2.45) corresponds to:

$$\begin{cases} W_{HZDx}(q, \dot{q})\ddot{\theta} + H_{HZDx}(q, \dot{q}) = 0 \\ [q, \dot{q}] = f_{HZDx}(\theta, \dot{\theta}, C_{q^d}) \end{cases} \quad (2.52)$$

Obviously, the walking stability can be investigated using the HZD by 2 states  $\theta, \dot{\theta}$ . In fact, if the same Poincaré section is chosen as in Subsection (2.5.7), in the restricted Poincaré map  $P^z : S_\theta \cap Z \rightarrow S_\theta \cap Z$  there is always:  $\theta^* = 0.4\theta_i^d + 0.6\theta_f^d$ . Thus only  $\dot{\theta}$  is the state to be analyzed. The known cyclic motion  $q^d(\theta)$  gives a fixed-point  $x^{z*} = \dot{\theta}^*$ . The resulted discrete-time system is denoted as  $x_{k+1} = P^z(x_k)$ . Define  $\delta x_k = x_k - x^*$ , the Poincaré map linearized about the fixed-point  $x^*$  gives rise to a linearized system,

$$\delta x_{k+1} = A^z \delta x_k, \quad (2.53)$$

where the Jacobian matrix of the Poincaré map  $A^z$  is a  $(1 \times 1)$  numerical value, and it can be calculated using:

$$A^z = \frac{P^z(x^{z*} + \Delta\dot{\theta}) - P^z(x^{z*} - \Delta\dot{\theta})}{2\Delta\dot{\theta}}. \quad (2.54)$$

According to **Theorem 2.1** and **Theorem 2.2** proposed in Subsection 1.4.3, if the eigenvalues of  $A^z$  have magnitude strictly less than one, the walking will be stable.

## Simulation results

The reduced dimensional zero dynamics (2.52) indicates that the walking stability is no longer influenced by the choice of controlled joints, i.e., the choice of  $M_1$ . Besides, the stability is analyzed in one dimensional space by using the state  $\dot{\theta}$ . Therefore, the maximum eigenvalue of the Jacobian matrix of the Poincaré map  $A^z$  is a scalar:

$$\lambda = 0.3719. \quad (2.55)$$

Apparently, the walking will be stable and that is also validated by the results Fig. 2.19 – Fig. 2.21. The simulation is done using the rigid ground model. The initial error of  $0.01 \text{ rad}$  is introduced on  $q_2$  and a velocity error of  $0.01 \text{ rad/s}$  is introduced on  $\dot{q}_2$  and  $\dot{\theta}$ , the errors on the other joints are introduced to have a double support configuration. This initial condition is the same as the previous simulation where both of two directions of ZMP are controlled. Fig. 2.20 and Fig. 2.21 show that the walking converges toward a cyclic movement and the walking is stable.

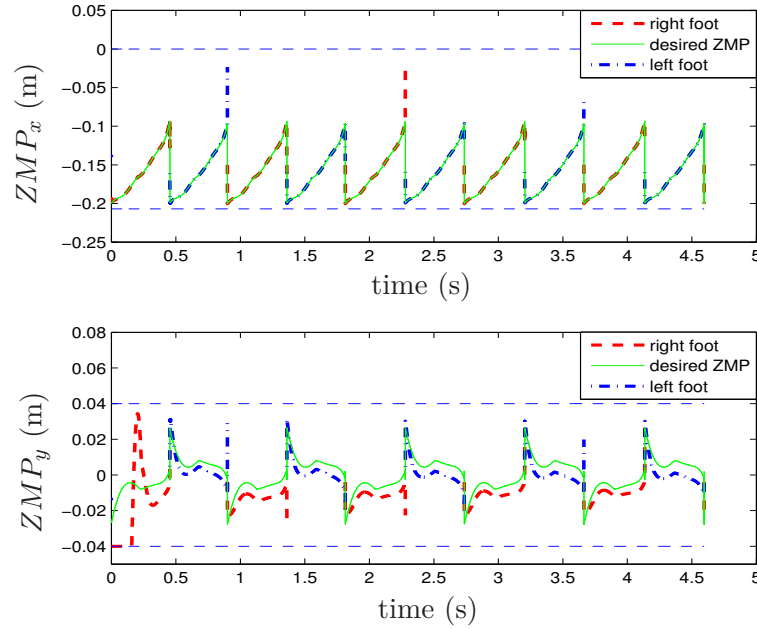


Figure 2.19: Position of ZMP in the foot sole for the control law without the regulation of  $ZMP_y$ : the position of ZMP moves periodically and is always within the limits but  $ZMP_y$  does not track  $ZMP_y^d$ .

Compared to Fig. 2.13, Fig. 2.20 indicates that the walking converges faster than the proposed control law where both two directions of  $ZMP$  are regulated. However, since  $ZMP_y$  is not controlled, there exist tracking errors about  $ZMP_y^d$  and the errors increase with the increase of initial errors. Therefore, if the initial errors are large or the maximum

values of the desired ZMP are near the edges of foot sole, the obtained  $ZMP_y$  in the simulation will be out of the foot sole.

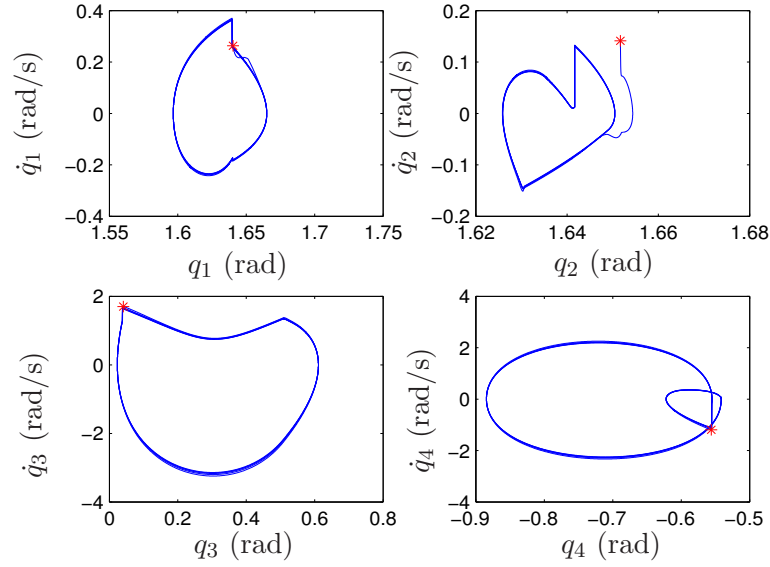


Figure 2.20: Phase-plane plots for  $q_i, i = 1, 2, 3, 4$  for the control law without the regulation of  $ZMP_y$ . The initial state is represented by a (red) star.

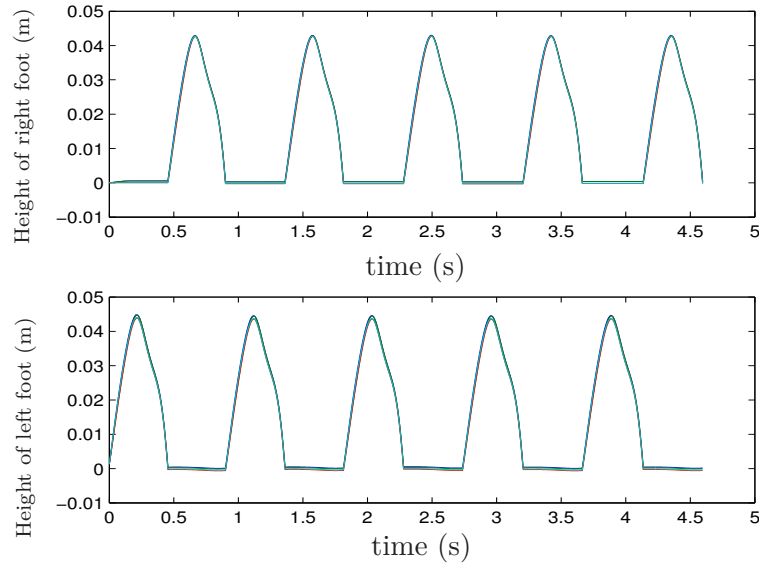


Figure 2.21: Height of feet for the control law without the regulation of  $ZMP_y$ .



## 2.7.2 A control law without the regulation of $ZMP_x$

### Principle of the control law

In this section, a control law without regulation of the forward position of ZMP, i.e.,  $ZMP_x$ , will be proposed. Fig. 2.2 shows that  $q_3$  influences  $ZMP_x$  directly, thus the control of joint angle  $q_3$  is used to compensate for the lack of control of  $ZMP_x$ . Because  $\theta = q_3 + 0.5q_4$ , the control of  $q_3$  is equivalent to the control of  $\theta$  and  $q_4$ . Since  $q_4$  has been included in the controlled partial joints  $u$  (see (2.21) and (2.22)), the output of the original control law in (2.26) is rewritten as:

$$\begin{cases} y_1 &= ZMP_y - ZMP_y^d(\theta) = 0 \\ y_{2c} &= \xi_{xy} - \xi_{xyc} = 0 \\ y_{3c} &= u - u^d(\theta) - u_c = 0 \\ y_4 &= \theta - \theta^d(t) = 0 \end{cases} \quad (2.56)$$

where the first equation denotes the regulation of  $ZMP_y$  which is related to  $M_{px}$  in (2.4) so the control is implemented using the first row of (2.14). The second and third equation of (2.56) describe the swing ankle rotation controller and partial joint angles controller. They are realized as the original controllers by using (2.31) and (2.32). The fourth equation denotes the control of  $\theta$  and it is achieved by a PD controller:

$$\ddot{\theta} - \ddot{\theta}^d(t) + \frac{K_d}{\varepsilon}(\dot{\theta} - \dot{\theta}^d(t)) + \frac{K_p}{\varepsilon^2}(\theta - \theta^d(t)) = 0 \quad (2.57)$$

where  $\theta^d(t)$ ,  $\dot{\theta}^d(t)$ ,  $\ddot{\theta}^d(t)$  are calculated by the reference trajectory expressed as a function of time before parametrization:  $q^d(t)$ ,  $\dot{q}^d(t)$ ,  $\ddot{q}^d(t)$ .

Because  $\theta$  is a linear function of  $q$  (see (A.11)), (2.57) can also be written as the linear equation of  $\ddot{q}$ :

$$W_\theta(q, \dot{q})_{1 \times 14} \ddot{q} + H_\theta(q, \dot{q})_{1 \times 1} = 0, \quad (2.58)$$

where  $W_\theta(q, \dot{q})$  denotes all the coefficient terms of  $\ddot{q}$  and  $H_\theta(q, \dot{q})$  denotes all the terms without  $\ddot{q}$  in (2.57).

Subsection 2.5.5 has proposed that the first three sub-controllers in (2.56) can be implemented by the first row of (2.14), (2.33) and (2.34) respectively. Combine them and (2.58), the new control law (2.56) yields 14 new equations about  $q, \dot{q}, \ddot{q}$ :

$$A(q, \dot{q})\ddot{q} + B(q, \dot{q}) = \mathbf{0}_{14 \times 1}, \quad (2.59)$$

with  $A = [W_1, W_s, W_j, W_\theta]^T$  and  $B = [H_1, H_s, H_j, H_\theta]^T$ . Here  $W_1$  and  $H_1$  are the first row of  $W$  and  $H$ .

Next, the  $\ddot{q}$  is resolved directly by using:

$$\ddot{q} = -A^{-1}B \quad (2.60)$$

and the desired torques  $\Gamma$  can be calculated with  $\ddot{q}$ ,  $\dot{q}$  and  $q$  by using the inverse dynamics via Newton-Euler algorithm (2.2).

### Stability analysis

According to the definition of HZD, (2.56) is satisfied. Subsection 2.5.6 has proposed that the states of robot  $q, \dot{q}$  are described by  $q_2, \theta, \dot{q}_2, \dot{\theta}$  by using the second and third equation of (2.56) and they are influenced by  $M_1$ . The fourth equation of (2.56) shows that  $\theta$  is controlled to follow  $\theta^d(t)$ , that means the HZD is also influenced by the time  $t$ , thus (2.40) is rewritten as:

$$[q, \dot{q}] = f_{HZDy}(q_2, \dot{q}_2, \tau, M_1, C_{q^d}) \quad (2.61)$$

where  $\tau$  is the time during each step, the relation between it and the time  $t$  has been presented in (1.53). Next, the  $ZMP_y$  controller described by the first equation of (2.56) is expressed only as a linear function of  $\ddot{q}_2$ . Therefore, the HZD of the new controller is:

$$\begin{cases} W_{HZDy}(q, \dot{q}, \tau) \ddot{q}_2 + H_{HZDy}(q, \dot{q}, \tau) = 0 \\ [q, \dot{q}] = f_{HZDy}(q_2, \dot{q}_2, \tau, M_1, C_{q^d}) \end{cases} \quad (2.62)$$

For the studied robot the dimension of the state space is  $n = 2 \times 14$ , the relative degree of ZMP controller is zero and that of other three sub-controllers described by using the last three equations of (2.56) are 2 for each controlled output, so the dimension of  $HZD$  will be  $2 \times 14 - (2 + 10 + 1) \times 2 = 2$ . Since the reference trajectory depends on time, one variable  $\tau$  should be added. The equation (2.62) shows that the 3 states to describe the property of  $q, \dot{q}$  are  $q_2, \dot{q}_2, \tau$ . Next, the Poincaré section is chosen at  $\theta^* = 0.4\theta_i^d + 0.6\theta_f^d$  as before. In the Poincaré section since  $\theta$  is fixed,  $\tau$  is fixed thus the known cyclic motion  $q^d(\theta(\tau))$  gives a fixed-point  $x^{z*} = (q_2^d(\theta^*), \dot{q}_2^d(\theta^*))$  for the proposed control law for any value of  $M_1$ . Using the same method as before, the Poincaré map linearized about the fixed-point  $x^*$  gives rise to a linearized system,

$$\delta x_{k+1} = A^z \delta x_k, \quad (2.63)$$

where the Jacobian matrix of the Poincaré map is a  $(2 \times 2)$  square matrix  $A^z$  and it can be calculated using:

$$A^z = \begin{bmatrix} A_1^z & A_2^z \end{bmatrix}_{2 \times 2}$$

with

$$A_i^z = \frac{P^z(x^{z*} + \Delta x_i^z) - P^z(x^{z*} - \Delta x_i^z)}{2\Delta x_i^z}, \quad i = 1, 2 \quad (2.64)$$

$$\text{and } \Delta x_i^z = \begin{cases} \Delta q_2, & i = 1 \\ \Delta \dot{q}_2, & i = 2 \end{cases}.$$

According to **Theorem 2.1** and **Theorem 2.2** proposed in Subsection 1.4.3, the task of stability analysis is to observe whether the eigenvalues of  $A^z$  have magnitude strictly less than one or not.

### Simulation results

The equation (2.62) shows that the walking stability will be influenced by  $M_1$  and the effect of that on the eigenvalues of  $A^z$  for the complete regulation of ZMP has been shown

in Fig. 2.7. Here  $M_1(6,1) = 5$  is still used and the resulted  $A^z$  is:

$$A^z = \begin{bmatrix} 0.6962 & -0.1709 \\ 3.7355 & -0.5728 \end{bmatrix}.$$

Its maximum eigenvalue is:

$$\lambda = 0.4893. \quad (2.65)$$

It is less than 1 so the walking will be stable. Since  $ZMP_x$  is not controlled and its desired minimum value  $(ZMP_x^d)_{min} = -0.1999$  is so close to its constraint value  $-0.207$  (the length of foot is  $0.207 \text{ m}$ ),  $ZMP_x$  will be out of the foot sole if the initial errors are as large as before, thus the robot will probably fall down. Therefore, here the initial errors of  $q_2$ ,  $\dot{q}_2$  and  $\dot{\theta}$  are decreased to  $0.0005 \text{ rad}$  and  $0.0005 \text{ rad/s}$ . The walking is stable and the simulation results are shown in Fig. 2.22 – Fig. 2.24. As explained before,  $ZMP_x$  is out of the foot sole during a short period at the beginning of every step in spite of the fact that the initial errors are very small.

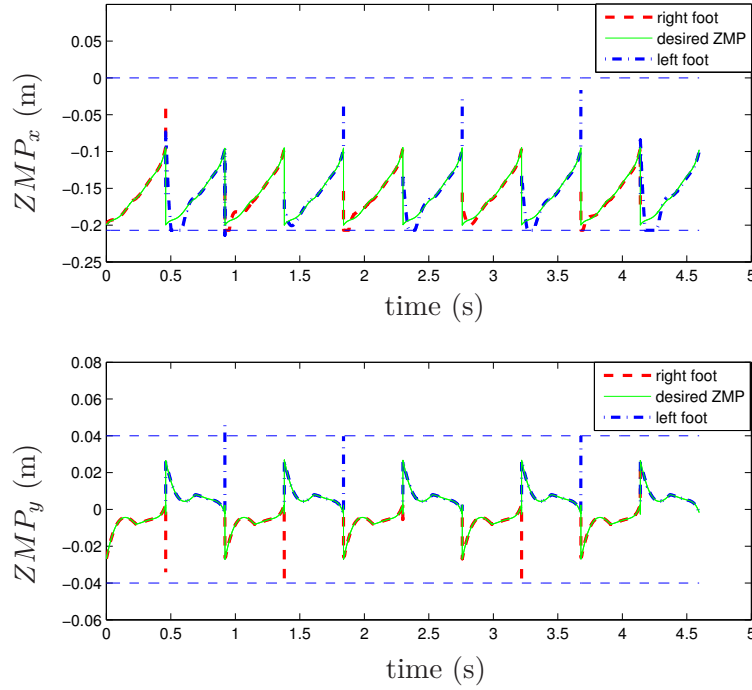


Figure 2.22: Position of ZMP in the foot sole for the control law without the regulation of  $ZMP_x$ : the position of ZMP moves periodically but  $ZMP_x$  is out of the limit during a short time.

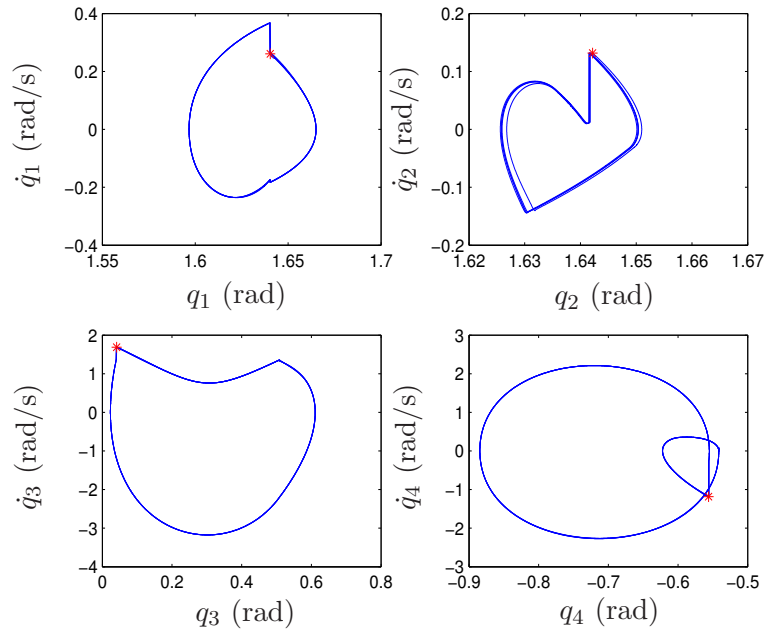


Figure 2.23: Phase-plane plots for  $q_i, i = 1, 2, 3, 4$  for the control law without the regulation of  $ZMP_x$ . The initial state is represented by a (red) star.

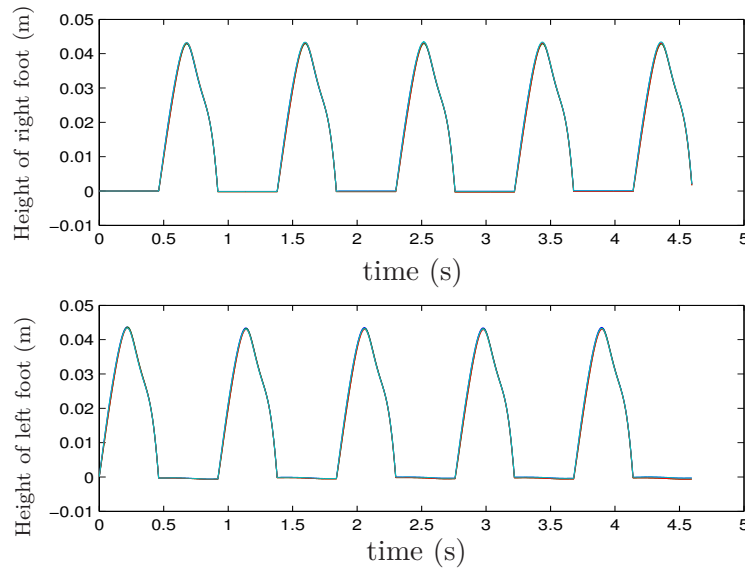


Figure 2.24: Height of feet for the control law without the regulation of  $ZMP_x$ .

### 2.7.3 A control law without the regulation of ZMP

#### Principle of the control law

This section will present a control law without the regulation of ZMP. Based on the analysis in the previous two sections, the control of forward and lateral position of ZMP can be transferred to the control of joint angle  $\theta$  and  $q_2$  respectively. Combine (2.45) and (2.56), the new control law without the regulation of ZMP can be described as:

$$\begin{cases} y_{2c} &= \xi_{xy} - \xi_{xyc} = 0 \\ y_{3c} &= u_e - u_e^d(\theta) - u_{ec} = 0 \\ y_4 &= \theta - \theta^d(t) = 0 \end{cases} \quad (2.66)$$

where the first equation corresponds to the swing ankle rotation controller, the second equation denotes the partial joint angles controller and  $u_e$  has been defined in (2.46) where  $q_2$  is controlled directly to regulate  $ZMP_y$ . The third equation of (2.66) regulates  $ZMP_x$  by using the control of  $\theta$ . The three sub-controllers described in (2.66) yield (2.33), (2.48) and (2.58) respectively, thus  $\ddot{q}$  can be resolved by using:

$$\ddot{q} = -A^{-1}B \quad (2.67)$$

with  $A = [W_s, W_{je}, W_\theta]^T$  and  $B = [H_s, H_{je}, H_\theta]^T$ . Thus the desired torques  $\Gamma$  can be calculated with  $\ddot{q}$ ,  $\dot{q}$  and  $q$  by using the inverse dynamics via Newton-Euler algorithm (2.2).

The equation (2.66) is always satisfied according to the definition of zero dynamics. Since the relative degree is  $28 - (2 + 11 + 1) \times 2 = 0$ , the reduced dimensional zero dynamics of (2.66) such as (2.52) and (2.62) does not exist. Therefore, the stability analysis is not necessary for this control law.

#### Simulation results

For the simulation of this control law without the regulation of ZMP, if an initial error of  $0.001 \text{ rad}$  is introduced on  $q_2$  and a velocity error of  $0.001 \text{ rad/s}$  is introduced on  $\dot{q}_2$  and  $\dot{\theta}$ , the walking is stable and the results are shown in Fig. 2.25 – Fig. 2.27. Since the position of ZMP is not controlled, there are tracking errors about  $ZMP_y^d$  and  $ZMP_x^d$ . Especially for  $ZMP_x$ , it cannot track  $ZMP_x^d$  at the beginning of every step. Furthermore, if the initial errors of the position and velocity are increased to  $0.01 \text{ rad}$  and  $0.01 \text{ rad/s}$  respectively, the walking is not stable because  $ZMP_x$  is out of the foot sole during a so long period at the sixth step ( $t = 2.5 \text{ s}$ ) that the support foot began to shake (see Fig. 2.28 and Fig. 2.30).

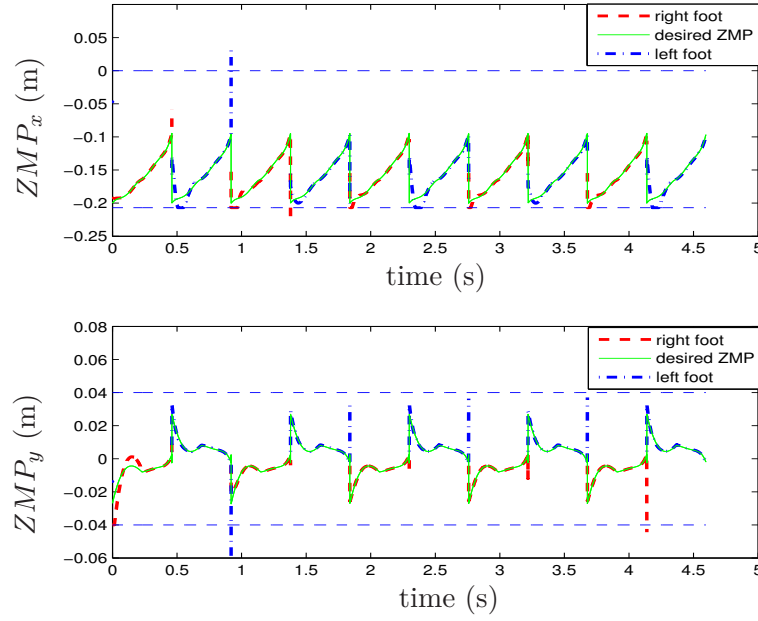


Figure 2.25: Position of ZMP in the foot sole for the control law without the regulation of ZMP.

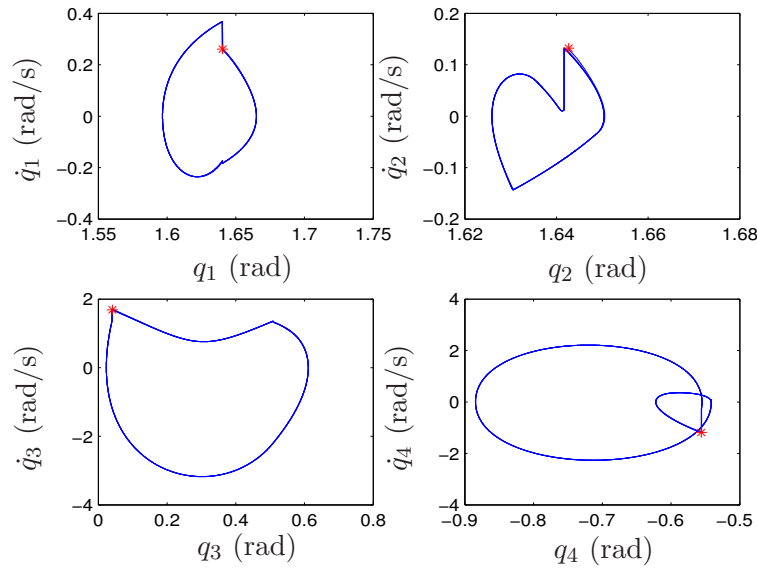


Figure 2.26: Phase-plane plots for  $q_i, i = 1, 2, 3, 4$  for the control law without the regulation of ZMP. The initial state is represented by a (red) star.

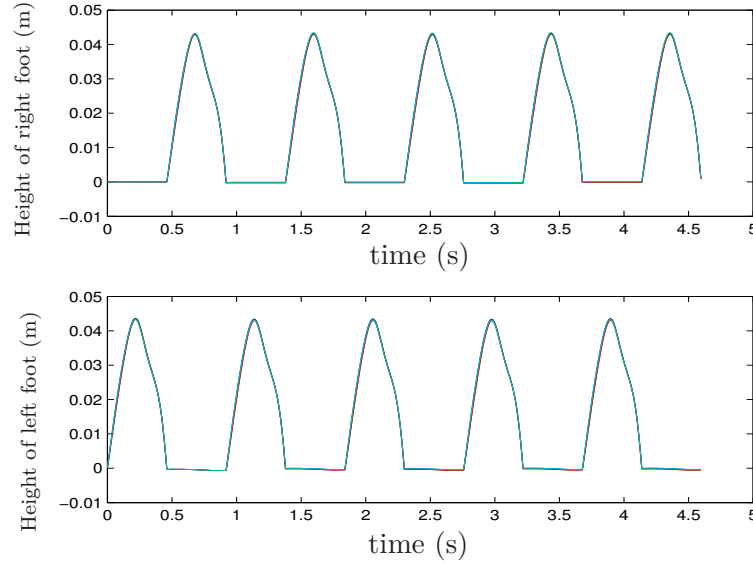


Figure 2.27: Height of feet for the control law without the regulation of ZMP.

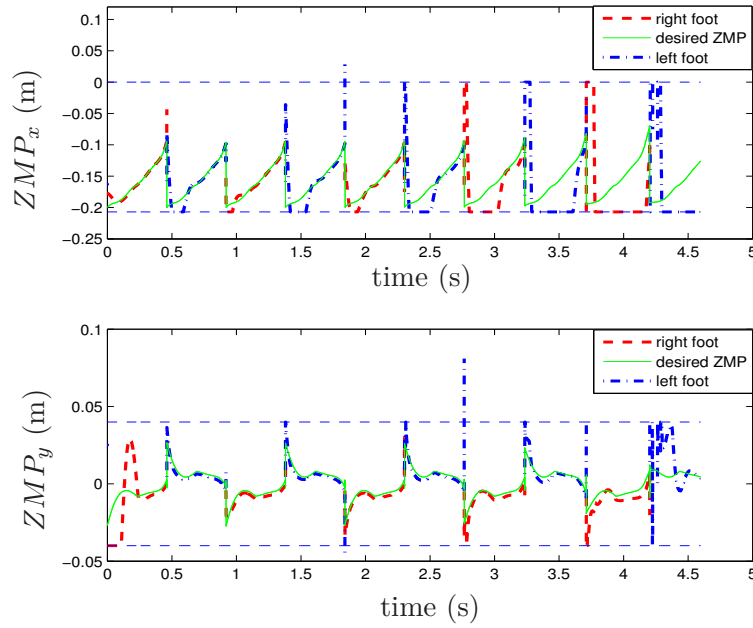


Figure 2.28: Position of ZMP in the foot sole for the control law without the regulation of ZMP: the position of  $ZMP_x$  is out of the limits when the larger initial errors are introduced.

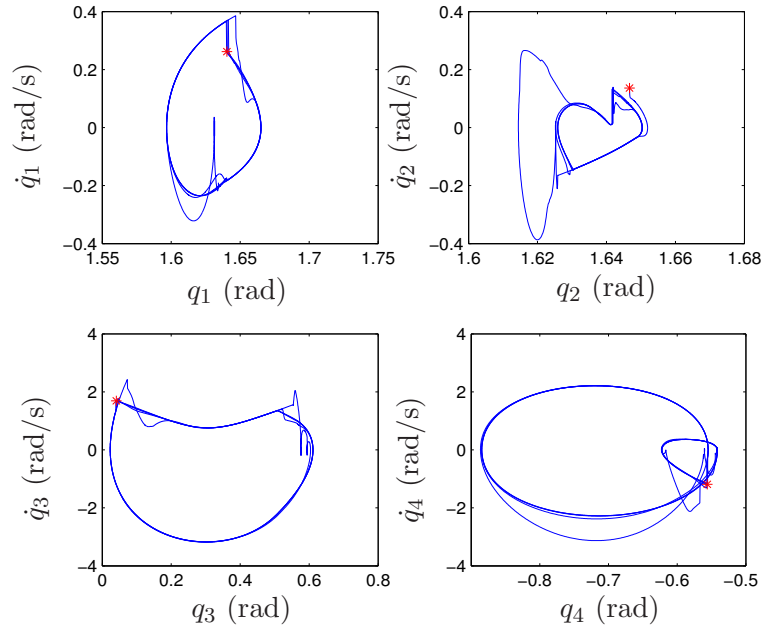


Figure 2.29: Phase-plane plots for  $q_i, i = 1, 2, 3, 4$  for the control law without the regulation of ZMP when the larger initial errors are introduced. The initial state is represented by a (red) star.

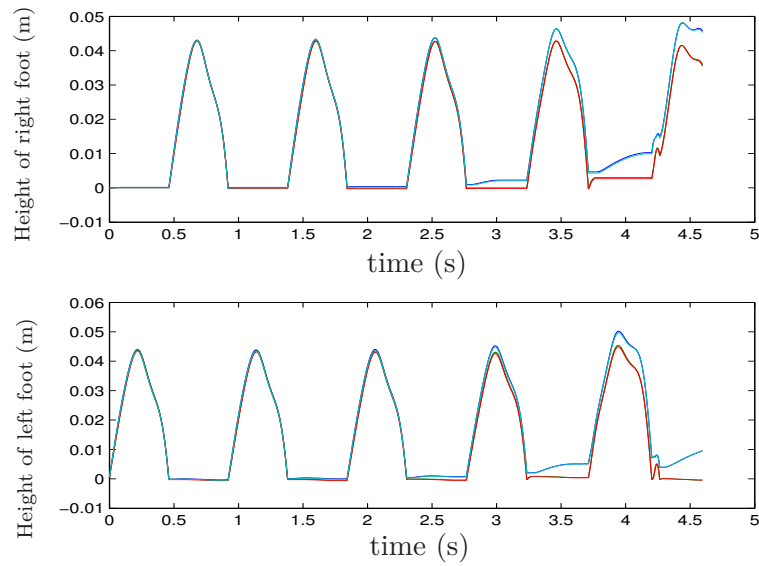


Figure 2.30: Height of feet for the control law without the regulation of ZMP when the larger initial errors are introduced.



### 2.7.4 A classical control law without the regulation of ZMP

In order to prove the validity and superiority of our control laws, the walking simulation is tested under a classical control law, in which all the joint angles are controlled and the desired property of the closed loop system is:

$$\ddot{q} = \ddot{q}^d - K_d(\dot{q} - \dot{q}^d) - K_p(q - q^d), \quad (2.68)$$

where  $K_d > 0$  and  $K_p > 0$ .

Then the torques can be obtained by (2.2) using  $q$ ,  $\dot{q}$  and  $\ddot{q}$ . Next, the same reference trajectory, the same simulator of the robot and the same simulation parameters are used for the walking simulation. For the control law (2.68), in order to limit the influence of errors at the beginning of the step, the reference trajectory in (2.68) is also modified as presented in section 2.5.4.

An initial error of  $0.01 \text{ rad}$  is introduced on  $q_2$  and a velocity error of  $0.01 \text{ rad/s}$  is introduced on  $\dot{q}_2$  and  $\dot{\theta}$ , the results are shown in Fig. 2.31 – Fig. 2.34. For this classical control law, since all the joint angles are controlled, the tracking error of the joint is close to zero at the end of the step (see Fig. 2.31 where the joint angle  $q_2$  is chosen to be compared with Fig. 2.11). However, the initial error is so high that the COP reaches the limits along the axis  $y$  as shown in Fig. 2.33. As a consequence, the stance foot rotates as shown in Fig. 2.32. Fig. 2.34 also shows that the height of hips changes irregularly and the robot will fall down.

The comparison reconfirms that the control of ZMP is much more important than the tracking of predefined joints trajectory. It also indicates that the swing ankle rotation controller is helpful for the stable contact with the ground.

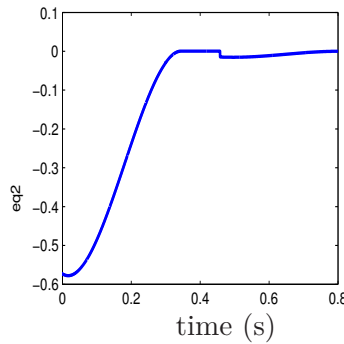


Figure 2.31: The tracking errors of  $q_2$  for the classical control law.

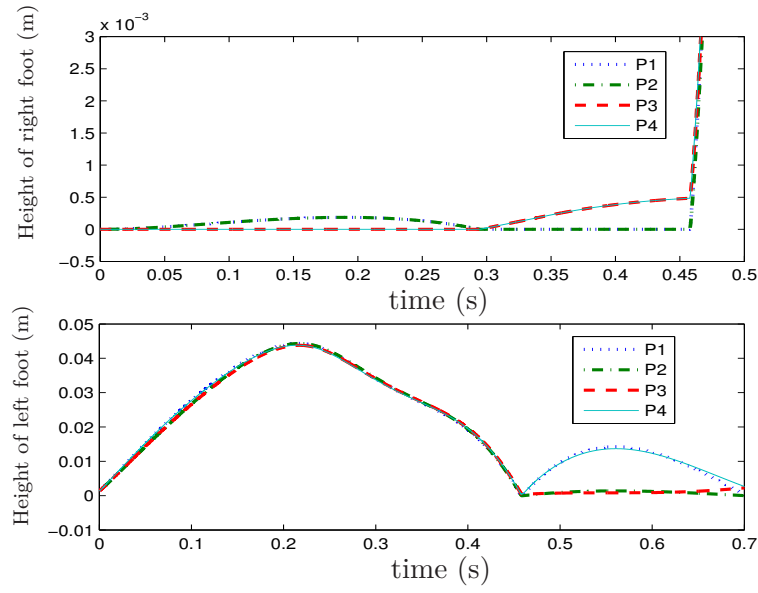


Figure 2.32: Height of feet with the classical control law, for the right foot a zoom is done along the vertical axis to show the unexpected rotation of the stance foot.

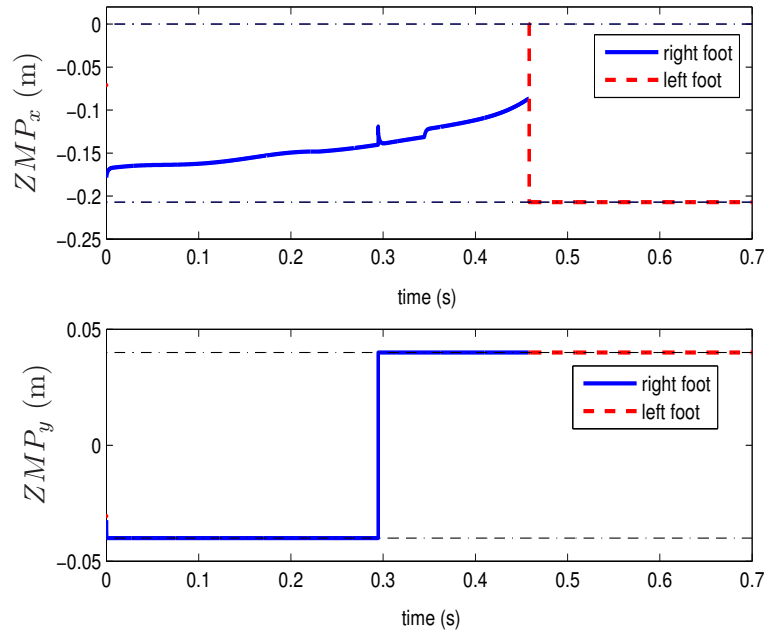


Figure 2.33: COP in the feet sole for the classical control law.

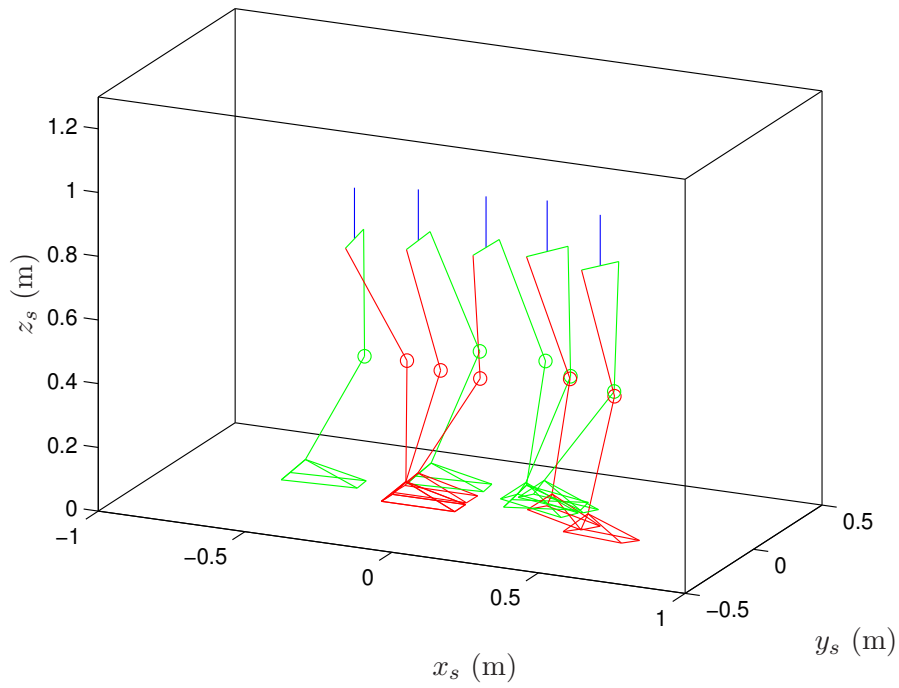


Figure 2.34: The walking motion of first two steps with the classical control law.

### 2.7.5 Comparisons of five control laws

Based on whether one or two directions of ZMP are controlled or not, the proposed four walking control methods are denoted as:  $Control_{ZMP}$ ,  $Control_{without-ZMP_y}$ ,  $Control_{without-ZMP_x}$  and  $Control_{without-ZMP}$ . Besides of these, a classical control law without the regulation of  $ZMP$  is also tested for the walking simulation and it is denoted as:  $Control_{joints}$ . In order to compare these control laws more fairly, they are tested in the simulation with the same initial conditions. Note that an initial error of  $\Delta$  is introduced on  $q_2$ ,  $\dot{q}_2$  and  $\dot{\theta}$ , the errors on the other joints are introduced to have a double support configuration. The results are summarized in Table 2.3.

$\Delta$ (rad)	0.0005	0.001	0.01	0.05
$Control_{ZMP}$	stable	stable	stable	stable
$Control_{without-ZMP_y}$	stable	stable	stable	not stable
$Control_{without-ZMP}$	stable	stable	not stable	not stable
$Control_{joints}$	stable	stable	not stable	not stable
$Control_{without-ZMP_x}$	stable	not stable	not stable	not stable

Table 2.3: Comparison of five control laws under the same initial conditions

It clearly shows that the the proposed control law where both of two directions of ZMP are controlled is the best one among them. The control principles of  $Control_{without-ZMP_y}$  and  $Control_{without-ZMP}$  show that the walking stability is not influenced by the choice of

controlled partial joints so the task of stability analysis is simplified. That is a strong point of these two control laws. In addition, their robustness is stronger than  $Control_{without-ZMP_x}$  because  $q_2$  is controlled directly in them. Furthermore,  $Control_{without-ZMP_y}$  is better than  $Control_{without-ZMP}$  because the minimum allowable error between  $ZMP_x^d$  and its constraint is much less than that between  $ZMP_y^d$  and its constraint. The property of the classical control law  $Control_{joints}$  is close to that of  $Control_{without-ZMP}$ , although in  $Control_{without-ZMP}$  the swing ankle is controlled to insure a good landing condition and the choice of controller partial joints is determined by the stability analysis. That also indicates the importance of the regulation of ZMP. In summary, for the latter four control methods, once ZMP is not completely controlled, there would be tracking errors about  $ZMP^d$  and the robot would fall down when the initial errors are large.

## 2.8 Conclusions

This chapter proposed four walking control strategies for a 3D bipedal robot with flat-feet based on tracking a reference path in the joint space instead of the general reference path expressed as a function of time. A computed-torque control method is implemented. In order to satisfy the ground contact condition, the first control law consists of a ZMP controller, a swing ankle rotation controller and a partial joint angles controller. By creating the hybrid zero dynamics, a stability study with application of Poincaré method was evaluated in a reduced dimensional space. The influence of the controlled partial joints selection on the stability of the control law was investigated. The examples showed that the stability can be improved by a pertinent choice of the controlled partial joints.

The other three walking control strategies are used to study the influences of ZMP control on the stable walking. They are a control law without regulation of ZMP and two control laws only regulating one direction of ZMP respectively, i.e.,  $ZMP_x$  and  $ZMP_y$ . In addition, an earlier classical control law without the regulation of ZMP is also tested in the simulation and compared with other four control laws with the same initial condition. The simulation results show that the first control law where both of two directions of ZMP are controlled is the best one. For other control laws where ZMP is not completely controlled, their robustness depends on the position of  $ZMP^d$  in the foot sole. For example, with the given reference trajectory the distance between the maximum value of  $ZMP_y^d$  and its constraint is larger than that between the maximum value of  $ZMP_x^d$  and its constraint, thus the control law without the regulation of  $ZMP_y^d$  is better than others.

The main contribution of this chapter is that the proposed control law consists of three sub-controllers, which can insure the position of ZMP, landing condition and walking stability, respectively. Parts of this work have been presented in conferences *Humanoids'2010* [Wang and Chevallereau, 2010a] and *Dynamic Walking 2011* [Wang and Chevallereau, 2011c]. A complete version is submitted to the journal *Robotics and Autonomous Systems* [Wang et al., 2011].

# Chapter 3

## Steering control of the 3D biped robot

### 3.1 Introduction

In Chapter 2, a stable walking control law which consists of a ZMP controller, a swing ankle rotation controller and a partial joint angles controller was proposed for the 3D biped robot with 14 actuated joints. With the proposed control law, the robot can achieve an asymptotically stable and periodic walking along a straight line. It can be observed that even though the frame  $R_0$  initially coincides with  $R_s$ , the walking motion is not exactly along the  $x_s$  axis when initial errors exist. For different initial errors, the walking direction of the biped robot is different. Moreover, the robot is expected to be able to move all over the working place in human environment. Thus we need the precise steering control not merely the simple straight walking. Therefore, the objective of this chapter is to adjust the net yaw rotation of the robot over a step in order to steer the robot to walk along paths with mild curvature.

There are few studies about direction control. In [Li et al., 2011] the walking direction of biped robot is modified by adjusting the yaw angle of the hip motors via fuzzy logic control law. [Nishiwaki et al., 2003] and [Kurazume et al., 2003] studied the turning motions for biped with ZMP-based footstep planning. Work in [Matsumoto and Kawamura, 2010] proposed the robust direction control system that used gyro sensor feedback under environment with disturbance. In [Yagi and Lumelsky, 2000], motion stability during turning is ensured by adjusting the swing leg center of mass (COM) and hip position trajectories in a trial and error fashion. In this chapter, an event-based feedback controller [Grizzle, 2003] is integrated with the control law proposed in Section 2.5 to regulate the walking direction through the net yaw motion about the stance foot over a step. It is appended to distribute set point commands to all the actuated joints in order to achieve a desired amount of turning, as opposed to the continuous corrections used in [Gregg and Spong, 2010]. Different from the previous studies, the stability during steering is maintained. In addition, an interesting feature of this work is that one is able to control the robot's motion along

various paths with limited curvature using only a single predefined periodic motion.

This chapter is organized as follows. At first, in order to control the walking direction of the biped robot, a walking direction angle is introduced to the original system as a state of robot. In Section 3.2, the stability of the extended system is analyzed. It will be shown that the walking direction of the original system is influenced by the initial errors, and the extended system is not stable. Therefore, in Subsection 3.3, the event-based control law that has been presented in Section 1.5.5 is used to stabilize the extended system. Next in Section 3.4, three examples are given to validate the proposed method. They are respectively steering the robot to walk along a desired direction, pass through a door and reach at a predefined destination. Finally, the conclusions are given in Section 3.5.

## 3.2 Stability analysis of the extended system with yaw motion

For some robots, *heading angle* is used to describe their moving direction and it is defined as a rotation of the robot about the vertical axis in the world coordinate system [Nair and Aggarwal, 1998]. It can be estimated relative to the earth's magnetic field by using compass module [Behnke, 2006]. However, since this angle is an absolute angle, it is difficult and not necessary to be known for the humanoid robots. Usually, in the steering control of the biped robot, it's the relative distance or relative angle between the robot and target that is measured by cameras with sensors [Sreenivasa et al., 2009]. In our simulation, in order to obtain these relative informations to be used in the control law, the walking direction angle  $q_0$  is defined at first. As shown in Fig. 3.1, let  $q_l$  and  $q_r$  denote the direction angle relative to  $x_s$  axis of left foot and right foot respectively, the walking direction angle of the whole body  $q_0$  is given by:

$$q_0 = \frac{q_l + q_r}{2}, \quad (3.1)$$

where  $q_l$  and  $q_r$  can be obtained by using the position of two feet in  $x_s y_s$  plane of the absolute frame.

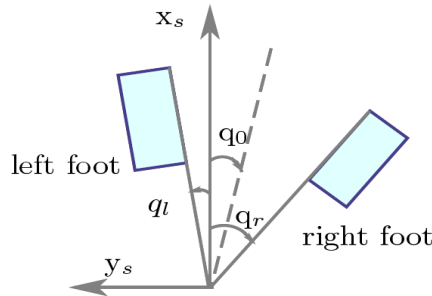


Figure 3.1: Description of walking direction

In the simulation, we have found that if there is no initial error on the states of the studied robot, the walking direction angle of two feet  $q_l$  and  $q_r$  are symmetric about  $x_s$  axis. Thus the robot will walk along  $x_s$  axis so the walking direction angle  $q_0 = 0$ . Otherwise,  $q_0 \neq 0$  and its value changes with the initial errors. For example, using the same simulation condition proposed in Subsection 2.6.4, the obtained feet positions at impacts are shown in Fig. 3.2. It clearly indicates that the robot departs from the direction of  $x_s$  axis.

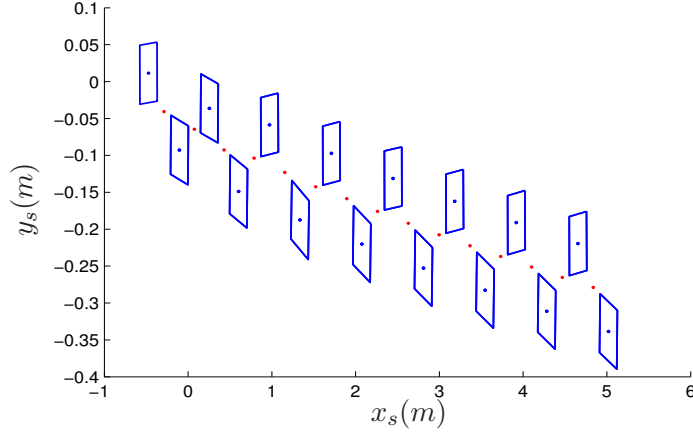


Figure 3.2: The positions of the feet at impacts with initial error of states, where the red points denote the midpoint of two feet. The robot departs from the direction of  $x_s$  axis.

In order to control the walking direction angle  $q_0$  to equal its desired value  $q_0^d$ ,  $q_0$  is regarded as a new state of robot to be considered in the configuration variables of the robot, that yields  $q^e = [q^T, q_0]^T$ . From Chapter 2 we know that under the proposed control law the original system is stable, thus during the walking phases the vector of joint angles  $q$  converges to  $q^d$  although there exist initial errors. But  $q_0$  does not converge to  $q_0^d = 0$  under the influence of initial errors. Therefore, it is necessary to analyze the stability of the extended system including  $q_0$ .

Next, the stability of the extended system is studied by using the same method presented in Subsection 2.5.6 and 2.5.7. With the proposed control law, the behavior of the robot is re-studied in the HZD (Hybrid Zero Dynamics). According to the definition of HZD, the original system is described by the states:  $x = [q_2, \dot{q}_2, \dot{\theta}]^T$  in Subsection 2.5.6. Hence, the extended system should be described by the states:  $x^e = [q_2, \dot{q}_2, \dot{\theta}, q_0]^T$ . Correspondingly, the linearized extended restricted Poincaré map at the fixed-point  $x^{e*} = [q_2^*, \dot{q}_2^*, \dot{\theta}^*, q_0^*]^T$  is written as:

$$\delta x_{k+1}^e = A^e \delta x_k^e, \quad (3.2)$$

where  $\delta x_k^e = x_k^e - x^{e*}$ ,  $x^{e*}$  and  $x_k^e$  are respectively the values of  $x^e$  at the fixed-point and the Poincaré section of the  $k^{th}$  step. Compared with the original linearized system (2.42), since  $q_0$  is added in  $x^e$ , here  $A^e$  is a  $4 \times 4$  matrix.

According to the linearization method of the Poincaré map about the fixed-point (see

the equation (1.47)),  $A^e$  can be described by:

$$A^e = \begin{bmatrix} A_{\delta x_k, x_{k+1}}^e & A_{\delta q_{0k}, x_{k+1}}^e \\ A_{\delta x_k, q_{0k+1}}^e & A_{\delta q_{0k}, q_{0k+1}}^e \end{bmatrix} \quad (3.3)$$

where the four components of  $A^e$  denote the effect of introduced errors  $\delta x_k$  or  $\delta q_{0k}$  on the states of the next step  $\delta x_{k+1}$  or  $\delta q_{0k+1}$  respectively. Obviously,  $A_{\delta x_k, x_{k+1}}^e = A^z$ , which has been obtained in subsection 2.5.7. Moreover, it has been shown that the impact surfaces and the dynamic model are invariant under the rotation around the  $z_s$  axis of the absolute frame [Spong and Bullo, 2005]. Therefore, during the complete walking phase, a perturbation on  $q_0$  is conserved after one step while the joints' configurations  $q$  are not affected. As a consequence the resulted  $A^e$  can be written as:

$$A^e = \begin{bmatrix} A^z & \mathbf{0}_{3 \times 1} \\ A_{\delta x_k, q_{0k+1}}^e & 1 \end{bmatrix} \quad (3.4)$$

Since the stability of the extended system is determined by the eigenvalues of  $A^e$ , in which the first three eigenvalues are the eigenvalues of  $A^z$  and the fourth eigenvalue is 1. According to **Theorem 2.1** and **Theorem 2.2**, the extended system is not stable. Exactly, the walking direction angle  $q_0$  cannot be controlled by the control law proposed in Section 2.5. Therefore, if the eigenvalues of the extended system can be modified to have magnitude strictly less than one, the walking direction angle  $q_0$  can converge to its value at the fixed-point:  $q_0^*$ , which is the walking direction angle at Poincaré section for the desired reference trajectory. Furthermore,  $q_0$  can also converge to another fixed-point:  $q_0^* + C$  for any constant  $C$ . As a result, the robot can converge to a motion with a desired direction of travel  $q_0^* + C$ . If  $x^{e*} = [q_2^*, \dot{q}_2^*, \dot{\theta}^*, q_0^*]^T$  is a fixed-point for the Poincaré return map,  $x^{e*} = [q_2^*, \dot{q}_2^*, \dot{\theta}^*, q_0^* + C]^T$  is also a fixed-point for any value of  $C$ . Moreover, the Jacobian matrix of the linearized Poincaré return map  $A^e$  is the same for the different fixed-points. In summary, the problem of steering control of the biped robot can be transformed to the problem of stabilizing the extended system at the chosen fixed-points. The detail is presented in the next section.

### 3.3 Stabilization of the yaw motion

In order to stabilize the extended system, all the eigenvalues of  $A^e$  in (3.4) must have magnitude strictly less than 1. Here an event-based feedback control [Grizzle, 2003] is introduced to modify the the eigenvalues of  $A^e$ . In Subsection 1.5.5, it has been used successfully to improve the walking stability for an under-actuated planar biped robot. In this chapter, for simplicity it is only supplemented to the partial joint angles controller, and then the desired property of the overall controller shown in (2.26) is rewritten as:

$$\begin{cases} y_1 &= ZMP - ZMP^d(\theta) = 0 \\ y_{2c} &= \xi_{xy} - \xi_{xyc} = 0 \\ y_{3cs} &= u - u^d(\theta) - u_c - u_s = 0 \end{cases} \quad (3.5)$$



where the supplemented term  $u_s$  is defined like  $u_c$  in (2.27)

$$u_s = b_0 + b_1\theta + b_2\theta^2 + b_3\theta^3 \quad (3.6)$$

with  $b_0, b_1, b_2, b_3$  defined such that:

$$\begin{cases} u_s(\theta_f^d) = \beta \\ u_s(\theta) \equiv 0, \quad \theta \leq \theta_s \text{ and } \theta^* \leq \theta_s < \theta_f^d. \end{cases} \quad (3.7)$$

where  $\beta$  is the feedback control term to be determined.  $\theta^*$  is the value of  $\theta$  in the Poincaré section defined in subsection 2.5.7 ( $\theta^* = 0.4\theta_i^d + 0.6\theta_f^d$ , where  $\theta_i^d$  and  $\theta_f^d$  are the initial and final value of  $\theta$  with desired trajectory during one step).  $\theta_s$  denotes the introduction moment of the event-based feedback control and it is limited by  $\theta^* \leq \theta_s < \theta_f^d$  to insure that the state of the robot is completely defined by  $x^e$  in the Poincaré section. In order to obtain sufficient time to control the walking direction before impact, here we choose  $\theta_s = \theta^*$ .

By introducing  $u_c$  and  $u_s$  to  $u^d$ , the resulted reference trajectory can be described by Fig. 3.3. It should be noted that  $u_c$  modifies only the first part of the stance phase ( $u_c = 0$  when  $\theta \geq \frac{\theta_i^d + \theta_f^d}{2}$ ), and  $u_s$  modifies only the last part of the stance phase ( $u_s = 0$  when  $\theta \leq \theta_s$ ). Therefore, the choice of  $u_s$  in (3.7) is convenient because it does not require a re-design of the controller that has created the HZD in Chapter 2.

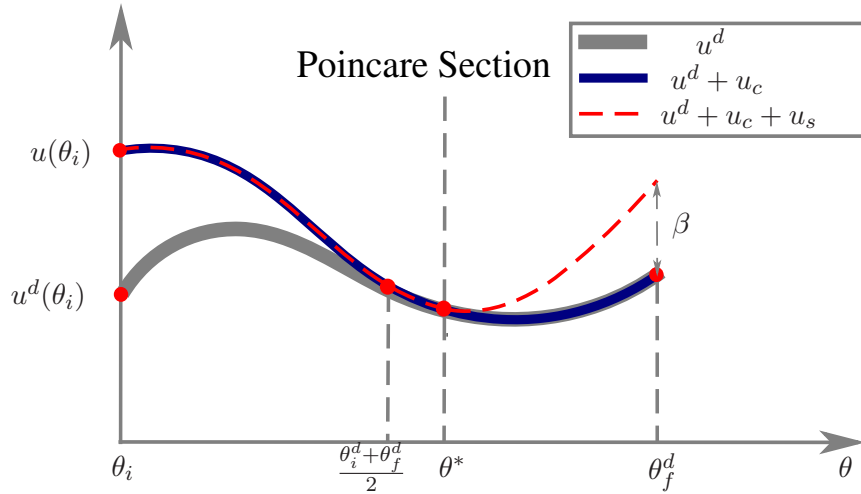


Figure 3.3: The modification of the reference path  $u^d$ .

In the thesis, for the studied biped robot with flat-feet, we always choose the Poincaré section before impact, specifically,  $\theta^* = 0.4\theta_i^d + 0.6\theta_f^d$ . According to the definition of  $u_s$  in (3.7), the modification term is maximum at each impact as shown in Fig. 3.3. As a result, the modification of the reference trajectory is maximal at each impact, that is helpful for reaching the desired walking direction quickly. However, if the Poincaré section was chosen

at impact, the modification of the reference trajectory will act essentially at the middle of the swing phase, but the joints' configurations will have to be unchanged at impact (to preserve the initial fixed-point). Therefore, a large change of reference trajectory (involving a large variation of torque) will produce a small change of walking direction angle  $q_0$ . Thus for the application considered in this chapter, it is convenient to choose the Poincaré section at the middle of the step. We recall that at the Poincaré section, the desired state of the robot is fixed. In the work [Perrin, 2011] N. Perrin also chose to impose fixed configuration at the middle of the step while modify impact configuration for "chaining" several steps with different walking direction.

As soon as the controlled output is redefined as (3.5), a new restricted Poincaré map is described from  $S_\theta \cap Z$  to  $S_\theta \cap Z$ , where  $Z = \{(\theta, q, \dot{q}, q_0) | y_1 = 0, y_{2c} = 0, \dot{y}_{2c} = 0, y_{3cs} = 0, \dot{y}_{3cs} = 0\}$  is the zero dynamics manifold (see (3.5)) and  $S_\theta = \{(\theta, q, \dot{q}, q_0) | \theta = 0.4\theta_i^d + 0.6\theta_f^d\}$  is the Poincaré section. The Poincaré map can be viewed as a nonlinear control system on  $S_\theta \cap Z$  with inputs  $\beta_k$ , namely  $x_{k+1}^e = P^z(x_k^e, \beta_k)$ , where  $\beta_k$  is the value of  $\beta$  during the  $k^{th}$  step. Linearizing the Poincaré map about the fixed-point  $x^{e*}$  and the nominal parameter value  $\beta^*$  leads to

$$\delta x_{k+1}^e = A^e \delta x_k^e + F \delta \beta_k, \quad (3.8)$$

where  $F$  is the Jacobian matrix of  $P^z$  with respect to  $\beta$ , and

$$\delta \beta_k = \beta_k - \beta^* \quad (3.9)$$

with

$$\beta^* = \mathbf{0}_{10 \times 1}. \quad (3.10)$$

Designing a feedback matrix

$$\delta \beta_k = -K \delta x_k^e \quad (3.11)$$

such that the eigenvalues of  $(A^z - FK)$  are strictly less than one will exponentially stabilize the fixed-point  $x^{e*}$ .

In (3.8),  $F$  is calculated numerically similarly to the calculation of  $A^e$ . The gain matrix  $K_{10 \times 4}$  is calculated via DLQR (design linear-quadratic state-feedback regulator for discrete-time state-space system), which is a function of control system toolbox in MATLAB. It calculates the optimal gain matrix  $K$  such that the state-feedback control law (3.11) minimizes the cost function  $\sum (\delta x_k^{e'} \delta x_k^e + r \delta \beta_k' \delta \beta_k)$ . For  $r = 5$  the eigenvalues of the linearized Poincaré map in closed loop  $(A^e - FK)$  are:

$$\begin{cases} \lambda_1 = -0.3154 \\ \lambda_2 = 0.1214 \\ \lambda_3 = -0.0016 \\ \lambda_4 = 0.0074 \end{cases} \quad (3.12)$$

All of them are less than 1 so the extended system will be stabilized and some examples of steering control are given in the next section.

## 3.4 Steering control of the walking

At the end of Section 3.2 we have announced that the problem of steering control of the biped robot can be transformed to the problem of stabilizing the extended system at different fixed-points  $q_0^* + C$ . It has been shown that the event-based feedback control law (3.11) can stabilize the extended system at the fixed-point  $x^{e*} = [q_2^*, \dot{q}_2^*, \dot{\theta}^*, q_0^* + C]^T$ . For the proposed control law, any value of  $C$  can be stabilized because the dynamic models of robot are invariant with respect to  $q_0$ . It is very interesting that  $C$  can be defined not only as a desired walking direction angle, but also as a relative distance or relative angle between the robot and a target. With different expressions of  $C$ , we are able to control the robot to walk along different paths.

### 3.4.1 Steering control of robot to walk along a desired direction

When the robot is desired to walk along a direction angle  $q_0^d$ , at the  $k^{th}$  step,  $C$  is defined as:

$$C_k = q_0^d. \quad (3.13)$$

According to  $\delta x_k^e = x_k^e - x^{e*}$ , there is:

$$\delta q_{0k} = q_{0k} - (q_0^* + C_k). \quad (3.14)$$

Here  $(q_0^* + C_k)$  is the desired walking direction angle at the Poincaré section.

It should be noted that the exchange of legs is considered but only one leg model is used in stability analysis, exactly, the right leg is always supposed to be the stance leg. In fact, the effects of the same  $\delta q_0$  on the walking direction angle of two feet are different. Therefore, when the stance leg is changed, (3.14) cannot be used. The definition of  $\delta q_{0k}$  for another stance leg is given in Appendix B.

Next, considering the saturation of torques, the feedback term  $\delta q_{0k}$  is chosen as:

$$\delta q_{0k-new} = \begin{cases} Q_{sat} & , \delta q_{0k} > Q_{sat} \\ -Q_{sat} & , \delta q_{0k} < -Q_{sat} \\ \delta q_{0k} & , otherwise. \end{cases} \quad (3.15)$$

where  $Q_{sat}$  is a saturation of torque that must be chosen appropriately.

Finally, using (3.15) in (3.11), the event-based feedback control law can be calculated by:

$$\delta \beta_k = -K \begin{bmatrix} q_{2k} - q_2^* \\ \dot{q}_{2k} - \dot{q}_2^* \\ \dot{\theta} - \dot{\theta}^* \\ \delta q_{0k-new} \end{bmatrix}. \quad (3.16)$$

From (3.9) and (3.10),  $\beta_k = \delta \beta_k$  obtained in (3.16) is known, and then the introduced term  $u_s$  is given by (3.7). Finally, the controlled outputs of the partial joint angles controller are redefined by  $y_{3cs}$  in (3.5) and the steering control feedback is created. A scheme describing this process is shown in Fig. 3.4.

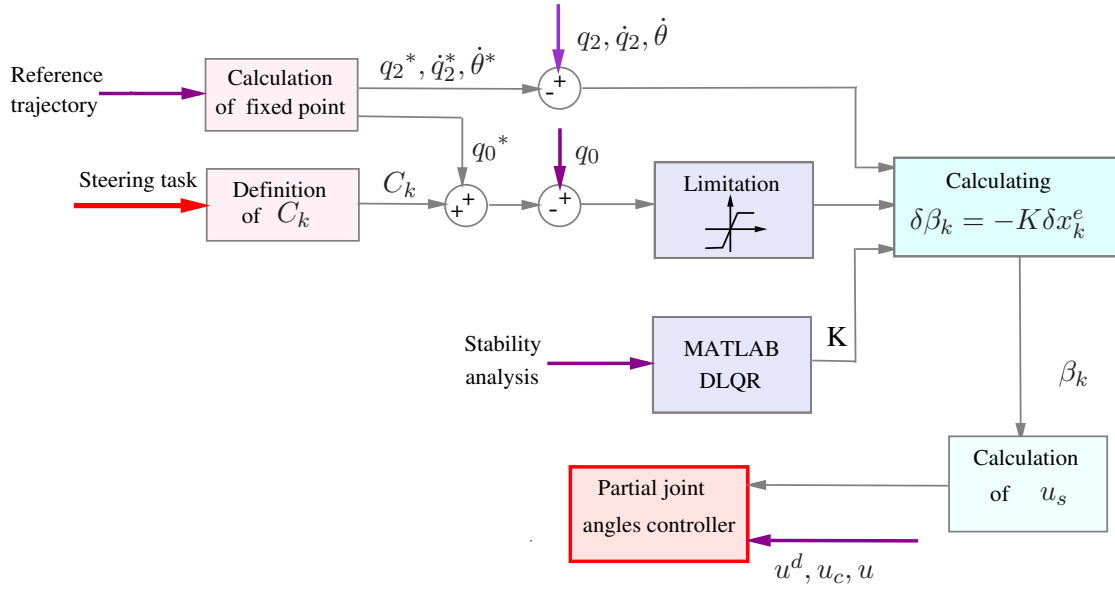


Figure 3.4: Scheme of the steering control law.

Here and in the following examples we always choose  $Q_{sat} = 9^\circ$ . For  $C = 0$ , the simulation result is shown in Fig. 3.5. It indicates that with the same initial error as in Fig. 3.2, the walking comes back to the direction of  $x_s$  axis by introducing the event-based feedback control law. In order to validate that the robot can turn with large extent, we

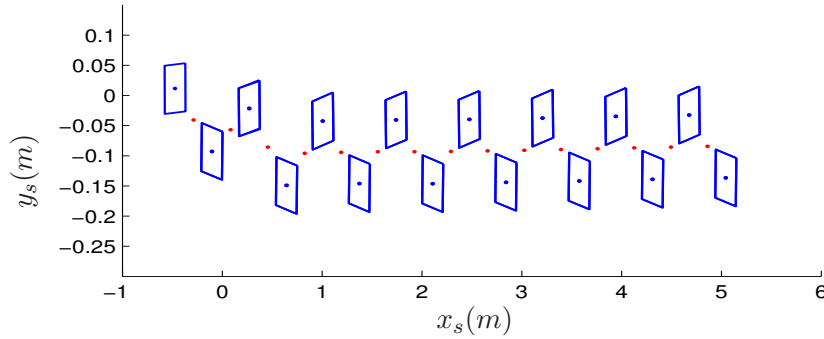


Figure 3.5: The positions of the feet at impacts under event-based feedback control, where the red points denote the midpoint of two feet. The robot walks along the direction of  $x_s$  axis .

choose  $C = 180^\circ$  and that means the robot will turn round and walk along the direction of  $-x_s$  axis. Fig. 3.6 describes the direction angle of two feet  $q_l, q_r$  and the walking direction angle  $q_0$ . It shows that  $q_0$  converges to  $180^\circ$ . The positions of the feet at impacts are shown in Fig. 3.7.

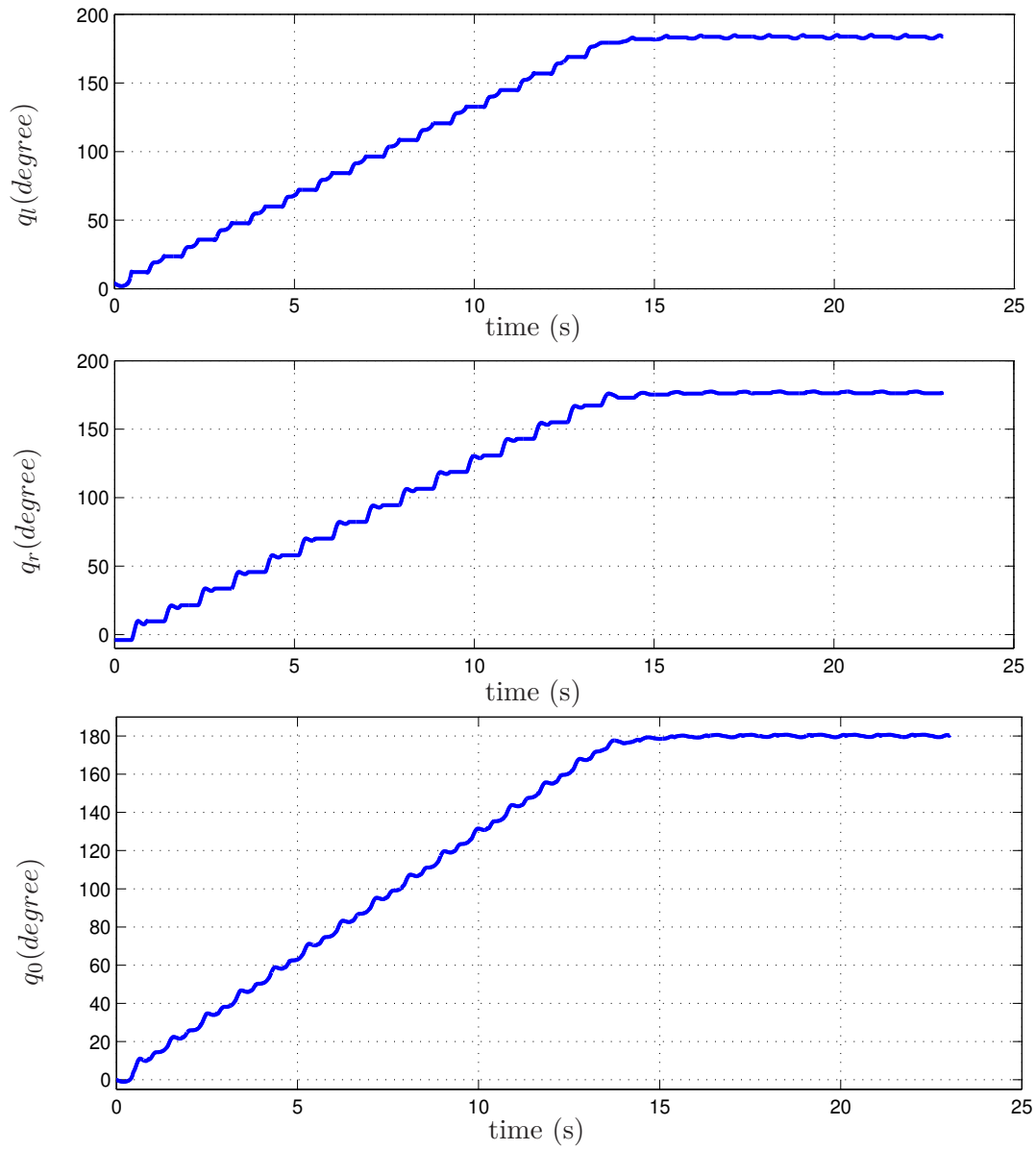


Figure 3.6: The direction angle of left foot  $q_l$ , right foot  $q_r$  and the walking direction angle  $q_0$ , where the straight lines in figures of  $q_l$  and  $q_r$  denote the single support phases.  $q_0$  converges to  $180^\circ$ .

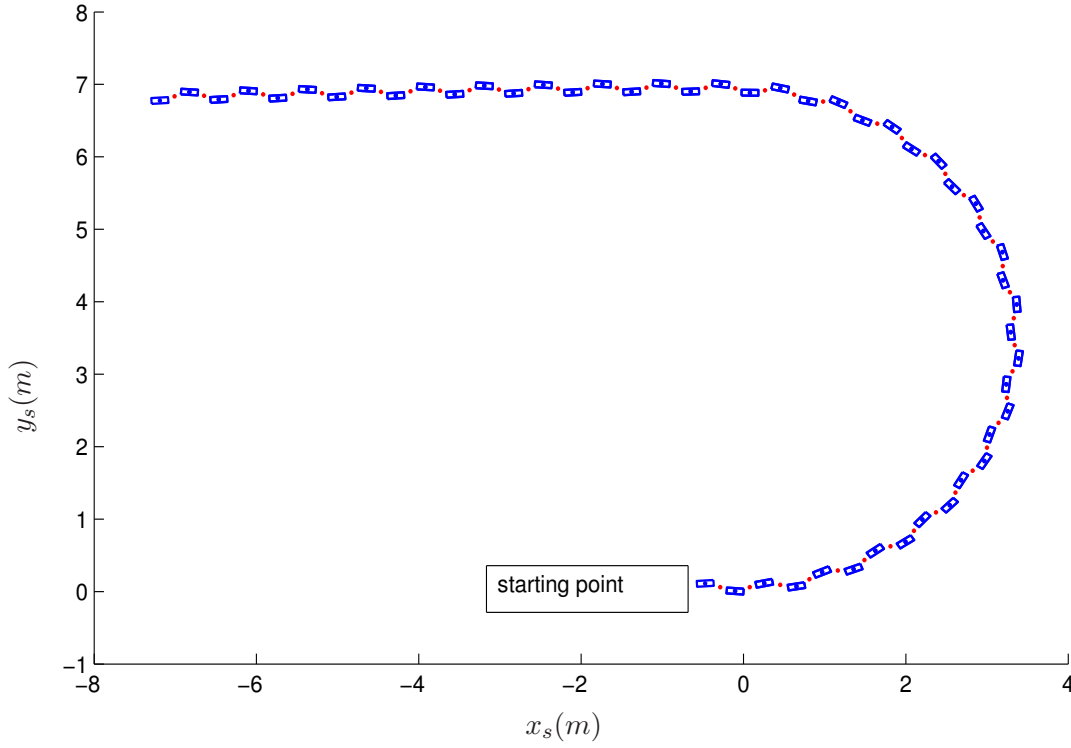


Figure 3.7: The positions of the feet at impacts under event-based feedback control, where the red points denote the midpoint of two feet. The robot walks along the direction of  $-x_s$  axis .

### 3.4.2 Steering control of robot to pass through a door

Generally, the robot is desired to be able to pass through a door like humans. It is described as *Path 1* in Fig. 3.8. With different definitions of  $C$ , the robot can be steered to walk along different paths. The control principle of *Path 1* is to regulate the walking direction to eliminate the distance between the midpoint of two feet and the goal along  $y_s$  axis , then to control the walking direction angle to 0. Therefore, at the  $k^{th}$  step,  $C$  is defined as:

$$C_k = k_1(y^d - y_k), \quad (3.17)$$

where  $y^d$  is the position of the door along  $y_s$  axis and  $y_k$  is the current position of the midpoint of two feet at the  $k^{th}$  step.  $k_1$  is the control gain and  $0 < k_1 < 1$ . In this case the frame  $R_s$  is defined with respect to the position of the door and not to coincide initially with the frame  $R_0$  which is attached to the stance foot. Substituting (3.17) in (3.14), and then using (3.15) and (3.16), the feedback control law to let the robot pass through a door is obtained.

Supposing  $y^d = -0.5$  and choosing  $k_1 = 0.8$ , the simulation results of *Path 1* are shown in Fig. 3.9 and Fig. 3.10. Fig. 3.9 indicates that the walking path converges to the desired

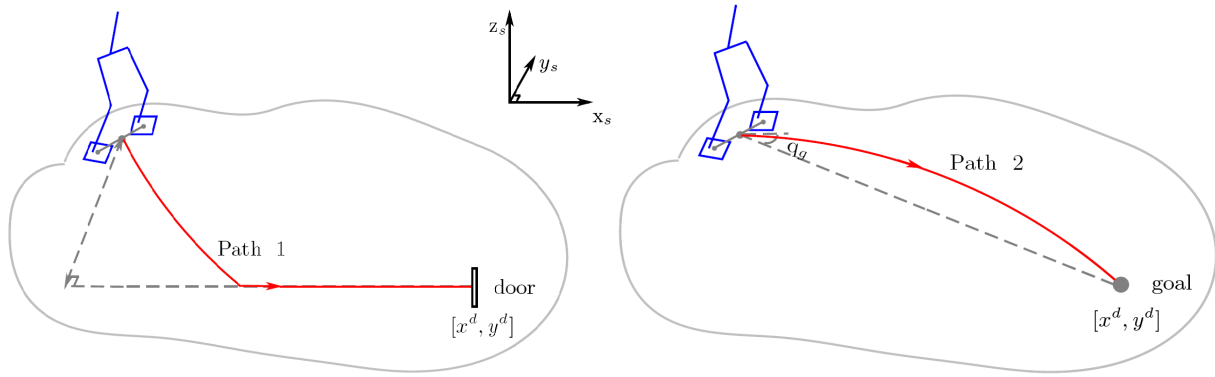


Figure 3.8: The layout of the robot and the targets.

one  $y^d = -0.5$ . Fig. 3.10 describes the direction angle of two feet  $q_l$ ,  $q_r$  and the walking direction angle  $q_0$ . It shows that  $q_0$  converges to 0 at last so the robot walks along the  $x_s$  axis, that means it can pass through the door shown in Fig. 3.8.

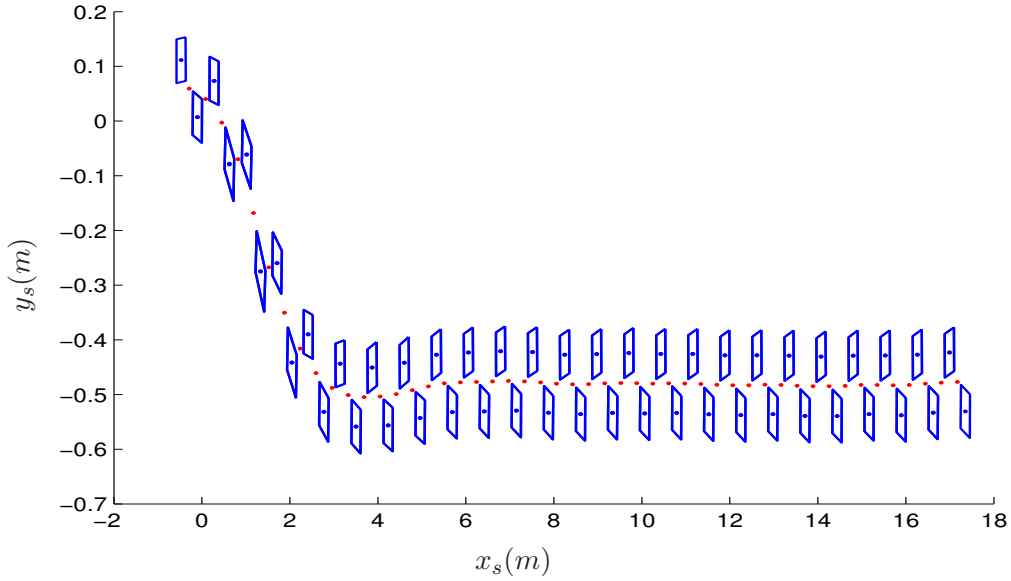


Figure 3.9: The positions of the feet at impacts for passing through the door, where the red points denote the midpoint of two feet. The walking path converges to the desired one  $y^d = -0.5$ .

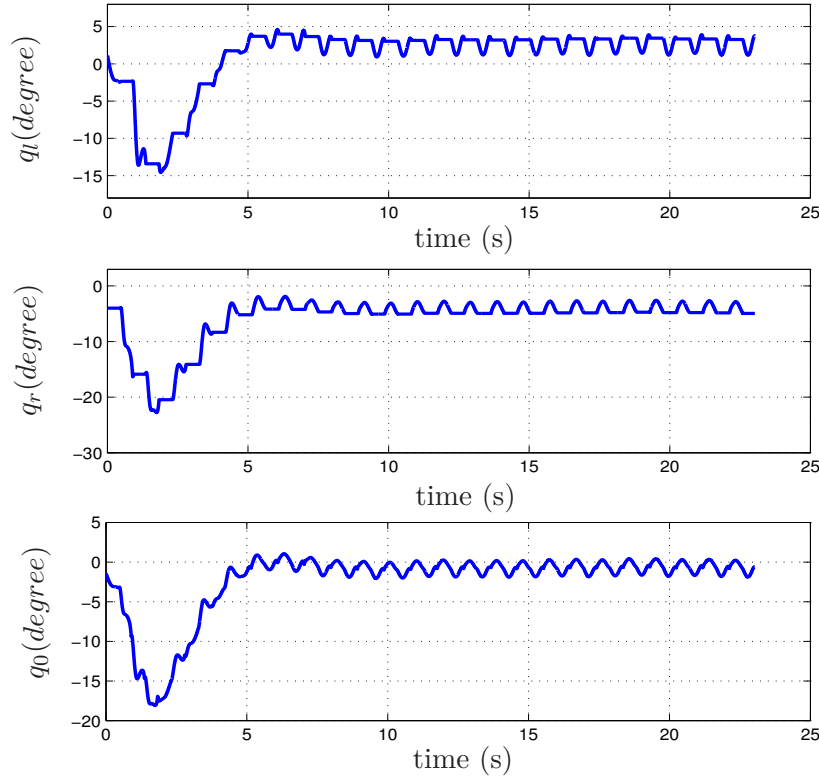


Figure 3.10: The direction angle of left foot  $q_l$ , right foot  $q_r$ , and the walking direction angle  $q_0$ , where the straight lines in figures of  $q_l$  and  $q_r$  denote the single support phases.  $q_0$  is regulated to obtain  $y^d = -0.5$  at first, then it converges to  $0^\circ$  so the robot walks along the  $x_s$  axis as shown in Fig. 3.9.

### 3.4.3 Steering control of robot to reach a destination

As shown in Fig. 3.8, if the robot is desired to reach a goal at the position  $[x^d, y^d]$ , the *Path 2* is more appropriate. The objective is to regulate the walking direction angle  $q_0$  to track the relative angle  $q_g$  between the robot and the goal in order that the walking direction of robot crosses the goal. Supposing the position of the midpoint of two feet in  $x_s y_s$  plane is  $[x_k, y_k]$  at the  $k^{th}$  step,  $q_g$  can be defined by:

$$q_{gk} = \begin{cases} \arctan\left(\frac{y^d - y_k}{x^d - x_k}\right) & , \quad x^d - x_k \geq 0 \\ \pi + \arctan\left(\frac{y^d - y_k}{x^d - x_k}\right) & , \quad otherwise. \end{cases} \quad (3.18)$$

According to the tracking objective,  $C$  is redefined to create a new fixed-point for the feedback event-based control law:

$$C_k = q_{gk}. \quad (3.19)$$



As soon as  $C_k$  is determined, using (3.14), (3.15) and (3.16), the feedback control law for the robot to reach a destination is obtained.

Two destinations at  $[6, -1]$  and  $[6, 1]$  in  $x_s y_s$  plane are chosen respectively for the simulation and Fig. 3.11 shows that the robot can reach these two points successfully. In addition, Fig. 3.12 describes the process of the robot approaching the destination at  $[6, 1]$ . As soon as the robot is close to the destination, the component of relative distance along  $y_s$  axis and  $x_s$  axis converge to 0.

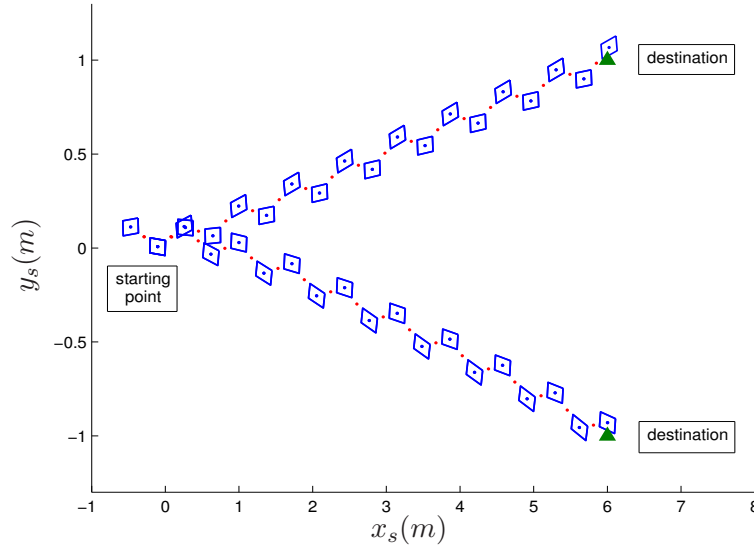


Figure 3.11: The positions of the feet at impacts for reaching two destinations at  $[6, 1]$  and  $[6, -1]$  respectively.

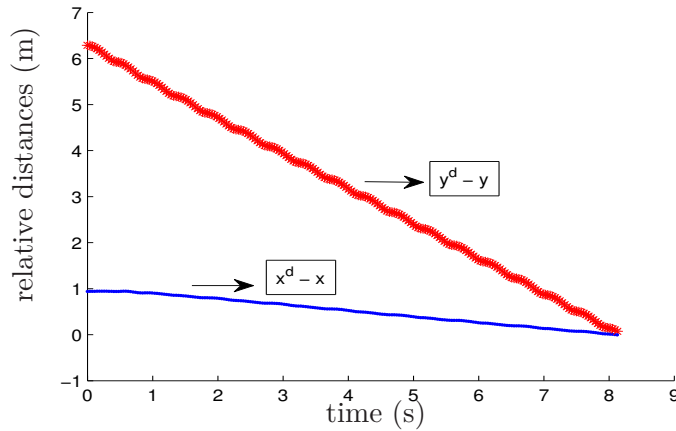


Figure 3.12: The relative distance of the robot and the destination at  $[6, 1]$ .

## 3.5 Conclusions

The main contribution of this chapter is proposing a steering control method for a 3D biped robot with flat-feet. Compared it with the previous studies, its feature is that only one single predefined periodic motion is used and the stability is ensured during the steering.

The control law proposed in Chapter 2 which consists of a ZMP controller, a swing ankle rotation controller and a partial joint angles controller, can stabilize all except the yaw motion of the robot. It was shown that the yaw rotation does not affect the dynamic model during single support phases and impacts in the closed-loop system. Therefore, a supplemental event-based feedback controller was then designed to stabilize the yaw motion.

By introducing an event-based feedback control, the eigenvalues of the extended system are modified to be less than 1. That means the yaw motion is stabilized. Since there exist an infinite number of fixed-points, at which the walking direction can be chosen, it is possible to achieve different objectives for the steering control. At last, the robot is steered successfully to walk along a predefined direction, to pass through a door and to reach a destination.

It should be noted that the event-based controller distributes commands to all of the actuated joints. Because of the restriction of the torque of joints, the robot only can turn with mild curvature.

The work of this chapter has been presented in the conference *CLAWAR'2011* [Wang and Chevallereau, 2011b], and it was awarded as one of the best technical papers.

# Chapter 4

## Walking control of a 3D biped robot with foot rotation

### 4.1 Introduction

The objective of this chapter is to extend the stable walking control method proposed in Chapter 2 to a more complicated biped robot with arms. More importantly, a *foot rotation phase* is considered in the single support phase, in which the stance heel lifts from the ground and the stance foot rotates about the toe. During the foot rotation phase, if the tracking requirements of the control law were posed in the time domain, the walking system would be under-actuated in the sense that the number of inputs would be less than the number of independent degrees of freedom.

For walking gaits that include foot rotation, various *ad-hoc* control solutions have been proposed in the previous literatures. For example, in [Takahashi and Kawamura, 2001] the robot is controlled to track desired trajectories during foot rotation phase. The toe is modeled as a free joint because the input torque cannot be applied to the toe. This kind of model becomes a non-holonomic constraint system, of which the degree of freedom degenerates. [Yi, 2000] proposed a walking control law for a biped robot with a compliant ankle mechanism. A pseudo static walking gait with dynamic gait modification method is presented by adjusting the position of a hip joint. The controller has two feedbacks, inner feedback for motor control and outer feedback for reference trajectory control. Besides, many related work considered the foot rotation phase in the jumping control [Hyon et al., 2006], [Goswami and Vadakkepat, 2009] or the running control of the robots [Kajita et al., 2007]. However, none of them can guarantee stability in the presence of the under-actuation that occurs during heel roll or toe roll.

To get around the under-actuation issue, the virtual constraints method was proposed to use a strict monotonic parameter of the robot to describe the reference trajectory instead of using the time parameter. In the previous work about the control of under-actuated biped robots with point feet [Grizzle et al., 2001], [Chevallereau et al., 2003], [Plestan et al., 2003], [Chevallereau et al., 2009], this method was used successfully to solve

the under-actuation problem, which has been introduced in Section 1.4. Next in [Chevallereau et al., 2008], it is applied for a 2D biped robot with foot rotation at the first time. It is shown that it is also effective for the under-actuation problem during the foot rotation phase. As a following work, the walking control law proposed in Chapter 2 used the same principle so it can be extended to this chapter directly. Moreover, by regarding the foot rotation angle as an actuated joint angle and considering all of its effects on the dynamic models of robot, a control law is proposed for both of fully-actuated phase and foot rotation phase. Furthermore, the stability during the foot rotation phase can also be taken into account, that is exactly what is missing in previous studies for walking gaits with foot rotation.

This chapter is organized as follows. At first, the studied robot is introduced in Section 4.2 and its dynamic models during different walking phases are presented in Section 4.3. Since the parametrized reference trajectory will be used to solve the under-actuation problem during the foot rotation phase, the parametrization of the reference trajectory is introduced in Section 4.4. Next, a control law considering ground contact and stability is proposed in Section 4.5. In order to show its validity, the simulation results of the control law considering initial errors and modeling errors are given in Section 4.6. Moreover, the simulation results of a classical control law are also shown to be compared with our control law. Finally, the conclusions are given in Section 4.7.

## 4.2 Description of the studied biped robot

Compared with the biped robot proposed in Chapter 2, the new biped robot is added two arms and the ankle joints are re-organized. The study of this robot is supported by R2A2 project of ANR and the participants are LIRMM, LISV, LCFC and IRCCyN. The robot's model is defined by LISV and it is shown in Fig. 4.1. It has 28 degrees of freedom: 3 at pelvis and each ankle, hip and shoulder, 1 at torso and each knee, elbow and toe of each foot. Since the toe is not actuated, there are 26 actuated joints in all. All the joints' configurations are described as a vector:

$$q_r = [q_1, \dots, q_{28}]_{28 \times 1}^T. \quad (4.1)$$

where  $q_1$  and  $q_{16}$  are used to describe the rotation angle of the toe in the sagittal plane of the robot, as shown in Fig. 4.2. In fact, for the swing foot, the rotation of the toe is not needed in the walking control so  $q_{16}$  is not considered here. As a result, the joint's configurations used in the dynamic model are written as:

$$q = [q_1, \dots, q_{15}, q_{17}, \dots, q_{28}]_{27 \times 1}^T. \quad (4.2)$$

Here we suppose that  $q_1$  can be measured or estimated for the real robot. Note that only the last 26 joints' configurations in  $q$  are actuated and the vector of actuated variables is written as:

$$q_a = [q_2, \dots, q_{15}, q_{17}, \dots, q_{28}]_{26 \times 1}^T. \quad (4.3)$$

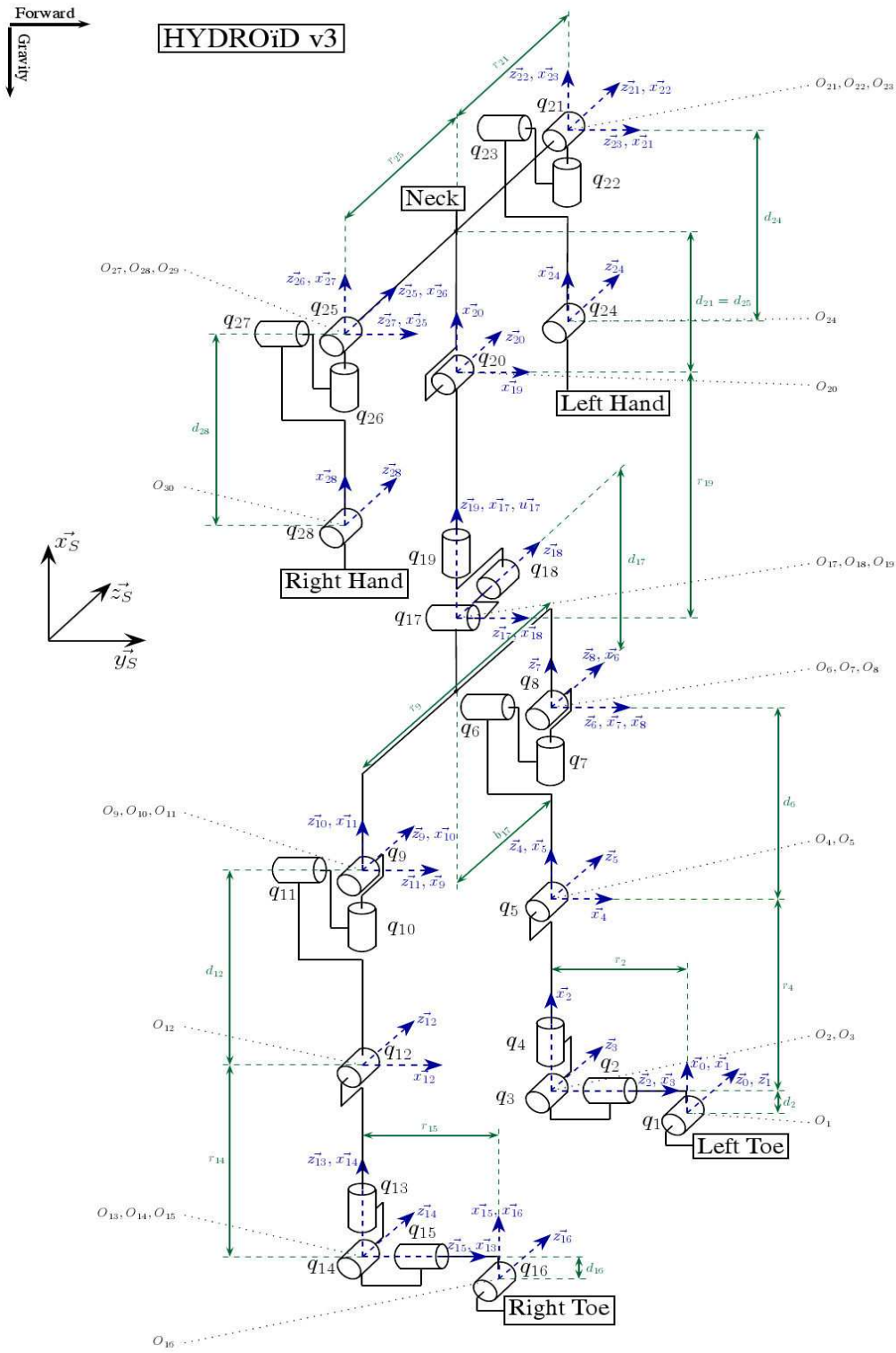


Figure 4.1: HYDROID: biped robot with arms.

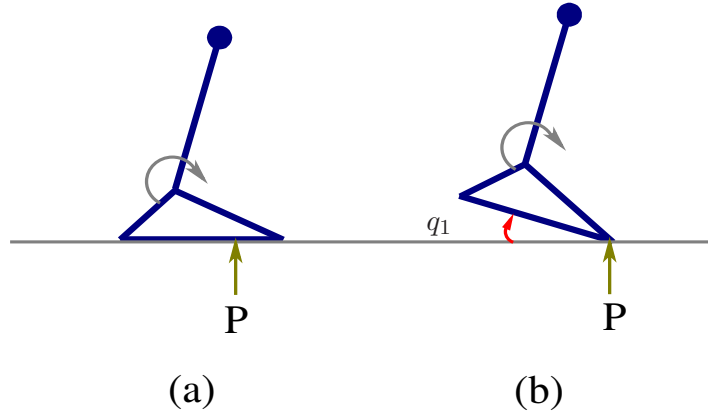


Figure 4.2: In case (a), the stance foot contacts the ground completely, the center of pressure of the forces on the foot,  $P$ , remains strictly within the interior of the footprint. In this case, the foot will not rotate,  $q_1 = 0$  and thus the system is fully actuated. In case (b), the center of pressure has moved to the toe, that allows the foot to rotate,  $q_1 \neq 0$ , thus the system is now under-actuated.

In order to design a control law which is suitable for both of two cases shown in Fig. 4.2, the vector  $q$  will be used in the dynamic models.  $q_1$  is regarded as an actuated joint angle, thus there are 27 torques corresponding to  $q$ :

$$\Gamma = [\Gamma_1, \Gamma_2, \dots, \Gamma_{27}]_{27 \times 1}^T. \quad (4.4)$$

In the following contents, we will add the constraint on the evolution of the ZMP during foot rotation phase, which corresponds to  $ZMP_x = 0$ , and thus  $\Gamma_1 = 0$ . In fact,  $\Gamma_1$  will never be used in the simulation because there is not any actuation at the toe.

The length of each body is given in Table 4.1. All links are assumed to be massive and rigid. The inertia of each link is also taken into account.

$d_2, d_{16}$	$d_6, d_{12}, r_4, r_{14}$	$d_{17}$	$d_{21}, d_{25}$	$d_{24}, d_{28}$	$b_{17}$	$r_2, r_{15}$	$r_9$	$r_{19}$	$r_{21}, r_{25}$
0.06425	0.392	0.16	0.01562	0.293	0.095	0.135	0.19	0.20478	0.191

Table 4.1: length parameters (m) of the biped model with arms

### 4.3 Dynamic model during different walking phases

The movement of human walking in one cycle is illustrated in Fig. 4.3. It shows that the stance phase consists of three periods: (1) first double support, where both feet are contacting with the ground; (2) single limb stance, where only one foot is in contact with the ground and the other foot is swinging, this phase is also called single support phase;

and (3) second double support, where both feet are in contact with the ground again. During the stance phase, there are five events: heel strike, foot-flat, mid-stance, heel-off, and toe-off. The heel strike initiates the gait cycle, and the toe-off terminates the stance phase because the foot lifts from the ground.

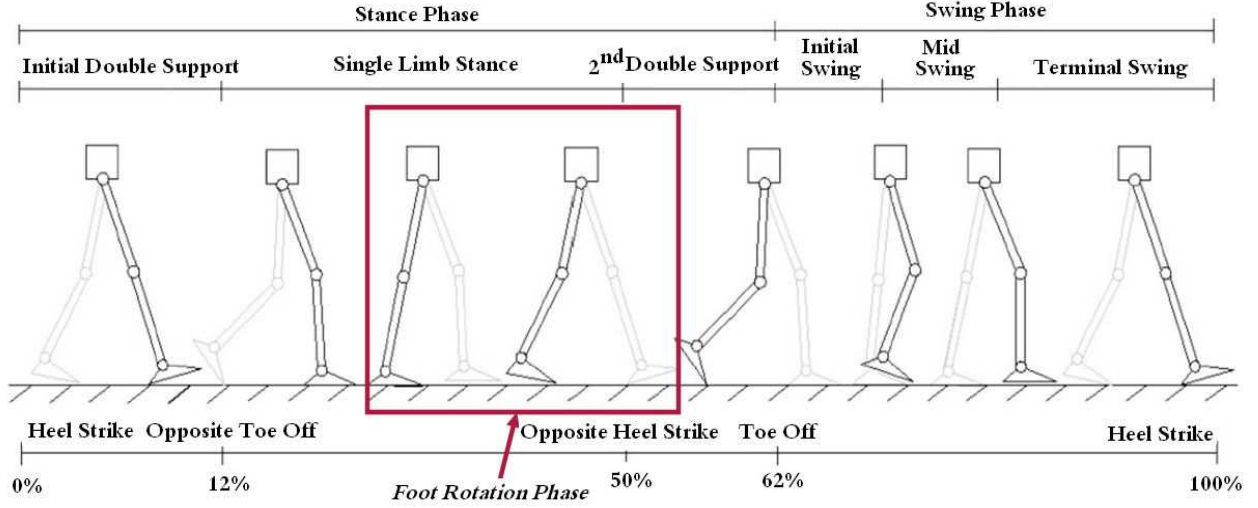


Figure 4.3: Human walking gait through one cycle, beginning and ending at heel strike. Percentages showing contact events are given at their approximate location in the cycle. Adapted from [Rose and Gamble, 1994].

In order to realize a more human-like walking gait as shown in Fig. 4.3, a *foot rotation phase* during which the stance heel lifts from the ground and the stance foot rotates about the toe is considered in the single support phase of our robot. It allows robot to reduce significantly the cost criterion for fast motions [Huang et al., 2001], [Tlalolini et al., 2009]. Work in [Kuo, 2002] shows that plantarflexion of the ankle, which initiates heel rise and toe roll, is the most efficient method to reduce energy loss at the subsequent impact of the swing leg. This motion is also necessary for the aesthetics of mechanical walking. Therefore, a whole walking phase of the studied robot is shown in Fig. 4.4. The walking begins from an instantaneous double support phase, during which one foot touches the ground completely and the other one is preparing to lift and only its toe touches the ground. The following single support phase is divided into fully support phase and foot rotation phase, which is also the under-actuated phase because during this phase the stance foot rotates around its metatarsal axis thus the robot has 28 DoF but only 26 actuated joints. At the end of foot rotation phase, the swing foot parallels to the ground and then the impact occurs.

The dynamic models for every walking phase are derived here by assuming support on left leg. They are described as follows and the models for support on right leg can be written in a similar way. It is worth mentioning that the models to be proposed are suitable for both of the fully support phase and foot rotation phase.

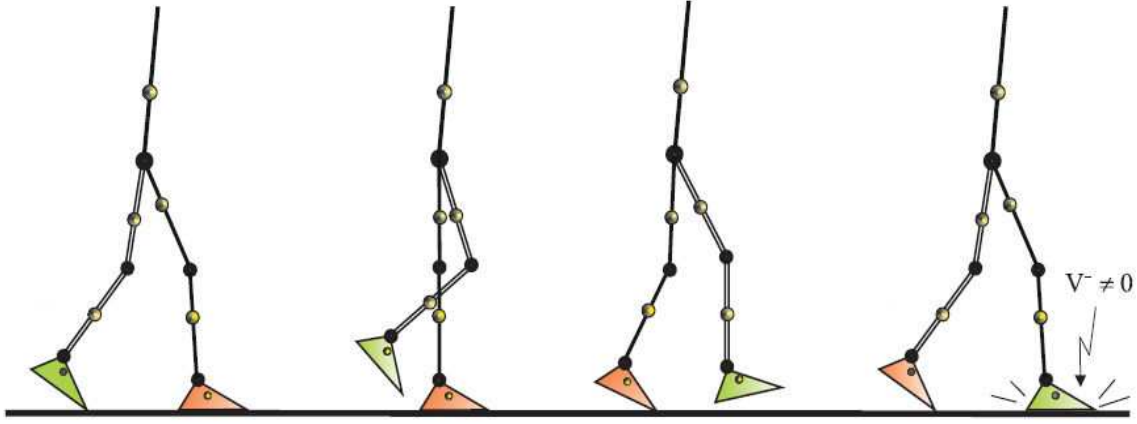


Figure 4.4: Walking gait of the studied robot with foot rotation phase. Adapted from [Tlalolini, 2008].

### 4.3.1 Dynamic model during single support phase

Compared with the dynamic model in Subsection 2.3.1, here an important point is that the effects of the rotation angle of the stance foot around its toe, i.e.,  $q_1$  on the dynamic models have to be considered. Similar to the equation (2.2), using Newton-Euler algorithm the dynamic model during foot rotation phase is written as:

$$\begin{bmatrix} F \\ M \\ \Gamma \end{bmatrix} = NE_{r1}(q)\ddot{q}_{27 \times 1} + NE_{r2}(q, \dot{q}) \quad (4.5)$$

where  $NE_{r1}(q)$  denotes all the coefficient terms of  $\ddot{q}$  and  $NE_{r2}(q, \dot{q})$  denotes all the terms without  $\ddot{q}$  and it includes Coriolis, centrifugal and gravitational terms.  $F$  and  $M$  compose the wrench vector exerted by the ground on the stance foot. They are expressed in the set of coordinate  $x_0y_0z_0$  and they will be used to calculate the position of ZMP. Since (4.5) is effective for any values of foot rotation angle  $q_1$ , it can be used in the case of  $q_1 = 0$ , i.e., the fully support phase. However, one difference between the results of two phases is that  $\Gamma_1 \neq 0$  during fully support phase while  $\Gamma_1 = 0$  during foot rotation phase because ZMP moves to the toe of stance foot.

### 4.3.2 ZMP dynamics

The calculation of ZMP dynamics has been presented in Subsection 2.3.2. It can be extended to the new biped model directly and the change is only due to the dimension of  $q$ . It should be noted that the definition of the absolute coordinate system  $x_sy_s z_s$  is modified in the new model shown in Fig. 4.1 because the naming order of the joints is changed. Compared with (2.4), now the components of the moment of an arbitrary point  $P$  in the



horizontal plane are rewritten as:

$$\begin{bmatrix} M_{py} \\ M_{pz} \end{bmatrix} = f_r(q, \dot{q}, \ddot{q}, \vec{OP}) = W\ddot{q}_{27 \times 1} + H \quad (4.6)$$

where the distance vector  $\vec{OP}$  is always defined in the coordinate system fixed in the foot, i.e.,  $x_0y_0z_0$  in Fig. 4.1. The function  $f_r()$  in (4.6) depends on (4.5) and (2.3), and  $W$ ,  $H$  can be obtained by:

$$H = f_r(q, \dot{q}, \ddot{q} = \mathbf{0}_{27 \times 1}, \vec{OP}), \quad (4.7)$$

and

$$\begin{cases} W(:, i) = f_r(q, \dot{q}, \ddot{q} = \mathbf{e}_{27 \times 1}, \vec{OP}) - H \\ \mathbf{e}(i) = 1, \quad i \in \{1, 2, \dots, 27\} \\ \mathbf{e}(j) = 0, \quad j \in \{1, 2, \dots, 27\} \quad \text{and} \quad j \neq i \end{cases} \quad (4.8)$$

(4.6) can be used to constrain the acceleration  $\ddot{q}$  in order that the ZMP which is such that

$$M_{py} = M_{pz} = 0 \quad (4.9)$$

is at a desired point  $P$ .

### 4.3.3 Impact model

For the new biped model, the stance foot touches the ground completely after impact, so there always exist  $q_1^+ = 0$  and  $\dot{q}_1^+ = 0$ , thus only the states of actuated joint  $q_a$ ,  $\dot{q}_a$  need to be calculated in the impact model and they are given by:

$$\begin{cases} q_a^+ = E q_a^- \\ \dot{q}_a^+ = EI(q^-) \dot{q}^- \end{cases} \quad (4.10)$$

where  $E_{26 \times 26}$  is a permutation matrix describing exchanges of legs and arms. The function  $EI_{26 \times 27}$  represents the linear jump of the joint velocity.

## 4.4 Parametrization of the reference trajectory

It is well known that  $q^d(t)$  should be parametrized by a quantity depending on the state of the robot that is strictly monotonic like time  $t$  during the walking phase. As presented in Section 2.4, in the sagittal plane the angle of a virtual stance leg defined by the line that connects the stance foot to the stance hip is chosen to replace the time  $t$  to parametrize the reference trajectory. As shown in Fig. 4.5, note that during the fully support phase, when the stance foot is fixed respect to the ground, this angle is considered as referenced to the initial frame, and hence becomes an absolute angle. Because the shin and the thigh have the same length, it can be calculated as (2.9):

$$\theta = \pi - q_3 + 0.5(q_3 + q_5) = \pi - 0.5q_3 + 0.5q_5. \quad (4.11)$$

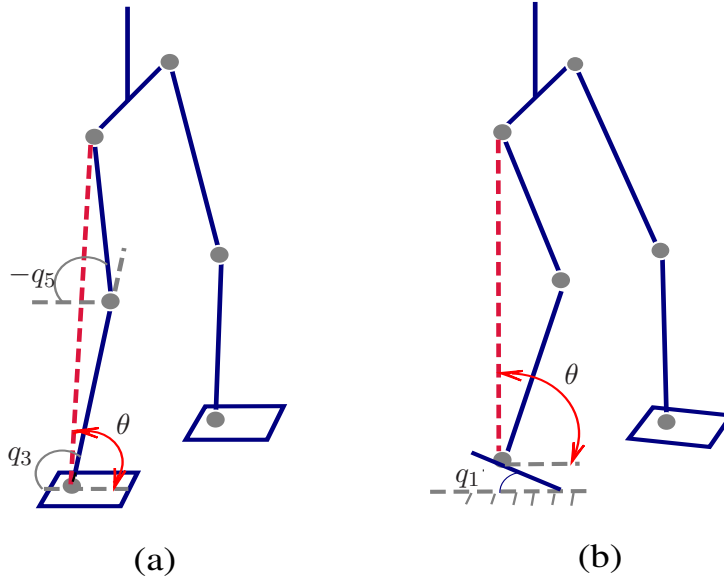


Figure 4.5: The definition of  $\theta$  during fully support phase (a) and foot rotation phase (b). Note that the definition of joint angle for the ankle and knee, i.e.,  $q_3$  and  $q_5$ , are different from that of the robot's model shown in Fig. 2.4. This is because the definition of coordinate systems for the two joints are changed in the new robot model.

However, during foot rotation phase, there exists a rotation angle of the stance foot  $q_1$ , since  $\theta$  obtained in (4.11) is just a relative angle of the virtual stance leg with respect to the stance foot, the absolute angle should be:

$$\theta = \pi - 0.5q_3 + 0.5q_5 - q_1. \quad (4.12)$$

Because  $\pi$  is a constant and it does not influence the monotonicity of  $\theta$ , in order to create a linear relation between  $\theta$  and  $q$  to be easily used in the control law, we choose:

$$\theta = -0.5q_3 + 0.5q_5 - q_1. \quad (4.13)$$

Obviously, (4.13) also can be used in the fully support phase because when  $q_1 = 0$  (4.12) is equivalent to (4.11).

Next, similar to Section 2.4, a one-dimensional Bezier polynomial is chosen to describe the reference trajectory and the reference path  $h^d(s)$  is designed in order to be compatible with a periodic solution of the biped model, as presented in (2.10), (2.11) and (2.12). Based on these equations, according to a known reference trajectory  $q^d(t)$ ,  $\dot{q}^d(t)$ ,  $\ddot{q}^d(t)$ , the corresponding reference joint path can be known.

## 4.5 A control law considering ground contact and stability

The control principle has been presented in Section 2.5. As shown in Fig. 2.5, the overall control law consists of ZMP controller, swing ankle rotation controller and partial joint angles controller. In addition, in order to create a continuous and cyclic desired trajectory, the reference motion is modified after the impact phase. Since the rotation angle of the stance foot in the sagittal plane, i.e.,  $q_1$ , has been considered in the joints' configurations vector  $q$ . It can be regarded as an actuated joint angle to be adjusted in the partial joint angles controller although  $\Gamma_1 = 0$ . Therefore, the proposed control law can be extended directly from 14 dimensions to 27 dimensions. The only point is taking account of the effect of  $q_1$  on the dynamic models in the control law. Its detail is given as follows.

### 4.5.1 ZMP controller

The objective of this controller is to obtain:

$$ZMP = ZMP^d(\theta). \quad (4.14)$$

According to the definition of ZMP, if  $P$  in Fig. 2.3 is  $ZMP^d(\theta)$ , (4.6) can be rewritten as:

$$W(q, \dot{q})\ddot{q} + H(q, \dot{q}) = \mathbf{0}_{2 \times 1} \quad (4.15)$$

where  $W$  and  $H$  are recalculated by (4.7) and (4.8) with  $\vec{OP} = ZMP^d(\theta)$ . The effect of  $q_1$  has been considered in the calculation of  $W$  and  $H$  by using the dynamic model (4.5), which is needed to obtain  $M_p$  in (4.6).

### 4.5.2 Swing ankle rotation controller

Compared this part with that for the biped robot proposed in Subsection 2.5.2, for the new model shown in Fig. 4.1, one change is the direction of the absolute system  $x_s y_s z_s$ , and the other change is that  $q_1$  influences the calculation of orientation matrix from the absolute system  $x_s y_s z_s$  to the coordinate systems of the swing ankle.

In Fig. 4.1 the angles  $q_{13}$ ,  $q_{14}$  and  $q_{15}$  are used to describe the orientation of the swing ankle. They are the rotation angles of the 13<sup>th</sup>, 14<sup>th</sup> and 15<sup>th</sup> joint around the axes  $z_{13}$ ,  $z_{14}$  and  $z_{15}$ , respectively. Moreover, they reflect the yaw, pitch and roll movement of the swing foot. Therefore, in order to control the pitch and roll movement of the swing foot to force it keep flat just before impact, the previous 15 joints should be constrained. Let  ${}^s R_{15}$  be a  $3 \times 3$  orientation matrix from the coordinate system  $x_s y_s z_s$  to  $x_{15} y_{15} z_{15}$ :

$${}^s R_{15} = [s, n, a]_{3 \times 3}, \quad (4.16)$$

where  $s_{3 \times 1}$ ,  $n_{3 \times 1}$  and  $a_{3 \times 1}$  are unitary vectors defining  $x_{15} y_{15} z_{15}$  in frame  $R_s$  respectively. Note that  ${}^s R_{15}$  is calculated by using:

$${}^s R_{15} = {}^s R_1^{-1} R_{15}, \quad (4.17)$$

where  ${}^1R_{15}$  describes the orientation matrix from the coordinate system fixed on the stance foot  $x_1y_1z_1$  to  $x_{15}y_{15}z_{15}$ .  ${}^sR_1$  is the orientation matrix from the absolute coordinate system  $x_sy_s z_s$  to  $x_1y_1z_1$ , and it is given as:

$${}^sR_1 = \begin{bmatrix} \cos(q_1) & -\sin(q_1) & 0 \\ \sin(q_1) & \cos(q_1) & 0 \\ 0 & 0 & 1 \end{bmatrix}. \quad (4.18)$$

Obviously, during the fully support phase,  $q_1 = 0$  and  ${}^sR_1$  is an identity matrix thus the proposed control law in the following contents is suitable for both of fully support phase and foot rotation phase.

Next  ${}^sR_{15}^d = [s^d, n^d, a^d]$  is used to denote the desired orientation of transformation matrix  ${}^sR_{15}$ . Small error in the orientation of the swing ankle can be defined as  $\xi$  [Luh et al., 1980]:

$$\xi = \frac{1}{2}(s \times s^d + n \times n^d + a \times a^d). \quad (4.19)$$

The derivatives of the orientation error are:

$$\begin{cases} \dot{\xi} = {}^s\omega_{15}^d - {}^s\omega_{15} \\ \ddot{\xi} = {}^s\dot{\omega}_{15}^d - {}^s\dot{\omega}_{15} \end{cases} \quad (4.20)$$

where  ${}^s\omega_{15}$  and  ${}^s\dot{\omega}_{15}$  are the angular velocity and acceleration of the joint 15 in the absolute coordinate system  $x_sy_s z_s$ . They can be efficiently computed by the forward recursive equations of the general serial robot with  $q_1, \dots, q_{15}$ , their velocity and acceleration [Khalil and Dombre, 2002] (see Appendix A.1).

Because only the pitch and roll angle of swing foot need to be regulated, that means the orientation of swing ankle around  $x_s$  direction is not necessary, thus the objective of this control law is:

$$\xi_{yz} = \mathbf{0}_{2 \times 1} \quad (4.21)$$

Next, a PD controller like (2.19) is used to realize that and two equations about  $q, \dot{q}, \ddot{q}$  can be obtained.

### 4.5.3 Partial joint angles controller

The proposed control law is a computed-torques control, thus 27 equations about the states of robot have to be obtained to resolve  $\ddot{q}_{27 \times 1}$  to be used in the calculation of torques  $\Gamma$ . Since (4.15) and (4.21) have offered 4 restrictions about the states of robot  $q, \dot{q}, \ddot{q}$ , there are only other 23 controlled outputs can be chosen.

Because the pitch and roll movement of the swing foot are actuated by the 14<sup>th</sup> and 15<sup>th</sup> joint (see Fig. 4.1), so we can suppose that  $q_{14}$  and  $q_{15}$  have been constrained by the swing ankle rotation controller using  $q_1, q_2, \dots, q_{13}$ . Thus there is no need to consider them again in the partial joint angles controller. In addition, because all the reference trajectory are parametrized by  $\theta$  and  $\theta = -0.5q_3 + 0.5q_5 - q_1$ ,  $q_3, q_5$  and  $q_1$  are not independent of each

other and  $q_3$  is excluded here. Therefore, the joint angles that are not directly controlled via the parametrization of the reference trajectory and the swing ankle controller are:

$$Q_r = [q_1, q_2, q_4, q_5, \dots, q_{13}, q_{17}, \dots, q_{28}]_{24 \times 1}^T \quad (4.22)$$

$Q_r$  has 24 elements but only 23 controlled outputs can be defined. Since the second joint influences the lateral position of ZMP directly, in order to distinguish  $q_2$  from other joints in  $Q_r$  and avoid singularity in the control law, the controlled joint angles are chosen as:

$$u = Q + M_1 q_2 \quad (4.23)$$

with

$$Q = [q_1, q_4, q_5, \dots, q_{13}, q_{17}, \dots, q_{28}]_{23 \times 1}^T \quad (4.24)$$

Chapter 1 and Chapter 2 have shown that the choice of controlled joints affects the stability of the robot thus the stability condition will be a criteria to select  $M_1$ . Therefore, here  $M_1$  is a  $23 \times 1$  constant matrix to be determined by the stability analysis. Next, a PD controller such as (2.23) is used to achieve  $u = u^d$  and it can offer 23 constraint equations about  $q, \dot{q}, \ddot{q}$ .

#### 4.5.4 Calculation of the input torques

As proposed in Subsection 2.5.4, besides of the above three sub-controllers, in order to avoid the discontinuity, the reference trajectory used in the swing ankle rotation controller and partial joint angles controller are modified stride to stride so that they are compatible with the initial state of the robot at the beginning of each step. The new output for the feedback control design is:

$$\begin{cases} y_1 &= ZMP - ZMP^d(\theta) = 0 \\ y_{2c} &= \xi_{yz} - \xi_{yzc} = 0 \\ y_{3c} &= u - u^d(\theta) - u_c = 0 \end{cases} \quad (4.25)$$

Here  $\xi_{xyz}$  and  $u_c$  are modification terms of the original reference motions. They can be calculated by using equations (2.27)–(2.30).

Since ZMP controller offers 2 linear equations of  $\ddot{q}$  (see (4.15)), and the other two sub-controllers can give other 25 linear equations of  $\ddot{q}$  (see Appendix A.2 and A.3). Therefore, three sub-controllers described in (4.25) offer 27 equations in all and they can be integrated as:

$$A(q, \dot{q})\ddot{q} + B(q, \dot{q}) = \mathbf{0}_{27 \times 1}, \quad (4.26)$$

thus  $\ddot{q}$  can be resolved (see Appendix A.5). Then, the desired torques  $\Gamma$  can be calculated with  $\ddot{q}, \dot{q}$  and  $q$  by using the inverse dynamics via Newton-Euler algorithm (4.5).

### 4.5.5 Stability analysis

In Subsection 2.5.6 we have deduced the hybrid zero dynamics (HZD) of the control system in a reduced dimensional space. Similarly, according to the definitions of HZD, (4.25) is supposed to be satisfied. The Poincaré section is still chosen at  $\theta = 0.4\theta_i^d + 0.6\theta_f^d$ . At this instant the swing foot does not touch the ground, and since  $\theta \geq \frac{\theta_i^d + \theta_f^d}{2}$  the controlled variables are not affected by  $u_c$  and  $\xi_{yzc}$  (see Fig. 1.7). Therefore, based on the swing ankle rotation controller and partial joint angles controller which are described as the last two sub-equations in (4.25), we have:

$$\begin{cases} [q_{14}, q_{15}] = f_\xi(q_1, q_2, \dots, q_{13}) \\ Q = u^d(\theta) - M_1 q_2 \end{cases} \quad (4.27)$$

where  $f_\xi$  expresses the solution of  $q_{14}, q_{15}$  to achieve  $\xi_{yzc} = \xi_{yzc}^d = 0$ . By using (4.27) and the definition of  $u$ ,  $Q$  and  $\theta$ , we know the state of robot  $q$  can be described by  $\theta, q_2, M_1, q^d$ . Consequently, a simplified expression of  $q, \dot{q}$  is defined by a function  $f_{HZD}$ :

$$[q, \dot{q}] = f_{HZD}(q_2, \theta, \dot{q}_2, \dot{\theta}, M_1, C_{q^d}) \quad (4.28)$$

where  $C_{q^d}$  denotes all the known terms introduced by the reference trajectory  $q^d$  and its derivatives.

Next the acceleration  $\ddot{q}$  can be expressed as a function of  $q_2, \theta, \dot{q}_2, \dot{\theta}, \ddot{q}_2, \ddot{\theta}$  and it depends on  $M_1$  and  $C_{q^d}$ . Based on that, (4.25) corresponds to:

$$\begin{cases} W_{HZD}(q, \dot{q}) \begin{bmatrix} \ddot{q}_2 \\ \ddot{\theta} \end{bmatrix} + H_{HZD}(q, \dot{q}) = \mathbf{0}_{2 \times 1} \\ [q, \dot{q}] = f_{HZD}(q_2, \theta, \dot{q}_2, \dot{\theta}, M_1, C_{q^d}) \end{cases} \quad (4.29)$$

It shows that the property of the closed-loop system can be analyzed using  $q_2, \theta, \dot{q}_2, \dot{\theta}$ . Since in the Poincaré section we have chosen  $\theta^* = 0.4\theta_i^d + 0.6\theta_f^d$ , the stability is studied at the fixed-point  $x^{z*} = (q_2^d(\theta^*), \dot{q}_2^d(\theta^*), \dot{\theta}^*)$  for the proposed control law for any value of  $M_1$ . The calculation of  $\ddot{q}_2$  and  $\ddot{\theta}$  from (4.29) is explained in Appendix A.4.

## 4.6 Simulation results

In order to validate the control law proposed above, the simulation results of two examples are given. In the first one, the rotation phase of the stance foot is not considered in the reference trajectory for the same model, i.e., there is always  $q_1 = 0$  in the control law. On the contrary, in the second example it is taken into account in the walking phase so the under-actuation phase exists.

### 4.6.1 Simulation results of an example without foot rotation phase

#### Reference trajectory

The reference trajectory has been calculated off-line using the same principle presented in Subsection 2.6.1. The cyclic walking gait is composed of successive single support phases and impulsive impacts with full contact between the sole of the feet and the ground. The obtained stick-diagram for one step of the periodic walking gait is shown in Fig. 4.6.

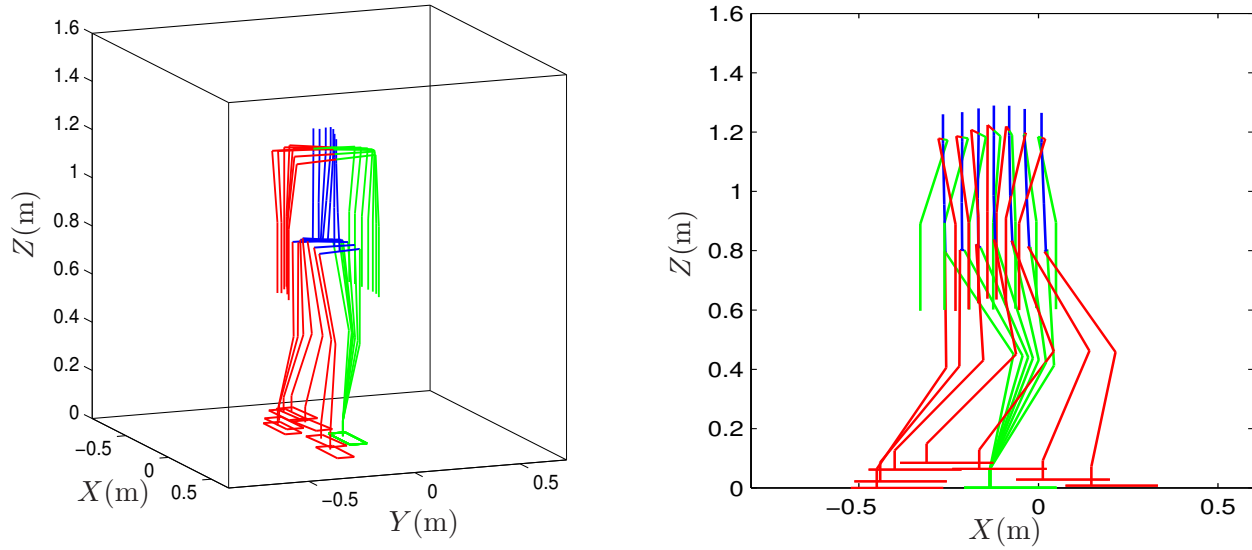


Figure 4.6: Stick-diagram for one step of the periodic walking gait in 3D space and sagittal plane.

#### The effect of different controlled partial joints on the walking stability

In order to determine the value of  $M_1$  for the controlled partial joint angles  $u$ , the effect of  $M_1$  on the walking stability should be studied. The exploration technique is used to illustrate the effect of the choice of  $M_{1(23 \times 1)}$ . Arbitrary 22 components of  $M_1$  are fixed to zero, then the largest magnitude of the eigenvalues of  $A^z$  are drawn as functions of the 23<sup>th</sup> component of  $M_1$ . If they are less than 1, the obtained walking is stable. By using this method,  $\max |\lambda_{1,2,3}|$  for  $M_1(j, 1)$ ,  $j = 1, \dots, 23$  are obtained but only in the case of  $j = 2$  the stable point is in evidence and it is shown in Fig. 4.7 (left one), where the red circle denotes that the largest magnitude of eigenvalues of  $A^z$  is less than one, that means the stable cases exist. By studying the values of  $\max |\lambda_{1,2,3}|$  for  $M_1(j, 1)$ ,  $j > 11$ , which means that the uncontrolled joint angle  $q_2$  is added to the joint angles of upper body, we find that  $M_1(j, 1)$  almost does not affect the stability in this case. An example of  $M_1(16, 1)$  is shown in the right figure of Fig. 4.7.

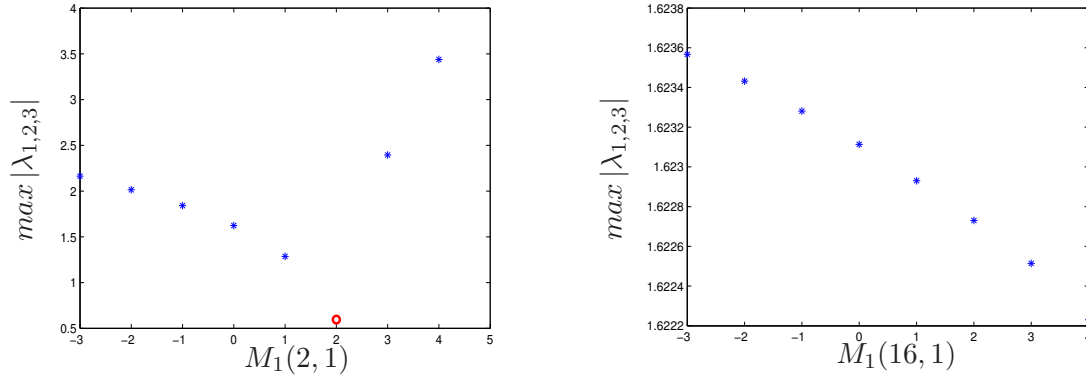


Figure 4.7:  $\max |\lambda_{1,2,3}|$  versus  $M_1(j, 1)$ ,  $j = 2, 16$ , when the other 22 components of  $M_1$  are zero.

### Simulation results

According to Fig. 4.7,  $M_1(2, 1) = 2$  is chosen to be tested in the simulator with the rigid ground model. The principle of the simulator has been presented in Section 2.6.3. For the controlled variable  $u = Q + M_1 q_2$ ,  $Q = [q_1, q_4, q_5, \dots, q_{13}, q_{17}, \dots, q_{28}]_{23 \times 1}^T$  and in  $M_1$  only  $M_1(2, 1)$  has non-zero value, thus the uncontrolled term  $M_1 q_2$  is added to  $q_4$ . An initial error of  $0.01 \text{ rad}$  is introduced on the uncontrolled joint angle  $q_2$  and a velocity error of  $0.01 \text{ rad/s}$  is introduced on  $\dot{q}_2$  and  $\dot{\theta}$ , the errors on the other joints are introduced to have a double support configuration.

The simulation results are shown in Fig. 4.8–Fig. 4.12. In Chapter 2, four points  $P_1$ ,  $P_2$ ,  $P_3$  and  $P_4$  are defined to note the vertices of the foot (see Fig. 2.3). Fig. 4.8 shows that the height of four points  $P_1$ ,  $P_2$ ,  $P_3$  and  $P_4$  are always the same, that means during the walking the swing foot keeps flat with the help of the swing ankle rotation controller. In addition, the stance foot always stays in the ground, that is because  $ZMP = ZMP^d$ , referring to Fig. 4.9. These results can also be found in the walking motion of the first three steps shown in Fig. 4.12. The phase planes for  $q_i, i = 2, 3, 4, 5$  are shown in Fig. 4.10. It clearly indicates that the walking converges to a periodic motion after some steps although there exist initial errors. The corresponding torques of these four joints  $q_i, i = 2, 3, 4, 5$  are displayed in Fig. 4.11, we can see that all the torques change periodically and they are always within the constraints. In a word, the proposed control law is effective and the stable walking can be obtained.



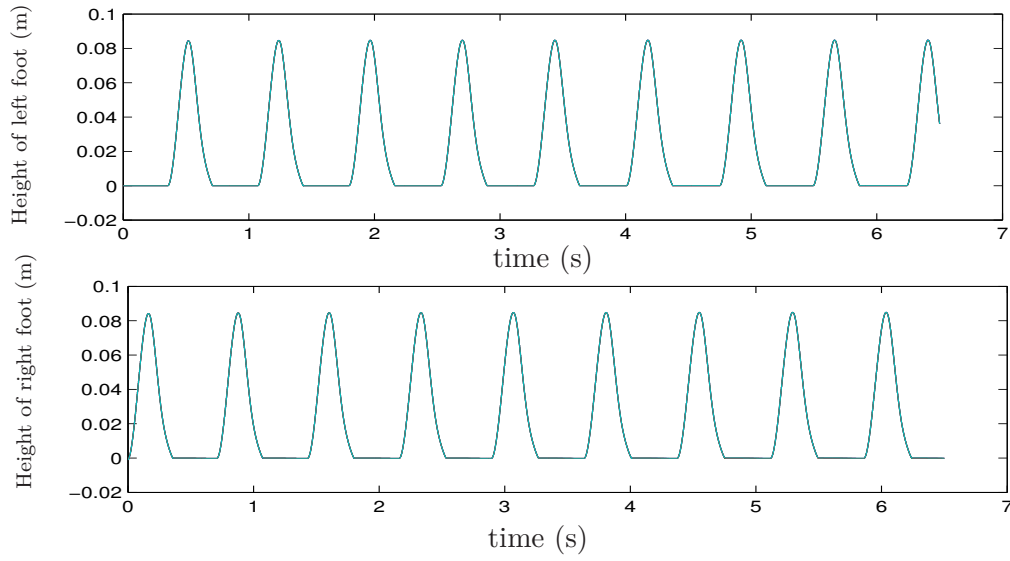


Figure 4.8: Height of feet for the walking without foot rotation phase.

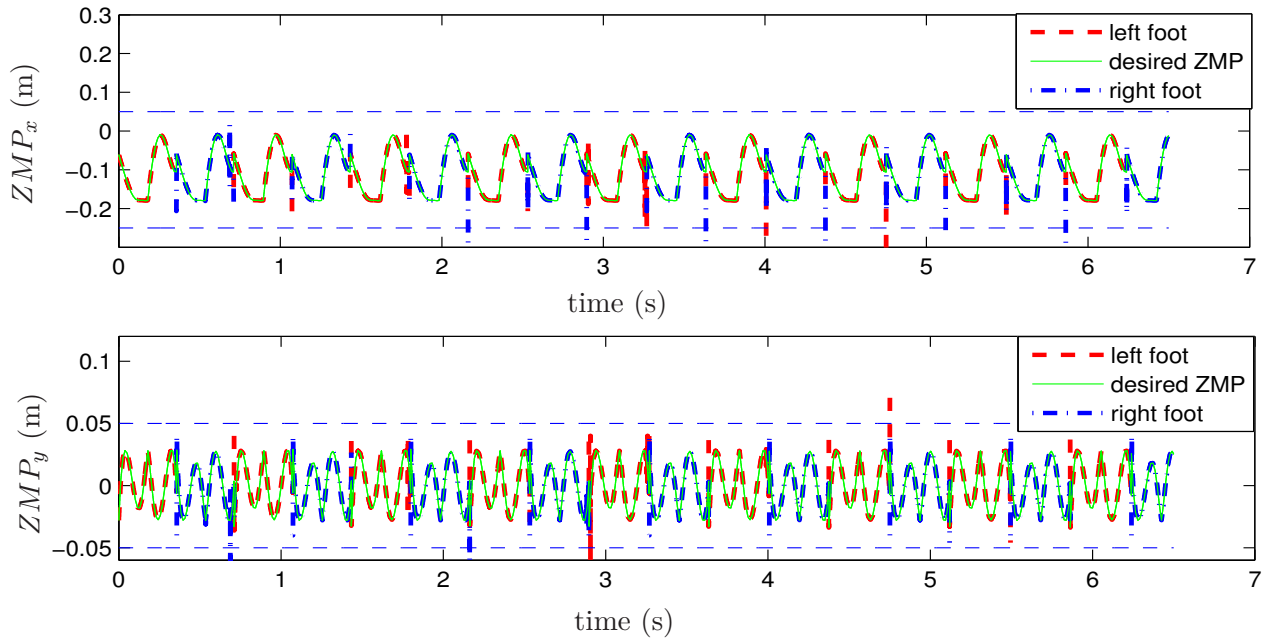


Figure 4.9: Position of ZMP in the foot sole for the walking without foot rotation phase: the position of ZMP moves periodically and is always within the limits.

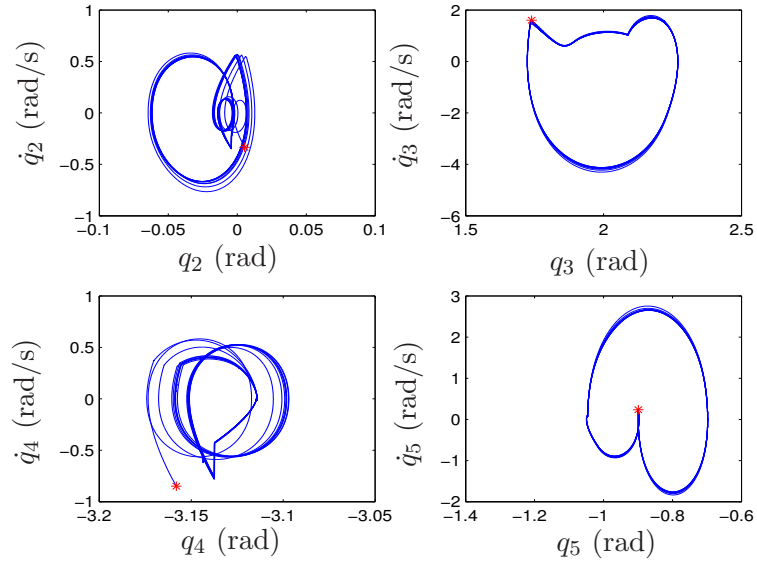


Figure 4.10: Phase-plane plots for  $q_i, i = 2, 3, 4, 5$  for the walking without foot rotation phase. The initial state is represented by a (red) star.

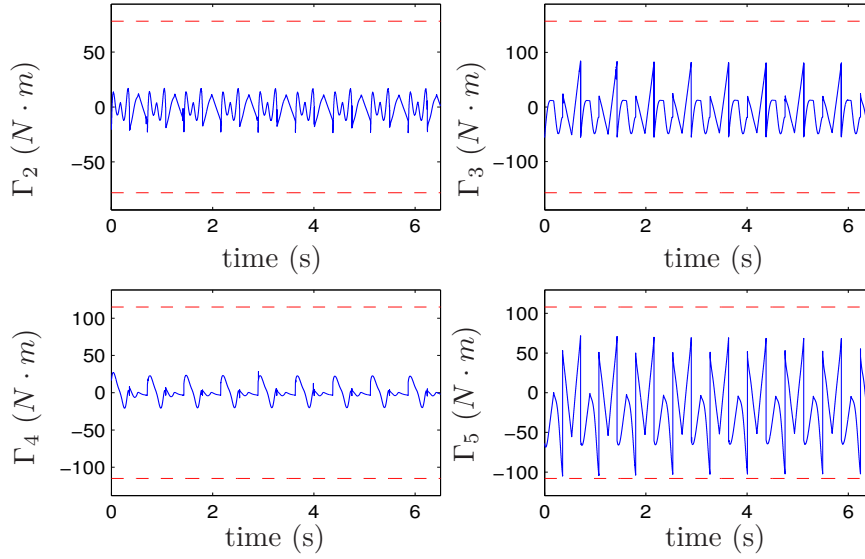


Figure 4.11: The corresponding torques of  $q_i, i = 2, 3, 4, 5$  for the walking without foot rotation phase.

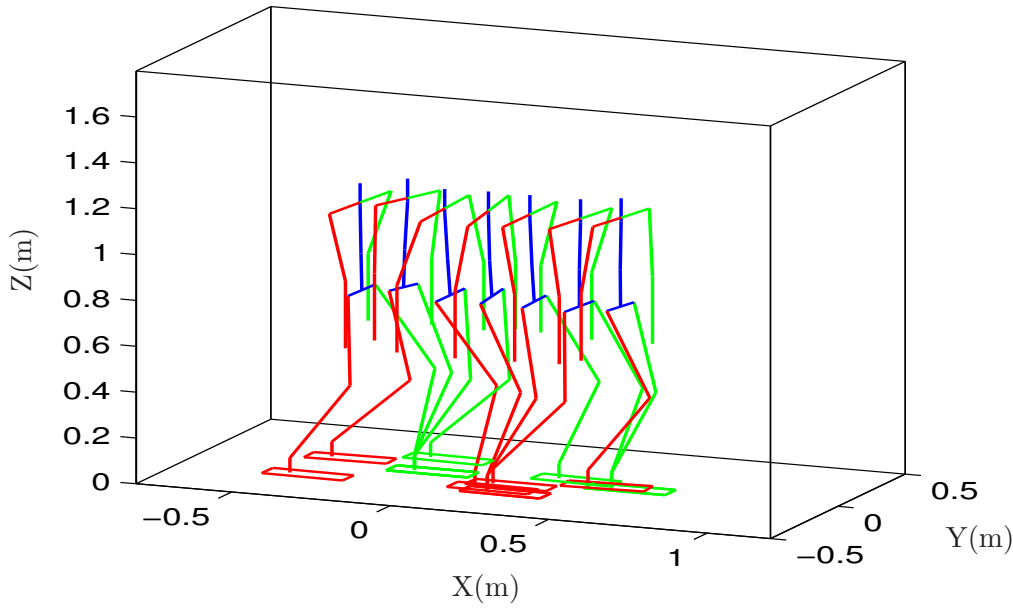


Figure 4.12: The walking motion of the robot without foot rotation phase during first three steps.

#### 4.6.2 Simulation results of the walking with foot rotation phase

##### Reference trajectory

D. Tlalolini has proposed the method to obtain the walking gait with foot rotation phase in [Tlalolini et al., 2011]. Different from previous bipedal structures, the studied model has one additional joint to take into account the foot twist rotation. During foot rotation phase, the center of pressure (CoP) remains strictly on the toe axis of the stance foot to allow the foot to rotate. The synthesis of the reference walking trajectories is stated under the form of a constrained parameter optimization problem. The resolution of this problem is obtained by sequential quadratic programming (SQP) methods. The performance criterion, based on the square of the torques, is optimized in order to increase the autonomy of energy of the biped robot. Furthermore, some constraints, such as actuator performances and limits on the ground reaction force in single support phases and at impacts, are taken into account. The obtained stick-diagram for one step of the periodic walking gait is shown in Fig. 4.13 and Fig. 4.14. From them we can clearly see that the stance heel lifts from the ground and the stance foot rotates about the toe.

Corresponding to the above walking movement, the evolution of the foot rotation angle  $q_1$  and the height of four vertices of the feet  $P_1$ ,  $P_2$ ,  $P_3$  and  $P_4$  (see Fig. 2.3) are shown in Fig. 4.15.

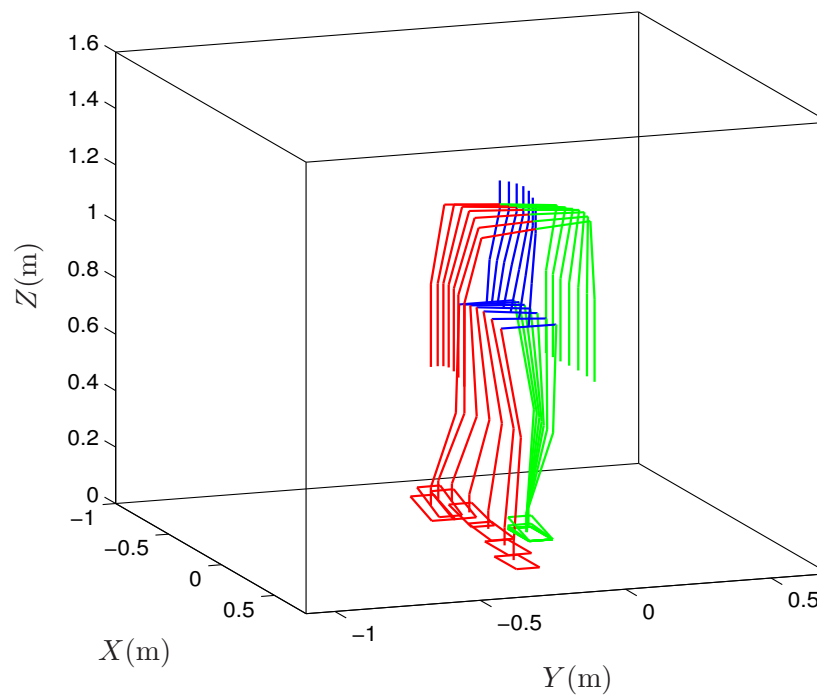


Figure 4.13: Stick-diagram for one walking step with foot rotation phase in 3D space.

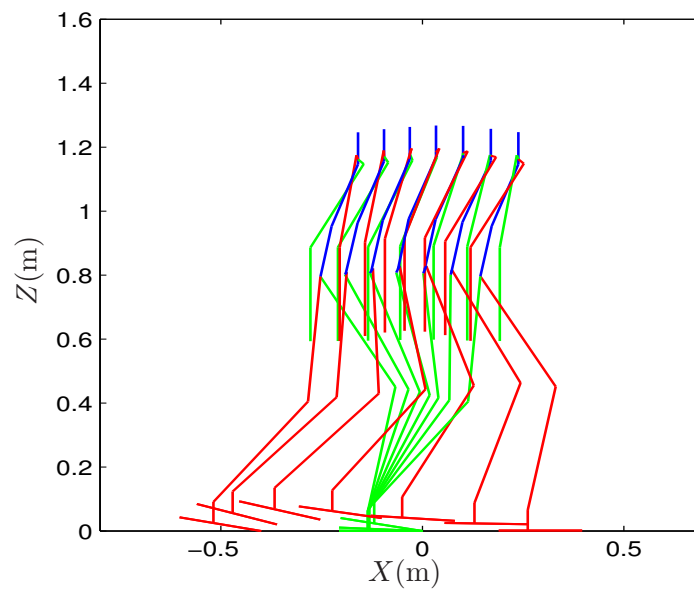


Figure 4.14: Stick-diagram for one walking step with foot rotation phase in sagittal plane.

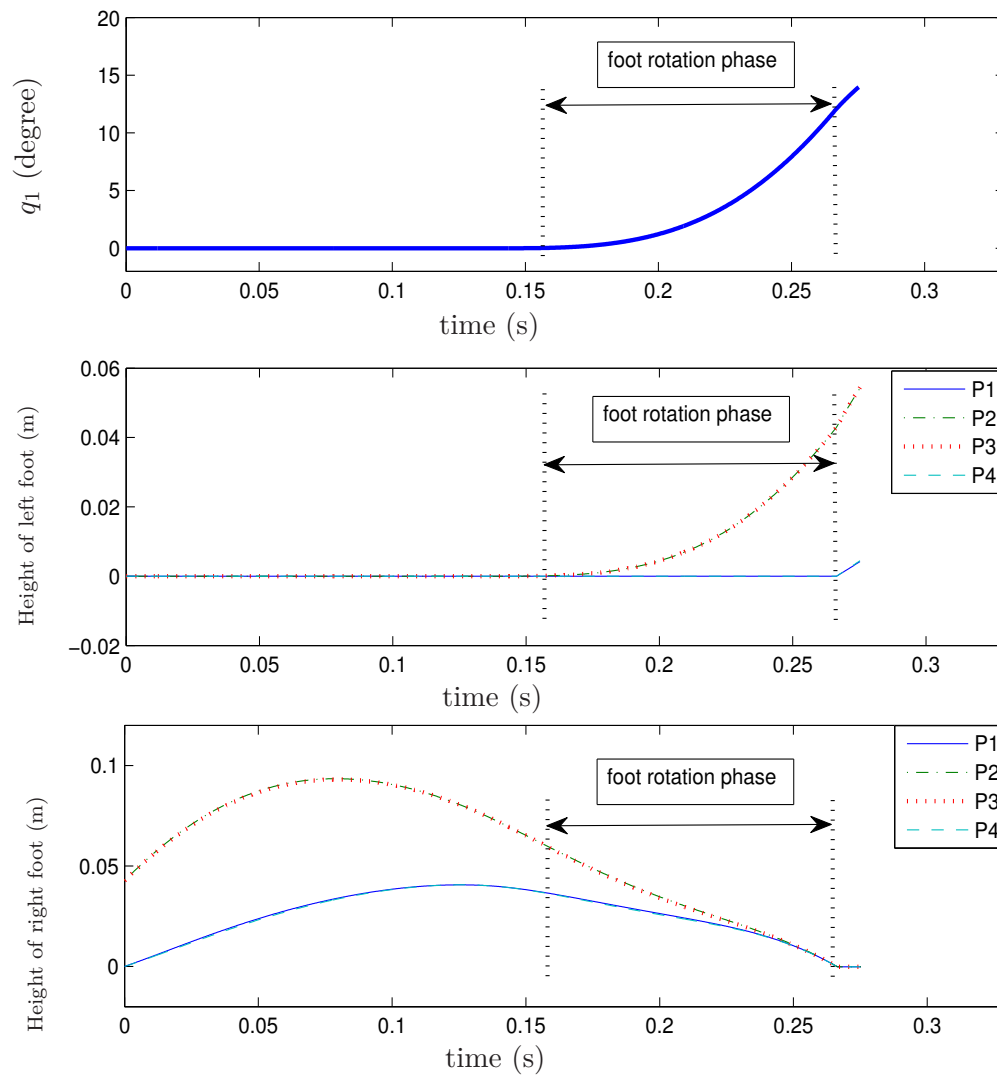


Figure 4.15: Foot rotation angle  $q_1$  and height of feet for the walking including foot rotation phase.

### The effect of different controlled partial joints on the walking stability

Using the same method proposed in Subsection 4.6.1, the analysis results of  $M_1$  for the new reference trajectory are obtained and only in the case of  $M_1(4, 1)$  a stable point is found, as shown in Fig. 4.16. We can see that if  $M_1(4, 1) = -1.5$ , the walking will be stable. According to  $u = Q + M_1 q_2$  and  $Q = [q_1, q_4, q_5, \dots, q_{13}, q_{17}, \dots, q_{28}]_{23 \times 1}^T$ , in this case, the uncontrolled term  $M_1 q_2$  is added to  $q_6$ .

It is worth mentioning that different from the right figure of Fig. 4.7, for the same biped robot but foot rotation phase is included, if  $M_1 q_2$  is added to the control of upper body joints in  $u$ , i.e.,  $M_1(j, 1), j > 11$ , it still affects the stability of the system.

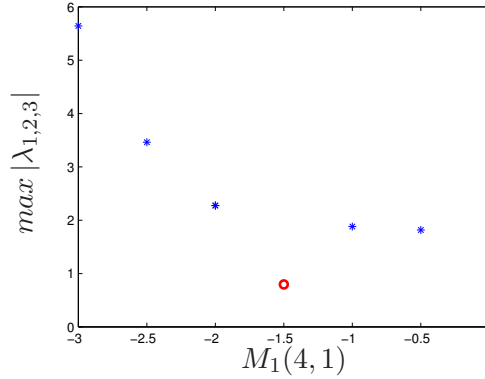


Figure 4.16:  $\max |\lambda_{1,2,3}|$  versus  $M_1(4, 1)$ , when the other 22 components of  $M_1$  are zero.

### Description of the simulator

Compared with the simulator for the walking without the foot rotation phase proposed in Section 2.6.3, here the foot rotation angle  $q_1$  and its velocity  $\dot{q}_1$  should be calculated in the new simulator to be used in the control law. In addition, in the torques obtained from the control law only  $\Gamma_2, \dots, \Gamma_{27}$  are applied on the robot. The block diagram of the simulator is shown in Fig. 4.17. Since the foot rotation angle  $q_1$  models the pitch angle of the foot, it can be calculated by using the foot posture defined in  $x_s y_s z_s$ . Similarly,  $\dot{q}_1$  is obtained from the foot velocity defined in  $x_s y_s z_s$ .

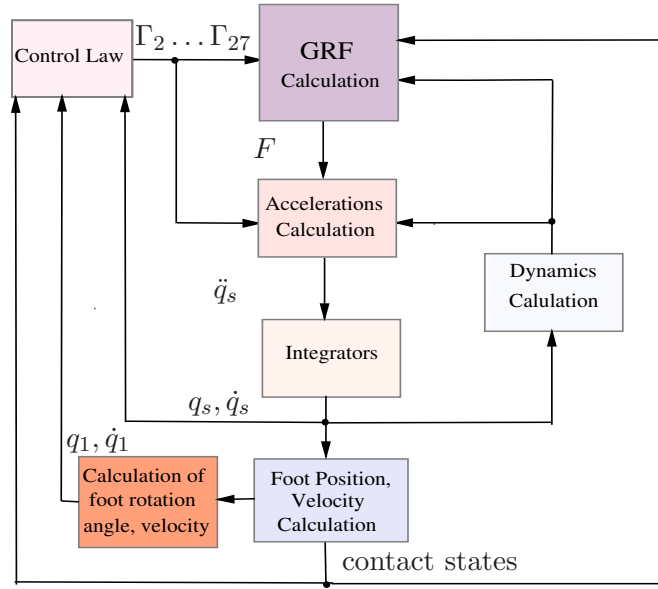


Figure 4.17: Block diagram of the simulator for the walking with foot rotation phase.

### Simulation results of the control law considering initial errors

Next use  $M_1(4, 1) = -1.5$  in the control law and test it in the simulator with the rigid ground model. An initial error of  $0.01 \text{ rad}$  is introduced on the uncontrolled joint angle  $q_2$  and a velocity error of  $0.01 \text{ rad/s}$  is introduced on  $\dot{q}_2$  and  $\dot{\theta}$ , the errors on the other joints are introduced to have a double support configuration.

The studied walking including foot rotation phase has been described in Fig. 4.4. Here it is realized by using the control law and the resulted walking motion of the first three steps are illustrated in Fig. 4.25. Fig. 4.18 shows that the height of two vertices of the toe ( $P_1$  and  $P_4$  in Fig. 2.3) are the same, the height of two vertices of the heel ( $P_2$  and  $P_3$ ) are also the same, that means both of two feet didn't roll during the whole walking phase. In the fully support phase, the stance foot keeps flat on the ground, which is also indicated by Fig. 4.19 because it shows  $ZMP = ZMP^d$ . In the foot rotation phase, the stance foot rotates around its metatarsal axis in the sagittal plane as we desired until impact phase, and the rotation angle  $q_1 = q_1^d$  as shown in Fig. 4.24. At the same time, the sole of swing foot parallels with the ground just before impact, thus the stable contact condition is satisfied.

The phase planes for  $q_i, i = 2, 3, 4, 5$  are shown in Fig. 4.20. It shows that the walking converges to a periodic motion after some steps. The corresponding torques of these four joints are given in Fig. 4.21, we can see that during the first two steps  $\Gamma_2$  and  $\Gamma_3$  are large because of the initial errors, but finally all the torques change periodically and they are always within the constraints. Moreover, the tracking errors of four uncontrolled joints  $q_2, q_3, q_{14}, q_{15}$  are shown in Fig. 4.22 and Fig. 4.23, where  $q_2$  is a additional term in the

controlled variable  $u$ ,  $q_3$  is a component of  $\theta$ ,  $q_{14}$  and  $q_{15}$  determine the pitch and roll motion of the swing foot which are controlled by swing ankle rotation controller indirectly. The figures reveal that the tracking errors of them converge to zero. In summary, the proposed control law conducted a stable walking although the under-actuated phase exists.

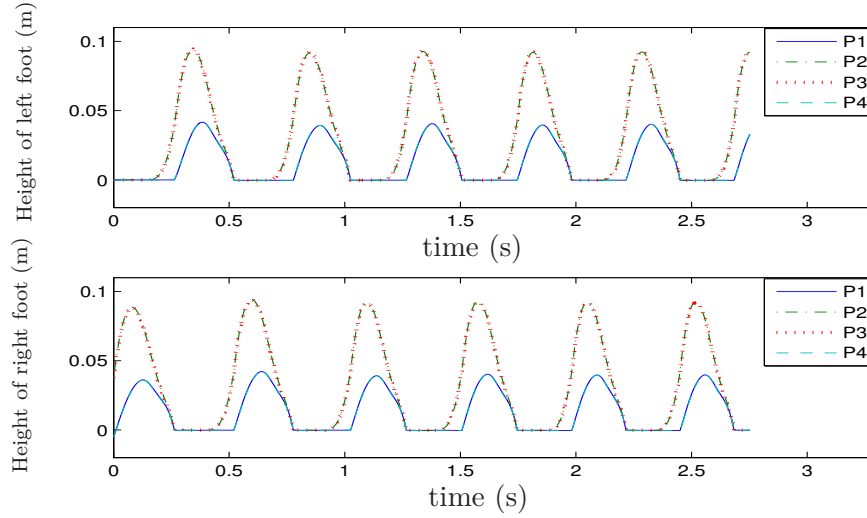


Figure 4.18: Height of feet for the walking including foot rotation phase.

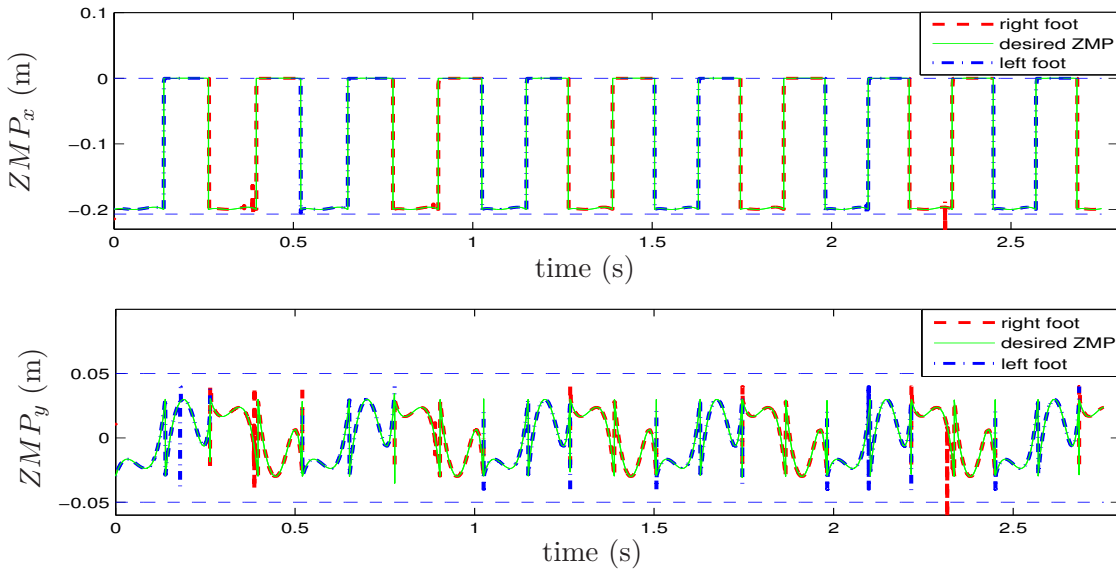


Figure 4.19: Position of ZMP in the foot sole for the walking including foot rotation phase: the position of ZMP moves periodically.  $ZMP_y$  is always within the limits and  $ZMP_x$  is zero during under-actuated phase.



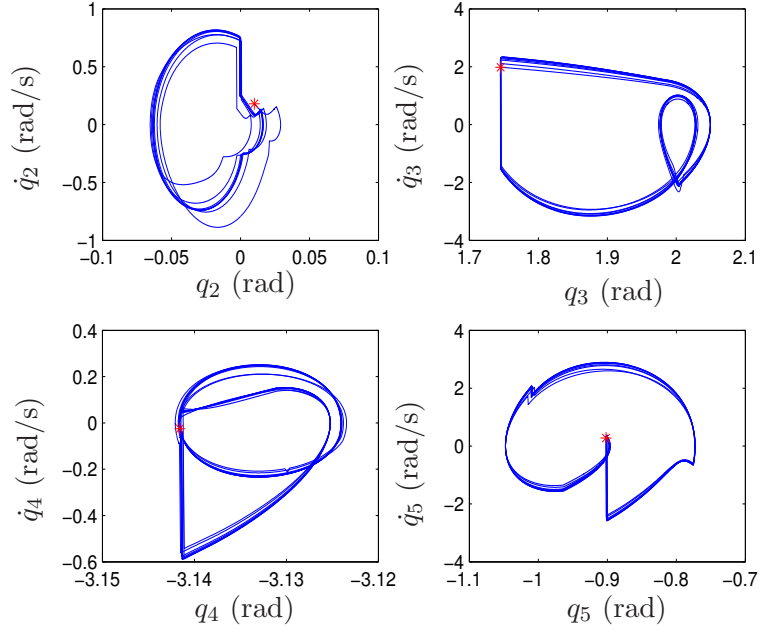


Figure 4.20: Phase-plane plots for  $q_i, i = 2, 3, 4, 5$  for the walking including foot rotation phase. The initial state is represented by a (red) star.

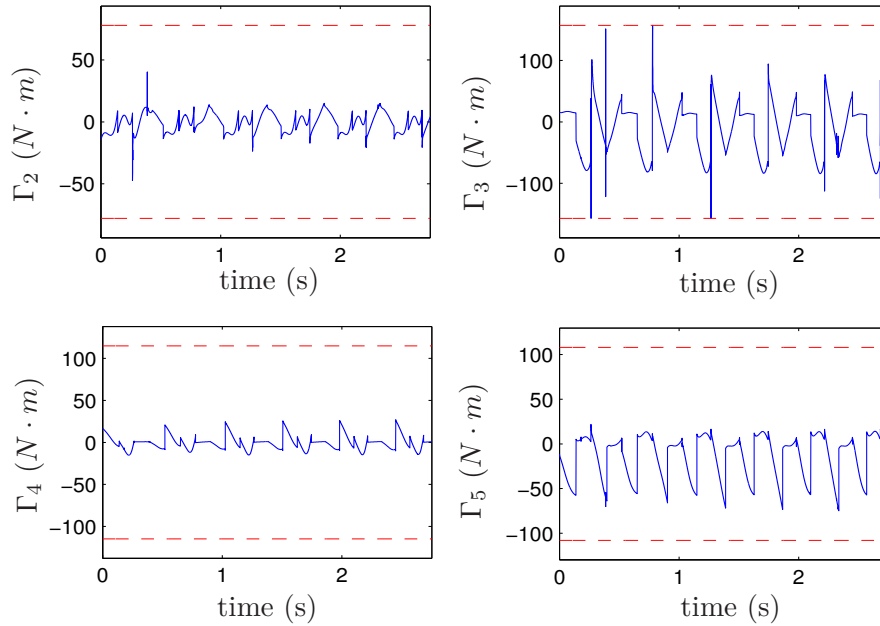


Figure 4.21: The corresponding torques of  $q_i, i = 2, 3, 4, 5$  for the walking including foot rotation phase.

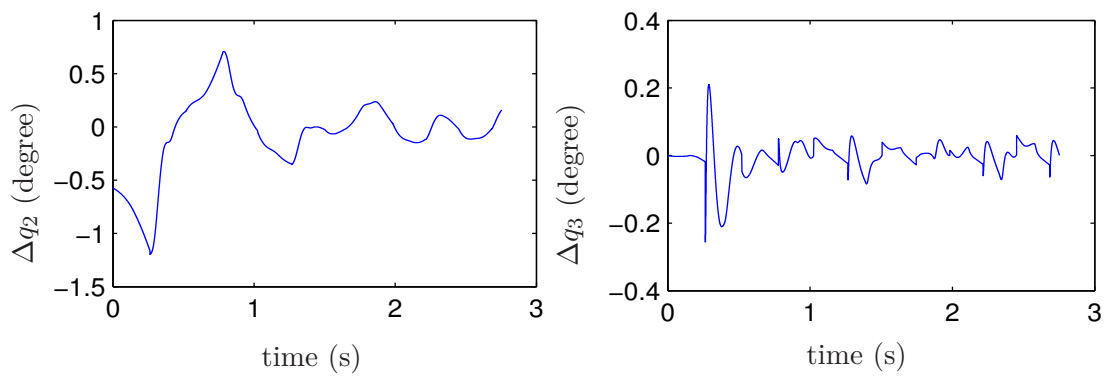


Figure 4.22: The tracking errors of  $q_2$  and  $q_3$  for the walking including foot rotation phase.

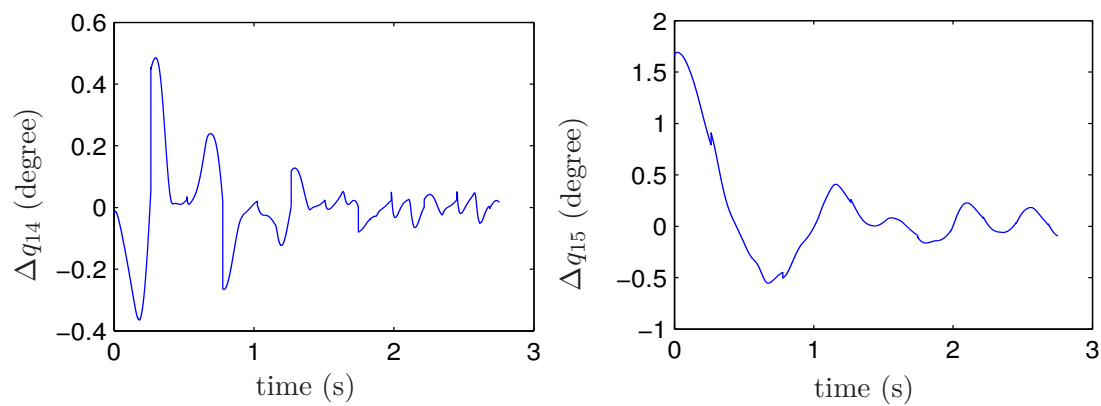


Figure 4.23: The tracking errors of  $q_{14}$  and  $q_{15}$  for the walking including foot rotation phase.

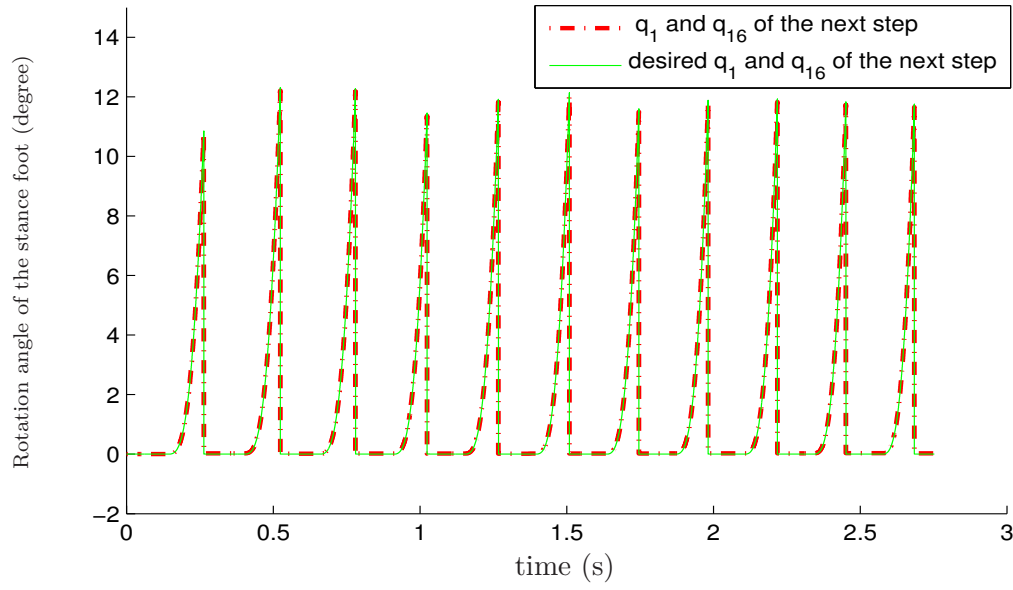


Figure 4.24: Rotation angle of the stance foot in the sagittal plane and its desired values. Note that in the first step it is  $q_1$  and in the next step is written as  $q_{16}$ , and so forth.

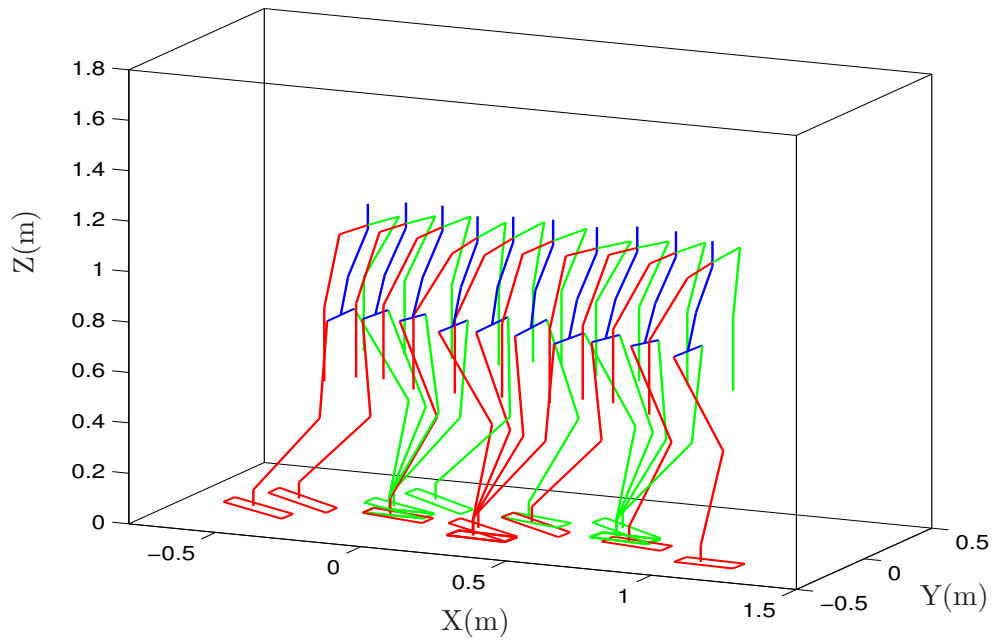


Figure 4.25: The walking motion of the robot with foot rotation phase during first three steps.

### Simulation results of the control law considering initial errors and modeling errors

In order to further verify the robustness of the control law, besides of the introduced initial errors, the modeling errors are also considered in the simulation. At first, all the inertial parameters are changed  $-20\%$  in the dynamic models of the control law, the simulation results are shown in Fig. 4.26–Fig. 4.30. By comparing them with the previous results that only considered initial errors shown in Fig. 4.18–Fig. 4.22, the influence of modeling errors on the walking of biped robot can be clearly seen.

Form the height of feet shown in Fig. 4.26, we know that the movement of feet in saggital plane evolves as we desired. During the whole walking phase both two feet didn't roll and during the fully support phases the stance foot keep flat in the ground. However, the maximum height of the swing foot during the first two steps are different from the desired value shown in the following steps because of the introduced initial errors and modeling errors. Besides, since the inertial parameters in the control law are not the same as that in the simulator, there exist tracking errors of the desired ZMP and these errors are constant, see Fig. 4.28. The figure also shows that the position of ZMP is always within the limits of the foot sole so at least the robot can keep balance until the simulation stop. Fig. 4.27 shows the tracking errors of  $q_2$  and  $q_3$ , compared it with Fig. 4.22, it indicates that the tracking errors of the joint angles still can converge although there exist modeling errors. However, they converge to certain constants but not to zero. The evolution of the joint in its phase plane can be seen in Fig. 4.29. Fig. 4.30 describes the evolution of torques corresponding to joint angles  $q_i, i = 2, 3, 4, 5$ , compared it with Fig. 4.21, it can be seen that the joint angle  $q_2$  and  $q_3$  consume much more torques in the vicinity of impact moment.

In summary, when all the inertial parameters are changed  $-20\%$  in the dynamic models of the control law, although there exist tracking errors of desired ZMP and joint angles, the stable walking still can be obtained. In general, the modeling errors are smaller, the converge properties of walking are better. However, the walking robustness also depends on the desired trajectory. If the margin of desired ZMP is very small, the acceptable modeling errors are small too. For example, when all the inertial parameters are changed  $+10\%$ , the resulted  $ZMP_x$  almost reaches the edge of the heel, as shown in Fig. 4.31. Luckily, the ZMP has not gotten out of the foot sole. As a result, the walking is stable as shown in Fig. 4.32. Moreover, compared with Fig. 4.27, Fig. 4.32 shows that in this case the walking converges better because the absolute value of introduced modeling errors are smaller. However, we have tested that when the errors are changed to  $+20\%$ , the ZMP gets out of the foot sole during certain time thus the walking is no longer stable.

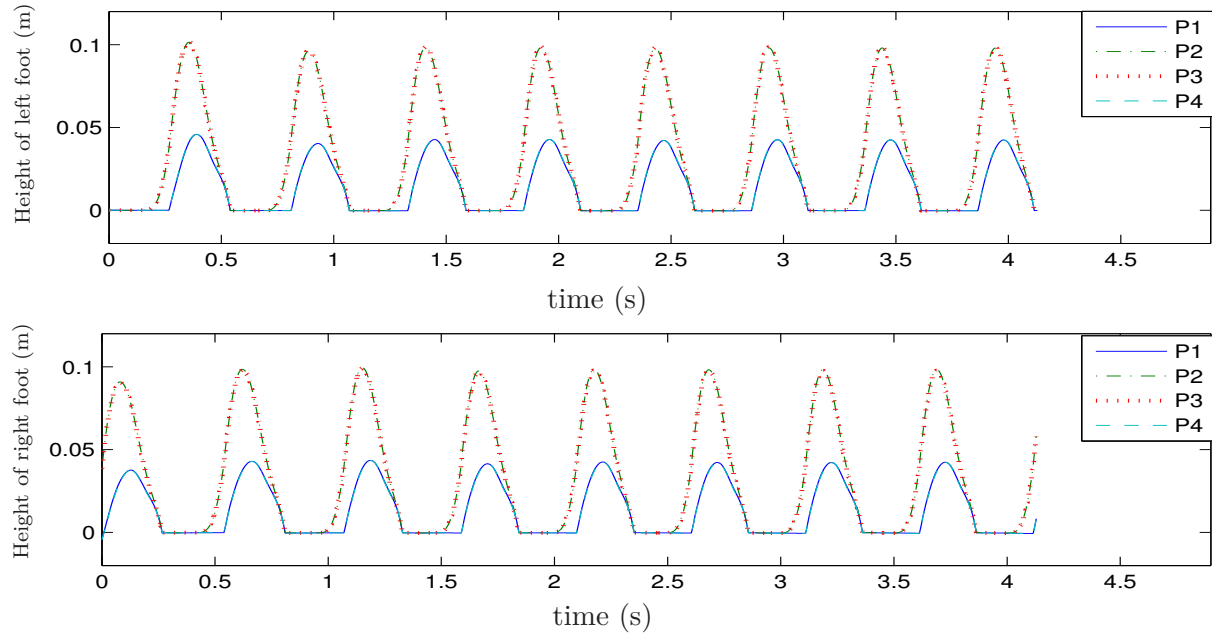


Figure 4.26: Height of feet for the proposed control law considering initials errors and  $-20\%$  modeling errors.

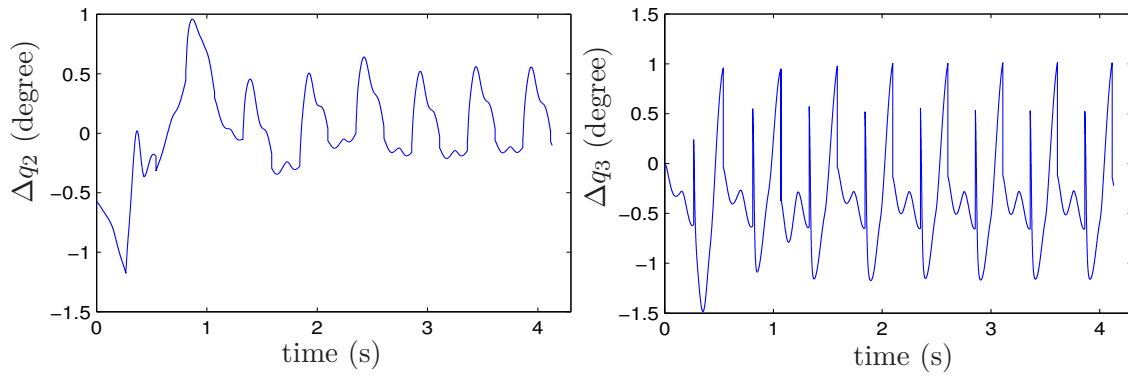


Figure 4.27: The tracking errors of  $q_2$  and  $q_3$  for the proposed control law considering initials errors and  $-20\%$  modeling errors.

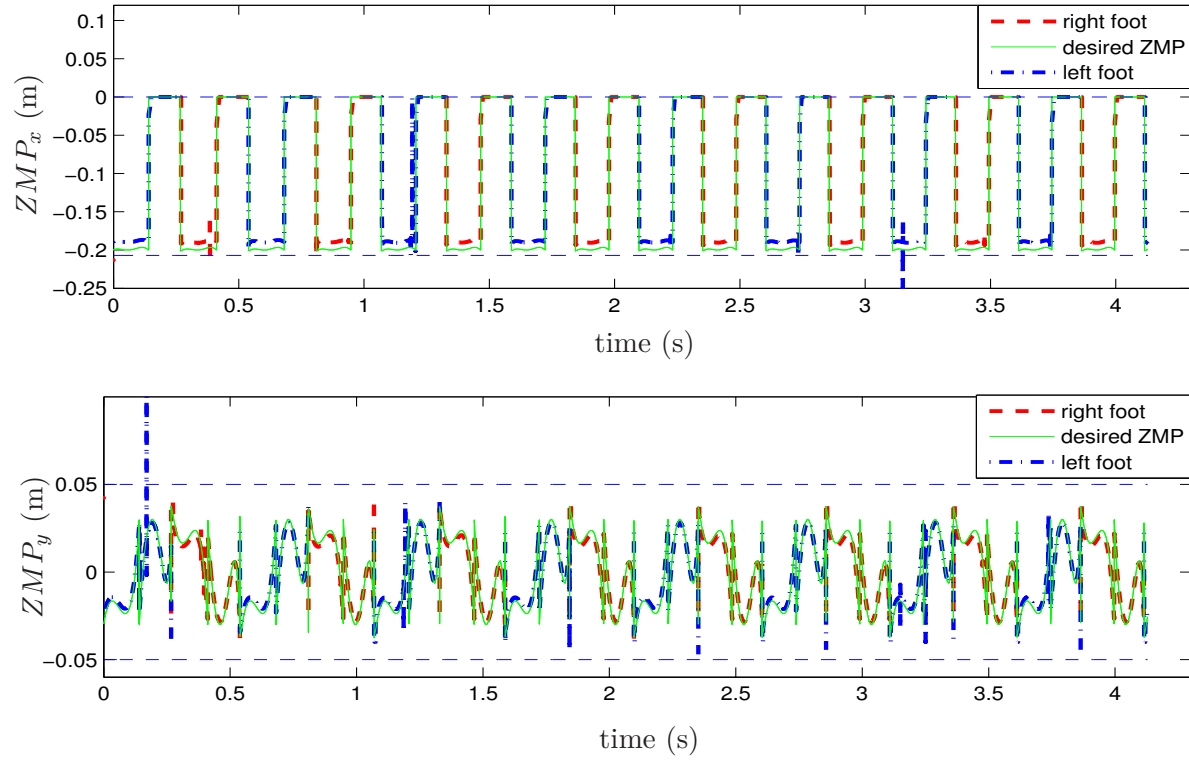


Figure 4.28: Position of ZMP for the proposed control law considering initials errors and  $-20\%$  modeling errors.  $ZMP_y$  is always within the limits and  $ZMP_x$  is zero during under-actuated phase.

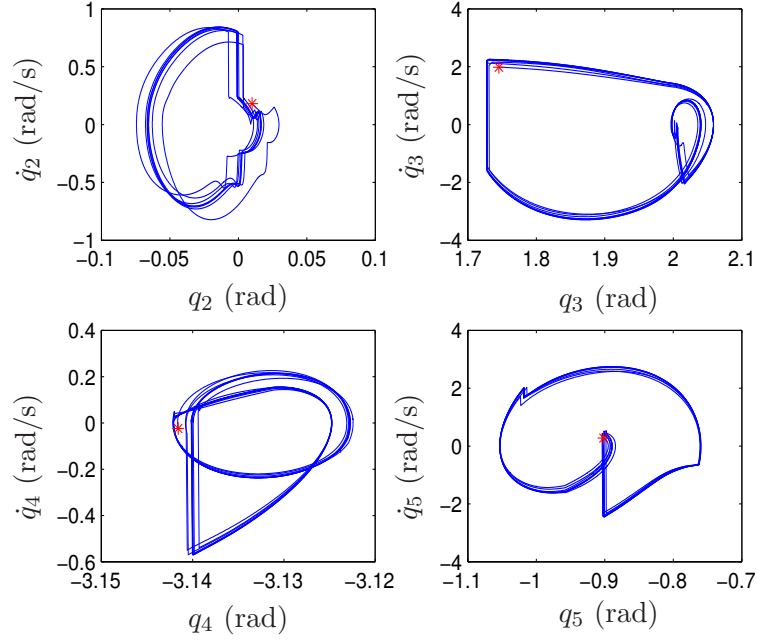


Figure 4.29: Phase-plane plots for  $q_i, i = 2, 3, 4, 5$  for the proposed control law considering initials errors and  $-20\%$  modeling errors. The initial state is represented by a (red) star.

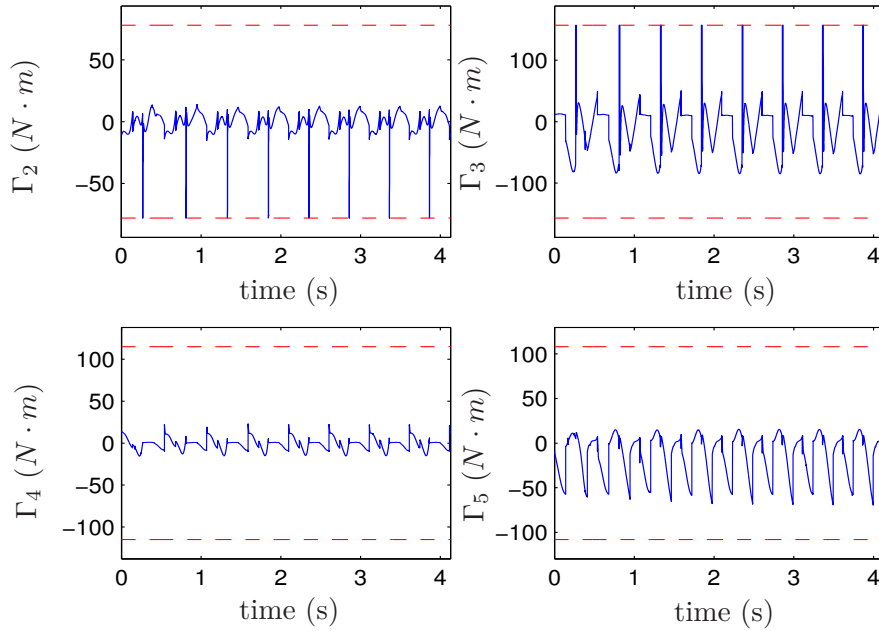


Figure 4.30: The corresponding torques of  $q_i, i = 2, 3, 4, 5$  for the proposed control law considering initials errors and  $-20\%$  modeling errors.

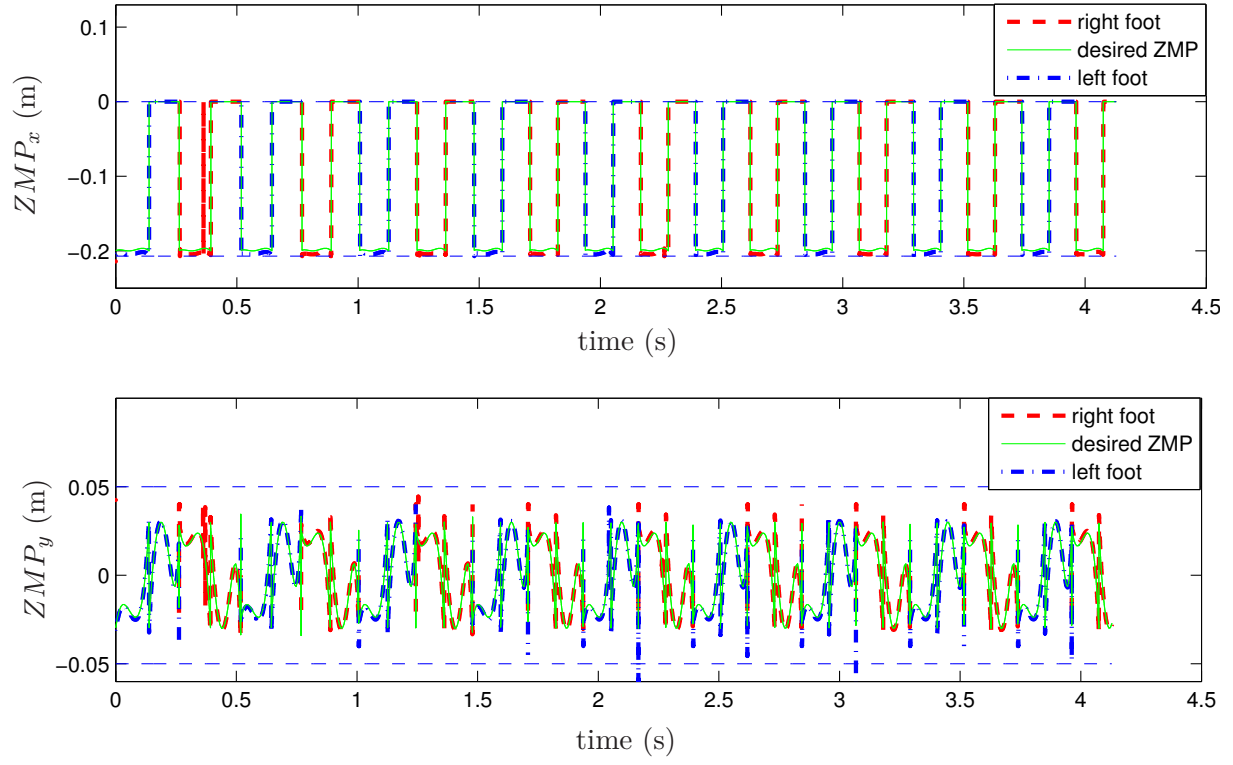


Figure 4.31: Position of ZMP for the proposed control law considering initials errors and +10% modeling errors.  $ZMP_x$  almost reaches the edge of the heel during the fully support phase.

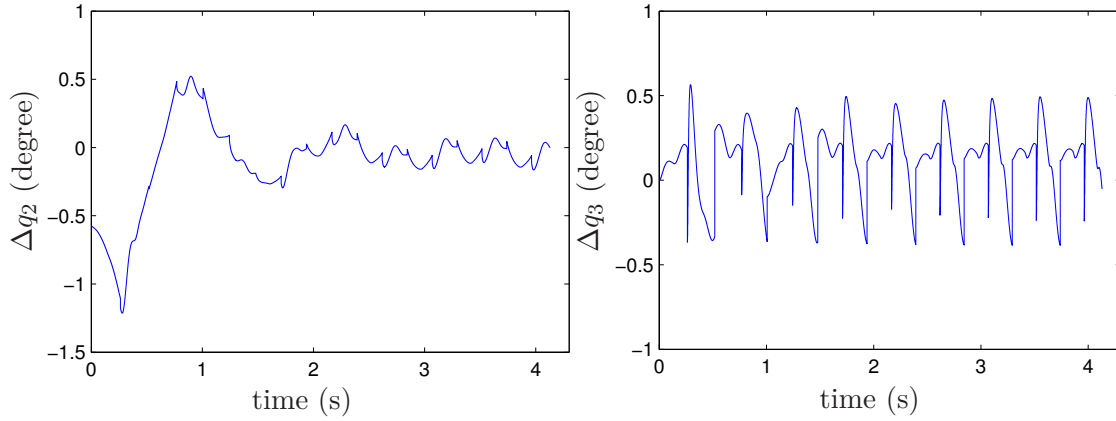


Figure 4.32: The tracking errors of  $q_2$  and  $q_3$  for the proposed control law considering initials errors and +10% modeling errors.



### Simulation results of a classical control law with initial errors

Next, the walking simulation with the same reference trajectory is tested under the classical control law that has been proposed in Subsection 2.7.4, in which all the joint angles are controlled and the desired property of the closed-loop system is:

$$\ddot{q} = \ddot{q}^d - K_d(\dot{q} - \dot{q}^d) - K_p(q - q^d), \quad (4.30)$$

where  $K_d > 0$  and  $K_p > 0$ .

The torques are obtained by using (4.5) with  $q$ ,  $\dot{q}$  and  $\ddot{q}$ . Similar to our control law, in order to limit the influence of errors at the beginning of the step, the reference trajectory in (4.30) is also modified as presented in section 2.5.4. In order to prove the validity and superiority of our control law, the walking simulation of this control law is tested in the same simulator and the simulation settings are also the same. A smaller initial error of  $0.001 \text{ rad}$  is introduced on  $q_2$  and a velocity error of  $0.001 \text{ rad/s}$  is introduced on  $\dot{q}_2$  and  $\dot{\theta}$ , the simulation results are shown in Fig. 4.33–Fig. 4.36.

The simulation results are similar to that for the walking without foot rotation phase (see Section 2.7.4). When there exists initial errors at the states of robot, since the classical control law only adjusts the joint angles, the position of ZMP can easily move out of the foot sole, as shown in Fig. 4.33. As a result, Fig. 4.34 shows that after the second impact ( $t > 0.53 \text{ s}$ ) the stance foot began to rotate about its edge so it can not keep flat in the ground. At the same moment, the robot tries to lift the other foot much higher to keep balance. Therefore, the maximum height of the swing foot (at  $t = 0.63 \text{ s}$ ) is higher than that of the previous step. Fig. 4.35 describes some postures of the robot during walking. Compared with the stable walking under our control law shown in Fig. 4.25, it clearly shows that under the classical control law the walking is unorderly and nonperiodic. Fig. 4.36 also indicates that the walking is divergent. Obviously, the comparison reconfirms that the control of ZMP is much more important than the tracking of predefined joints trajectory.

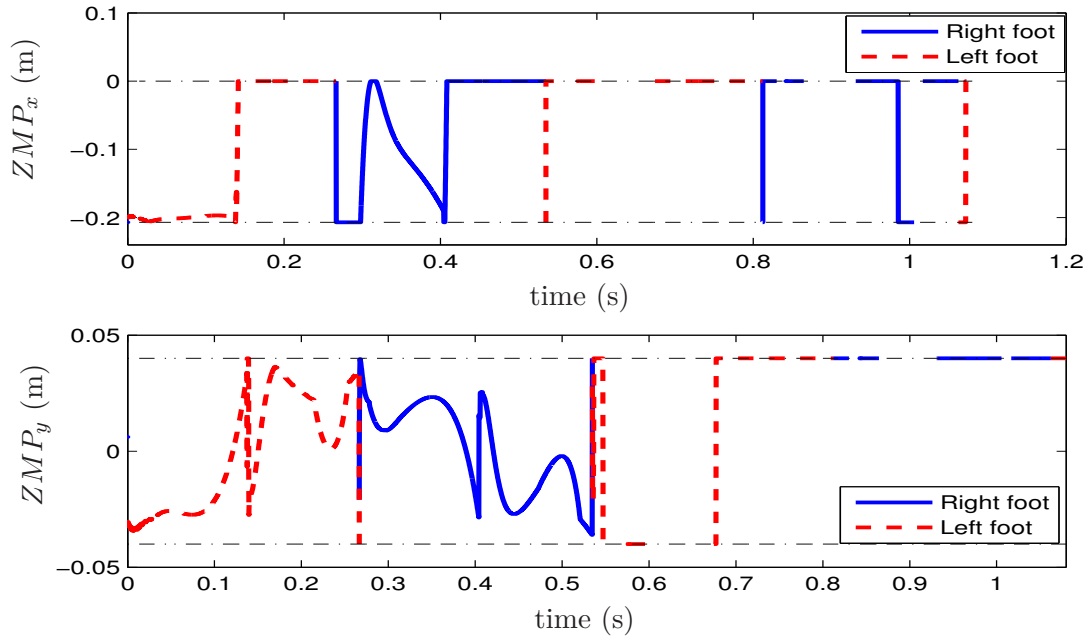


Figure 4.33: Position of CoP in the foot sole for the walking with foot rotation phase under the classical control law: it moves out of the foot sole after walking two steps.

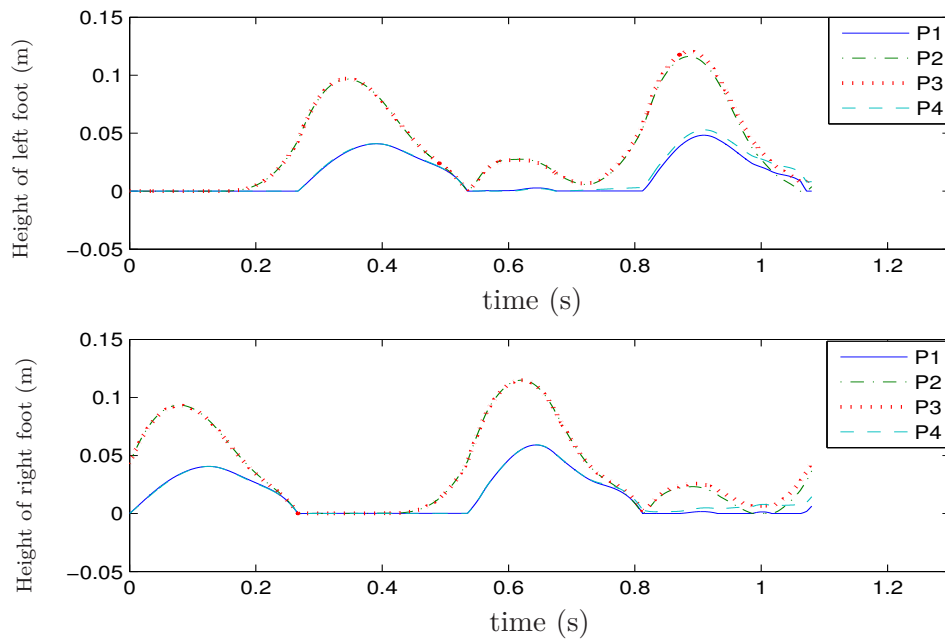


Figure 4.34: Height of feet for the walking with foot rotation phase under the classical control law.

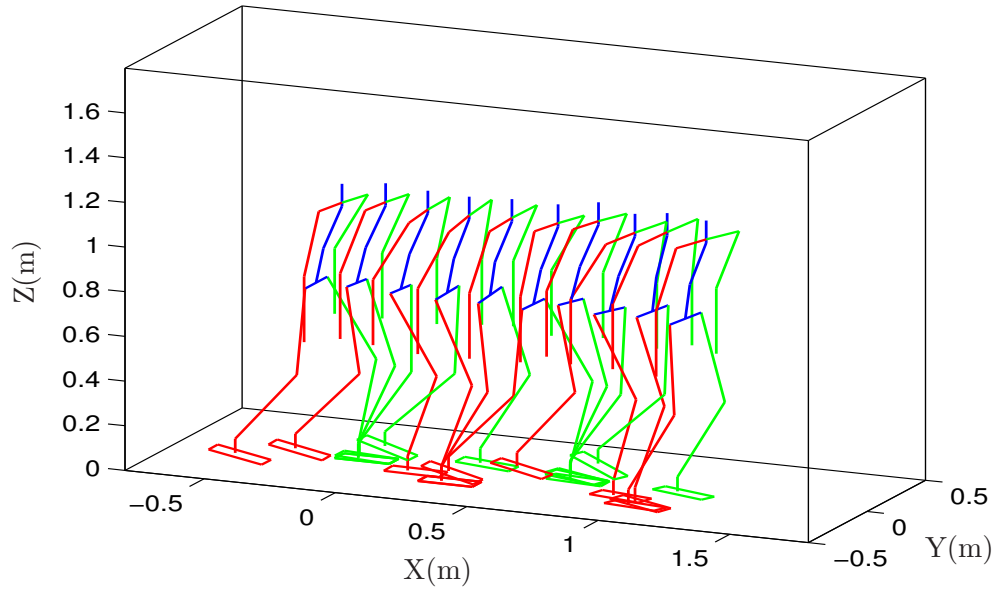


Figure 4.35: The walking motion of the robot with foot rotation phase under the classical control law.

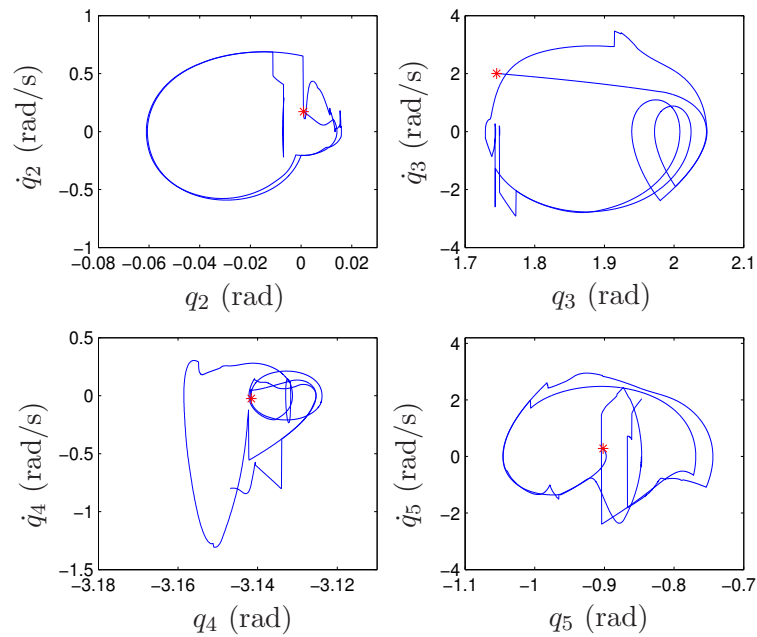


Figure 4.36: Phase-plane plots for  $q_i, i = 2, 3, 4, 5$  for the walking with foot rotation phase under the classical control law. The initial state is represented by a (red) star.

## 4.7 Conclusions

The main contribution of this chapter is that a walking control law proposed in Chapter 2 is successfully extended to a 3d biped robot considering foot rotation phase. In addition, the control law is suitable for both of fully support phase and foot rotation phase.

The studied biped robot has 27 DoF and 26 actuated joints during foot rotation phase, which means the system is under-actuated. In Chapter 2, a control strategy was proposed based on tracking a reference path in the joint space instead of a reference motion expressed as a function of time. The parameterized reference trajectory helps to solve the problem of under-actuation during foot rotation phase.

The control law still consists of ZMP controller, swing ankle rotation controller and partial joint angles controller. The rotation angle of the stance foot is added in the overall joint configuration vector as an actuated joint angle. The corresponding torque of this angle is also calculated by using Newton-Euler algorithm. However, the computed torque for the toe is zero since the constraints on the ZMP position are taken into account. Therefore, the proposed dynamic model in the foot rotation phase is still useful in the fully support phase because that can be viewed as a special case of that the foot rotation angle is zero.

Compared with the control law proposed previously for the walking without foot rotation phase, in this chapter ZMP controller and swing ankle rotation controller are always the same as before, the difference is that the foot rotation angle is also adjusted in the partial joint angles controller as other actuated joint angles. Finally, two examples are given and the simulation results validate the effectiveness of the control law even in presence of initial errors and modeling errors.

# Conclusions and perspectives

## Conclusions

This thesis studied the walking control problem for three biped robots. The reference trajectory for them have been calculated off-line using optimization technical method. The objective of the control law is to achieve an asymptotically stable, periodic walking gait.

Firstly, in Chapter 1, the studied model is an under-actuated planar biped robot based on RABBIT. This robot has point contact with the ground. The rotation of the stance leg with respect to the ground is passive. Three control laws are presented for this robot. The first one is the virtual constraints method which has been proved successfully to control this kind of under-actuated robot. It uses a state quantity of the biped that is strictly monotonic along a typical walking gait to replace the time  $t$  to parameterize the reference trajectory. By using this method, only the kinematic evolution of the robot's state is regulated but not its temporal evolution. Therefore, it makes for a stable walking. For the under-actuated robot, the number of input torques is less than the number of its independent degrees of freedom. Since the state quantity of the biped to parametrize the reference trajectory is also a linear function of the actuated joint angles, it can be regarded as a new actuated joint used in the control law. Its acceleration is chosen to satisfy the dynamic equation corresponding to the global rotation of the robot around the point contact, which helps to solve the under-actuation problem.

In order to validate the effectiveness of the control law, a stability analysis is necessary. A classical technique for determining the existence and stability properties of periodic orbits in nonlinear system is using Poincaré return map. A periodic solution corresponds to a fixed-point of a Poincaré return map. Stability of the periodic solution is equivalent to stability of the fixed-point. In order to simplify the stability analysis, the definitions of zero dynamics and hybrid zero dynamics (HZD) are introduced. The zero dynamics is defined to describe the behavior of the system when the outputs of the control law are assumed to be zero, that means the control law is perfect and all the tracking errors are zero. Since the torques of the biped are calculated only based on the dynamic model during swing phase, if the impact model is incorporated into the notion of the maximal internal dynamics compatible with the output being identically zero, a zero dynamics of the complete model of the biped robot is obtained, which is called *hybrid zero dynamics* (HZD). According to the definitions of zero dynamics and HZD, the full order system can be simplified to a reduced dimensional system. Thus the stability can be analyzed in a

reduced dimensional space.

The results of stability analysis show that the walking is stable using the method of virtual constraints. However, the parameterized reference trajectory is not usual in robotics, while the definition of that as a function of time is more traditional. In addition, it is difficult to find the strictly monotonic state for some robots, for example, robot-semiquad, quadruped with a curvet gait, or biped with frontal motion. As a consequence, two other control laws are proposed based on tracking the reference motion described as a function of time. The first method is using event-based feedback control to improve the walking stability. With this control law, a vector of parameters that is updated just after each impact is introduced to modify the walking stride to stride. In contrast to this strategy, the second method does not need supplemental feedback controller. It is based on the choice of controlled joint angles which will influence the walking stability. Thus by studying its effects on the stability some pertinent choices of controlled joint angles are determined and the stability is ensured at the same time. Furthermore, by analyzing some walking characteristics of many stable cases a necessary condition for stable walking is conjectured, which helps to choose the controlled outputs leading to stable walking. At the end of Chapter 1, three control laws are compared with each other. It shows that the converge property of the method based on choice of controlled joint angles is better than that of the event-based feedback control. Especially, its tracking error of the velocity converges faster than that of the virtual constraints method.

Next, the walking control of a 3D biped robot with 14 joint actuators is studied in Chapter 2. The robot is modeled based on HYDROID and it is comprised of a torso and two identical legs that are independently actuated and terminated with flat-feet. The walking phase consists of single support phases and impacts. We suppose that the double support phase is instantaneous and the ground is flat. In addition, during the single support phase, the supported foot does not slide nor rotate. The Newton Euler algorithm is used to calculate the dynamic model of biped during the single support phase. The actuator torques and the ground reaction (forces and torques) to the stance foot can be computed as soon as the joint position, velocity and acceleration are known. Since the control law is based on the compute-torques control, the desired acceleration of the robot for the actuated joint has to be defined. The control law is based on tracking of the parameterized reference trajectory because the efficiency of this approach has been proved for the robot with point feet.

In view of the importance of ZMP for the stability, a ZMP controller is used to regulate the position of ZMP to its desired value in the horizontal plane, that can offer 2 constraint equations about the states of robot. Moreover, in order to ensure that the robot could touch the ground with flat foot at impact, the pitch and roll angles of the swing foot are controlled to be their desired values by a swing ankle rotation controller, which can also offer 2 constraint equations. Because not all the joints can be controlled directly since 4 constraints on acceleration have already been defined, the other controlled outputs are chosen from the joint configuration according to stability analysis of the whole system. This method is called partial joint angles controller. By using the control law composed by these three sub-controllers, the stance foot does not move because of ZMP controller,

the stable contact condition is satisfied with the help of swing ankle rotation controller, and the stability of the overall system is ensured by the partial joint angles controller. Finally, the simulation results validate the proposed control law. Furthermore, in order to study the effects of ZMP control on the walking of robot, the same method but without the control of  $ZMP_y$ ,  $ZMP_x$  and  $ZMP$  respectively, are presented and compared with each other.

With the proposed control law, the robot can achieve an asymptotically stable and periodic walking along a straight line. It can be observed that the walking motion is not exactly along the  $x$ -axis if there exists initial error. However, the robot is expected to be able to move all over the working place when it works in human environment. Thus in Chapter 3, the steering control of the robot is studied. We introduce a walking direction angle to the states of the robot to create an extended system. In fact, with the proposed control strategy the walking direction of the robot is not controllable and the extended system is not stable. Precisely, the yaw motion of the robot is not stable. In Chapter 1 we have validated that the event-based feedback control law can improve the stability of the system. Therefore, a supplemental event-based feedback controller is then introduced to the original control system and it distributes commands to all of the actuated joints. As a result, the extended system is stabilized. Since the behavior of the robot is invariant with respect to the walking direction, it is possible to achieve different objectives of steering control by using different definitions of desired walking direction. At last, the robot is steered successfully to turn to a predefined direction, to pass through a door and to reach a destination. Considering the restriction of the torque of joints, the robot can only turn with mild curvature.

Finally, Chapter 4 studied the walking control of a biped robot with arm motion and foot rotation. A walking phase describing the stance foot rotation around its metatarsal axis is considered in the single support phase. During this phase, the robot is under-actuated because there is no actuation at the toe. A disequilibrium phase which is unusual for humanoid robot but existing in human walking is introduced. This phase is useful to reduce the energy cost of walking by increasing the step length. Fortunately, the explicit control of the ZMP, that has to be along the metatarsal axis during the foot rotation phase, helps to solve this problem and that has been used in the control of the biped model proposed in Chapter 2. Therefore, the control law presented in Chapter 2 is extended directly to the new biped model. The control law still consists of ZMP controller, swing ankle rotation controller and partial joint angles controller. The key point is that the rotation angle of the supported foot is added in the overall joint configuration vector as an actuated joint angle. The corresponding torque of this angle is also calculated by using Newton Euler algorithm. However, the computed torque for the toe is zero since the constraints on the ZMP position are taken into account. Therefore, the proposed dynamic model in the foot rotation phase is still useful in the fully support phase because that can be viewed as a special case of that the foot rotation angle is zero. Different from the previous studies, the stability of the control law is insured during foot rotation phase. The simulation results indicate that the proposed control law can lead to stable walking for the biped robot with foot rotation even in presence of initial errors and modeling errors.

## Perspectives

Until now, the proposed control law in this thesis can realize an asymptotically stable, periodic walking gait for a biped robot model based on HYDROID. More importantly, the reference trajectory is relative human-like because it includes a walking phase during which the stance foot rotates around its toe in the sagittal plane. Thus the work is original and significant. In the future, the proposed control law will be tested in the robot Roméo. As a consequence, there are still many interesting and challenging questions to be answered.

Firstly, going back to the reference trajectory, the method of virtual constraints is presented in Chapter 1, in which the reference trajectory is parametrized by a state quantity of the biped that is strictly monotonic during the whole walking phase. It is shown that this method can reduce the dimension of hybrid zero dynamics to simplify the stability analysis, and it helps to solve the under-actuation problem. Therefore, it is still used for the 3D biped robot with foot rotation phase. However, for the biped model studied in 3D, as soon as the frontal motion is considered, it is not very easy to obtain an ideal reference trajectory that can give the strictly monotonic state. Hence, it is regarded as a constraint to be considered in the generation of the trajectory. In the next step, maybe it will be a better choice that if we can generate a parametrized reference joint path directly using optimization techniques.

The next problem is the stability analysis. It is very important for our control law because it determines the choice of controlled partial joint angles. We have found that for the studied robot with foot rotation, it is difficult to find many good choices of controlled outputs which can lead to stable walking. In Chapter 1, by studying some walking characteristics of many stable cases, we found a necessary condition for stable walking. Based on this condition, the choice of controlled outputs is constrained, and then two stable domains for the controlled outputs selection are given. Thus in the next step, we should test that if the proposed necessary condition is still useful for the biped robot with foot rotation or if there exist other conditions.

Besides, when the control law is tested in the real robot, there are many practical things have to be considered. For example, in our steering control law, the present walking direction angle is an input of the system, thus the measurement of this angle by using some sensors should be considered. Similarly, for the walking including foot rotation phase, the absolute rotation angle of the stance foot should be measured. Moreover, in the numerical simulation we suppose that the ground is flat, so we want to know if the proposed control law can be extended to the walking on the uneven or inclined floor. In addition, presently the double support phase is supposed to be instantaneous and the robot touches the ground with flat foot. In future, if we add a walking phase during which the swing leg strikes the ground with the heel at first and then the foot sole touches the ground completely, the control law should be updated according to the dynamic models and ZMP. Furthermore, even though the reference trajectory of our robot is calculated off-line, Chapter 3 has shown that it is possible to change it a little to adjust the walking direction of the biped robot. Therefore, it is also interesting to study if it is possible to define a reference trajectory on-line.



In summary, there are still lots of work to do for the walking control of biped robot. We hope that the biped robot can not only walk like human, it can even turn, jump and run swifter, higher and faster than us.



# Bibliography

- [Acary et al., 2008] Acary, Vicent, Brogliato, and Bernard (2008). *Numerical Methods for Nonsmooth Dynamical Systems: Applications in Mechanics and Electronics*, volume 35 of *Lecture Notes in Applied and Computational Mechanics*. Springer Verlag.
- [Alfayad, 2009] Alfayad, S. (2009). *Robot humanoïde HYDROÏD : Actionnement, Structure Cinématique et Stratégie de contrôle*. PhD thesis, Université de Versailles Saint Quentin en Yvelines.
- [Anderle and Celikovsky, 2009] Anderle, M. and Celikovsky, S. (2009). Analytical design of the acrobot exponential tracking with application to its walking. In *IEEE International Conference on Control and Automation*, pages 163–168, Christchurch, New Zealand.
- [Aoustin et al., 2005] Aoustin, Y., Chevallereau, C., and Formal’sky, A. (2005). Numerical and experimental study of a virtual quadrupedal walking robot - semiquad. *Multibody System Dynamic*.
- [Asano and Luo, 2007] Asano, F. and Luo, Z.-W. (2007). Asymptotically stable gait generation for biped robot based on mechanical energy balance. In *Proceedings of the 2007 IEEE/RSJ International Conference on Intelligent Robots and Systems*, pages 3328–3333, San Diego, USA.
- [Asano and Luo, 2008] Asano, F. and Luo, Z.-W. (2008). Asymptotic stability of dynamic bipedal gait with constraint on impact posture. In *Proceedings of 2008 IEEE International Conference on Robotics and Automation*, pages 1246–1251, USA.
- [Behnke, 2006] Behnke, S. (2006). Online trajectory generation for omnidirectional biped walking. In *IEEE International Conference on Robotics and Automation*, pages 1597–1603, Orlando, Florida.
- [Bergmann, 2004] Bergmann, M. (2004). *Optimisation aérodynamique par réduction de modèle POD et contrôle optimal. Application au sillage laminaire d’un cylindre circulaire*. PhD thesis, Institut National Polytechnique de Lorraine / LEMTA. in French.
- [Bezier, 1972] Bezier, P. (1972). *Numerical control: Mathematics and Applications*. J. Wiley, New York. Wiley series in computing.

- [Bhat and Bernstein, 2000] Bhat, S. and Bernstein, D. (2000). Finite-time stability of continuous autonomous systems. *SIAM Journal of Control and Optimization*, 38(3):51–766.
- [Buschmann et al., 2007] Buschmann, T., Lohmeier, S., Bachmayer, M., Ulbrich, H., and Pfeiffer, F. (2007). A collocation method for real-time walking pattern generation. In *IEEE-RAS International Conference on Humanoid Robots*, pages 1–6, Pittsburgh, PA.
- [Buschmann et al., 2009] Buschmann, T., Lohmeier, S., and Ulbrich, H. (2009). Humanoid robot lola: Design and walking control. *Journal of Physiology-Paris*, 103:141–148.
- [Chemori and Loria, 2004] Chemori, A. and Loria, A. (2004). Control of a planar under-actuated biped on a complete walking cycle. *IEEE Transactions on Automatic Control*, 49(5):838–843.
- [Chenglong et al., 2006] Chenglong, F., Shuai, M., and Chen., K. (2006). Proving asymptotic stability of dynamic walking for a five-link biped robot with feet. In *IEEE Conference on Robotics, Automation and Mechatronics*.
- [Chevallereau, 1999] Chevallereau, C. (1999). *Modern Control Theory*, chapter 7, "Under actuated biped robot". Esculapio, Bologna (Italy).
- [Chevallereau et al., 2003] Chevallereau, C., Abba, G., Aoustin, Y., Plestan, F., Westervelt, E., and et al. (2003). Rabbit: A testbed for advanced control theory. *IEEE Control Systems*, 23(5):57–78.
- [Chevallereau and Aoustin., 2001] Chevallereau, C. and Aoustin., Y. (2001). Optimal reference trajectories for walking and running of a biped robot. *Robotica*, 19(5):557–569.
- [Chevallereau et al., 2008] Chevallereau, C., Djoudi, D., and Grizzle, J. (2008). Stable bipedal walking with foot rotation through direct regulation of the zero moment point. *IEEE Transactions on Robotics*, 24(2):390–401.
- [Chevallereau et al., 2004] Chevallereau, C., Formal'sky, A., and Djoudi, D. (2004). Tracking of a joint path for the walking of an underactuated biped. *Robotica*, 22:15–28.
- [Chevallereau et al., 2009] Chevallereau, C., Grizzle, J., and Shih, C. (2009). Asymptotically stable walking of a five-link underactuated 3d bipedal robot. *IEEE Trans. on Robotics*, 25(1):37–50.
- [Chevallereau et al., 2010] Chevallereau, C., Grizzle, J., and Shih, C. (2010). Steering of a 3d bipedal robot with an underactuated ankle. In *Proceedings of the 2010 IEEE/RSJ International Conference on Intelligent Robots and Systems*, Taipei, Taiwan. To be appeared.
- [Choi and Grizzle, 2005] Choi, J. H. and Grizzle, J. W. (2005). Planar bipedal walking with foot rotation. In *Proc. of the American Control Conference*, pages 4909–4916.

- [Coros et al., 2010] Coros, S., Beaudoin, P., and van de Panne, M. (2010). Generalized biped walking control. In *Proceedings of the 37th International Conference on computer graphics and interactive techniques*, Los Angeles, USA. To be appeared.
- [Djoudi et al., 2005] Djoudi, D., Chevallereau, C., and Aoustin, Y. (2005). Optimal reference motions for walking of a biped robot. In *IEEE International Conference on Robotics and Automation*, pages 2002–2007, Barcelona, Spain.
- [Dombre and Khalil, 1999] Dombre, E. and Khalil, W. (1999). *Modélisation, identification et commande des robots*. Hermes Sciences. in French, Paris.
- [Fantoni and Lozano, 2002] Fantoni, I. and Lozano, R. (2002). *Non-linear control of underactuated mechanical systems*. Springer-Verlag.
- [Ferreira et al., 2006] Ferreira, J., Crisostomo, M., and Coimbra, A. (2006). Neuro-fuzzy zmp control of a biped robot. In *Proceedings of the 6th WSEAS International Conference on Simulation, Modeling and Optimization*, pages 331–337, Lisbon, Portugal.
- [Fukuda et al., 2006] Fukuda, T., Doi, M., Hasegawa, Y., and Kajima, H. (2006). *Fast Motions in Biomechanics and Robotics*, volume 340. Springer-Verlag. chapter Multi-Locomotion Control of Biped Locomotion and Brachiation Robot.
- [Goswami, 1999] Goswami, A. (1999). Postural stability of biped robots and the foot-rotation indicator (FRI) point. *International Journal of Robotics Research*, 18(6):523–533.
- [Goswami and Vadakkepat, 2009] Goswami, D. and Vadakkepat, P. (2009). Planar bipedal jumping gaits with stable landing. *IEEE Transactions on Robotics*, 25(5):1030–1046.
- [Gouaillier, 2009] Gouaillier, D. (2009). *Conception mécanique et commande de l'appareil locomoteur d'un robot humanoïde*. PhD thesis, Université de Versailles Saint Quentin, France.
- [Gregg and Spong, 2010] Gregg, R. and Spong, M. (2010). Reduction-based control of three dimensional bipedal walking robots. *International Journal of Robotics Research*, 29(6):680–702.
- [Grizzle, 2003] Grizzle, J. (2003). Remarks on event-based stabilization of periodic orbits in systems with impulse effects. In *Proceedings of the Second International Symposium on Communications, Control and Signal Processing*.
- [Grizzle et al., 2001] Grizzle, J., Abba, G., and Plestan, F. (2001). Asymptotically stable walking for biped robots: Analysis via systems with impulse effects. *IEEE Transactions on Automatic Control*, 46:51–64.

- [Grizzle et al., 2005] Grizzle, J., Moog, C., and Chevallereau, C. (2005). Nonlinear control of mechanical systems with an unactuated cyclic variable. *IEEE Transactions on Automatic Control*, 50(5):559–576.
- [Guckenheimer and Johnson, 1995] Guckenheimer, J. and Johnson, S. (1995). Planar hybrid systems. In *Proceedings of Hybrid Systems II, Lecture Notes in Computer Science*, volume 999, pages 202–225, London, UK. Springer-Verlag.
- [Hiskens, 2001] Hiskens, I. (2001). Stability of hybrid system limit cycles: Application to the compass gait biped robot. In *Proceedings of 40th IEEE Conference on Decision and Control*, pages 775–779, Florida, USA.
- [Huang et al., 2000] Huang, Q., Kaneko, K., Yokoi, K., Kajita, S., Kotoku, T., Koyachi, N., Arai, H., Imamura, N., Komoriya, K., and Tanie, K. (2000). Balance control of a biped robot combining off-line pattern with real-time modification. In *Proceedings of International Conference on Robotics and Automation*, pages 3346–3352, San Francisco, USA.
- [Huang et al., 2001] Huang, Q., Yokoi, K., Kajita, S., Kaneko, K., Arai, H., Koyachi, N., and Tanie, K. (2001). Planning walking patterns for a biped robot. *IEEE Transactions on Robotics and Automation*, 17(3):280–289.
- [Hurmuzlu and Chang, 1992] Hurmuzlu, Y. and Chang, T. (1992). Rigid body collisions of a special class of planar kinematic chains. *IEEE Transactions on Systems, Man, and Cybernetics*, 22(5):964–971.
- [Hurmuzlu and Marghitu, 1994] Hurmuzlu, Y. and Marghitu, D. (1994). Rigid body collisions of planar kinematic chains with multiple contact points. *International Journal of Robotics Research*, 13(1):82–92.
- [Hyon et al., 2006] Hyon, S., Yokoyama, N., and Emura, T. (2006). Back handspring of a multi-link gymnastic robot - reference model approach. *Advanced Robotics*, 20(1):93–113.
- [Ishida, 2004] Ishida, T. (2004). Development of a small biped entertainment robot qrio. In *Proceedings of the 2004 international symposium on micro-nano mechatronics and human science and International symposium on micro-nano mechatronics and human science*.
- [Isidori, 1995] Isidori, A. (1995). *Nonlinear Control Systems*. Springer-Verlag, Berlin, third edition.
- [Isidori and Moog, 1988] Isidori, A. and Moog, C. (1988). On the nonlinear equivalent of the notion of transmission zeros. In C., B. and Kurzhanski, A., editors, *Proc. of the IIASA Conference: Modeling and Adaptive Control*, pages 146–157, Berlin. Springer-Verlag.

- [Ito et al., 2008] Ito, S., Amano, S., Sasaki, M., and Kulvanit, P. (2008). A zmp feedback control for biped balance and its application to in-place lateral stepping motion. *Journal of Computers*, 3(8):23–31.
- [Kajita et al., 2002] Kajita, S., Kanehiro, F., Kaneko, K., Fujiwara, K., Yokoi, K., and Hirukawa, H. (2002). A real-time pattern generator for biped walking. In *IEEE International Conference on Robotics and Automation*, pages 31–37.
- [Kajita et al., 2007] Kajita, S., Kaneko, K., Morisawa, M., Nakaoka, S., and H., H. (2007). Zmp-based biped running enhanced by toe springs. In *IEEE International Conference on Robotics and Automation*, pages 3963–3969, Roma, Italy.
- [Kajita et al., 2001] Kajita, S., Matsumoto, O., and Saigo, M. (2001). Real-time 3d walking pattern generation for a biped robot with telescopic legs. In *Proceedings of International Conference on Robotics and Automation*, pages 2299–2306, Seoul, Korea.
- [Kajita and Tani, 1991] Kajita, S. and Tani, K. (1991). Study of dynamic biped locomotion on rugged terrain. In *IEEE International Conference on Robotics and Automation*, pages 1405–1410.
- [Kajita and Tani, 1995] Kajita, S. and Tani, K. (1995). Experimental study of biped dynamic walking in the linear inverted pendulum mode. In *Proc. of the IEEE International Conference on Robotics and Automation, Nagoya, Japan*, pages 2885–2891.
- [Kaneko et al., 2004] Kaneko, K., Kanehiro, F., Kajita, S., Hirukawa, H., Kawasaki, T., Hirata, M., Akachi, K., and Isozumi, T. (2004). Humanoid robot hrp-2. In *IEEE international conference on robotics and automation*, New Orleans, LA.
- [Khalil, 2002] Khalil, H. (2002). *Nonlinear Systems - 3rd Edition*. Prentice Hall, Upper Saddle River, NJ.
- [Khalil and Dombre, 2002] Khalil, W. and Dombre, E. (2002). *Modeling, identification and control of robots*. Hermes Sciences, Europe. Paris.
- [K.Hirai et al., 1998] K.Hirai, Hirose, M., Haikawa, Y., and T.Takenaka (1998). The development of honda humanoid robot. In *Proceedings of the IEEE International Conference on Robotics and Automation*, pages 1321–1326, Leuven, Belgium.
- [Kim et al., 2006] Kim, J., Park, I., and Oh, J. (2006). Experimental realization of dynamic walking of the biped humanoid robot khr-2 using zero moment point feedback and inertial measurement. *Advanced Robotics*, 20(6):707–736.
- [Kuo, 1999] Kuo, A. (1999). Stabilization of lateral motion in passive dynamic walking. *International Journal of Robotics Research*, 18(9):917–930.
- [Kuo, 2002] Kuo, A. D. (2002). Energetics of actively powered locomotion using the simplest walking model. *Journal of Biomechanical Engineering*, 124:113–120.

- [Kurazume et al., 2003] Kurazume, R., Hasegawa, T., and Yoneda, K. (2003). The sway compensation trajectory for a biped robot. In *Proceedings of the 2003 IEEE International Conference on Robotics and Automation*, pages 925–931, Taipei, Taiwan.
- [Li et al., 2011] Li, T., Su, Y., Lai, S., and Hu, J. (2011). Walking motion generation, synthesis, and control for biped robot by using pgrl, lpi, and fuzzy logic. *IEEE Transactions on Systems, Man, and Cybernetics, Part B: Cybernetics*, 41:736–748.
- [Luh et al., 1980] Luh, J., Walker, M., and Paul, R. (1980). On line computational scheme for mechanical manipulators. *Trans. of ASME, J. of Dynamic Systems, Measurement and Control*, 102(2):69–76.
- [Matsumoto and Kawamura, 2010] Matsumoto, K. and Kawamura, A. (2010). The direction control of a biped robot using gyro sensor feedback. In *Proceedings of the 11th IEEE International Workshop on Advanced Motion Control*, pages 137–142, Nagaoka, Niigata.
- [Mitobe et al., 2000] Mitobe, K., Capi, G., and Nasu, Y. (2000). Control of walking robots based on manipulation of the zero moment point. *Robotica*, 18:651–657.
- [Mitobe et al., 2010] Mitobe, K., Satoh, M., and Capi, G. (2010). A zmp control of a powered passive dynamic walking robot. In *Proceedings of 2010 World Automation Congress (WAC)*, pages 1–7, Japan.
- [Miura and Shimoyama, 1984] Miura, H. and Shimoyama, I. (1984). Dynamic walk of a biped. *The International Journal of Robotics Research*, 3(2):60–74.
- [Miura et al., 2008] Miura, K., Nakaoka, S., Morisawa, M., Harada, K., and Kajita, S. (2008). A friction based 'twirl' for biped robots. In *Proceedings of 2008 IEEE-RAS International Conference on Humanoid Robots*, pages 279–284.
- [Morris and Grizzle, 2005] Morris, B. and Grizzle, J. (2005). A restricted Poincaré map for determining exponentially stable periodic orbits in systems with impulse effects: Application to bipedal robots. In *IEEE Conf. on Decision and Control*, Seville, Spain. IEEE Press.
- [Morris and Grizzle, 2009] Morris, B. and Grizzle, J. (2009). Hybrid invariant manifolds in systems with impulse effects with application to periodic locomotion in bipedal robots. *IEEE Transactions on Automatic Control*, 54(8):1751–1764.
- [Nagasaka et al., 1999] Nagasaka, K., Inoue, H., and Inaba, M. (1999). Dynamic walking pattern generation for a humanoid robot based on optimal gradient method. In *IEEE international conference on systems, man, and cybernetics*.
- [Nair and Aggarwal, 1998] Nair, D. and Aggarwal, J. (1998). Moving obstacle detection from a navigating robot. *IEEE Transactions on robotics and automation*, 14(3):404–416.



- [Napoleon et al., 2002] Napoleon, Nakaura, S., and Sampei, M. (2002). Balance control analysis of humanoid robot based on zmp feedback control. In *Proceedings of the 2002 IEEE/RSJ International Conference on Intelligent Robots and Systems*, pages 2437–2442, Lausanne, Switzerland.
- [Nijmeijer and van der Schaft, A. J., 1989] Nijmeijer, H. and van der Schaft, A. J. (1989). *Nonlinear Dynamical Control Systems*. Springer-Verlag, Berlin.
- [Nishiwaki et al., 2003] Nishiwaki, K., Kagami, S., Kuffner, J., Inaba, M., and Inoue, H. (2003). Online humanoid walking control system and a moving goal tracking experiment. In *Proceedings of the 2003 IEEE International Conference on Robotics and Automation*, pages 911–916, Taipei, Taiwan.
- [Oda and Ito, 2010] Oda, N. and Ito, M. (2010). Visual walking direction control by regulating torsional deflection for biped robot. In *The 11th IEEE International Workshop on Advanced Motion Control*, pages 143–148, Nagaoka, Japan.
- [Parker and Chua, 1989] Parker, T. and Chua, L. (1989). *Practical Numerical Algorithms for Chaotic Systems*. Springer-Verlag, New York.
- [Perrin, 2011] Perrin, N. (2011). *Footstep Planning for Humanoid Robots: Discrete and Continuous Approaches*. PhD thesis, Universite de Toulouse, Toulouse, France.
- [Plestan et al., 2003] Plestan, F., Grizzle, J., Westervelt, E., and Abba, G. (2003). Stable walk-ing of a 7-dof biped robot. *IEEE Transactions on Robotics and Automation*, 19(4):653–668.
- [Rengifo, 2010] Rengifo, C. (2010). *Contributions à la commande d’un robot bipède 3D*. PhD thesis, Ecole Centrale de Nantes, Nantes, France.
- [Rengifo et al., 2009] Rengifo, C., Aoustin, Y., Chevallereau, C., and Plestan, F. (2009). A penalty-based approach for contact forces computation in bipedal robots. In *Proceedings of the 9th IEEE-RAS International Conference on Humanoid Robots*, pages 121–127, Paris, France.
- [Rose and Gamble, 1994] Rose, J. and Gamble, J. (1994). *Human walking*. Williams and Wilkins, Baltimore, 2nd edition.
- [Sakagami et al., 2002] Sakagami, Y., Watanabe, R., Aoyama, C., Matsunaga, S., Higaki, N., and Fujimura, K. (2002). The intelligent asimo: System overview and integration. In *IEEE/RSJ international conference on intelligent robots and systems*, Lausanne, Switzerland.
- [S.Aoi et al., 2004] S.Aoi, Tsuchiya, K., and Tsujita, K. (2004). Turning control of a biped locomotion robot using nonlinear oscillators. In *Proceedings of the 2004 IEEE International Conference on Robotics and Automation*, pages 3043–3048, New Orleans, LA.

- [Seydel, 1994] Seydel, R. (1994). *Practical Bifurcation and Stability Analysis: From Equilibrium to Chaos*, volume 5 of *Interdisciplinary Applied Mathematics*. Springer-Verlag, New York, second edition.
- [Shih et al., 2007] Shih, C., Grizzle, J., and Chevallereau, C. (2007). Asymptotically stable walking of a simple underactuated 3D bipedal robot. In *The 33rd Annual Conference of the IEEE Industrial Electronics Society (IECON)*, pages 2766–2771, Taipei, Taiwan.
- [Shih et al., 2010] Shih, C., Grizzle, J., and Chevallereau, C. (2010). From stable walking to steering of a 3d bipedal robot with passive point feet. *Robotica*. in press.
- [Sira-Ramirez, 1990] Sira-Ramirez, H. (1990). Structure at infinity, zero dynamics and normal forms of systems undergoing sliding motions. *International journal of systems science*, 21(4):665–674.
- [S.Kajita et al., 2006] S.Kajita, F.Kanehiro, K.Kaneko, K.Fujiwara, K.Harada, K.Yokoi, and H.Hirukawa (2006). Biped walking pattern generator allowing auxiliary zmp control. In *Proceedings of the 2006 IEEE/RSJ International Conference on Intelligent Robots and Systems*, pages 2993–2999, Beijing, China.
- [S.Kajita et al., 2003] S.Kajita, M.Morisawa, K.Harada, K.Kaneko, F.Kanehiro, K.Fujiwara, and H.Hirukawa (2003). Biped walking pattern generation by using preview control of zero-moment point. In *Proceedings of the ICRA '03 IEEE International Conference on Robotics and Automation*, pages 1620–1626, Taipei, Taiwan.
- [Spong and Bullo, 2005] Spong, M. and Bullo, F. (2005). Controlled symmetries and passive walking. *IEEE Transactions on Automatic Control*, 50(7):1025–1031.
- [Sreenivasa et al., 2009] Sreenivasa, M., Soueres, P., Laumond, J., and Berthoz, A. (2009). Steering a humanoid robot by its head. In *IEEE/RSJ International Conference on Intelligent Robots and Systems*, pages 4451–4456, St.Louis, USA.
- [Sugihara and Nakamura, 2002] Sugihara, T. and Nakamura, Y. (2002). Whole-body cooperative balancing of humanoid robot using cog jacobian. In *IEEE/RSJ International Conference on Intelligent Robots and Systems*.
- [Sugihara et al., 2002] Sugihara, T., Nakamura, Y., and Inoue, H. (2002). Realtime humanoid motion generation through zmp manipulation based on inverted pendulum control. In *Proceedings of the IEEE International Conference on Robotics and Automation*, pages 1404–1409.
- [Takahashi and Kawamura, 2001] Takahashi, T. and Kawamura, A. (2001). Posture control for biped robot walk with foot toe and sole. In *27th Annual Conference of the IEEE Industrial Electronics Society*, pages 329–334.
- [Takeuchi, 2001] Takeuchi, H. (2001). Development of 'mel horse'. In *Proceedings of International Conference on Robotics and Automation*, pages 3165–3171, Seoul, Korea.

- [Tlalolini, 2008] Tlalolini, D. (2008). *Generation de mouvements optimaux de marche pour des robots bipides 3d*. PhD thesis, Ecole Centrale de Nantes, Université de Nantes, Nantes, France.
- [Tlalolini et al., 2010] Tlalolini, D., Aoustin, Y., and Chevallereau, C. (2010). Design of a walking cyclic gait with single support phases and impacts for the locomotor system of a thirteen-link 3d biped using the parametric optimization. *Multibody System Dynamics*, 23(1):33–56.
- [Tlalolini et al., 2009] Tlalolini, D., Chevallereau, C., and Aoustin, Y. (2009). Comparison of different gaits with rotation of the feet for a planar biped. *Robotics and Autonomous Systems*, 57(4):371–383.
- [Tlalolini et al., 2011] Tlalolini, D., Chevallereau, C., and Aoustin, Y. (2011). Human-like walking: Optimal motion of a bipedal robot with toe-rotation motion. *IEEE/ASME Transactions on Mechatronics*, 16(2):310–320.
- [Varghese et al., 1991] Varghese, M., Fuchs, A., and Mukundan, R. (1991). Chaotic zero dynamics in kinematically redundant robots. *IEEE Transactions on aerospace and electronic systems*, 27(5):784–795.
- [Vukobratovic et al., 1990] Vukobratovic, M., Borovac, B., Surla, D., and Stokic, D. (1990). *Biped Locomotion - Dynamics, Stability, Control and Application*. Springer-Verlag, Berlin.
- [Wang and Chevallereau, 2010a] Wang, T. and Chevallereau, C. (2010a). A new control law for a 3d biped robot based on regulation of the zero moment point and joint path. In *Proceedings of 2010 IEEE-RAS International Conference on Humanoid Robots*, pages 27–32, Nashville, USA.
- [Wang and Chevallereau, 2010b] Wang, T. and Chevallereau, C. (2010b). Stability of time-varying control for an underactuated biped robot based on choice of controlled outputs. In *Proceedings of the 2010 IEEE/RSJ International Conference on Intelligent Robots and Systems*, pages 4083–4088, Taipei, Taiwan.
- [Wang and Chevallereau, 2011a] Wang, T. and Chevallereau, C. (2011a). Stability analysis and time-varying walking control for an under-actuated planar biped robot. *Robotics and Autonomous Systems*, 59(6):444–456.
- [Wang and Chevallereau, 2011b] Wang, T. and Chevallereau, C. (2011b). Steering control for a 3d biped robot considering ground contact and stability. In *14th International Conference on Climbing and Walking Robots and the Support Technologies for Mobile Machines*, Paris, France. To be appeared.
- [Wang and Chevallereau, 2011c] Wang, T. and Chevallereau, C. (2011c). Walking control for a 3d biped robot considering ground contact and stability. In *Dynamic Walking*, Jena, Germany. To be appeared.

- [Wang et al., 2011] Wang, T., Chevallereau, C., and Rengifo, C. (2011). Walking and steering control for a 3d biped robot considering ground contact and stability. *Robotics and Autonomous Systems*. Submitted.
- [Wang et al., 2009] Wang, T., Chevallereau, C., and Shih, C.-L. (2009). Choice of output for time-variant walking control for a five-link underactuated planar biped robot. In *Proceedings of 2009 IEEE-RAS International Conference on Humanoid Robots*, pages 373–378, Paris, France.
- [Westervelt et al., 2007] Westervelt, E., Grizzle, J., Chevallereau, C., Choi, J., and Morris, B. (2007). *Feedback Control of Dynamic Bipedal Robot Locomotion*. Control and Automation. CRC Press, Boca Raton.
- [Westervelt et al., 2002] Westervelt, E., Grizzle, J., and Koditschek, D. (2002). Zero dynamics of planar biped walkers with one degree of under actuation. In *IFAC 2002, Barcelona, Spain*.
- [Westervelt et al., 2003] Westervelt, E., Grizzle, J., and Koditschek, D. (2003). Hybrid zero dynamics of planar biped walkers. *IEEE Transactions on Automatic Control*, 48(1):42–56.
- [Yagi and Lumelsky, 2000] Yagi, M. and Lumelsky, V. (2000). Synthesis of turning pattern trajectories for a biped robot in a scene with obstacles. In *Proceedings of the 2000 IEEE/RSJ International Conference on Intelligent Robots and Systems*, pages 1161–1166.
- [Yamaguchi et al., 1993] Yamaguchi, J., Takanishi, A., and Kato, I. (1993). Development of a biped walking robot compensating for three axis moment by trunk motion. In *IEEE/RSJ international conference on intelligent robots and systems*, Yokohama, Japan.
- [Yi, 2000] Yi, K. (2000). Walking of a biped robot with compliant ankle joints: implementation with kubca. In *Proc. of the 39th IEEE Conf. Dec. and Control, Sydney, Australia*, pages 4809–4814.
- [Zikmund and Moog, 2006] Zikmund, J. and Moog, C. (2006). The structure of 2-bodies mechanical systems. In *Proceedings of the 45th IEEE Conf. on Decision and Control*, pages 6464–6469, San Diego, CA, USA.

# Appendix A

## Calculation details of the control law

### A.1 Calculation of ${}^s\omega_n$ and ${}^s\dot{\omega}_n$

${}^s\omega_n$  and  ${}^s\dot{\omega}_n$  are the angular acceleration and velocity of the joint  $n$  in the absolute coordinate system  $x_sy_s z_s$ . For the biped model proposed in Chapter 2,  $n = 13$ , and for the biped model proposed in Chapter 4,  $n = 15$ . They can be efficiently computed by the forward recursive equations of the general serial robot [Khalil and Dombre, 2002]. For the serial number of joints  $j = 1, \dots, n$ , there exist:

$$\begin{cases} {}^j\omega_{j-1} &= {}^jR_{j-1}{}^{j-1}\omega_{j-1} \\ {}^j\omega_j &= {}^j\omega_{j-1} + \dot{q}_j {}^ja_j \\ {}^j\dot{\omega}_j &= {}^jR_{j-1}{}^{j-1}\dot{\omega}_{j-1} + \ddot{q}_j {}^ja_j + {}^j\omega_{j-1} \times \dot{q}_j {}^ja_j \end{cases} \quad (\text{A.1})$$

where  ${}^ja_j = [0, 0, 1]^T$ ,  ${}^jR_{j-1}$  denotes the orientation matrix from the coordinate system  $x_jy_jz_j$  to  $x_{j-1}y_{j-1}z_{j-1}$ , and the initial condition are  ${}^0\omega_0 = 0$ ,  ${}^0\dot{\omega}_0 = 0$ . If  ${}^n\omega_n$  and  ${}^n\dot{\omega}_n$  have been computed by (A.1),  ${}^s\omega_n$  and  ${}^s\dot{\omega}_n$  in (2.17) can be obtained by:

$$\begin{cases} {}^s\omega_n = {}^sR_n {}^n\omega_n \\ {}^s\dot{\omega}_n = {}^sR_n {}^n\dot{\omega}_n \end{cases} \quad (\text{A.2})$$

### A.2 Simplification of calculations for swing ankle rotation controller

The swing ankle rotation controller is:

$$\ddot{\xi}_{xy} - \ddot{\xi}_{xyc} + \frac{K_1}{\varepsilon}(\dot{\xi}_{xy} - \dot{\xi}_{xyc}) + \frac{K_2}{\varepsilon^2}(\xi_{xy} - \xi_{xyc}) = \mathbf{0}_{2 \times 1} \quad (\text{A.3})$$

It's worth noting that when the calculations of this section are used for the biped robot model proposed in Chapter 4, all the subscript  $xy$  have to be changed to  $yz$  because the

definition of the absolute coordinate system  $x_s y_s z_s$  is modified. According to the definition of  $\dot{\xi}$  and  $\ddot{\xi}$  (see (2.17)), (A.3) can be rewritten as:

$${}^s\dot{\omega}_n^d{}_{xy} - {}^s\dot{\omega}_{nxy} - \ddot{\xi}_{xyc} + \frac{K_1}{\varepsilon}(\dot{\xi}_{xy} - \dot{\xi}_{xyc}) + \frac{K_2}{\varepsilon^2}(\xi_{xy} - \xi_{xyc}) = \mathbf{0}_{2 \times 1} \quad (\text{A.4})$$

where  $\xi_{xy}$  is obtained by (2.15) (or (4.16) for Chapter 4) and (2.16).  $\dot{\xi}_{xy}$  can be calculated by (A.1), (A.2) with  $q, \dot{q}$  and  $q^d, \dot{q}^d$ . Based on (2.29) and (2.30),  $\dot{\xi}_{xyc}$  and  $\ddot{\xi}_{xyc}$  can be calculated with:

$$\begin{cases} \dot{\xi}_{xyc} &= \frac{\partial \xi_{xyc}}{\partial \theta} \dot{\theta}, \\ \ddot{\xi}_{xyc} &= \frac{\partial \xi_{xyc}}{\partial \theta} \ddot{\theta} + \frac{\partial^2 \xi_{xyc}}{\partial \theta^2} \dot{\theta}^2 \end{cases} \quad (\text{A.5})$$

and

$$\begin{cases} \frac{\partial \xi_{xyc}}{\partial \theta} &= c_1 + 2c_2\theta + 3c_3\theta^2 + 4c_4\theta^3 \\ \frac{\partial^2 \xi_{xyc}}{\partial \theta^2} &= 2c_2 + 6c_3\theta + 12c_4\theta^2. \end{cases} \quad (\text{A.6})$$

According to Appendix A.1,  ${}^s\dot{\omega}_n$  is a linear function of  $\ddot{q}$ . Similar to (2.4),  ${}^s\dot{\omega}_{nxy}$  can be defined as:

$${}^s\dot{\omega}_{nxy} = F_a \ddot{q} + F_v, \quad (\text{A.7})$$

where  $F_a$  and  $F_v$  can be obtained according to the functions to compute  ${}^s\dot{\omega}_n$ . Accordingly, as the same as (2.5) and (2.6), they can be calculated by:

$$F_v = {}^s\dot{\omega}_{nxy}(q, \dot{q}, \ddot{q} = \mathbf{0}_{N \times 1}), \quad (\text{A.8})$$

and

$$\begin{cases} F_a(:, i) = {}^s\dot{\omega}_{nxy}(q, \dot{q}, \ddot{q} = \mathbf{e}_{N \times 1}) - F_v \\ \mathbf{e}(i) = 1, \quad i \in \{1, 2, \dots, N\} \\ \mathbf{e}(j) = 0, \quad j \in \{1, 2, \dots, N\} \quad \text{and} \quad j \neq i \end{cases} \quad (\text{A.9})$$

Where  $N$  is the number of joints used in the dynamic models.  $N = 14$  in Chapter 2 and  $N = 27$  in Chapter 4.

According to (A.7), we can deduce  ${}^s\dot{\omega}_{nxy}$  and its desired value  ${}^s\dot{\omega}_n^d{}_{xy}$  are linear functions of  $\ddot{q}$  and  $\ddot{q}^d$  respectively.  ${}^s\dot{\omega}_n^d{}_{xy}$  can be written as:

$${}^s\dot{\omega}_n^d{}_{xy} = F_a^d \ddot{q}^d + F_v^d, \quad (\text{A.10})$$

where  $F_a^d$  and  $F_v^d$  are calculated by using (A.9) and (A.8) with  $q^d, \dot{q}^d$ . Since  $\ddot{q}^d$  includes a term about  $\ddot{\theta}$  (see (2.12)), which is also a linear function of  $\ddot{q}$ . There exists:

$$\theta = M_\theta q \quad (\text{A.11})$$

where  $M_\theta$  is determined by (2.9) or (4.13) for two biped models respectively.

Based on (A.10), (2.12) and (A.11),  ${}^s\dot{\omega}_n^d{}_{xy}$  can be obtained using:

$${}^s\dot{\omega}_n^d{}_{xy} = F_a^d \frac{\partial h^d(\theta)}{\partial \theta} M_\theta \ddot{q} + F_a^d \frac{\partial^2 h^d(\theta)}{\partial \theta^2} (M_\theta \dot{q})^2 + F_v^d. \quad (\text{A.12})$$

Finally, (A.5), (A.7), (A.12) and (A.11) show that (A.4) is a linear equation of  $\ddot{q}$ , and it can be rewritten as:

$$W_s(q, \dot{q})\ddot{q} + H_s(q, \dot{q}) = \mathbf{0}_{2 \times 1}, \quad (\text{A.13})$$

where  $W_s(q, \dot{q})$  denotes all the coefficient terms of  $\ddot{q}$  and  $H_s(q, \dot{q})$  denotes all the terms without  $\ddot{q}$  in (A.4). Specifically, they are calculated with:

$$W_s = F_a^d \frac{\partial h^d(\theta)}{\partial \theta} M_\theta - F_a - \frac{\partial \xi_{xyc}}{\partial \theta} M_\theta \quad (\text{A.14})$$

and

$$H_s = F_a^d \frac{\partial^2 h^d(\theta)}{\partial \theta^2} (M_\theta \dot{q})^2 + F_v^d - F_v - \frac{\partial^2 \xi_{xyc}}{\partial \theta^2} (M_\theta \dot{q})^2 + \frac{K_1}{\varepsilon} (\dot{\xi}_{xy} - \dot{\xi}_{xyc}) + \frac{K_2}{\varepsilon^2} (\xi_{xy} - \xi_{xyc}). \quad (\text{A.15})$$

### A.3 Simplification of calculations for partial joint angles controller

The partial joint angles control law is:

$$\ddot{u} - \ddot{u}^d - \ddot{u}_c + \frac{K_d}{\varepsilon} (\dot{u} - \dot{u}^d - \dot{u}_c) + \frac{K_p}{\varepsilon^2} (u - u^d - u_c) = \mathbf{0}_{J \times 1}, \quad (\text{A.16})$$

where  $J$  denotes the dimension of  $u$ ,  $J = 10$  in Chapter 2 and  $J = 23$  in Chapter 4. Because the controlled partial joint angles  $u$  is a linear function of the joint angles  $q$  (see (2.21) or (4.23)), so it can be written as:

$$u = Mq \quad (\text{A.17})$$

Obviously,  $\ddot{u}$  is a linear function of  $\ddot{q}$ . In addition, using (2.12), (A.17) and (A.11),  $u^d, \dot{u}^d, \ddot{u}^d$  can be calculated as:

$$\begin{cases} u^d(t) &= Mh^d(\theta) \\ \dot{u}^d(t) &= M \frac{\partial h^d(\theta)}{\partial \theta} \dot{\theta} \\ \ddot{u}^d(t) &= M \left( \frac{\partial^2 h^d(\theta)}{\partial \theta^2} (M_\theta \dot{q})^2 + \frac{\partial h^d(\theta)}{\partial \theta} M_\theta \ddot{q} \right) \end{cases} \quad (\text{A.18})$$

(A.18) shows that  $\ddot{u}^d$  is also a linear function of  $\ddot{q}$ .

Next, similar to the calculation of  $\dot{\xi}_{xyc}, \ddot{\xi}_{xyc}$  (see (A.5) and (A.6)),  $\dot{u}_c$  and  $\ddot{u}_c$  can be given by:

$$\begin{cases} \dot{u}_c &= \frac{\partial u_c}{\partial \theta} \dot{\theta}, \\ \ddot{u}_c &= \frac{\partial u_c}{\partial \theta} \ddot{\theta} + \frac{\partial^2 u_c}{\partial \theta^2} \dot{\theta}^2 \end{cases} \quad (\text{A.19})$$

and

$$\begin{cases} \frac{\partial u_c}{\partial \theta} &= a_1 + 2a_2\theta + 3a_3\theta^2 + 4a_4\theta^3 \\ \frac{\partial^2 u_c}{\partial \theta^2} &= 2a_2 + 6a_3\theta + 12a_4\theta^2. \end{cases} \quad (\text{A.20})$$



Finally, substitute (A.17), (A.18) and (A.19) into (A.16), the resulted equation can be written as:

$$W_j(q, \dot{q})_{J \times N} \ddot{q} + H_j(q, \dot{q})_{J \times 1} = \mathbf{0}_{J \times 1}, \quad (\text{A.21})$$

where  $W_j(q, \dot{q})$  denotes all the coefficient terms of  $\ddot{q}$  and  $H_j(q, \dot{q})$  denotes all the terms without  $\ddot{q}$  in (A.16). They are obtained by using:

$$W_j = M - M \frac{\partial h^d(\theta)}{\partial \theta} M_\theta - \frac{\partial u_c}{\partial \theta} M_\theta \quad (\text{A.22})$$

and

$$H_j = -M \frac{\partial^2 h^d(\theta)}{\partial \theta^2} (M_\theta \dot{q})^2 - \frac{\partial^2 u_c}{\partial \theta^2} (M_\theta \dot{q})^2 + \frac{K_d}{\varepsilon} (\dot{u} - \dot{u}^d - \dot{u}_c) + \frac{K_p}{\varepsilon^2} (u - u^d - u_c). \quad (\text{A.23})$$

## A.4 Calculation of zero dynamics

According to the definition of zero dynamics, there is:

$$\begin{cases} y_1 &= ZMP - ZMP^d(\theta) = 0 \\ y_2 &= \xi_{xy} = 0 \\ y_3 &= u - u^d(\theta) = 0 \end{cases} \quad (\text{A.24})$$

Based on the latter two equations of (A.24),  $q, \dot{q}$  are simplified as function of  $q_2, \theta$  and their derivatives (see (2.40) and (4.28)). As a result, (A.24) is rewritten as:

$$\begin{cases} W(q, \dot{q}) \ddot{q} + H(q, \dot{q}) = \mathbf{0}_{2 \times 1} \\ [q, \dot{q}] = f_{HZD}(q_2, \theta, \dot{q}_2, \dot{\theta}, M_1, C_{q^d}) \end{cases} \quad (\text{A.25})$$

where the first equation of (A.25) comes from the ZMP control law (2.14). In order to solve (A.25),  $\ddot{q}$  should be replaced by  $\ddot{q}_2, \ddot{\theta}$  and other known terms. The detail is shown in the following contents.

Using the second line of (A.24), the definition of  $\xi$  (see (2.17)) and (A.7), we have:

$${}^s\dot{\omega}_n^d{}_{xy} = F_a \ddot{q} + F_v, \quad (\text{A.26})$$

Similarly, the third line of (A.24) and (A.17) result in:

$$\ddot{u}^d = M \ddot{q}. \quad (\text{A.27})$$

In addition, because  $\theta = M_\theta q$  and  $q_2 = M_{q_2} q$ , here  $M_{q_2}$  is a constant matrix,  $\ddot{q}_2$  and  $\ddot{\theta}$  can also be written as linear functions of  $\ddot{q}$ . Therefore, there exists:

$$\ddot{q} = T_a \begin{bmatrix} \ddot{q}_2 \\ \ddot{\theta} \\ {}^s\dot{\omega}_n^d{}_{xy} - F_v \\ \ddot{u}^d \end{bmatrix}, \quad (\text{A.28})$$



with

$$T_a = \begin{bmatrix} M_{q_2} \\ M_{\theta} \\ F_a \\ M \end{bmatrix}^{-1}. \quad (\text{A.29})$$

Next, substituting (A.28) into the first line of (A.25) yields:

$$WT_a \begin{bmatrix} \ddot{q}_2 \\ \ddot{\theta} \\ {}^s\dot{\omega}_n^d - F_v \\ \ddot{u}^d \end{bmatrix} + H = \mathbf{0}_{2 \times 1} \quad (\text{A.30})$$

It should be noted that the calculations of  ${}^s\dot{\omega}_n^d$  and  $\ddot{u}^d$  need  $\ddot{q}^d$  (see (A.10) and (A.17)), which also includes a term about  $\ddot{\theta}$  (see (2.12)). Therefore, using (A.10), (A.17) and (2.12) in (A.30) leads to:

$$W_{HZD}(q, \dot{q}) \begin{bmatrix} \ddot{q}_2 \\ \ddot{\theta} \end{bmatrix} + H_{HZD}(q, \dot{q}) = \mathbf{0}_{2 \times 1} \quad (\text{A.31})$$

where

$$W_{HZD} = \begin{bmatrix} W_1 \\ W_2 + (W_3 F_a^d + W_4 M) \frac{\partial h^d(\theta)}{\partial \theta} \end{bmatrix}^T, \quad (\text{A.32})$$

$$H_{HZD} = (W_3 F_a^d + W_4 M) \frac{\partial^2 h^d(\theta)}{\partial \theta^2} \dot{\theta}^2 + W_3 (F_v^d - F_v) + H \quad (\text{A.33})$$

and

$$[W_{1(2 \times 1)}, W_{2(2 \times 1)}, W_{3(2 \times 2)}, W_{4(2 \times 10)}] = WT_a \quad (\text{A.34})$$

## A.5 Calculation of joint accelerations

Appendix A.2 and A.3 have shown that both of the swing ankle rotation controller and partial joint angles controller can be written as the linear equations of  $\ddot{q}$  such as ZMP controller (2.14). Thus, (2.14), (A.13) and (A.21) can be combined as:

$$A(q, \dot{q})\ddot{q} + B(q, \dot{q}) = \mathbf{0}_{N \times 1}, \quad (\text{A.35})$$

with  $A = [W, W_s, W_j]^T$  and  $B = [H, H_s, H_j]^T$ . Next, the  $\ddot{q}$  can be resolved by using:

$$\ddot{q} = -A^{-1}B \quad (\text{A.36})$$

Generally, the calculation of  $A_{N \times N}^{-1}$  is not very easy especially for the biped model with large number of DOF. Therefore, in the implementation process the calculation of  $\ddot{q}$  is not done directly using (A.36). In fact,  $\ddot{q}_2$  and  $\ddot{\theta}$  are resolved from the ZMP controller, exactly, the first two equations of (A.35), then  $\ddot{q}$  is calculated by using  $\ddot{q}_2$ ,  $\ddot{\theta}$  and other  $N - 2$

equations. The detail is presented as follows. The equation (A.28) shows that for the complete dynamic model without using the definition of zero dynamics,  $\ddot{q}$  can be described as:

$$\ddot{q} = T_a \begin{bmatrix} \ddot{q}_2 \\ \ddot{\theta} \\ {}^s\dot{\omega}_{nxy} - F_v \\ \ddot{u} \end{bmatrix}, \quad (\text{A.37})$$

where  ${}^s\dot{\omega}_{nxy}$  and  $\ddot{u}$  can be respectively calculated by using the PD controllers (A.3) and (A.16). Substituting (A.37) into ZMP controller (2.14), it yields two equations where only  $\ddot{q}_2$  and  $\ddot{\theta}$  are unknown, thus they can be resolved directly. As a result,  $\ddot{q}$  can be obtained by using  $\ddot{q}_2$ ,  $\ddot{\theta}$  and (A.37).

# Appendix B

## Steering control for different legs

In stability analysis, the exchange of legs is considered but only one leg model is used, exactly, the right leg is always supposed to be the stance leg. All the work about the exchange of legs is based on a natural symmetry of the hybrid robot model. When both of two legs are considered in the simulation, the effects of the same tracking error  $\delta q_0$  (see (3.14)) on the walking direction angle of two feet are different. In order to understand that clearly, some values of  $\delta q_0$  are used in the feedback event-based control law (3.11) during the first step and second step, that means the steered foot is the left foot and the right foot respectively. Fig. B.1 and Fig. B.2 give the resulted walking direction angle of two feet just before impact and they can show that:

- 1) The larger the value of  $|\delta q_0|$ , the larger the turning extent of the transfered foot.
- 2) The effect of  $\delta q_0$  on the walking direction angle of two feet is exactly opposite and symmetrical. For example, in the first step, the left leg is transfered. When  $\delta q_0 = 0$ ,  $q_l \approx 4^\circ$  before impact. If  $\delta q_0 = -9^\circ$ ,  $q_l \approx -2^\circ$  before impact. The change is  $-6^\circ$ . On the contrary, in the next step, the right leg is transfered. When  $\delta q_0 = 0$ ,  $q_r \approx -4^\circ$ . If  $\delta q_0 = -9^\circ$ ,  $q_r \approx 2^\circ$ . The change is  $6^\circ$ .
- 3) If the desired walking direction angle of the robot is a large positive value, for example,  $C = 30^\circ \gg 0$ , according to (3.14),  $\delta q_0 < 0$ . Fig. B.2 has shown that  $\delta q_0 < 0$  is helpful to obtain  $q_r > 0$ . However, Fig. B.1 shows that  $\delta q_0 > 0$  is a better choice to obtain  $q_l > 0$ .

Therefore, based on the above three points, (3.14) should be rewritten to distinguish the steering control of two feet. In the case of that the left (or right) foot is transfered at the  $k^{th}$  step, its definition of  $\delta q_0$ , which is written as  $\delta q_{0lk}$  (or  $\delta q_{0rk}$ ), can be calculated by using  $\Delta q_{0k}$ :

$$\Delta q_{0k} = \begin{cases} \delta q_{0lk} &= -[q_{0k} - (q_{0l}^* + C_k)] \\ \delta q_{0rk} &= q_{0k} - (q_{0r}^* + C_k) \end{cases} \quad (B.1)$$

where  $q_{0l}^*$  and  $q_{0r}^*$  denote the value of  $q_0^*$  when the left and right leg is transfered respectively. They have been denoted as red points shown in Fig. B.1 and Fig. B.2. It is obviously that  $q_{0l}^* = -q_{0r}^*$ .

Finally, using (B.1) to replace (3.14), and substituting it to (3.15) to (3.16), the event-based feedback control law for two legs are obtained.

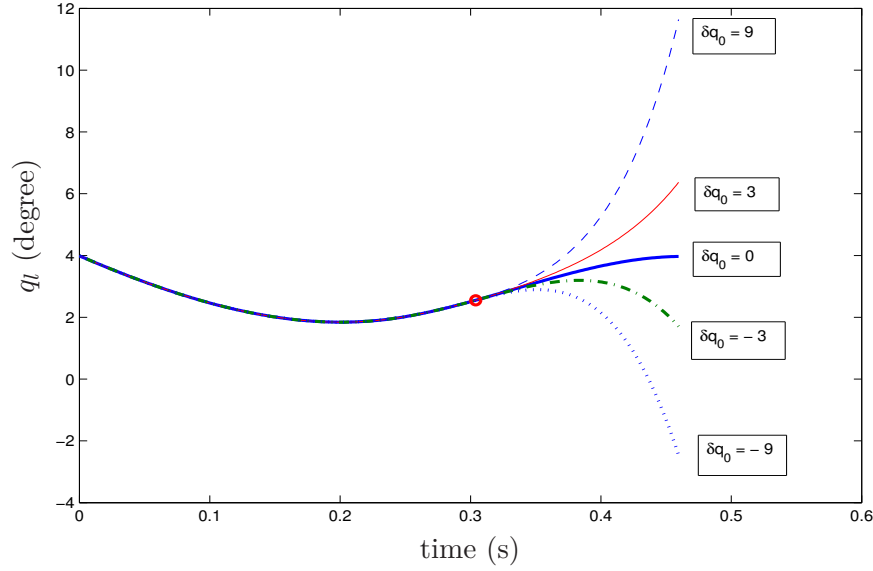


Figure B.1: The walking direction angle of the left foot before the impact of the first step with different  $\delta q_0$ . The red point denotes the moment at Poincaré section when  $\delta q_0$  is introduced in the feedback event-based control law.

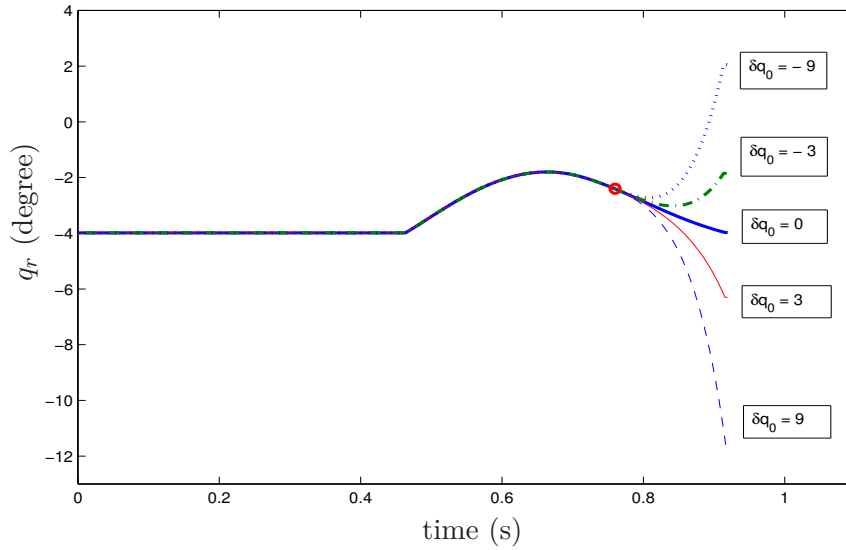


Figure B.2: The walking direction angle of the right foot before the impact of the second step with different  $\delta q_0$ . Here the straight line denotes the right leg is supported by the ground in the first leg. The red point denotes the moment at Poincaré section where  $\delta q_0$  is introduced in the feedback event-based control law.

# Appendix C

## Publications

### Journal Papers

**T. Wang**, C. Chevallereau. Stability analysis and time-varying walking control for an under-actuated planar biped robot. *Robotics and Autonomous Systems (Elsevier)*, 59: 444-456, 2011.

**T. Wang**, C. Chevallereau, C. Rengifo. Walking and steering control for a 3d biped robot considering ground contact and stability. *Robotics and Autonomous Systems (Elsevier)*, 2011, **Submitted**.

### Conference Papers

**T. Wang**, C. Chevallereau. Steering control for a 3D biped robot considering ground contact and stability. *The 14th International Conference on Climbing and Walking Robots and the Support Technologies for Mobile Machines (CLAWAR'11)*, Paris, France, September 2011. **Best Paper Award**.

**T. Wang**, C. Chevallereau. Walking control for a 3D biped robot considering ground contact. *Dynamic Walking*, Jena, Germany, July 2011.

**T. Wang**, C. Chevallereau. A new control law for a 3D biped robot based on regulation of the zero moment point and joint path. *The 10th IEEE-RAS International Conference on Humanoid Robots (Humanoids'10)*, Pages: 27-32, Nashville, TN, USA, December 2010.

**T. Wang**, C. Chevallereau. Stability of time-varying control for an under-actuated biped robot based on choice of controlled outputs. *IEEE/RSJ International Conference on Intelligent Robots and Systems (IROS'10)*, Pages: 4083-4088, Taipei, October 2010.

**T. Wang**, C. Chevallereau, C-l. Shih. Choice of output for time-variant walking control for a five-link under-actuated planar biped robot. *The 9th IEEE-RAS International Conference on Humanoid Robots (Humanoids'09)*, Pages: 373-378, Paris, France, December 2009.